DEUTSCHES ELEKTRONEN-SYNCHROTRON DESY

DESY 86-040
March 1986

STRUCTURE OF WEAK CURRENTS

by

Paul-Dieter Gall

II. Institut für Experimentalphysik der Universität Hamburg

ISSN 0418-9833

NOTKESTRASSE 85 · 2 HAMBURG 52

To be sure that your preprints are promptly included in the
HIGH ENERGY PHYSICS INDEX ,
send them to the following address (if possible by air mail) :

DESY
Bibliothek
Notkestrasse 85
2 Hamburg 52
Germany

DESY 86-040
March 1986

ISSN 0418-9833

STRUCTURE OF WEAK CURRENTS

by

Paul-Dieter Gall

II. Institut für Experimentalphysik der Universität Hamburg

July 1985

CONTENTS

1. INTRODUCTION AND MOTIVATIONS

Weak interaction phenomena have been known for a long time. Already 1934 Fermi /1/ proposed a first theoretical model for describing weak interaction processes by an effective Lagrangian which is the product of two weak currents. This is known as four-Fermion interaction theory.

Since that time, a great amount of experimental and theoretical knowledge on weak interactions at low energy has been derived from the study of nuclear β-decay, muon-capture, muon-decay and the semi-leptonic decays of low-mass mesons and baryons /2/.

These processes were phenomenologically described to good accuracy by the Cabibbo theory /3/ and the Kobayashi-Maskawa extension of it /4/. This was the latest form of Fermi's current-current theory of weak interactions. It fixes the space-time structure of these low-energy charge-changing currents to V-A, i.e. from the five possible interactions – vector (V), axialvector (A), scalar (S), pseudoscalar (P), and tensor (T) - only V and A contribute with equal strength and prescribed phase.

A subject of great interest during the last years has been the detailed study of weak charged-current processes in large-scale detectors such as bubble chambers and electronic counters using calorimetric devices which have been exposed to intense high-energy neutrino and antineutrino beams. Recent results (such as the measurement of μ^+ polarization in $\bar{\nu}_\mu$ induced reactions, the study of inverse μ-decay $\nu_\mu e^- \rightarrow \mu^- \nu_e$, and the discovery of multilepton events) provide useful information on the general space-time structure of the weak charged currents at high energies and large momentum transfers.

It was known that the current-current theory had to be modified at high energies because the amplitudes grow with energy and eventually violate the unitarity limit. Unitarity could not be restored simply by including higher order diagrams, because the four-Fermion interaction theory was non-renormalizable /5/. Even the hypothesis that the four-Fermion interaction is just a low-energy approximation to a finite range interaction mediated by the exchange of massive intermediate vector bosons failed to produce a unitary renormalizable theory.

It turns out that the only renormalizable theories involving massive vector bosons are those in which the bosons are the quanta associated with a gauge symmetry /6/. However, embedding an intermediate vector boson theory into a spontaneously broken gauge theory requires the existence of at least one neutral current and an associated neutral gauge boson. Therefore, the discovery of weak neutral currents in 1973 - 1974 in elastic /7-10/ and single pion production /11,12/ processes induced by neutrinos had drastically enhanced the possible relevance of gauge theory principles in weak interactions.

It is possible to develop gauge theories, incorporating both charged and neutral currents, for the weak interactions alone /13,14/. A more satisfactory and attractive approach is to combine the electromagnetic and weak forces into a single electroweak force and thus to attain partial success in the unification of the four fundamental interactions.

A model proposed by Glashow /15/ and later by Salam and Ward /16/ satisfies this requirement. It has subsequently been improved by Weinberg /17/ and Salam /18/ by incorporating the idea of spontaneous breakdown of local gauge symmetry /6/ in this model. Its single free parameter, the electroweak mixing angle Θ_W, characterizes the amount of

mixing between the neutral weak and electromagnetic current. This model originally intended to describe the weak and electromagnetic interactions of leptons could be extended /17/ to hadrons by implementing a mechanism due to Glashow, Iliopoulos, and Maiani (GIM) /19/.

Precise and beautiful experiments have been performed which confirm the existence of weak neutral currents in a wide variety of particle reactions. Most of the existing measurements agree quite well with the predictions of this Glashow-Weinberg-Salam (GWS) model, the so-called standard model. However, the data cover a range of relatively low momentum transfers ($Q^2 \ll M_Z^2$) and thus probe only the low-energy limits of this model. The value of the electroweak mixing angle extracted from these low-energy data allows an unambiguous prediction of the masses of the charged and neutral vector bosons $W^\pm$ and Z^0 which mediate the interactions. The recent discovery of these particles /20/ in $\bar{p}p$ collider experiments at CERN, with the theoretically predicted masses, is therefore a major triumph for the standard model.

Yet the experimental proof of the standard model is not complete. In particular, the Higgs sector of the theory needed for implementing spontaneous symmetry breaking has not been tested at all. Attempts /21-24/ to modify the theory, or to embed it into a larger framework, usually involve a modification of the neutral current sector. Therefore, detailed experimental information on the neutral-current structure (e.g. on $\sin^2\Theta_W$) is needed to test the theory to second order to establish that it really is a renormalizable theory and to distinguish it from other models with the same leading order low-energy predictions. A precise determination of the parameter $\sin^2\Theta_W$ is interesting moreover as a discriminant for different grand unified theories (GUTS) /25/ which try to unify strong, weak, and electromagnetic interactions in a simple group.

Since different experiments are sensitive to different higher order contributions and possible deviations from the theory, it should be tested in as many ways as possible. That is why the structure of neutral current interactions has been studied in neutrino-nucleon, muon-nucleon, neutrino-electron, nucleon-nucleon, and in electron-positron reactions and very recently in the production and decays of the intermediate vector bosons into electron and muon channels. This variety of neutral current phenomena covers an enormously wide range of energy and momentum transfer, from space-like $Q^2 \sim 10^{-11}\ GeV^2$ in radiative atomic transitions to time-like Q^2 exceeding $10^3\ GeV^2$ in the colliding-beam experiments.

In general, non-neutrino experiments are of valuable help in revealing the space-time structure of the neutral weak interaction by its possible interference with some other interaction whose properties are known. Such an interference, e.g. between the weak and electromagnetic interaction, can only occur if both interactions have certain characteristics in common. They must, for instance, contribute to the same helicity amplitudes, allowing thus a discrimination between SPT and VA spatial structures which are strongly favoured by gauge models. With neutrino scattering experiments alone (the main experimental technique in neutral current studies for a long time) it is extremely difficult to discriminate between all a priori possible coupling types, since in most of the processes studied, there is actually a confusion theorem /26-28/ that states that an appropriate mixture of S, P, and T covariants can mimic the effects of a V, A space-time structure.

The purpose of this review is to summarize the present knowledge on neutral-current physics, especially in view of a comparison with the standard weak interaction theory. No attempt has been made to give a balanced survey of all experiments which have contributed to

the field. Only the main conclusions which may be extracted from the experimental work are pointed out. Usually this is done by discussing only those data which do not rely too much on model-dependent assumptions. Thus, for example, various nuclear physics experiments have been omitted, whose interpretation depends strongly on nuclear matrix element calculations.

The outline of this article is as follows:
Chapter 2 will provide, in a historical and phenomenological approach (to an extent necessary for this review), the theoretical framework needed to describe the electroweak interaction processes. Chapter 3 is devoted to a brief review of the charged-current structure. The elucidation of the space-time structure of the neutral weak force is the main topic of the subsequent chapters. For this reason Chapter 4 deals with the experimental results based on the analysis of neutrino-electron and neutrino-hadron interactions. Additional information on the neutral-current structure will be extracted from parity-violating effects in muon-hadron (Chapter 5), electron-hadron (Chapter 6) and electron-positron reactions (Chapter 7). Having surveyed the diverse neutral-current phenomena, Chapter 8 will summarize the state of the knowledge about the parameters of the neutral-current interactions. Chapter 9 concludes this review with a discussion of some outstanding problems.

Finally, I want to acknowledge several excellent reviews that have been a valuable help and guide in preparing this article. I would like to mention especially P. Langacker's review of Grand Unified Theories and Proton Decay /5/, the review of Weak Neutral Current by J.E. Kim, P. Langacker, M. Levine and H.H. Williams /29/, J.J. Sakurai's work on The Structure of Charged Currents /30/, P.Q. Hung's and J.J. Sakurai's review of The Structure of Neutral Currents /31/, and the articles of F.W. Büsser on The Structure of Weak Currents in High Energy Neutrino Reactions /32,33/. It will be apparent in the following that I have benefited heavily from the material presented in those papers.

2. THEORETICAL FRAMEWORK

2.1. Coupling types

The interaction Lagrangian governing the four-fermion reaction $a + b \rightarrow c + d$, e.g. the inverse μ-decay $\nu_\mu e^- \rightarrow \nu_e \mu^-$, is assumed to depend directly (i.e. without derivatives) on the wave functions of the particles involved in this process. If one then requires Lorentz invariance (excluding space inversion), the most general four-fermion interaction Lagrangian can be written as /2/

$$\mathcal{L} = \frac{G}{\sqrt{2}} \sum_i \left[\bar{\Psi}_d \Gamma_i \Psi_a \right] \cdot \left[\bar{\Psi}_c \Gamma_i \left(C_i + \gamma_5 C_i' \right) \Psi_b \right] + \text{h. c.}, \tag{2.1}$$

where i runs over the five coupling types V, A, S, P, and T discussed below. Ψ are Dirac spinors and $G \simeq 1.027 \cdot 10^{-5} m_p^{-2}$ /34/ is the Fermi coupling constant and m_p the proton mass.

$\mathcal{L}$ contains all the 16 independent matrices Γ_i which can be built in terms of the Dirac γ-matrices /35/ and the unit matrix. The bilinear terms $\bar{\Psi}\Gamma_i\Psi$ transform under the Lorentz group (including space inversion) as indicated in Table 2.1.

Table 2.1. Covariants in weak interactions.

Γ_i	Number of independent matrices	$\bar{\psi}\,\Gamma_i\,\psi$	Tensor
1	1	$\bar{\psi}\psi$	S (scalar)
γ^μ	4	$\bar{\psi}\gamma^\mu\psi$	V (vector)
$\sigma^{\mu\nu}$	6	$\bar{\psi}\sigma^{\mu\nu}\psi$	T (antisymmetric tensor)
$i\gamma^\mu\gamma_5$	4	$\bar{\psi}i\gamma^\mu\gamma_5\psi$	A (axial vector)
γ_5	1	$\bar{\psi}\gamma_5\psi$	P (pseudoscalar)

The coefficients C_i and C_i' are the coupling constants corresponding to the different space-time coupling types V, A, S, P, and T. They describe the strength of the interaction, are in general complex and have to be determined experimentally. But the number of independent C_i can be reduced when the invariance of $\mathcal{L}$ under space inversion (P), charge conjugation (C),

and time reversal (T) is taken into account. All C_i (or all C_i') have to vanish if one assumes that the interaction Lagrangian (2.1) is invariant under parity operations, whereas time reversal invariance restricts the coupling strengths C_i and C_i' to real values and C-invariance involves real constants C_i but purely imaginary C_i', as summarized in Table 2.2.

Table 2.2. Invariance constraints of the weak interaction Lagrangian (2.1) under P,C, and T operations.

Transformation	Invariance constraints
P	$C_i' = 0$ (or $C_i = 0$)
C	$C_i = C_i^*$, $C_i' = -C_i'^*$
T	$C_i = C_i^*$, $C_i' = C_i'^*$

Due to the analogy between the vectorial Dirac covariant $\bar{\Psi}\gamma^\mu\Psi$ and the electromagnetic current density, the bilinear terms $\bar{\Psi}\Gamma_i\Psi$ are usually called weak currents, so that in terms of this picture the weak interaction between four fermions $a + b \to c + d$ is described by a Lagrangian which is proportional to the product of two currents (current-current interaction)

$$\mathcal{L} = \frac{G}{\sqrt{2}}\left[J_{a\to d} \times J_{b\to c} \right]. \qquad (2.2)$$

2.2. Nomenclature

Phenomenologically, all known weak interactions can be devided into three classes according to the proportion of lepton currents present:

- *Purely leptonic processes*
  Since leptons do not undergo strong interactions, such processes offer a unique opportunity to study weak interactions in a relatively pure state. In contrast to neutral leptons $(\nu_e, \nu_\mu, \nu_\tau)$, charged leptons (e, μ, τ) are subject to weak as well as electromagnetic interactions giving rise to distortions of the pure weak interactions.
  Examples: $\mu^- \to e^-\bar{\nu}_e\nu_\mu$, $\nu_e e^- \to \nu_e e^-$, $\nu_\mu e^- \to \nu_\mu e^-$, $e^+e^- \to e^+e^-$, $\mu^+\mu^-$.

- *Semileptonic processes*
  They involve interactions between a leptonic and a hadronic weak current. Therefore, the theory of weak interactions must necessarily be concerned with renormalizing effects of both the electromagnetic and strong interactions. Because of the great difference in relative strength between the weak interaction on the one hand and the strong and electromagnetic interactions on the other hand, the weak processes are overwhelmed by nonweak interactions, unless selection rules suppress the nonweak with respect to the weak processes.
  Examples: $n \to pe^-\bar{\nu}_e$, $\nu_\mu N \to \mu^- X$, $\nu_\mu N \to \nu_\mu X$, $e^- D \to e^- X$, atomic parity experiments.

- *Nonleptonic processes*
  Those involve interactions between two hadronic weak currents. Again, the strong interactions preponderate the tiny effect of the weak interaction unless selection rules suppress the strong with respect to the weak processes.
  Examples: $\Lambda \to \pi^- p$, $K^+ \to \pi^+\pi^0$, nuclear parity mixing experiments.

According to the character of the currents involved, one distinguishes weak interactions between *charged currents* (CC) (i.e. the two fermion fields forming the current differ in charge by one unit) and weak interactions between *neutral currents* (NC), consequently connecting fermions of equal charge.

Charged-current interactions are responsible for all known weak decays (e.g. μ, β, and Λ decay) and for such neutrino reactions which have a charged lepton (of the same type as the neutrino) in the final state (e.g. $\nu_\mu e^- \to \mu^-\nu_e$, $\nu_\mu N \to \mu^- X$, $\bar{\nu}_e e^- \to \bar{\nu}_e e^-$).

Neutral weak currents were predicted in the framework of gauge field theories for electroweak interactions /16-18/ and discovered 1973 in the famous GARGAMELLE experiment /7/. In an antineutrino exposure, a single electron event was found which was interpreted as being due to the process $\bar{\nu}_\mu e^- \to \bar{\nu}_\mu e^-$. Subsequently, reactions induced by muon-neutrinos and producing hadrons, but no charged lepton, have been observed /8/. These events behaved as expected if they arise from neutral current induced processes $\nu_\mu N \to \nu_\mu +$ hadrons. Further examples of experimentally investigated neutral-current weak interactions are processes such as $e^+e^- \to e^+e^-$, $\mu^+\mu^-$, $e^- D \to e^- X$, but also studies of atomic and nuclear parity mixing effects.

For reactions such as $e^+e^- \to e^+e^-$, $\mu^+\mu^-$ or $e^- + quark \to e^- + quark$, neutral current weak and electromagnetic transitions coexist. Processes such as the scattering of $\nu_e\,(\bar{\nu}_e)$ off electrons receive contributions from both the product of two neutral currents and the product of two charged currents. Therefore, the effects of the weak neutral currents are not cleanly separated out in such processes. Nevertheless, they are of great importance for the study of the neutral-current structure since they offer a possibility to search for interference effects between the neutral weak interaction and another interaction whose properties are known. Thus, if an interference is observed, one can use the knowledge of the other interaction (e.g. charged-current interaction or electromagnetism) to get information about the properties of the neutral weak force.

2.3. The Fermi theory

As early as 1934 Fermi /1/ proposed a first theoretical model describing the β-decay of the neutron by a four-fermion (zero-range) effective Lagrangian

$$\mathcal{L}_{eff} = \frac{G}{\sqrt{2}}\left\{ J^\mu J_\mu^+ + J^{\mu+} J_\mu \right\}, \qquad (2.3)$$

which is the product of two weak currents. It took many years to elucidate the form of the weak charged current J_μ. As illustrated in Chap. 3, the weak charged-current interactions are phenomenologically decribed to good accuracy by the Cabibbo theory /3/ and the Kobayashi-Maskawa six quark generalization of it /4/. The weak current J_μ, written in terms of quark and lepton fields (for abbreviation a spinor is just marked by its index), is in the Cabibbo-modified Fermi theory

$$\begin{aligned} J_\mu &= \bar{e}\gamma_\mu \frac{1}{2}(1+\gamma_5)\nu_e + \bar{\mu}\gamma_\mu \frac{1}{2}(1+\gamma_5)\nu_\mu \\ &+ \cos\Theta_C \bar{d}'\gamma_\mu \frac{1}{2}(1+\gamma_5)u + \sin\Theta_C \bar{s}'\gamma_\mu \frac{1}{2}(1+\gamma_5)u \\ &- \sin\Theta_C \bar{d}'\gamma_\mu \frac{1}{2}(1+\gamma_5)c + \cos\Theta_C \bar{s}'\gamma_\mu \frac{1}{2}(1+\gamma_5)c\,, \end{aligned} \tag{2.4}$$

where the Cabibbo angle Θ_C measures the relative strength of strangeness-changing and strangeness-conserving interactions; it can be determined to $\Theta_C = 13.2^\circ \pm 0.7^\circ$ by comparing the strength of super-allowed Fermi β-decays in nuclei ($0^+ \to 0^+$ transitions) to the strength of muon decay /36/. Since J_μ, composed of leptonic and hadronic parts, contains equal admixtures of vector and axialvector contibutions, charge conjugation C and parity P are maximally violated by $\mathcal{L}_{eff}$ but CP is conserved.

The Lagrangian (2.3) is phenomenologically successful since it describes correctly all known charged-current weak processes below the b quark threshold, except CP violation, observed in kaon decays, and some aspects of nonleptonic hyperon decay. Figure 2.1 shows typical diagrams for β-decay ($n \to p e^- \bar{\nu}_e$) and $\nu_\mu e^- \to \nu_e \mu^-$ scattering (inverse μ-decay) described by $\mathcal{L}_{eff}$, where the circles represent the four-fermion interaction. The indices L and R mark the left-handed and right-handed fermion states (Chap. 3), respectively.

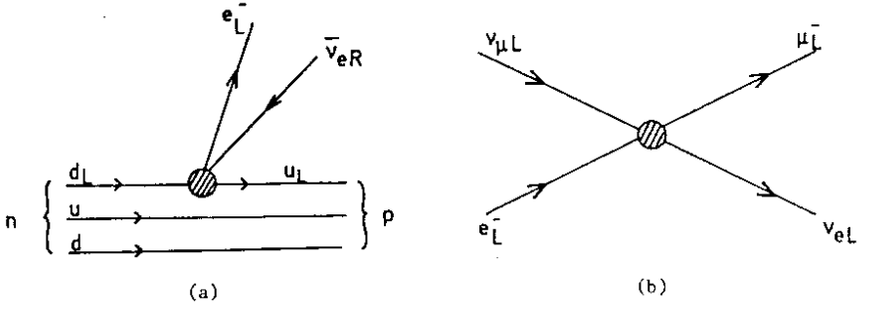

Fig. 2.1 Diagrams for β-decay ($n \to p e^- \bar{\nu}_e$) (a) and $\nu_\mu e^- \to \nu_e \mu^-$ (b) in the Cabibbo-modified Fermi theory.

At this level, the effective current-current theory gives a prediction for inverse μ-decay $\nu_\mu e^- \to \nu_e \mu^-$, where "effective" means that the first-order matrix element of $\mathcal{L}_{eff}$ is supposed

to give directly the transition amplitude of this weak interaction process and no higher-order matrix elements are to be considered. The total cross section for $\nu_\mu e^- \to \nu_e \mu^-$, calculated from $\mathcal{L}_{eff}$, is thus /2/

$$\sigma_{tot}(s) = \frac{G^2}{\pi} \cdot \frac{(s-m_\mu^2)^2}{s} \xrightarrow{E_\nu \gg m_\mu} \frac{G^2}{\pi} s\,, \tag{2.5}$$

where s is the square of the total center-of-mass energy.

Because of this strong energy dependence, the cross section grows indefinitely with increasing energy, so that at some point one gets into conflict with conservation of probability. Since $\mathcal{L}_{eff}$ describes a point interaction, it can only produce S-wave scattering implying that σ_{tot} should satisfy the unitarity limit

$$\sigma_{tot} < \frac{4\pi}{s}\,. \tag{2.6}$$

This unitarity bound is violated for a center-of-mass neutrino energy of about 300 GeV, so that the Fermi theory must break down before this energy. One might take this as an indication that higher-order calculations should be included. But $\mathcal{L}_{eff}$ decribes a non-renormalizable field theory, i.e. to renormalize all divergent amplitudes involves an infinite number of arbitrary constants. This non-renormalizability is basically caused by the negative mass dimension of the Fermi coupling constant $G \sim m_p^{-2}$.

2.4. The intermediate vector boson theory

A possible modification of this Fermi theory has been found by the assumption that the four-fermion interaction is the low-energy approximation to a finite range interaction mediated by electrically-charged massive vector particles $W^\pm$ (*intermediate vector boson theory*) /37/. These hypothetical particles have recently been discovered in $\bar{p}p$ collider experiments at CERN /20/. The intermediate vector bosons couple to the Cabibbo current by the interaction

$$\mathcal{L}_{weak} = \frac{g}{\sqrt{2}} \left\{ J^\mu W_\mu^- + J^{\mu +} W_\mu^+ \right\}. \tag{2.7}$$

The corresponding diagrams for neutron decay and inverse muon decay, described by $\mathcal{L}_{weak}$, are shown in Fig. 2.2 /5/. The emission and reabsorption of the field particle in such a picture is described by a propagator term.

The intermediate vector boson propagator, expressed in momentum space, is /38/

$$D^{\mu\nu}(q) = \frac{q^\mu q^\nu / M_W^2 - g^{\mu\nu}}{q^2 - M_W^2} \xrightarrow{|q^2| \ll M_W^2} \frac{g^{\mu\nu}}{M_W^2}\,, \tag{2.8}$$

where q denotes the four-momentum of the virtual vector boson and M_W its mass. Hence, for momentum transfers small compared to M_W which is the case for weak decays, intermediate vector boson theory and Fermi theory coincide for

$$\frac{G}{\sqrt{2}} = \frac{g^2}{8 M_W^2}\,. \tag{2.9}$$

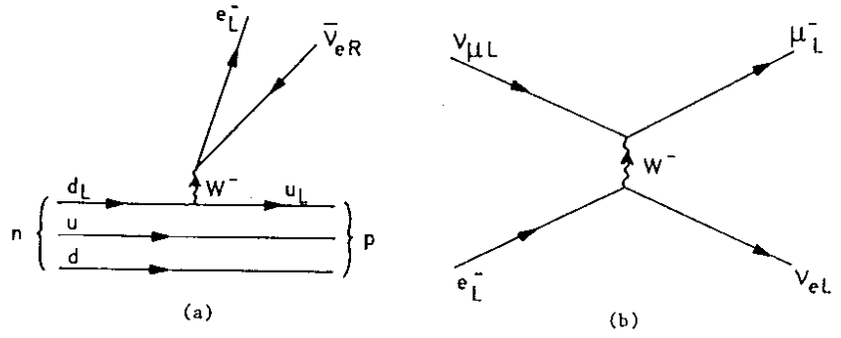

Fig. 2.2 Diagrams for β-decay ($n \to p e^- \bar{\nu}_e$) (a) and $\nu_\mu e^- \to \nu_e \mu^-$ (b) in the intermediate vector boson theory.

Therefore, the weakness of the weak interaction could be caused by either g being small, or M_W very heavy, or both. If one assumes that the intermediate vector boson couples basically with electromagnetic strength to left-handed leptons and quarks and right-handed antiparticles, M_W is of the order of about 90 GeV in agreement with the experimental result of $M_W = (81 \pm 2)$ GeV /20/.

The corrections introduced by the intermediate vector boson theory into current-current theory predictions are, e.g. for the muon decay parameters, of order $(m_\mu/M_W)^2 \sim 1.7 \cdot 10^{-6}$ (using the experimental value for M_W), and thus within the experimental errors /2/.

The high energy behaviour of $\nu_\mu e^- \to \nu_e \mu^-$ is now no longer such a severe problem since in the intermediate vector boson theory the amplitude is no longer purely S-wave. It can be shown /2/ that the introduction of intermediate vector bosons in the theory only postpones the unitarity crisis to higher energies but does not remove it - the divergence becomes now only logarithmic just as in the electromagnetic case.

However, in contrast to quantum electrodynamics (QED) which describes the electromagnetic interactions also by exchange of a vector particle, the intermediate vector boson theory fails to produce a unitary renormalizable theory /5/. In fact, no renormalizable theory can be constructed from interactions for which the propagators of the various fields depend on dimensional parameters like masses if the energies involved become large /35/. This is the case for the massive vector boson propagator (2.8) whose asymptotic form is $(q^\mu q^\nu)/M_W^2 q^2$. So diverges the cross section for external boson production $\nu_\mu + \bar{\nu}_\mu \to W^+ + W^-$ or $e^+ + e^- \to W^+ + W^-$ again with the square of the total center-of-mass energy and not logarithmically as a result of the non-renormalizability of such models. The divergent terms arise herein from the longitudinal polarization states of the massive bosons which effectively reintroduce a dimensional coupling constant.

The good high-energy behaviour of QED has its origin in the absence of longitudinal polarization states of real external photons, respectively in cancellation effects between divergent contributions caused by such states for virtual internal photons. This can be traced to the

gauge invariance property of QED. It was therefore suggested to incorporate the intermediate vector boson theory into a gauge theory. However, embedding it into a spontaneously broken gauge theory – since actually only a theory with massless vector bosons is renormalizable /6/ - requires the existence of at least one neutral massive intermediate vector boson and thus experimentally observable weak neutral currents. The interactions mediated by this new gauge boson cancel many of the divergencies in the intermediate vector boson theory and, due to gauge invariance, the troublesome $q^\mu q^\nu$ term in the vector boson propagator (2.8) is effectively unobservable /5/.

It is in principle possible to develop gauge theories, incorporating both charged and neutral currents, for the weak interactions alone /13,14/. Another approach used in the Glashow-Weinberg-Salam (GWS) model /15-18/ is to consider both the weak and electromagnetic interactions as pieces of a larger unifying gauge group, which includes electromagnetic, charged-current and neutral-current weak interactions. The present theoretical and experimental knowledge, in particular the discovery of $W^\pm$ and Z^0 with the theoretically anticipated masses, favours clearly the GWS approach.

2.5. Neutral-current coupling types

The modification of the non-renormalizable intermediate vector boson theory by incorporating it into a gauge theory involves quite restrictive selections of possible neutral-current coupling types. The GWS theory, for instance, implies that the weak neutral current is made up of a linear combination of vector and axialvector covariants, since only those contribute to the same helicity amplitudes as the electromagnetic interaction. This is strongly supported experimentally by the neutral-current data on cross section asymmetries with longitudinally polarized electrons /41,42/ (Chap 6.1) and by the appearance of a forward-backward asymmetry in the angular distribution of the muons (taus) in $e^+e^- \to \mu^+\mu^- (\tau^+\tau^-)$ reactions (Chap. 7). But these asymmetries are not very sensitive to small admixtures of S, P, and T currents.

The experimental observation in charged-current reactions that the neutrino behaves like a two-component field being invariant under chirality transformations (Chap. 3) is also not a definite indication that neutral-current weak interactions of neutrinos (e.g. $\nu_\mu N \to \nu_\mu +$ hadrons) would have to be through V and A currents, too. It could be that the observed helicity of neutrinos is not an intrinsic property of the particles themselves, but is due to a bias in the charged-current interactions /42/.

In general, it turns out to be extremely difficult to reveal the Lorentz structure of the weak neutral current by performing usual neutrino scattering experiments since, in most of the processes studied, there is actually a confusion theorem that states that an appropriate mixture of S, P, and T covariants can mimic the effects of a V, A space-time structure /26,27/.

It is even impossible in principle to study the question of parity violation in neutral weak interactions using neutrinos. Ideally, one would like to test parity conservation by comparing the cross section for a process induced by left-handed neutrinos to that for the same process induced by right-handed neutrinos which are not available. If one therefore compares instead the cross sections for left-handed neutrinos and right-handed antineutrinos, it can be shown that the observation of unequal neutrino and antineutrino cross sections cannot possibly prove that the neutral weak interaction violates parity /43,44/. These points demonstrate the necessity to study the neutral-current structure in non-neutrino experiments, too.

Furthermore, there appear to be inconsistencies between theoretical predictions and experimental results concerning the reactor-neutrino scattering on nucleons /45/, the solar-neutrino observation /46/, and possibly the ratio of prompt $(\nu_e + \bar{\nu}_e)$ to $(\nu_\mu + \bar{\nu}_\mu)$ rates in beam-dump experiments /47/. It has been suggested that some of these puzzles may be solved by the lepton mixing hypothesis (neutrino oscillation) /48/. Other approaches, not relying on the neutrino oscillation hypothesis, tried to attack these problems by scalar-boson exchange theories /49/ which at low energy can mimic a vector-axialvector interaction /50/.

Although the GWS model is self-consistent and in good agreement with most of the data, there are several viewpoints that suggest that it may be an approximate or incomplete description of the weak interactions. It contains very many parameters which are not predicted and whose origin remains unclear. Furthermore, the accuracy to which some of the experimental information is known, is only limited so that there is room for sizeable deviations from the GWS model. There are therefore good reasons for a careful study of the space-time structure of the weak charged- and neutral-current interactions in order to detect departures from this model.

2.6. The Glashow-Weinberg-Salam model

Because of its success in describing low energy processes and its economy in the number of fundamental fields involved, the electroweak GWS theory /15-18/, based on the spontaneously broken $SU_2 \times U_1$ gauge group, has become the "standard" model. In order to be able to discuss the predictions of this model meaningfully, and introduce the terminology, only a brief description of its general features and properties will be given, the more so since this theory has been widely reviewed /51-58/.

There is a well-defined prescription for constructing gauge models of the weak and electromagnetic interactions /51/. It requires that the relevant gauge group, the multiplet structure of the fermions, the gauge bosons and their couplings, and the symmetry breaking mechanism are to be specified. One starts with an underlying gauge symmetry which is then broken by the presence of scalar fields with non-vanishing vacuum expectation values (Higgs mechanism) /6/. When the symmetry is broken in this way some of the gauge fields acquire masses, but the theory remains renormalizable.

Invariance group

In the standard (GWS) model the basic gauge group is $SU_2 \times U_1$. SU_2 has three generators T^i (weak isospin generators), i = 1,2,3, and therefore three gauge bosons W^i_μ. The weak hypercharge generator Y and thus one gauge boson B_μ is connected with the U_1 subgroup. g and g' are the gauge coupling constants associated with SU_2 and U_1 transformations respectively. $SU_2 \times U_1$ is the minimum invariance group needed to accommodate the weak charged, weak neutral and electromagnetic currents.

Representation of the fermions

To specify the theory further, one has to decide how the fermions (leptons and quarks) transform under the invariance group. The original Weinberg-Salam model /16-18/ described only the weak and electromagnetic interactions of leptons. It could be extended to hadrons by implementing a mechanism due to Glashow, Iliopoulos, and Maiani (GIM) /19/, where the hadrons in weak currents are represented by quarks.

In the GWS model all left-handed (negative helicity) fermions are assumed to transform according to doublet representations of SU_2, while the right-handed (positive helicity) components are taken as SU_2 singlets. Therefore, parity violation is put in by hand by assigning left- and right-handed fermions to different representations. This assignment is motivated by the fact that it is the simplest way to reproduce the successful V-A form of the charged-current interactions (Chap. 3).

The minimal number of lepton (quark) SU_2 doublets needed to describe the present phenomenology is 3:

$$\text{leptons} \quad \begin{pmatrix} \nu_m \\ e_m \end{pmatrix}_L = \begin{pmatrix} \nu_e \\ e^- \end{pmatrix}_L \quad \begin{pmatrix} \nu_\mu \\ \mu^- \end{pmatrix}_L \quad \begin{pmatrix} \nu_\tau \\ \tau^- \end{pmatrix}_L \tag{2.10}$$

$$\text{quarks} \quad \begin{pmatrix} u_m \\ d'_m \end{pmatrix}_L = \begin{pmatrix} u \\ d' \end{pmatrix}_L \quad \begin{pmatrix} c \\ s' \end{pmatrix}_L \quad \begin{pmatrix} t \\ b' \end{pmatrix}_L \tag{2.11}$$

where m labels the doublet. u, c, t are the charge $+\frac{2}{3}$ quarks and d', s', b' are related by a unitary transformation /4/ (Kobayashi-Maskawa matrix) to the charge $-\frac{1}{3}$ fields d, s, b involved in strong interactions.

Here the notation u_{mL} resp. u_{mR} stands for the chirality states

$$\begin{aligned} u_{mL} &= \frac{1}{2}(1+\gamma_5)\, u_m \,, \\ u_{mR} &= \frac{1}{2}(1-\gamma_5)\, u_m \,, \end{aligned} \tag{2.12}$$

which are equivalent to -1 resp. +1 helicity states if the mass is neglected.

The fermions in the first two generations (m = 1,2) have all been found, whereas the last generation (m = 3) is still incomplete. ν_τ has not yet been observed directly. One has indirect evidence /59/ from b-quark decays that the t-quark (top) must exist. Searches for top in the reaction $e^+e^- \rightarrow$ hadrons indicate /60/ that the mass of the t-quark, if it exists, must be above 22.5 GeV. Recently, events consistent with intermediate boson decays $W \rightarrow t\bar{b}$ has been found /61/, from which the bounds 30 GeV $< m_t <$ 50 GeV on the mass of the t-quark can be infered. The other quark flavours (up, charm, down, strange, and bottom) are well established with current masses /62-66/ satisfying $m_s \simeq 150$ MeV, $m_c \simeq 1.2$ GeV, $m_b \simeq 4.5$ GeV, $m_u/m_d = 0.47 \pm 0.11$, and $m_d/m_s = 0.042 \pm 0.007$.

Fermion-boson couplings

The fundamental fermions are assumed to carry the weak isospin $(\vec{T})$ and the weak hypercharge (Y) which for any fermion is given by

$$Q = T^3 + Y \,, \tag{2.13}$$

where Q is its electric charge. The weak and electromagnetic interactions are given by a $SU_2 \times U_1$ symmetric interaction /68/

$$\mathcal{L}_{int} = g\vec{J}_\mu \vec{W}_\mu + g' J^Y_\mu B_\mu \tag{2.14}$$

involving a set of gauge bosons $\vec{W}$ and B which couple to weak isospin and hypercharge respectively. The currents associated with $\vec{T}$ and Y are

$$\begin{aligned} \vec{J}_\mu &= \sum_F \bar{F}\gamma_\mu \frac{\vec{\tau}}{2} F \qquad \text{(sum over all isodoublets F)} \\ J^Y &= \sum_f \left[\bar{f}_L \gamma_\mu Y_L f_L + \bar{f}_R \gamma_\mu Y_R f_R\right] \quad \text{(sum over all fermions f)}, \end{aligned} \tag{2.15}$$

where $\vec{\tau} = (\tau_1, \tau_2, \tau_3)$ with τ_i being the i^{th} Pauli matrix.

Weak bosons

The gauge bosons are initially massless. In order to endow them with masses and to preserve the renormalizability of the theory, one relies on a spontaneous breakdown of the gauge symmetry. It is achieved by introducing Higgs scalar fields into the theory whose self-interaction causes them to develop non-vanishing expectation values. This leads finally to a mass matrix for the spin-1 particles whose eigenstates represent the physical particles with masses corresponding to the mass matrix eigenvalues (Higgs mechanism) /6/.

The GWS model involves one complex doublet of scalar particles whose neutral member has a non-vanishing vacuum expectation value. As a consequence the theory is spontaneously broken, whereby three out of the four hermitian Higgs fields are absorbed in a redefinition of the gauge bosons, three of which (W^+, W^-, Z) are endowed with masses, while the fourth (the photon A) remains massless corresponding to the unbroken group U_1^{em}. The fourth neutral Higgs is realized as a physical spin-zero particle and should be found. However, the experimental search for this predicted Higgs particle is very difficult since it is electrically neutral, conserves flavour and parity, and couples very weakly to low-mass fermions such as the electron and proton. With two or more Higgs multiplets, however, there should exist additional Higgs particles, left over after symmetry breaking, which do not have to conserve flavour, might have electric charge, etc. One might learn about such Higgs particles through virtual effects in low-energy processes, such as possible departures from a pure V-A structure of weak charged currents (due to charged Higgs bosons) or observation of lepton-number violating decays (due to flavour-changing neutral Higgs particles) /69,70/.

Detailed studies show that the mass matrix eigenstates

$$W_\mu^\pm = \frac{1}{\sqrt{2}}\left(W_\mu^1 \pm i W_\mu^2\right) \tag{2.16}$$

acquire the mass $M_{W^\pm} = \frac{1}{2}vg$ (v being the vacuum expectation value of the neutral Higgs field), whereas in the neutral sector the mass matrix eigenstates Z_μ (mediator of the neutral weak current) and A_μ (photon) are orthogonal combinations of the neutral gauge fields W_μ^3 and B_μ associated with the SU_2 and U_1 subgroups:

$$\begin{aligned} A_\mu &= \sin\Theta_W\, W_\mu^3 + \cos\Theta_W\, B_\mu \\ Z_\mu &= \cos\Theta_W\, W_\mu^3 - \sin\Theta_W\, B_\mu\,. \end{aligned} \tag{2.17}$$

They have masses $M_Z = \frac{1}{2}v\sqrt{g^2+g'^2}$ resp. $M_A = 0$, where

$$\tan\Theta_W = \frac{g'}{g} \tag{2.18}$$

defines the electroweak mixing angle (Weinberg angle).

The unknown parameters g, g', and v in the model are constrained by the relations (2.22/2.26). Therefore, the vector boson masses are predicted in terms of the single parameter $\sin^2\Theta_W$:

$$\begin{aligned} M_W &= \frac{gv}{2} = \left(\frac{\pi\alpha}{\sqrt{2}G}\right)^{1/2} \cdot \frac{1}{\sin\Theta_W} = \frac{37.3\ \text{GeV}}{\sin\Theta_W} \\ M_Z &= \frac{M_W}{\cos\Theta_W} = \frac{74.6\ \text{GeV}}{\sin 2\Theta_W}\,, \end{aligned} \tag{2.19}$$

Higher order corrections to the lowest order amplitudes modify these predictions /71-75/. The precise form of these radiative corrections – finite by virtue of the renormalizability of the standard model – depends on the definition of $\sin^2\Theta_W$ which depends on the renormalization scheme. The fact that these corrections turn out to be significant for the intermediate boson masses M_W and M_Z, which are predicted to lie 3–4 % higher than the lowest order expectations, is very interesting since a precise measurement of $\sin^2\Theta_W$ and the boson masses would allow to test the theory to second order (Chap. 8).

Interactions

Rewriting the interaction (2.14) in terms of the mass matrix eigenstates $W^\pm$, Z and A one obtains

$$\begin{aligned} \mathcal{L}_{int} = &\frac{g}{\sqrt{2}}\left(J_\mu^+ W_\mu^- + J_\mu^- W_\mu^+\right) \\ &+ \left[g\sin\Theta_W J_\mu^3 + g'\cos\Theta_W J_\mu^{em} - g'\cos\Theta_W J_\mu^3\right] A_\mu \\ &+ \left[g\cos\Theta_W J_\mu^3 - g'\sin\Theta_W J_\mu^{em} + g'\sin\Theta_W J_\mu^3\right] Z_\mu\,, \end{aligned} \tag{2.20}$$

where the U_1 symmetry current J_μ^Y has been written as

$$J_\mu^Y = J_\mu^{em} - J_\mu^3 \tag{2.21}$$

according to Eq. (2.13).
If the second term in (2.20) is identified with the usual electromagnetic interaction $eJ_\mu^{em}A_\mu$ (e being the positron charge), one gets the so-called "unification condition"

$$e = g\sin\Theta_W = g'\cos\Theta_W\,. \tag{2.22}$$

This leads finally to the interaction Lagrangian

$$\mathcal{L}_{int} = \frac{g}{\sqrt{2}}\left(J_\mu^+ W_\mu^- + J_\mu^- W_\mu^+\right) + \frac{g}{\cos\Theta_W} Z_\mu \left(J_\mu^3 - \sin^2\Theta_W J_\mu^{em}\right) + eJ_\mu^{em}A_\mu \tag{2.23}$$

which contains a charged-current, a neutral-current and an electromagnetic contribution.

Charged current

The charged-current interaction

$$\mathcal{L}^{CC} = \frac{g}{\sqrt{2}}\left(J_\mu^+ W_\mu^- + J_\mu^- W_\mu^+\right) \tag{2.24}$$

leads, for momentum transfers Q^2 small to M_W^2, to an effective four-fermion charged-current interaction

$$\mathcal{L}_{eff}^{CC} = \frac{G}{\sqrt{2}} J_\mu J_\mu^+ , \tag{2.25}$$

where the Fermi coupling constant is given by

$$\frac{G}{\sqrt{2}} = \frac{g^2}{8M_W^2} = \frac{1}{2v^2} . \tag{2.26}$$

The charged weak current (SU_2 symmetry current)

$$J_\mu = \sum_m \left\{ \bar{e}_m \gamma_\mu \frac{1}{2}(1+\gamma_5)\nu_m + \bar{d}'_m \gamma_\mu \frac{1}{2}(1+\gamma_5) u_m \right\} \tag{2.27}$$

consists of a lepton and a hadron part.

Neutral current

The weak neutral-current interaction

$$\mathcal{L}^{NC} = \frac{g}{\cos\Theta_W} Z_\mu \left(J_\mu^3 - \sin^2\Theta_W J_\mu^{em} \right) \tag{2.28}$$

leads (for $Q^2 \ll M_Z^2$) to an effective current-current interaction

$$\mathcal{L}_{eff}^{NC} = \frac{1}{2} \frac{g^2}{M_Z^2 \cos^2\Theta_W} \left(J_\mu^3 - \sin^2\Theta_W J_\mu^{em} \right) \cdot \left(J_\mu^3 - \sin^2\Theta_W J_\mu^{em} \right) = 4 \frac{G}{\sqrt{2}} \rho J_\mu^Z \cdot J_\mu^Z , \tag{2.29}$$

where J_μ^Z is identified as the neutral weak current which couples to the massive neutral gauge boson Z_μ. The parameter

$$\rho = \frac{M_W^2}{M_Z^2 \cos^2\Theta_W} \tag{2.30}$$

controls the relative strength of charged versus neutral current interactions.

In the minimal GWS model (i.e. with only one complex Higgs doublet) one gets:

$$M_W^2 = M_Z^2 \cos^2\Theta_W , \tag{2.31}$$

a relation that still holds true if, for example, additional doublets and singlets of Higgs scalars are introduced. However, it would be spoiled by the existence of Higgs triplets etc. More generally, one finds /54/

$$\frac{M_W^2}{M_Z^2 \cos^2\Theta_W} = \frac{\sum_i v_i^2 \left(t_i^2 + t_i - t_i^{(3)\,2} \right)}{2 \sum_i v_i^2 t_i^{(3)\,2}} , \tag{2.32}$$

where the summation has to be carried out over the various representations of scalar fields with weak isospin t_i; $t_i^{(3)}$ and v_i are the third component of weak isospin and the vacuum expectation value of the neutral member of the i^{th} multiplet, respectively.

From the most general form of the third component of the weak isospin current

$$J_\mu^3 = \sum_i \bar{f}_i \gamma_\mu \left[\frac{(1+\gamma_5)}{2} T_{3,i}^L + \frac{(1-\gamma_5)}{2} T_{3,i}^R \right] f_i \tag{2.33}$$

and

$$J_\mu^{em} = \sum_i Q \bar{f}_i \gamma_\mu f_i , \tag{2.34}$$

one gets for the neutral current

$$J_\mu^Z = \frac{1}{2} \sum_i \bar{f}_i \gamma_\mu \left[(1+\gamma_5) T_{3,i}^L + (1-\gamma_5) T_{3,i}^R - 2\sin^2\Theta_W Q_i \right] f_i , \tag{2.35}$$

where the sum extends over all fermions with charge Q_i and third component of weak isospin $T_{3,i}^L$ for the left-handed resp. $T_{3,i}^R$ for the right-handed states. The assignments for the fermions inply $T_{3,i}^L = \pm 1/2$ and $T_{3,i}^R = 0$ in the standard $SU_2 \times U_1$ model.

Using the parametrization

$$J_\mu^Z = \frac{1}{2} \sum_i \bar{f}_i \gamma_\mu \left[g_{V,i} + g_{A,i}\gamma_5 \right] f_i ,$$

the axialvector (g_A) and vector couplings (g_V) of the fermion to the neutral current are given by:

$$\begin{aligned} g_A &= T_3^L - T_3^R \\ g_V &= T_3^L + T_3^R - 2\sin^2\Theta_W Q . \end{aligned} \tag{2.36}$$

2.7. Fermion mass eigenstates

The original Weinberg-Salam model /16-18/ described only the weak and electromagnetic interactions of leptons. The model has then been extended successfully by replacing the hadron currents by quark currents within the framework of the quark model. The quark model /76-78/ describes many aspects of the spectra, decays and interactions of the hadrons. Strong additional evidence for the quark picture was provided by the observed scaling behaviour in deep inelastic ep scattering /79-81/. It supports the hypothesis that the nucleon consists of non-interacting point-like spin-$\frac{1}{2}$ constituents.

These quarks (or partons as they were originally called in the scaling concept) carry two types of internal quantum numbers: the flavour quantum number (representing all the internal quantum numbers conserved by the strong interaction) and the colour quantum number. Each quark flavour - u, c, and t (electric charge 2/3) and d, s, and b (electric charge -1/3) - is believed to occur in three colour states. The underlying Lagrangian acquires an additional global invariance under a group SU_3^C which acts on the quark colour indices without changing the flavour. The baryons are believed to be made of three quarks (e.g. p = uud, n = udd), whereas mesons are supposed to be bound states of a quark-antiquark pair (e.g. $\pi^+ = u\bar{d}$, $K^+ = u\bar{s}$, $D^+ = c\bar{d}$). All hadrons are assumed to be neutral with respect to colour. These aspects are taken into account in quantum chromodynamics (QCD) /82-85/, the theory of strong interaction.

How do now the quarks fit in $SU_2 \times U_1$? It is found experimentally by the study of weak charged-current processes that the rates of strangeness-changing ($|\Delta S| = 1$) semileptonic decays (involving $u \rightleftharpoons s$ charged currents, e.g. $\Lambda \to pe^-\bar{\nu}_e$) are lower by a factor of about 20 compared with those of $\Delta S = 0$ semileptonic decays (involving $u \rightleftharpoons d$ charged weak currents, e.g. $n \to pe^-\bar{\nu}_e$). In order to save the universality of weak interaction, Cabibbo /3/ hypothesized that the most general charged hadronic weak current is a linear combination of $\Delta S = 0$ and $|\Delta S| = 1$ currents. In terms of quark degrees of freedom it can be written as

$$\begin{aligned} J_\mu^{hadr.} &= \bar{d}\gamma_\mu \frac{1}{2}(1+\gamma_5)u\cos\Theta_C + \bar{s}\gamma_\mu \frac{1}{2}(1+\gamma_5)u\sin\Theta_C \\ &= (\bar{d}\cos\Theta_C + \bar{s}\sin\Theta_C)\gamma_\mu \frac{1}{2}(1+\gamma_5)u = \bar{d}'\gamma_\mu \frac{1}{2}(1+\gamma_5)u\,, \end{aligned} \tag{2.37}$$

where Θ_C is the Cabibbo angle. This current is of the V-A form. But this does not imply that for the hadronic matrix elements the axialvector and the vector form factors will be identical since the weak interactions among quarks are expected to be modified by the QCD strong interactions which bind those quarks into hadrons.

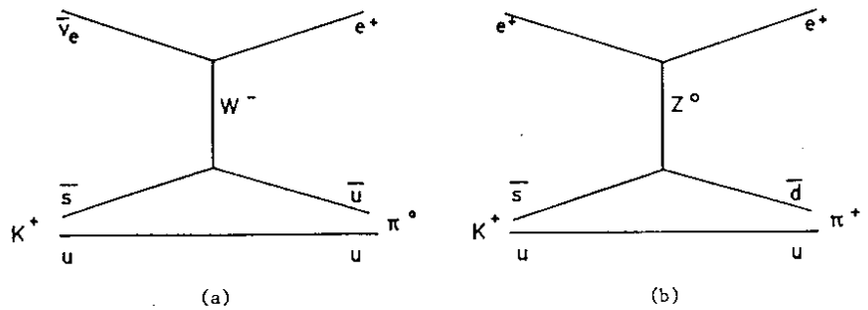

Fig. 2.3 Diagram for the charged-current process $K^+ \to \pi^0 e^+ \nu_e$ (a) and neutral-current process $K^+ \to \pi^+ e^+ e^-$ (b) in terms of intermediate bosons.

To incorporate the current (2.37) into the $SU_2 \times U_1$ model, one assigns the quarks under the weak SU_2 group as

$$\begin{pmatrix} u \\ d\cos\Theta_C + s\sin\Theta_C \end{pmatrix}_L = \begin{pmatrix} u \\ d' \end{pmatrix}_L ; u_R\,, d_R\,, s_R\,.$$

This assignment, however, predicts the existence of substantial strangeness-changing neutral currents ($|\Delta S| = 1$), since the neutral weak current J_μ^Z contains now a piece which mixes the

d and s quark (Eq. 2.33). This is in sharp contradiction to the experimental data which put quite stringent limits on the existence of strangeness-changing neutral currents /86/. The strangeness-changing neutral-current process $K^+ \to \pi^+ e^+ e^-$, for instance, is suppressed by at least five orders of magnitude relative to the already Cabibbo-suppressed charged-current decay $K^+ \to \pi^0 e^+ \nu_e$. Fig. 2.3 shows the diagrams in terms of intermediate bosons for both decays.

The solution to this problem, presented in 1970 by Glashow, Iliopoulos and Maiani (*GIM mechanism*) /19/, was to add an extra weak doublet which contains a new quark (charm) and corresponding to d' an orthogonal linear combimation s':

$$\begin{pmatrix} c \\ -d\sin\Theta_C + s\cos\Theta_C \end{pmatrix}_L = \begin{pmatrix} c \\ s' \end{pmatrix}_L ; c_R\,.$$

On the one hand, the existence of this new doublet adds new pieces to the charged current (2.37)

$$\begin{aligned} J_\mu^{hadr.} &= \bar{d}\gamma_\mu \frac{1}{2}(1+\gamma_5)u\cos\Theta_C + \bar{s}\gamma_\mu \frac{1}{2}(1+\gamma_5)u\sin\Theta_C \\ &\quad - \bar{d}\gamma_\mu \frac{1}{2}(1+\gamma_5)c\sin\Theta_C + \bar{s}\gamma_\mu \frac{1}{2}(1+\gamma_5)c\cos\Theta_C \\ &= \bar{d}'\gamma_\mu \frac{1}{2}(1+\gamma_5)u + \bar{s}'\gamma_\mu \frac{1}{2}(1+\gamma_5)c\,, \end{aligned} \tag{2.38}$$

implying that in the GIM picture the $c \to d$ transition amplitude ($\sim \sin\Theta_C$) should be suppressed relative to that for the $c \to s$ transition ($\sim \cos\Theta_C$). This will result in a preponderance of strange particles in the decays of charmed particles, in agreement with observation.

On the other hand, the weak neutral current has now no lowest-order strangeness-changing pieces, since the $|\Delta S| = 1$ neutral currents from the new weak doublet cancel the ones from the first doublet. The next to lowest order terms depend on the quark masses. The experimentally observed decay rates are compatible with the mass difference of the c- and u-quark.

The Cabibbo-GIM formalism has to be generalized to take account of the mixing of the third generation quarks b, t with the first and second generation sector and to insure the absence of flavour-changing neutral currents. The three-doublet (six flavour) generalization of the Cabibbo-GIM structure is originally due to Kobayashi and Maskawa /4/. Here the mismatch between the states d', s', b' (2.11) with definite weak interaction properties and the eigenstates of the mass matrix (which the unprimed quark labels refer to) is characterized by a generalized unitary Cabibbo matrix U_{KM}, sometimes referred to as the KM (Kobayashi-Maskawa) matrix:

$$\begin{pmatrix} d' \\ s' \\ b' \end{pmatrix} = U_{KM} \begin{pmatrix} d \\ s \\ b \end{pmatrix} \tag{2.39}$$

It can be shown /57/ that the neutral current couplings are diagonal both in the primed and unprimed basis. This ensures automatically flavour conservation in the neutral current couplings.

In the six quark case, U_{KM} is a 3×3 unitary matrix with nine real parameters: 3 mixing angles (generalized Cabibbo angles) and six relative phases of quarks. A redefinition of quark phases can transform away only five of the six phases. The remaining phase is important and welcome because it allows for an elegant accounting of CP violation in the theory /4,87,88/. The mixing matrix U_{KM} can be written in the form

$$U_{KM} = \begin{pmatrix} c_1 & c_3 s_1 & s_1 s_3 \\ -c_2 s_1 & c_1 c_2 c_3 - s_2 s_3 e^{i\delta} & c_1 c_2 s_3 + c_3 s_2 e^{i\delta} \\ s_1 s_2 & -c_1 c_3 s_2 - c_2 s_3 e^{i\delta} & -c_1 s_2 s_3 + c_2 c_3 e^{i\delta} \end{pmatrix} \qquad (2.40)$$

where s_i and c_i represent $\sin\Theta_i$ and $\cos\Theta_i$ (Θ_i denoting the generalized Cabibbo angles) and δ the CP violating phase.

CP violation has only been observed so far in the K-$\bar{K}$ system. Of particular importance are the amplitudes for $K_{S,L} \to \pi\pi$ decays. Possible experimental tests to distinguish the different models accommodating CP violation may be provided by precise measurements of the ratios

$$\eta_{+-} = \frac{A(K_L \to \pi^+\pi^-)}{A(K_S \to \pi^+\pi^-)} \simeq \epsilon + \epsilon', \qquad \eta_{00} = \frac{A(K_L \to \pi^0\pi^0)}{A(K_S \to \pi^0\pi^0)} \simeq \epsilon - 2\epsilon' \qquad (2.41)$$

and the weak interaction contribution to the electric dipole moment of the neutron d_N^e. ϵ is the CP impurity parameter which measures essentially the departure of mass eigenstates in K^0-$\bar{K}_0$ and analogous particle systems from being CP eigenstates. The parameter ϵ' characterizes the difference in phase of the weak amplitudes for $K^0 \to \pi\pi$ (isospin I = 0) and $K^0 \to \pi\pi$ (I = 2). The present status of experimental and theoretical knowledge on these parameters is summarized in /89,90/:

In superweak theories /91/ all of the CP violation arises from the mass matrix, implying $\epsilon' = 0$ and $\eta_{+-}/\eta_{00} = 1$.

In gauge theories CP violation can arise through:

i) quark mixings as in the KM model, predicting $|\epsilon'/\epsilon| \leq 0.02$ (ϵ'/ϵ is almost certainly positive /90/) and $\eta_{+-}/\eta_{00} = 1$ /92/;

ii) Higgs couplings (for more than one doublet) /93-95/, giving $|\epsilon'/\epsilon| \leq 0.02$ but a rather large $d_N^e \sim 10^{-25}$ e-cm compared with $d_N^e \sim 10^{-32}$ e-cm in the other model;

iii) more gauge bosons /96/ (for example $SU_{2L} \times SU_{2R} \times U_1$), giving $\epsilon' \simeq 0$, η_{+-}/η_{00} different from unity, and $d_N^e \sim 10^{-25}$ e-cm,

or a combination of the above mechanisms.

The experimental data impose constraints on the KM parameters U_{ij}, showing that the diagonal elements are large and the couplings become weaker as the quark generations involved in the mixings become more distant /97/. The total hadronic charged current is in the sequential six quark scheme given by

$$J_\mu^{hadr.} = (\bar{u}, \bar{c}, \bar{t})\, \gamma_\mu \frac{1}{2}(1+\gamma_5)\, U_{KM} \begin{pmatrix} d \\ s \\ b \end{pmatrix}. \qquad (2.42)$$

In the lepton sector, the neutrinos are assumed to be massless. Therefore, any possible mixing of the mass eigenstates can be removed by a redefinition of the neutrino fields /98/. If, however, the neutrinos are massive and there are no global conservation laws of the different lepton numbers, there will in general exist mixings between the lepton generations (2.10) similar to those in the quark sector /48/. Experimental methods of constraining neutrino masses and mixings can, for example, be found in /99-101/.

2.8. Alternatives to the standard model

Whereas until recently mainly theoretical reasons justified the demand for extensions of the standard model, now new experimental discoveries, if confirmed in further experiments, provide evidence for such extensions. A number of classes of unusual events has been observed in the $\bar{p}p$ collider experiments (e.g. radiative Z^0 decays /102/ of unexpectedly high rate and of unusual kinematic configuration, jet events with large missing transverse momentum /103,104/, and dimuon events containing an abundance of strange particles /105/) which are difficult to be accommodated in the standard model.

Another potential problem for the standard model may arise from a new experimental result /89/ indicating that the ratio ϵ'/ϵ is negative, whereas the standard model predicts probably a positive ϵ'/ϵ value /90/. Furthermore, if weak CP violation is explained within the KM framework of the standard model, the long b-quark lifetime $\tau_b = (1.5 \pm 0.4 \pm 0.3) \cdot 10^{-12}$ s /106/ involves a t-quark mass significantly higher than the possible value extracted from the UA1 experiment /61/.

Finally the already mentioned indirect hints for neutrino oscillations (Chap. 2.5) obtained some support by the recent possible evidence for neutrino masses and/or neutrino oscillations /101/ indicating that extensions to the standard model may be demanded.

Such extensions have been obtained, for instance, by varying the number of fermion generations or their SU_2 representation assignments, by increasing the number of Higgs fields or changing their multiplet structure, by enlarging the symmetry group, by using a supersymmetric framework /108/ where bosons are related to fermions, or by assuming that the bosons and/or fermions are composites /107/.

An *increase of the number of Higgs fields* implies that there will exist additional neutral and charged Higgs particles left over after symmetry breaking. This may involve Higgs mediated flavour-changing neutral current effects and possible contributions to CP violating effects /69,70/. In models involving Higgs triplets or higher multiplets the mass relation (2.31) would be spoiled (i.e. $\rho \neq 1$).

The possibility to modify the standard model by *increasing the number of lepton and/or quark generations* turns out to be very restricted. Cosmological arguments /109/, based on the observed abundance of primordial helium, suggest that the number of neutrinos (with masses $m_\nu \leq 1$ MeV) should not be greater than 4. The best laboratory limits on the number n_ν of light neutrino species are $n_\nu < 6$ (25) from indirect (direct) limits on the Z width /20/. A theoretical limit on the number of quark flavours can be set by demanding asymptotic freedom for the strong interactions. QCD interactions become weaker for high momentum transfers (i.e. short distances) as quantified by the running strong coupling constant /110/

$$\alpha_s(Q^2) \overset{Q^2 \to \infty}{\longrightarrow} \frac{12\pi}{33 - 2N_f} \cdot \frac{1}{\ln(Q^2/\Lambda^2)}, \qquad (2.43)$$

with N_f being the number of quark flavours (actually, only those quarks which are light compared to $\sqrt{Q^2}$ are counted in N_f). The requirement that α_s has to be greater than zero for $Q^2 > \Lambda^2$ leads to $2N_f < 33$, i.e. the number of quark doublets N_D $(= N_f/2)$ must be, at most, eight.

The measurement of the parameter ρ which controls the relative strength of charged- vs. neutral-current interactions can be used to put bounds on the mass of possible heavy fermions. In the standard model ρ is equal to unity, but radiative corrections with a fermion loop in the W and Z propagator modify this value. For example, a doublet of fermions with masses m_1 and m_2 leads to a correction to ρ given by /111/

$$\rho = 1 + \left\{ \begin{matrix} 1 \\ 3 \end{matrix} \right\} \frac{G}{8\sqrt{2}\pi^2} \left[\frac{2m_1^2 m_2^2}{m_1^2 - m_2^2} \ln \frac{m_2^2}{m_1^2} + m_1^2 + m_2^2 \right], \tag{2.44}$$

where the factors 1 and 3 (colour) apply to leptons and quarks respectively. In particular, for a quark doublet $\binom{t}{b}$ one obtains /112/:

$$\rho - 1 \simeq \frac{3Gm^2}{8\sqrt{2}\pi^2} \simeq 2.8 \cdot 10^{-2} \left(\frac{m}{300 \text{ GeV}} \right)^2 . \tag{2.45}$$

The present limits on ρ imply that $m \leq 300$ GeV. The existence of bounds on the fermion masses suggests that the number of fermion generations are limited.

Further customary modifications to the standard model are obtained by *changing the multiplet structure of the fermions* in that way that some right-handed fermions are placed in doublets, too (b-quark models /113/, q-quark models /114/, vector models /115/, etc.). Experimentally there is only evidence (and only at low energies) that u, d, and s couple in a left-handed way (β-decay, success of Cabibbo theory in semileptonic hyperon decay, y-distributions of di-leptons in neutrino-hadron collisions). In principle u_R and d_R could be in a higher multiplet with heavier quarks. If one allows that the right-handed fermion f_R has a component $f_R \cos\alpha_f$ in a singlet but $f_R \sin\alpha_f$ is in a doublet, then the experimental data place the following limits for such a mixing /29/:

$$\sin^2\alpha_u \leq 0.103\,, \; \sin^2\alpha_d \leq 0.348\,, \; \sin^2\alpha_e \leq 0.064\,.$$

The extension of the standard model by adding the extra group factor SU_{2R} leads to *left-right symmetric models* /116/ which thus are based on the gauge group $SU_{2L} \times SU_{2R} \times U_1$. The subscripts mean that left-handed fermions are assumed to transform as doublets and singlets with respect to SU_{2L} and SU_{2R}, respectively (and correspondingly for right-handed fermions). The structure of these models is arranged so that no large right-handed charged currents appear between the known leptons and quarks so as to avoid experimental contradiction. This can be done either by arranging the doublets under SU_{2R} carefully or by introducing appropriate Higgs mesons which guarantee that the charged boson which mediates all right-handed processes is very heavy. ($M_{W_R}^2 > 10 M_{W_L}^2$ from the success of the V - A theory in various decay processes and $M_{W_R} > 1.6$ TeV from the evaluation of higher-order charged-current contributions to $M_{K_L^0} - M_{K_S^0}$ /117/). Choosing the second option implies that parity violation observed at low energies is attributed to an accident of spontaneous symmetry breaking. Depending on the details of this symmetry breaking, the

neutral current interactions in these models may or may not be the same as in the standard model. Quite generally, the effective neutral-current interaction Lagrangian resulting from such theories can be parametrized as:

$$\begin{aligned} \mathcal{L}_{eff}^{NC} = 4\frac{G}{\sqrt{2}} \Big[& \rho_L \left(J_{\mu L}^3 - \sin^2\Theta_W J_\mu^{em} \right)^2 + \rho_R \left(J_{\mu R}^3 - \sin^2\Theta_W J_\mu^{em} \right)^2 \\ & - 2\rho_{LR} \left(J_{\mu L}^3 - \sin^2\Theta_W J_\mu^{em} \right) \left(J_{\mu R}^3 - \sin^2\Theta_W J_\mu^{em} \right) \Big] , \end{aligned} \tag{2.46}$$

where the standard model is obtained in the limit $\rho_L = 1$, $\rho_R = \rho_{LR} = 0$.

The term proportional to ρ_R escapes in neutrino-induced reactions because available neutrino beams are left-handed. It should show up in parity-violating weak-electromagnetic interference effects. Neutrino data may be used to constrain ρ_{LR}, the relative strength of the left-right symmetric contribution. This class of models has two neutral intermediate bosons Z_1^0 and Z_2^0 whose masses M_1 and M_2 are given by

$$\begin{aligned} \left(\frac{37.3}{M_1} \right)^2 + \left(\frac{37.3}{M_2} \right)^2 &= \sin^2\Theta_W \left[(1 - \sin^2\Theta_W)(\rho_L + \rho_R) + 2\sin^2\Theta_W \rho_{LR} \right] \; GeV^{-2} \\ \left(\frac{37.3}{M_1} \right)^2 \cdot \left(\frac{37.3}{M_2} \right)^2 &= \sin^4\Theta_W (1 - 2\sin^2\Theta_W)(\rho_L \rho_R - \rho_{LR}^2) \; GeV^{-4} , \end{aligned} \tag{2.47}$$

where the mass of the lighter of the two Z bosons (Z_1^0) is lower than the standard theory limit (2.19).

Supersymmetry (SUSY) /108/ is also being considered as a possible non-trivial extension of the standard theory. It is a symmetry which can transform bosons into fermions and viceversa. There are simple supersymmetries (only one supersymmetry generator) and extended supersymmetries (more generators). Since no fermion-boson degeneracy is observed in nature, supersymmetry must be broken. SUSY provides new particles (so-called sparticles: sleptons $\tilde{l}$, squarks $\tilde{q}$, gluinos $\tilde{g}$, "light" Higgs, ...) that may be responsible for the recent experimental discoveries. It makes substantial contributions to weak CP-violating processes, thus resolving the incompatibility between measured long b-quark lifetime and the possible UA1 t-quark mass region /105/.

It was shown by Bjorken /23/ and by Hung and Sakurai /24/ that the effective Lagrangian of the standard model can be reproduced by assuming a global SU_2 symmetry with universality and electromagnetic mixing of the neutral field W_μ^3 with the photon field A_μ. This W^0–γ mixing implies that the W^0 is a *composite* object containing charged constituents /68/. As a result of this mixing with strength λ one obtains a neutral weak boson with a mass shifted upwards with respect to the charged bosons $W^\pm$:

$$M_Z = \frac{M_W}{\sqrt{1 - \lambda^2}} \tag{2.48}$$

At low Q^2, the effective neutral current interaction becomes

$$\mathcal{L} = \frac{4G}{\sqrt{2}} \left(J_\mu^3 - \frac{e}{g}\lambda J_\mu^{em} \right) \cdot \left(J_\mu^3 - \frac{e}{g}\lambda J_\mu^{em} \right) . \tag{2.49}$$

Both the strength ($\rho = 1$) and the $J_\mu^3 - \text{"sin}^2\,\Theta\text{"} J_\mu^{em}$ structure of the standard model are reproduced, provided one identifies $\lambda e/g$ as "$\sin^2\Theta$". The $W^\pm$ and Z masses, however, do not necessarily coincide with the GWS model relations (2.19). One expects a weaker mass relation /24/

$$M_W = \frac{37.3\ \text{GeV}}{\text{"sin}^2\,\Theta\text{"}}\lambda\,, \qquad M_Z = \frac{37.3\ \text{GeV}}{\text{"sin}^2\,\Theta\text{"}}\frac{\lambda}{\sqrt{1-\lambda^2}}\,. \tag{2.50}$$

The standard model mass spectrum (2.19) is obtained only if the W^0-γ mixing parameter is fixed by the "unification condition" $\lambda^2 = e^2/g^2 = \text{"sin}^2\,\Theta\text{"}$.

If one allows a whole spectrum of weak bosons (discrete or continuous), W-γ mixing leads to an effective neutral-current Lagrangian of the form /21,22/

$$\mathcal{L}_{eff}^{NC} = \mathcal{L}_{eff}^{standard} + 4\frac{G}{\sqrt{2}}C\left(J_\mu^{em}\right)^2\,. \tag{2.51}$$

The extra term ($C > 0$) remains invisible in neutrino interactions because the neutrino has no electric charge and escapes also in parity-violating electron-quark processes because it is purely parity-conserving. It could potentially be dectected in Bhabha scattering and in electron-positron annihilation into muon or tau pairs. As pointed out by Gounaris and Schildknecht /118/, the C term measures the deviation of the total e^+e^- cross section from the standard theory, integrated over all energy with the weighting factor $1/s$:

$$C = \frac{1}{16}\frac{\left|\int \frac{ds}{s}\sigma(e^+e^- \to ALL\right|_{\substack{TRUE\\THEORY}} - \left|\int \frac{ds}{s}\sigma(e^+e^- \to ALL\right|_{\substack{STANDARD\\THEORY}}}{\left|\int \frac{ds}{s}\sigma(e^+e^- \to ALL\right|_{\substack{STANDARD\\THEORY}}}\,. \tag{2.52}$$

In more radical subcomponent models both bosons and fermions are allowed to be composites /105,107/, whose constituents are held together by a strong confining interaction. Such theories may eventually explain the weak interaction energy scale and the nature of the lepton and quark generations and their mixing angles. The rich structure of composite models has been exploited in order to explain the recent experimental discoveries at the $\bar{p}p$ collider /119/. Composite fermions would imply the existence of excited leptons and quarks (explaining the radiative Z^0 decays via $Z^0 \to ll^* \to ll\gamma$), while composite gauge bosons would support the existence of a scalar or pseudoscalar partner X_0 of the Z^0 (allowing thus $Z^0 \to \gamma X_0 \to \gamma ll$).

2.9. Neutral current parametrization

In the following it will be assumed that neutral-current phenomena at low energies (i.e. s, $Q^2 \ll M_Z^2$) can be decribed by an effective current-current interaction between the different types of elementary fermions: neutrinos, electrons, muons and quarks

$$\mathcal{L}_{eff}^{NC} = \mathcal{L}^{\nu H} + \mathcal{L}^{\nu e} + \mathcal{L}^{eH} + \mathcal{L}^{e\mu} + \cdots \tag{2.53}$$

where $\mathcal{L}^{\nu H}$ contains the terms relevant for neutrino hadron scattering, etc. The various branches of the neutral current network (Sakurai tetragon /120/, Fig. 2.4) can then be parametrized in the following way /29,31,68/.

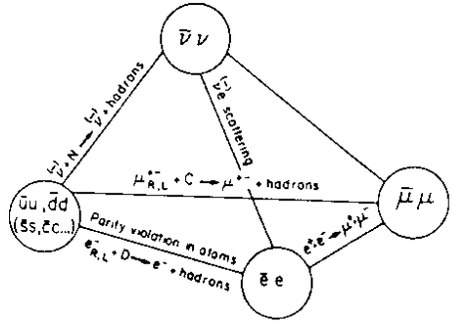

Fig. 2.4 Sakurai tetragon of neutral-current interactions.

The *neutrino-hadron interaction* $\mathcal{L}^{\nu H}$ is of the form

$$\mathcal{L}^{\nu H} = \frac{G}{\sqrt{2}}\bar{\nu}\gamma^\mu(1+\gamma_5)\nu\, J_\mu^H\,, \tag{2.54}$$

where the fact is used that in accelerator beams the neutrinos are left-handed (Chap. 3) and where the hadronic neutral current is given by

$$\begin{aligned} J_\mu^H &= \sum_i \left[\epsilon_L(i)\bar{q}_i\gamma_\mu(1+\gamma_5)q_i\right] + \left[\epsilon_R(i)\bar{q}_i\gamma_\mu(1-\gamma_5)q_i\right] \\ &= \sum_i \bar{q}_i\gamma_\mu\left(g_V^i + g_A^i\gamma_5\right)q_i \end{aligned} \tag{2.55}$$

The sum extends over the quark flavours (q_i = u,d,s,c, ...). The vector (g_V^i) and axialvector couplings (g_A^i) are related to the left-handed (ϵ_L) and right-handed chiral couplings (ϵ_R) by

$$\begin{aligned} g_V^i &= \epsilon_L(i) + \epsilon_R(i) \\ g_A^i &= \epsilon_L(i) - \epsilon_R(i) \end{aligned} \tag{2.56}$$

If generation universality holds, one expects for the neutral-current parameters:

$$\epsilon_{L,R}(c) = \epsilon_{L,R}(u)\,; \qquad \epsilon_{L,R}(s) = \epsilon_{L,R}(d)\,. \tag{2.57}$$

The quite stringent upper limits on strangeness and charm changing neutral currents strongly suggest, also do not necessarily imply, the validity of this assumption /29/.

In addition an alternate notation is used which emphasizes the isospin structure /31/ (Sakurai's notation)

$$\begin{aligned} J_\mu^H &= \frac{\alpha}{2}\left[\bar{u}\gamma_\mu u - \bar{d}\gamma_\mu d\right] + \frac{\beta}{2}\left[\bar{u}\gamma_\mu\gamma_5 u - \bar{d}\gamma_\mu\gamma_5 d\right] \\ &\quad + \frac{\gamma}{2}\left[\bar{u}\gamma_\mu u + \bar{d}\gamma_\mu d\right] + \frac{\delta}{2}\left[\bar{u}\gamma_\mu\gamma_5 u + \bar{d}\gamma_\mu\gamma_5 d\right] + \cdots \\ &= \alpha V_\mu^3 + \beta A_\mu^3 + \gamma V_\mu^0 + \delta A_\mu^0 + \cdots \end{aligned} \tag{2.58}$$

where V_μ^3 (V_μ^0) is the isovector (isoscalar) vector current, and similarly for A_μ^3 (A_μ^0). The dots denote analogous terms for heavy quarks. The relationship between these two sets of couplings is

$$\begin{aligned}
\epsilon_L(u) &= \frac{1}{4}(\alpha+\beta+\gamma+\delta) \\
\epsilon_R(u) &= \frac{1}{4}(\alpha-\beta+\gamma-\delta) \\
\epsilon_L(d) &= \frac{1}{4}(-\alpha-\beta+\gamma+\delta) \\
\epsilon_R(d) &= \frac{1}{4}(-\alpha+\beta+\gamma-\delta)\,.
\end{aligned} \tag{2.59}$$

The effective Lagrangian for *neutrino-electron interactions* is written as:

$$\mathcal{L}^{\nu e} = \frac{G}{\sqrt{2}}\bar{\nu}\gamma^\mu(1+\gamma_5)\nu\, J_\mu^e \tag{2.60}$$

with

$$\begin{aligned}
J_\mu^e &= \epsilon_L(e)\,\bar{e}\gamma_\mu(1+\gamma_5)e \;+\; \epsilon_R(e)\,\bar{e}\gamma_\mu(1-\gamma_5)e \\
&= \bar{e}\gamma_\mu\,(g_V^e + g_A^e\gamma_5)\,e
\end{aligned} \tag{2.61}$$

where

$$\begin{aligned}
g_V^e &= \epsilon_L(e) + \epsilon_R(e) \\
g_A^e &= \epsilon_L(e) - \epsilon_R(e)\,.
\end{aligned} \tag{2.62}$$

The parity violating Lagrangian in the *electron-hadron interaction* (and equivalently in *muon-hadron interaction* by replacing e by μ if μ-e universality holds) is parametrized as:

$$\begin{aligned}
\mathcal{L}^{eH} &= \frac{G}{\sqrt{2}}\sum_i\left[C_{1i}\,\bar{e}\gamma^\mu\gamma_5 e\cdot\bar{q}_i\gamma_\mu q_i \;+\; C_{2i}\,\bar{e}\gamma^\mu e\cdot\bar{q}_i\gamma_\mu\gamma_5 q_i\right] \\
&= \frac{G}{\sqrt{2}}\left[\bar{e}\gamma^\mu\gamma_5 e\,(\tilde{\alpha}V_\mu^3+\tilde{\gamma}V_\mu^0) \;+\; \bar{e}\gamma^\mu e\,(\tilde{\beta}A_\mu^3+\tilde{\delta}A_\mu^0) \;+\; \cdots\right],
\end{aligned} \tag{2.63}$$

emphasizing that this effective Lagrangian has the form: $A_{lepton}\cdot V_{quark} + V_{lepton}\cdot A_{quark}$. The two sets of coupling constants are related by

$$\begin{aligned}
C_{1u} &= \frac{1}{2}(\tilde{\alpha}+\tilde{\gamma})\,, \qquad & C_{2u} &= \frac{1}{2}(\tilde{\beta}+\tilde{\delta}) \\
C_{1d} &= \frac{1}{2}(-\tilde{\alpha}+\tilde{\gamma})\,, \qquad & C_{2d} &= \frac{1}{2}(-\tilde{\beta}+\tilde{\delta})\,.
\end{aligned} \tag{2.64}$$

Finally, the effective interaction Lagrangian for *electron-positron annihilation into muon pairs* is

$$\begin{aligned}
\mathcal{L}^{e\mu} \;=\; \frac{G}{\sqrt{2}}\big[&h_{VV}\,(\bar{e}\gamma_\mu e+\bar{\mu}\gamma_\mu\mu)\,(\bar{e}\gamma^\mu e+\bar{\mu}\gamma^\mu\mu) \\
&+\; 2h_{VA}\,(\bar{e}\gamma_\mu e+\bar{\mu}\gamma_\mu\mu)\,(\bar{e}\gamma^\mu\gamma_5 e+\bar{\mu}\gamma^\mu\gamma_5\mu) \\
&+\; h_{AA}\,(\bar{e}\gamma_\mu\gamma_5 e+\bar{\mu}\gamma_\mu\gamma_5\mu)\,(\bar{e}\gamma^\mu\gamma_5 e+\bar{\mu}\gamma^\mu\gamma_5\mu)\big]
\end{aligned} \tag{2.65}$$

where μ-e universality has been assumed. If μ-e-τ universality holds, the interaction relevant for $e^+e^- \to \tau^+\tau^-$ can be derived from (2.65) by replacing μ by τ.

The neutral-current parameters defined in this section are independent of specific weak interaction models. Their expressions in terms of the parameters of specific models can be obtained by comparing the above model-independent parametrizations with the effective Lagrangian of the different models (e.g. Eqs. 2.28, 2.46 or 2.51). The 13 coupling constants in terms of the $SU_2\times U_1$ parameters (ρ and T_{3R}^i arbitrary, $T_{3L}^i = \pm 1/2$) are listed in Table 2.4, together with the corresponding expressions for the one-parameter standard $SU_2\times U_1$ model.

The phenomenological aim of neutral-current physics is to determine all the discussed couplings. It is clear that, if the effective Lagrangians are all generated by a single intermediate boson, connections will exist between different sectors. They take the form of *factorization relations* /121/ which relate the coupling constants entering the eH and $e\mu$ Lagrangian to the νH and νe couplings. These factorization relations may be schematically visualized as shown in Fig. 2.5.

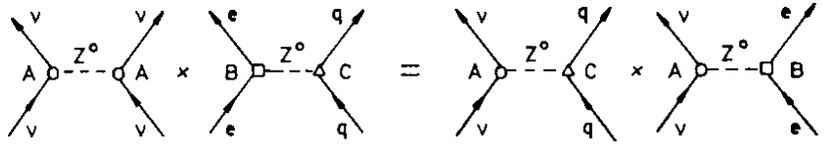

Fig. 2.5 Schematic representation of factorization.

Any single process can only measure the product of the two relevant coupling constants (e.g. $B\cdot C$ for electron-hadron scattering). The factorization hypothesis implies that the coupling strengths thus extracted will satisfy the expression stated graphically in Fig. 2.5, i.e.

$$A\cdot A\times B\cdot C = A\cdot B\times A\cdot C\,.$$

This is certainly true if all neutral-current processes are mediated by a unique intermediate Z^0 boson, but generally will not be true if there are more than one Z^0 /122/.

For models with a single Z^0 boson and under the assumption of μ-e universality, the interactions appearing in the neutral-current tetragon of Fig. 2.4 (involving 13 phenomenological parameters altogether) are completely determined by specifying seven independent parameters corresponding to the couplings of ν_L, u_L, d_L, e_L (and μ_L), u_R, d_R and e_R (and μ_R). Thus six factorization relations must exist which impose testable constraints on the data /121/. From the example illustrated in Fig. 2.5 one can derive

$$\begin{aligned}
\tilde{\gamma}/\tilde{\alpha} &= \gamma/\alpha \\
\tilde{\delta}/\tilde{\beta} &= \delta/\beta \\
g_V^e/g_A^e &= \alpha\tilde{\beta}/\beta\tilde{\alpha}\,.
\end{aligned} \tag{2.66}$$

Table 2.3. Values of the neutral-current parameters in the $SU_2 \times U_1$ model where $x = \sin^2\theta_W$. The (minimal) GWS model is the special case $\rho = 1$, $T^e_{3R} = T^u_{3R} = T^d_{3R} = 0$ of the general $SU_2 \times U_1$ model /31/.

	Parameter	$SU_2 \times U_1$ general	$SU_2 \times U_1$ minimal
νH	α	$\rho\left[1+(T^u_{3R} - T^d_{3R}) - 2x\right]$	$1 - 2x$
	β	$\rho\left[1-(T^u_{3R} - T^d_{3R})\right]$	1
	γ	$\rho\left[(T^u_{3R} + T^d_{3R}) - \frac{2}{3}x\right]$	$-\frac{2}{3}x$
	δ	$-\rho\left[T^u_{3R} + T^d_{3R}\right]$	0
νe	g^e_V	$\rho\left[-\frac{1}{2} + T^e_{3R} + 2x\right]$	$-\frac{1}{2} + 2x$
	g^e_A	$-\rho\left[\frac{1}{2} + T^e_{3R}\right]$	$-\frac{1}{2}$
$e\mu$	h_{VV}	$\rho\left[-\frac{1}{2} + T^e_{3R} + 2x\right]^2$	$\left[-\frac{1}{2} + 2x\right]^2$
	h_{AA}	$\rho\left[\frac{1}{2} + T^e_{3R}\right]^2$	$\frac{1}{4}$
	h_{VA}	$-\rho\left[\frac{1}{2} + T^e_{3R}\right]\left[-\frac{1}{2} + T^e_{3R} + 2x\right]$	$\frac{1}{4} - x$
eH	$\tilde{\alpha}$	$-2\rho\left[\frac{1}{2} + T^e_{3R}\right]\left[1+(T^u_{3R} - T^d_{3R}) - 2x\right]$	$-(1 - 2x)$
	$\tilde{\beta}$	$2\rho\left[-\frac{1}{2} + T^e_{3R} + 2x\right]\left[1-(T^u_{3R} - T^d_{3R})\right]$	$-(1 - 4x)$
	$\tilde{\gamma}$	$-2\rho\left[\frac{1}{2} + T^e_{3R}\right]\left[T^u_{3R} + T^d_{3R} - \frac{2}{3}x\right]$	$\frac{2}{3}x$
	$\tilde{\delta}$	$-2\rho\left[-\frac{1}{2} + T^e_{3R} + 2x\right]\left[T^u_{3R} + T^d_{3R}\right]$	0

The first two relations mean that the isoscalar-isovector ratios measureable in eH interactions must be equal to the corresponding ratios measurable in νH interactions. The third relation implies that the vector-to-axialvector ratio in νe scattering can be infered from νH and eH experiments. The remaining three factorization relations all concern the lepton sector

$$\begin{aligned} h_{VV} &= g_V^{e^2}/c_\nu^2 \\ h_{AA} &= g_A^{e^2}/c_\nu^2 \\ h_{VA} &= \sqrt{h_{VV}h_{AA}} = g_V^e g_A^e/c_\nu^2 , \end{aligned} \tag{2.67}$$

where c_ν^2 is a model-dependent positive quantity proportional to the square of the $Z\nu\nu$ coupling constant:

$$\mathcal{L}^{\nu\nu}_{eff} = \frac{G}{\sqrt{2}} c_\nu^2 \left[\bar{\nu}\gamma^\mu(1+\gamma_5)\nu\right] \cdot \left[\bar{\nu}\gamma_\mu(1+\gamma_5)\nu\right] . \tag{2.68}$$

In $SU_2 \times U_1$ gauge models $c_\nu^2 = 4\rho\,(T^\nu_{3L})^2$ and thus $c_\nu^2 = \rho$ for $T^\nu_{3L} = \frac{1}{2}$.

One can write down from these relations various factorization tests. So it turns out that one gets a practicable test by combining the relations (2.66) since $\tilde{\beta}$ and $\tilde{\delta}$ have not yet been determined separately:

$$\frac{g_V^e}{g_A^e} = \frac{(\alpha + \gamma/3)\,(\tilde{\beta} + \tilde{\delta}/3)}{(\tilde{\alpha} + \tilde{\gamma}/3)\,(\beta + \delta/3)} . \tag{2.69}$$

The right-hand side can be evaluated from neutrino hadron data and the SLAC asymmetry ed experiment.

Bernabéu and Jarlskog /123/ pointed out that there are two relations among the neutral-current couplings which are a consequence of the existence of an underlying $SU_2 \times U_1$ gauge symmetry for low and medium energies and which do not rely on a particular model:

$$2c_\nu^2 - (\alpha + \beta) + 3(\gamma + \delta) = 0 \tag{2.70}$$

$$2(g_V^e + g_A^e) + (\alpha + \beta) + 3(\gamma + \delta) = 0 . \tag{2.71}$$

A similar relation by Sidhu /124/ provides a more specific test of the GWS model:

$$(\alpha - \beta) + 3(\gamma - \delta) + 2(g_V^e - g_A^e) = 0 \tag{2.72}$$

For more general $SU_2 \times U_1$ models this has to be modified to:

$$(\alpha - \beta) + 3(\gamma - \delta) + 2(g_V^e - g_A^e) = 4c_\nu^2\left[2T^u_{3R} + T^d_{3R} + T^e_{3R}\right] . \tag{2.73}$$

To test the standard model one can either analyse each process of the neutral current tetragon (Fig. 2.4) in terms of its own characteristic parameters and subsequently check whether the factorization relations are satisfied, or analyse all processes in terms of the seven independent parameters (ν_L, u_L, d_L, e_L, u_R, d_R, e_R) and see if a unique solution exists.

3. CHARGED CURRENT STRUCTURE

3.1. Introduction

β-decay processes of nuclei and decay processes of elementary particles (such as μ, τ, π decay) played an important role in helping to formulate the weak interaction theory. It was proposed in the late 1950's /125/ that the effective charged weak interactions are of the current-current form with a V-A space-time structure for each current, implying maximal parity violation. This so-called V-A theory was established by a variety of crucial experiments /126-129/ and is still in agreement with all experiments. In describing neutron β-decay $n \to pe^-\bar{\nu}_e$, for instance, one starts from the most general interaction Lagrangian given by formula (2.1):

$$\mathcal{L} = \frac{G}{\sqrt{2}} \sum_{i=V,A,S,P,T} \left[\bar{p}\,\Gamma_i\, n\right] \cdot \left[\bar{e}\,\Gamma_i\,(C_i + \gamma_5 C_i')\,\nu_e\right], \tag{3.1}$$

where, for abbreviation, the particle symbols are used instead of the spinors. The leptonic current can be decomposed into two parts

$$\frac{1}{2}\,(C_i + C_i')\,\bar{e}\,\Gamma_i\,(1+\gamma_5)\,\nu_e + \frac{1}{2}\,(C_i - C_i')\,\bar{e}\,\Gamma_i\,(1-\gamma_5)\,\nu_e\,,$$

where the expression $(1+\gamma_5)\nu_e$ projects out the negative helicity state (ν_{eL}) and $(1-\gamma_5)\nu_e$ the positive one (ν_{eR}). The helicity of a fermion with momentum $\vec{p}$ and spin $\frac{\hbar}{2}\vec{\sigma}$ is defined by $H = \vec{\sigma}\cdot\vec{p}/|\vec{p}|$. The neutrino helicity was first determined in an elegant experiment by Goldhaber and co-workers /126/ to be $H_\nu = -1$. This implies maximal parity violation (i.e. $C_i = C_i'$) and reduces formula (3.1) to

$$\mathcal{L} = \frac{G}{\sqrt{2}} \sum_i \left[\bar{p}\,\Gamma_i\, n\right] \cdot \left[\bar{e}\,\Gamma_i\,(1+\gamma_5)\,\nu_e\right] C_i\,. \tag{3.2}$$

A theory of neutrinos formulated on only the basis of a left-handed (or right-handed) component is known as *two-component neutrino theory* /130-132/. Theories of this kind cannot, by itself, decide whether the neutrino is left-handed ($H_\nu = -1$) or right-handed ($H_\nu = +1$). The experiments clearly favour the solution with left-handed neutrinos and right-handed antineutrinos.

Since γ_5 anticommutes with Γ_i for V, A couplings and commutes with Γ_i if the couplings are of S, P or T type, the lepton current in (3.2) is

$$\bar{e}\,\Gamma_i\,(1+\gamma_5)\,\nu_e = \begin{cases} \bar{e}\,(1+\gamma_5)\,\Gamma_i\nu_e & \text{for i=S,P,T,} \\ \bar{e}\,(1-\gamma_5)\,\Gamma_i\nu_e & \text{for i=V,A.} \end{cases} \tag{3.3}$$

S, P, T type interactions should therefore produce a right-handed electron in neutron β-decay, whereas a left-handed final-state electron is expected for V, A type couplings. The experiments /133/ show that the electrons in β^--decays have a polarization $P_e = -1.001 \pm 0.008$, implying thus the dominance of vector and axialvector currents in nuclear β-decay.

If possible small S, P, T contributions are neglected, the formula (3.2) reduces to

$$\mathcal{L} = \frac{G}{\sqrt{2}} \left[\bar{p}\,\gamma_\mu\,(C_V - \gamma_5 C_A)\,n\right] \cdot \left[\bar{e}\,\gamma_\mu\,(1+\gamma_5)\,\nu_e\right]. \tag{3.4}$$

Measurements show that V and A couplings contribute with about equal amount but opposite sign. The fact that $C_A/C_V = -1.250 \pm 0.009$ in nuclear β-decay /134/ was attributed to a "renormalization effect" due to strong interactions, so that in the absence of strong interactions, one should have $C_A = -C_V$, i.e. pure V-A.

The standard $SU_{2L} \times U_1$ model is a renormalizable realization of this V-A hypothesis. Within the framework of this model, the charged current phenomena are described by the interaction Lagrangian (2.24) which reduces at low momentum transfers ($Q^2 \ll M_W^2$) to the phenomenological current-current form (2.25), as discussed in Chapter 2. In the standard model the V-A structure of charged currents

$$J_\mu = (\bar{u},\,\bar{c},\,\bar{t})_L\,\gamma_\mu U_{KM} \begin{pmatrix} d \\ s \\ b \end{pmatrix}_L + (\bar{\nu}_e,\,\bar{\nu}_\mu,\,\bar{\nu}_\tau)_L\,\gamma_\mu \begin{pmatrix} e^- \\ \mu^- \\ \tau^- \end{pmatrix}_L \tag{3.5}$$

is exact and due to the asymmetric assignment of chiral fermion states (Chap. 2.6). The many extensions of the standard model, however, include charged current interactions with other space-time structures. Therefore, careful studies of the structure of charged weak interactions are of interest for detecting possible small departures from the standard model.

In *left-right symmetric models* /116/ based on the $SU_{2L} \times SU_{2R} \times U_1$ gauge group, the assignment of chiral fermion states is symmetrical. The observed predominance of the V-A nature of the charged currents is then due to the mass difference of the two groups of gauge bosons ($W_L^\pm$, $W_R^\pm$), implying $M_{W_R} \gg M_{W_L}$ for the boson masses. The right- handed vector bosons can induce V+A interactions, so that the observed preferential V-A structure of the charged weak interactions could be a strictly low-energy phenomenon. The charged current sector of left-right symmetric models can be parametrized in terms of only two parameters, the ratio δ of the two boson masses squared ($\delta = M_{W_L}^2/M_{W_R}^2$) and their possible mixing angle ς. Pure V-A is recovered in the limit $\varsigma \to 0$ and $\delta \to 0$.

Many family unified theories which try to explain the experimentally observed replication of the fermion families (i.e. mixing angles and mass ratios between the various fermion generations, etc.), predict the existence of so-called *mirror fermions* which may have V+A couplings /135/. They may mix with ordinary fermions and thus give rise to a small V+A component in charged weak interactions even in the low-Q^2 region, depending on the mirror fermion mass scale /136/. The origin of such right-handed components is in general independent from the source of the W_R-mediated contributions in left-right symmetric models.

Deviations from pure V-A are also expected in models with *charged Higgs* bosons contributing as the intermediary to the charged weak interactions /30/. Charged Higgs bosons arise naturally in the GWS model with a complex Higgs structure (two or more Higgs multiplets) /69,70/. The Lagrangian for the charged Higgs couplings can be written as /69,70/

$$\mathcal{L} = 2^{\frac{3}{4}}\sqrt{G}\,m_{H^+} \left\{ \bar{f}\left[\alpha_{ff'}^L \left(\frac{1+\gamma_5}{2}\right) + \alpha_{ff'}^R \left(\frac{1-\gamma_5}{2}\right)\right] f' \right\} H^+ + \text{h. c.}\,, \tag{3.6}$$

where f and f' are two fermions differing in charge by one unit and m_{H^+} is the mass of the charged Higgs H^+. In general the effects of charged Higgs particles will lead to a scalar or pseudoscalar interaction at the four-fermion level with effective strength $\sim G\left(\alpha_{ff'}^{L,R}\right)^2$ and to

a violation of μ-e universality. But $\alpha^L_{ff'}$ and $\alpha^R_{ff'}$ must be small because of the success of the V-A theory. Theoretically these coupling strenghts are predicted to be roughly determined either by the mass of the fermions the Higgs interact with ($\alpha^{L,R}_{eff'} \sim [m_f + m_{f'}]/m_{H^+}$), or by the mass m_F of some heavy fermion F ($\alpha^{L,R}_{ff'} \sim m_F/m_{H^+}$) /69,70/. Because m_H is likely to be at least several GeV /137,138/, high-precision experiments are needed to detect the effects of charged Higgs in low-energy processes.

In *composite models* /105,107/ where the intermediate bosons, as well as the quarks and leptons, are composites of fundamental constituents (rishons, preons, etc.), bosons with a higher spin may occur, giving rise to tensor couplings /139/.

This demonstrates the necessity to test the V-A structure of charged weak interactions even at low energies in order to rule out or establish some of the possible alternatives to the standard model.

3.2. Decay experiments

Essential experimental information concerning the Lorentz structure of charged-current weak interactions (i.e. the determination of the 10 complex coupling constants C_i and C'_i in the Lagrangian (2.1)) has been obtained from a series of experiments studying decay processes. They have mainly been designed to detect parity-violating effects by measuring pseudoscalar quantities such as $< \vec{\sigma} > \cdot \vec{p}_l$ in decay processes of elementary particles /140,141/ or $< \vec{J} > \vec{p}_l$ in β-decay processes of nuclei /142-144/. $\vec{\sigma}$ and $\vec{p}_l$ are the spin and the momentum of the decay lepton respectively, and $\vec{J}$ is the spin of the polarized nuclei. In the low-energy and low-momentum domain accessible to such decay reactions, the data are in good agreement with the effective V-A coupling, still admit, however, relatively large deviations from it. This will be quantified in the subsequent sections.

3.2.1. Nuclear β-decay

Deviations from the effective V-A coupling may be determined by measuring the longitudinal electron (positron) polarization in nuclear β-decay, predicted to be $P = \mp A \frac{v}{c}$ for $e^{\mp}$, where the factor A accounts for small Coulomb and screening effects. The current status of these measurements has been summarized by Koks and van Klinken /145/ who measured the polarization for low-energy electrons by analysing the decay products from ^{3}H-decay (Fig. 3.1).

The v/c-law agrees with the V-A prediction within ~ 1 % for rather slow electrons (^{3}H-decays) as well as for relativistic electrons (^{32}P, ^{60}Co Gamow-Teller transitions). This can be translated into an upper limit of ~ 10 % on the contribution from a possible V+A amplitude, since the polarization measurements directly determine /30/

$$\left(|C_{V-A}|^2 - |C_{V+A}|^2\right) / \left(|C_{V-A}|^2 + |C_{V+A}|^2\right) . \qquad (3.7)$$

The anomalous behaviour of older polarization measurements in the intermediate energy region (Fig. 3.1) is still not very well understood.

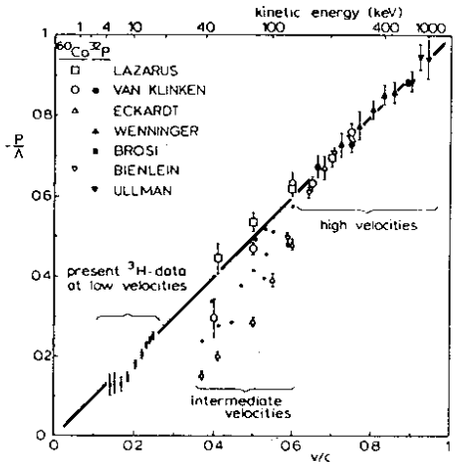

Fig. 3.1 Summary of data on electron polarization from nuclear ß-decay /145/. A stands for the correction factor due to Coulomb and screening effects. The straight line represents P= -A v/c.

Nuclear β-decay data allow to constrain the parameters δ ($= M^2_{W_L}/M^2_{W_R}$) and ζ (W_L-W_R mixing angle) in left-right symmetric models. As can be seen in Fig. 3.3 which shows the existing two-standard-deviation limits on these parameters, the mixing angle is limited by the measured angular asymmetry of positrons emitted in the decay of polarized ^{19}Ne /146/, combined with decay rate measurements and calculations using the CVC hypothesis /147/. The electron polarization measured in Gamow-Teller β-decays /148/ imposes constraints on the mass ratio δ.

Pseudoscalar interactions are negligible in nuclear β-decay as their matrix element is proportional to the electron velocity. Upper limits for possible S and T contributions have been obtained by the experimental observation that β-decay spectra in allowed Fermi and Gamow-Teller transitions (lepton pair in a singlet or triplet state respectively) are not distorted by interference terms between S and V or those between T and A, which should show a marked energy dependence ($\sim m_e/E_e$). Together with the assumption that the neutrino helicity is negative, the absence of these so-called Fierz interference terms puts a very stringent limit on S and T contributions /149/

$$C_S/C_V = -0.001 \pm 0.006 , \qquad C_T/C_A = -0.0004 \pm 0.0003 . \qquad (3.8)$$

This has to be loosened quite drastically if the neutrino helicity is left free /149-151/

$$\begin{aligned} C_S/C_V &= 0.08 \pm 1.2 , & C'_S/C_V &= -0.07 \pm 1.0 , \\ C_T/C_A &= 0.006 \pm 0.2 , & C'_T/C_A &= -0.006 \pm 0.2 . \end{aligned} \qquad (3.9)$$

The strongest constraint on charged Higgs couplings in β-decay experiments /69,70/ comes from measurements of the Fierz interference term (distorting the low-energy part of the decay-electron spectrum) in pure Fermi transitions (e.g. $^{14}O \rightarrow {}^{14}N^* e^+ \nu_e$ /152/):

$$-0.0025 \leq \left(\alpha_{du}^R + \alpha_{du}^L\right) \alpha_{e\nu}^L \leq 0.0035 \,. \tag{3.10}$$

The corresponding limit imposed by a measurement of the e^+-polarization in $^{14}O \rightarrow {}^{14}N^* e^+ \nu_e$ /69,70/ is much weaker:

$$\left|\alpha_{du}^R + \alpha_{du}^L\right| \cdot \left|\alpha_{e\nu}^L\right| \leq 0.33 \,. \tag{3.11}$$

All limits evaluated in nuclear β-decay refer to possible scalar-type quark couplings, i.e. $|\alpha_{ud}^R + \alpha_{ud}^L|$. In order to put limits on possible pseudoscalar quark couplings, $|\alpha_{ud}^R - \alpha_{ud}^L|$, one has to consider pion decay data.

3.2.2. Decay processes of elementary particles

Further suitable tests of the V-A structure of charged weak interactions are provided by studying the purely leptonic decays of μ /153-163/ and τ /106,164/ which are free from any complications due to hadronic structure. Analyses of the two-lepton decays of π /165-167/ and K /168,169/ add another piece of information.

μ^+-decay ($\mu^+ \rightarrow e^+ \nu_e \bar{\nu}_\mu$) in the intermediate vector boson theory is described by the diagram of Fig. 3.2.

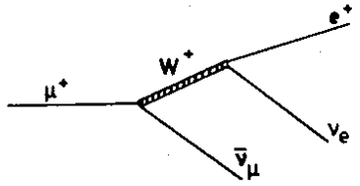

Fig. 3.2 μ^+-decay diagram in the intermediate vector boson theory.

The double differential decay probability as a function of the reduced positron energy $x = E_e/E_e^{max}$ and the emission angle Θ of the positron relative to the μ^+ spin in the muon's rest frame has the form /160/

$$\frac{d^2\Gamma}{dx\, d(\cos\Theta)} = \Gamma\Big[f_1(x,\eta,\rho) + P_\mu \xi \cos\Theta f_2(x,\delta) + \text{terms giving rise to } P_l,\ P_{T_1} \text{ and } P_{T_2} \text{ of } e^+\Big] \,. \tag{3.12}$$

P_μ is the degree of polarization of the muon. The shape of the spectrum of the decay positrons from unpolarized muons is described by the Michel parameter ρ and a parameter η affecting the low-energy end of the spectrum. The correlation between the muon spin direction and the positron momentum vector is taken into account by two more parameters: the parameter ξ which is related to the magnitude of the forward-backward asymmetry, and δ which parametrizes the difference in momentum spectrum of the positrons emitted at different angles. The remaining observables of the positron are the three components of its polarization vector $\vec{P}_e$ which is decomposed in a longitudinal component P_l along the positron momentum and two components P_{T_1}, P_{T_2} perpendicular to that direction, with the choice that P_{T_1} lies in the plane determined by muon spin and positron momentum, whereas P_{T_2} is the component perpendicular to that plane and forbidden by time reversal invariance. P_{T_1} and P_{T_2} are functions of both reduced positron energy x and emission angle Θ and determine four parameters α/A, β/A and α'/A, β'/A, respectively, where A is the rate parameter $\Gamma = \frac{m_\mu^5 G^2}{192\pi^3} \cdot \frac{A}{16}$ /160/.

All these μ-decay parameters can be expressed /153/ in terms of V, A, S, P, and T coupling coefficients that occur in the muon decay Lagrangian. They thus measure directly the form of interaction responsible for the decay. Their current best values are listed in Table 3.1.

The values for β/A and β'/A quoted in Table 3.1 represent fits under the assumption of total cancellation of scalar and pseudoscalar coupling ($\alpha = \alpha' = 0$). For small values of β, the polarization component P_{T_1} essentially measures the parameter η without the disturbing suppression factors of order m_e/m_μ which appear if η is obtained from the shape of the decay spectrum /153/. For $\alpha = 0$, the quoted β/A result gives therefore a very accurate value for η /160/

$$\eta = 0.004 \pm 0.034 \,. \tag{3.13}$$

The LBL-Northwestern-TRIUMF Collaboration /97/ has performed a precision experiment to search for deviations from the V-A structure in muon decay using two largely independent methods. In the first method the momentum spectrum of the positrons from μ^+-decay was measured in the direction opposite to the μ^+ polarization near the end point (x = 1). In the second method they measured the amplitude of the spin precession oscillation of the stopped μ^+ in a weak transverse magnetic field. Near the e^+ spectrum endpoint, $d^2\Gamma$ is proportional to $\left[1 - P_\mu \xi \frac{\delta}{\rho} \cos\Theta\right]$, and thus the experimental quantity extracted from these measurements is the combination of muon decay parameters $P_\mu \xi \delta/\rho$ listed in Table 3.1 for the two approaches /97/. The two consistent results can be combined to give the limit

$$P_\mu \xi \frac{\delta}{\rho} \geq 0.9966 \tag{3.14}$$

at the 90 % confidence level. This can be used to derive a limit for a possible (V+A) decay amplitude

$$\frac{|(V+A) - \text{Ampl.}|}{|(V-A) - \text{Ampl.}|} \leq 0.029 \qquad (90\ \%\ \text{C.L.}) \,. \tag{3.15}$$

The result (3.14) can also be used to deduce that the tensor couplings in addition to the standard V-A coupling are limited to

$$(C_T + C_T') \leq 0.027 \qquad (90\ \%\ \text{C.L.})$$

and the scalar and pseudoscalar couplings to

$$(C_S - C'_P)^2 + (C'_S - C_P)^2 \leq 0.054 \qquad (90\ \%\ \text{C.L.})\,.$$

One may thus conclude that this high precision experiment does not find any evidence of a deviation from the V-A structure as assumed in the standard model.

Table 3.1. μ^+-decay parameters: experiment vs. theory

Parameter		Experimental value	V-A Prediction	Reference
ρ	(Shape)	0.7517 ± 0.026	0.750	/161/
η	(Low energy shape)	-0.12 ± 0.21	0	/154/
		+0.027 ± 0.098		/160/ (prelim.)
δ	(Shape difference)	0.7551 ± 0.0085	0.750	/161/
		0.748 ± 0.004(stat) ± 0.003(syst)		/156/ (prelim.)
ξP_μ	(P_μ*Asymmetry)	0.972 ± 0.013	1	/162/
$\xi P_\mu \delta/\rho$		> 0.9959 (90 % C.L.)	1	/97/
		> 0.9948 (90 % C.L.)		
P_ℓ	(Long. Polarization)	0.998 ± 0.045	1	/159,163/
P_{T_1}	(Transv. Polarization)	β/A = -0.002 ± 0.017 (α/A = 0.0)	0	/159/
P_{T_2}	(Transv. Polarization - T violation)	β'/A = -0.007 ± 0.016 (α'/A = 0.0)	0	/159/

A systematic analysis of all available information on charge-changing leptonic interaction vertices (i.e. μ-decay, three-lepton decays of τ ($\to \mu\bar{\nu}\nu$, $e\bar{\nu}\nu$) /106,164/, two-lepton decays

of π, K ($\to \mu\nu$, $e\nu$) /165-169/, inverse μ-decay and the reaction $\bar{\nu}_\mu Fe \to \mu^+ X$ described in the subsequent chapters) has recently been performed /136,170/. It was found that effective tensor couplings are bounded by the data to ≤ 0.03 (at 1 σ and relative to the V-A coupling strength), whilst scalar/pseudoscalar couplings are not so well constrained and could still be present at the level of 0.08 relative to the V-A coupling. Noncanonical vector/axialvector couplings are excluded at the level of about 0.04.

Constraints on charged Higgs contributions which would manifest themselves as presence of effective scalar and pseudoscalar couplings, can be obtained from the μ-decay parameters, too. Using the value (3.13) for η one gets

$$-0.060 \leq \alpha^L_{\mu\nu} \cdot \alpha^L_{e\nu} \leq 0.076\,, \tag{3.16}$$

while the ξ value from Table 3.1 leads to the not very stringent limits

$$0.17 \leq |\alpha^L_{\mu\nu}| \sqrt{(\alpha^L_{e\nu})^2 + (\alpha^R_{e\nu})^2} \leq 0.29\,. \tag{3.17}$$

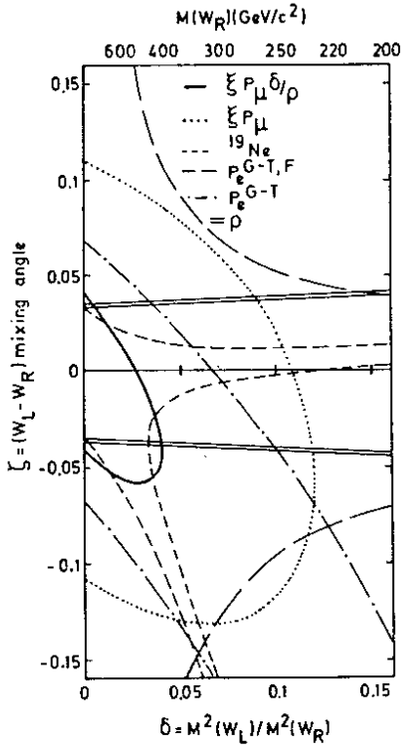

Fig. 3.3 Constraints on left-right symmetric models imposed by different low-energy experiments /97/.

The obserables of μ-decay can also be used to place limits on the parameters δ and ς of left-right symmetric models (Chap. 3.1). The precision experiment of the LBL-Northwestern-TRIUMF Collaboration /97/ constrains δ and ς by

$$1 - \frac{\delta\xi}{\rho} P_\mu \simeq 2\,(2\delta^2 + 2\delta\varsigma + \varsigma^2)$$

as displayed in Fig. 3.3 (bold contour). Other 90 % confidence limits are obtained from the measurement of ξP_μ in muon decay within nuclear emulsion /162/ (dotted contour), from the measurement of the ρ parameter in μ-decay /161/ (solid lines), from the β-asymmetry in ^{19}Ne-decay /146,97/ (short-dashed contours), from a comparison of the Fermi and Gamow-Teller β-polarizations /148/ (long-dashed contours), and from the measurements of the electron polarization in Gamow-Teller β-decay /148/ (dot-dashed lines). If it is assumed that a possible (V+A) contribution is due to a right-handed gauge boson W_R and a right-handed neutrino with less than 10 MeV mass, then the result (3.15) suggest the mass limit /156/

$$M_{W_R} > 400 \text{ GeV } (470 \text{ GeV}) \qquad (90\ \%\ \text{C.L.})$$

if arbitrary (in parentheses zero) mixing angles between left- and right-handed gauge bosons are allowed.

The ratio of pion decays $R_\pi = \Gamma(\pi \to e\nu)/(\pi \to \mu\nu)$ is very sensitive to possible pseudoscalar couplings. Between the experimental value /166/, $R_\pi^{exp} = (1.274 \pm 0.024)\cdot 10^{-4}$, and the radiative corrected V-A value /171/, $R_\pi^{V-A} \simeq 1.23 \cdot 10^{-4}$, there is a two standard deviation discrepancy which may be attributed /69/ to a possible existence of charged Higgs particles. In Higgs models with couplings proportional to fermion masses, a comparison of $\pi \to e\nu$ to $\pi \to \mu\nu$ decay rates does not provide any information about Higgs couplings, since in the V-A theory the ratio of the matrix elements is also proportional to m_e/m_μ. But in models where the Higgs couplings are independent of fermion masses (Chap.3.1), the discrepancy between R_π^{exp} and R_π^{V-A} would impose a quite stringent limit on pseudoscalar quark couplings /69/

$$\left|\alpha_{ud}^R - \alpha_{ud}^L\right| \cdot \left|\alpha_{e\nu}^L\right| \simeq 6.5 \cdot 10^{-4}\,, \qquad (3.18)$$

if one assumes that the Higgs couple only to left-handed neutrinos, i.e. $\alpha_{\mu\nu}^R = \alpha_{e\nu}^R = 0$.

Finally, it may be concluded that the charged weak interactions studied in the low-momentum transfer regime accessible in decay processes, are in very good agreement with the V-A theory as assumed in the standard model. The current limits on right-handed components and S, P, T couplings are quite tight now, and further increase in precision (e.g. for P_l- and ξ-parameter in μ-decay) can still narrow down these limits.

3.3. Neutrino experiments

Weak decay processes allow to test the V-A structure of charged weak interactions in a rather limited range of energy and momentum transfer. This range has been extended substantially by studying high-energy neutrino scattering processes. It involves the questions whether at higher energies and larger momentum transfers the weak processes are still describable in the framework of a local current-current interaction and, if so, whether the space-time structure of this interaction is still a V and A combination. These questions can only be answered by experiments and will be discussed in the subsequent chapters.

3.3.1. Polarization of μ^+ from inclusive $\bar{\nu}_\mu Fe \to \mu^+ X$ scattering

The most general Lagrangian specified in Chapter 2 leads /27/, neglecting antiquarks, to the following inelasticity distribution for the process $\bar{\nu}_\mu N \to \mu^+ X$:

$$\begin{aligned}\frac{d\sigma}{dy} \sim & 2(g_V - g_A)^2 + 2(g_V + g_A)^2(1-y)^2 + (|g_S|^2 + |g_P|^2)y^2 \\ & + 32\,|g_T|^2\,(1 - \tfrac{1}{2}y)^2 + 8\,\Re\left[g_T(g_S^* + g_P^*)\right]y(1 - \tfrac{1}{2}y)\,,\end{aligned} \qquad (3.19)$$

where g_i (defined by $g_i^2 = C_i^2 + C_i'^2$) are the coupling constants of the different Lorentz invariant combinations of the spinors participating in the reaction.

The experimental y-distributions ($y = 1 - E_\mu/E_\nu$) in inclusive neutrino and antineutrino charged-current scattering on nucleons /172-174/ turn out to be consistent with the expectations for a V-A structure of the interaction. The same y-distributions, however, could be obtained with appropriate mixtures of S, P, and T contributions (*confusion theorem*) /26,27/.

Measurements of the helicity of muons produced in neutrino interactions can resolve this ambiguity /175/, as currents of V and A type conserve the helicity of the incident neutrino, whereas interactions of S, P, and T type flip the lepton helicity in the zero-mass limit (Chap. 3.1). Hence positive muons from antineutrino-initiated reactions are expected to be of positive helicity if the interaction is V or A, and of negative helicity if any combination of S, P, and T is responsible, since the incident antineutrinos originating from pion and kaon decays are known to be of positive helicity /176,177/. For neutrino-induced reactions, the expectations would be just the reverse.

An experiment to measure the helicity of positive muons from inclusive $\bar{\nu}_\mu$ scattering on iron ($\bar{\nu}_\mu Fe \to \mu^+ X$) has been performed in the CERN SPS horn-focussed wide-band beam with a maximum antineutrino flux around 25 GeV.

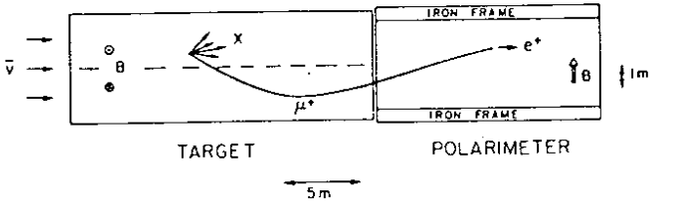

Fig. 3.4 Layout of the experiment to measure the polarization of muons produced in $\bar{\nu}_\mu$Fe → μ^+X (CDHS-CHARM experiment).

The CERN-Dortmund-Heidelberg-Saclay (CDHS) detector /178/ has been used as an instrumented target where the antineutrino interactions took place, and the CERN-Hamburg-

Amsterdam-Rome-Moscow (CHARM) detector /179/ as a polarimeter for the primary produced muons (Fig. 3.4) using the parity-violating decay process $\mu^+ \rightarrow e^+\nu_e\bar{\nu}_\mu$ as helicity analyser /180-182/. The polarization is derived from the measured forward-backward asymmetry of the decay positrons from muons stopping in the CHARM-calorimeter. This asymmetry

$$R(t) = \frac{N_B(t) - N_F(t)}{N_B(t) + N_F(t)} = R_0 \cos(\omega t + \phi) + \text{const.} \qquad (3.20)$$

is shown in Fig. 3.5 and is determined from $\sim$ 17000 detected $\mu^+ \rightarrow e^+$ decays in the CHARM polarimeter. $N_{B,F}(t)$ are the numbers of decay positrons measured in the backward and forward regions with respect to the detector plate in which the muon had stopped and decayed after a time t.

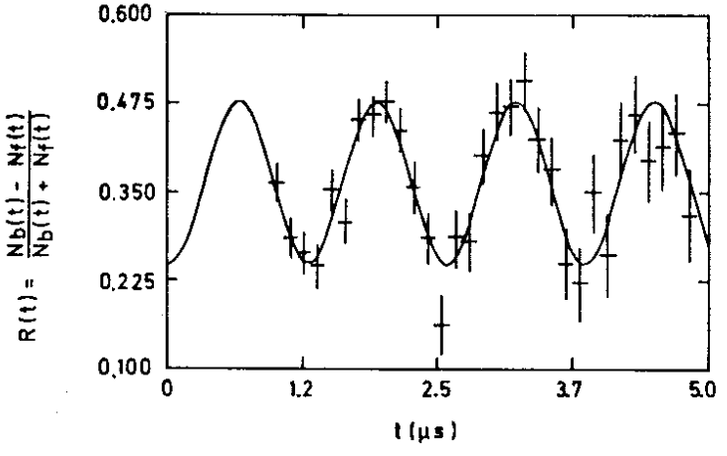

Fig. 3.5 Observed time dependence of the relative forward backward positron asymmetry. The sinusoidal function is the best fit to the data /180,182/.

R(t) exhibits a characteristic oscillation pattern since the muon spin is precessing in a low magnetic dipol field perpendicular to the neutrino beam direction with a period of $1.3\,\mu sec$. The best fit to the data is obtained for

$$R_0 = 0.116 \pm 0.010\,, \qquad \phi = -3.02 \pm 0.08\,. \qquad (3.21)$$

The oscillation amplitude R_0 is proportional to the magnitude of the longitudinal polarization P of the μ^+ with the polarimeter analysing power α as proportionality constant ($R_0 = \alpha P$).

ϕ is related to the sign of the helicity, and $\phi = 0$ is expected for negative and $\phi = -\pi$ for positive helicity. The measured phase is consistent with the value of $-\pi$ and shows that in charged-current interactions at a mean momentum-transfer of $< Q^2 >= 4\ GeV^2/c^2$ the muon spin is found to be oriented forward with respect to the muon momentum vector with an average polarization of

$$P = 0.82 \pm 0.07\ (\text{stat}) \pm 0.12\ (\text{syst})\,. \qquad (3.22)$$

The polarimeter analysing power α has been determined by a comparison of experimental data and Monte Carlo calculation results. The polarization value (3.22) sets an upper limit to possible S, P, and T contributions to charged-current interactions of $\sigma_{S,P,T}/\sigma_{all} < 20$ % at the 95 % confidence level.

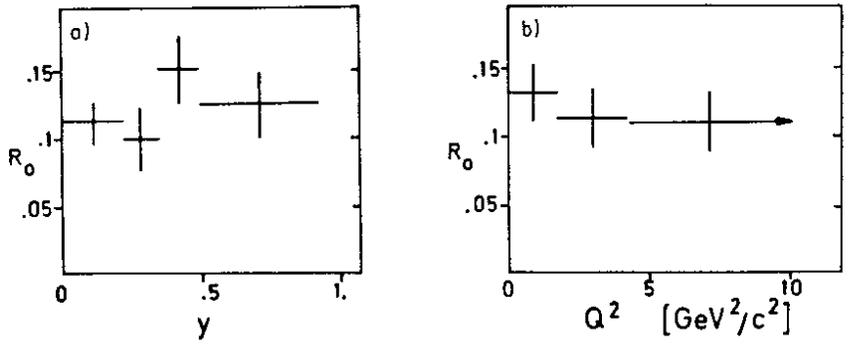

Fig. 3.6 Measured oscillation amplitude R_0
(a) as a function of the inelasticity $y = 1-E_\mu/E_\nu$,
(b) as a function of momentum-transfer Q^2.

No obvious dependence of the polarization on the kinematical quantities y and Q^2 was found (Fig. 3.6), although the sensitivity to scalar contributions (neglecting T contributions) has been increased in analysing the asymmetry in terms of y (Eq. 3.19) and Q^2 respectively. The absence of scalar contributions as, for instance, induced by charged Higgs exchange could be a strictly low-energy phenomenon. Comparison of the forward-backward asymmetry for $y < 0.2$ where S and P contributions are negligible (since they are proportional to y^2), and for $y > 0.5$ where they would dominate over V, A terms (Eq. 3.19), gives an upper limit on S and P contributions of

$$\sigma_{S,P}/\sigma_{all} < 7\,\% \qquad (95\%\ \text{C.L.}) \qquad (3.23)$$

which is unaffected by the systematic errors of the integrated polarization value.

A search for a polarization component perpendicular to the muon production plane sets a limit on time-reversal violation of

$$\sigma_{\left(\substack{\text{time}\\ \text{violating}}\right)}/\sigma_{all} < 16\,\% \tag{3.24}$$

at the 95 % confidence level for $< Q^2 >= 4\ GeV^2/c^2$.

3.3.2. Inverse muon decay

Muon-decay experiments (except those which determine the transverse polarization components of the decay positrons /155/) can never uniquely determine the interaction as V-A because all are only sensitive to the sum of the squares of the coupling constants $g_V^2 + g_A^2$. To go any further, the out-going neutrinos in muon decay ($\mu^+ \rightarrow e^+\nu_e\bar{\nu}_\mu$) must be observed so that, for instance, the positron-neutrino angular correlation is available. In this case, the measured decay rate would depend on a factor

$$(1 + \lambda\gamma_5) \quad \text{where} \quad \lambda = \frac{-2\,\Re(g_V^- g_A)}{|g_V|^2 + |g_A|^2}\,. \tag{3.25}$$

A determination of λ (= 1 for V-A) would therefore fully establish the structure of the weak leptonic charged-current interaction free from any assumptions, such as the validity of the two-component neutrino theory /183/.

The investigation of the inverse muon-decay reaction /184/

$$\nu_\mu + e^- \rightarrow \mu^- + \nu_e \tag{3.26}$$

provides essentially the same information as the observation of the outgoing ν_μ in μ-decay. The center-of-mass energy $\sqrt{s}$ of this process is low because of the small target mass, but the energy threshold in the laboratory system is high ($E_{th} = (m_\mu^2 - m_e^2)/(2m_e) \sim 10.9$ GeV), requiring thus high-energy neutrino beams.

Assuming completely left-handed charged leptons and making no assumptions on the helicity of the neutral leptons, the differential cross section for $s \gg m_\mu^2$ can be parametrized as a function of the quantity λ and $P = [N(\nu_R) - N(\nu_L)]/[N(\nu_R) + N(\nu_L)]$, the polarization of the beam neutrinos /184,185/:

$$\frac{d\sigma}{dy} = \frac{G^2 s}{4\pi}\left[(1+P)\cdot(1-\lambda)y^2 + (1-P)\cdot(1+\lambda)\right] \tag{3.27}$$

where again $y = (1 - E_\mu/E_\nu)$.

The y^2-term describes the scattering of possible right-handed ν_μ by left-handed e^-, coupled by S, P terms in the effective Lagrangian.

A pure V-A structure of the interaction implies $\lambda = 1$, and left-handed two-component neutrinos imply $P = -1$.

Events of reaction (3.26) have been observed recently /186-188/, identified by the particular characteristics of the kinematics of neutrino-electron scattering compared with that

of neutrino-nucleon processes. The muon produced in the inverse muon decay is expected to be emitted at very small angles given by $E_\mu\Theta_\mu^2 = 2m_e(1-y)$; i.e. $\Theta_\mu < 10$ mrad for $E_\nu > 11$ GeV. This results in an event pattern with a single forward going μ^- and no evidence of nuclear effects at the vertex.

Quasi-elastic neutrino scattering on nucleons ($\nu_\mu n \rightarrow \mu^- p$, $\nu_\mu N \rightarrow \mu^- \pi N$) can simulate the same event pattern. But the Q^2-dependence of these background processes is expected to be energy independent and equal for ν_μ and for $\bar{\nu}_\mu$ on an isoscalar target, whereas the inverse muon decay is expected to occur at very low values of Q^2 and only for incident ν_μ. This fact allows a separation of the background from the signal in the ν_μ sample, in the region $0 < Q^2 < 0.02\ (GeV/c)^2$, by subtracting the Q^2 distribution of the $\bar{\nu}_\mu$ sample normalized to the equivalent ν_μ sample in the range $0.02 \leq Q^2 < 0.1\ (GeV/c)^2$, where the inverse muon-decay reaction does not contribute. For $Q^2 < 0.02\ (GeV/c)^2$ an excess of μ^- events has been observed /188/. Fig. 3.7a shows the Q^2-distribution of these excess events compared to the prediction for inverse muon decay assuming V-A coupling and left-handed neutrinos.

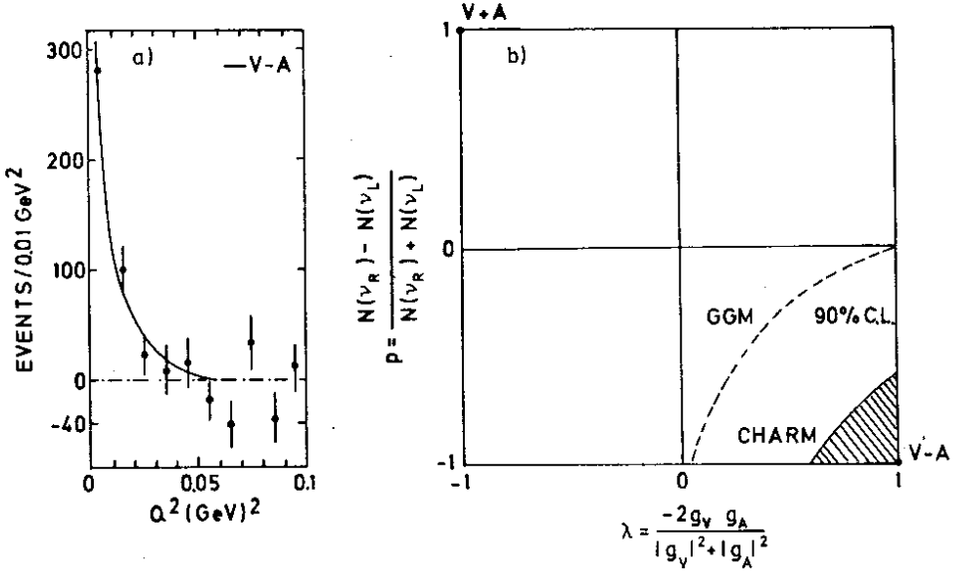

Fig. 3.7 (a) Observed Q^2-distribution of μ^- excess events. The solid line shows the V-A prediction for $\nu_\mu e^- \rightarrow \mu^- \nu_e$ (CHARM data /188/)
(b) 90 % confidence contour of the beam polarization (P) and the V/A coupling parameter (λ) deduced from the observed rates of the inverse muon decay reaction (GARGAMELLE and CHARM data /186,188/).

Taking the efficiencies for the acceptance criteria into account, the event rate for the inverse muon decay is

$$N(\nu_\mu e^- \to \mu^- \nu_e) = 594 \pm 56\ (\text{stat}) \pm 22\ (\text{syst})\,. \tag{3.28}$$

This has to be compared with the expected rates for inverse muon decay assuming respectively left-handed ($N_L = 607 \pm 35$) or right-handed neutrinos ($N_R = 226 \pm 13$):

$$\begin{aligned} R_L &= \frac{N_{exp}}{N_L} = 0.98 \pm 0.12 \\ R_R &= \frac{N_{exp}}{N_R} = 2.63 \pm 0.33\,. \end{aligned} \tag{3.29}$$

R_L expresses the ratio between the observed rate and the rate expected from V-A coupling among all the leptons in reaction (3.26), while R_R excludes at the level of 6 standard deviations the dominance of S, P couplings in the interaction. Fig. 3.7b shows the result of the CHARM experiment /188/ in terms of upper limits (90 % C.L.) in the P-λ plane, together with the result obtained by the GARGAMELLE experiment /186/. The data are in very good agreement with left-handed incoming neutrinos interacting on electrons trough a V-A interaction or left-handed current.

The inverse muon decay reaction (3.26) can also be analysed in terms of left-right symmetric models where the exchange of the vector bosons W_L and W_R produces respectively the constant part and the y^2 part in the cross section (3.27). In these models the rate R_L of reaction (3.26), normalized to the integrated V-A cross section, is a function of the mass ratio $\delta = M^2_{W_L}/M^2_{W_R}$ and of the (W_L-W_R) mixing angle ς /189/. The measurement /188/ of the rate R_L thus limits the mass ratio of the two charged bosons and their mixing angle to

$$\varsigma \leq 15^o \ \text{ and } \ M_{W_R} \geq 1.9\, M_{W_L} \qquad (90\ \%\ \text{C.L.}) \tag{3.30}$$

Most of the observed leptonic processes cannot distinguish between the so-called additive lepton number conservation law (implying separate conservation of electron and muon number) and the less stringent multiplicative law /190/. However, one can discriminate between these two alternatives by searching for the reaction $\bar{\nu}_\mu e^- \to \mu^- \bar{\nu}_e$ which is allowed by the multiplicative law but forbidden by additive lepton number conservation. The CHARM Collaboration /188/ has searched for this process and quotes a limit for the cross-section ratio of

$$\frac{\sigma(\bar{\nu}_\mu e^- \to \mu^- \bar{\nu}_e)}{\sigma(\nu_\mu e^- \to \mu^- \nu_e)} < 0.05 \qquad (90\ \%\ \text{C.L.})\,, \tag{3.31}$$

which seems to exclude multiplicative lepton number conservation. This is an improvement of the constraint

$$\frac{\sigma(\mu^+ \to e^+ \bar{\nu}_e \nu_\mu)}{\sigma(\mu^+ \to e^+ \nu_e \bar{\nu}_\mu)} < 0.098 \qquad (90\ \%\ \text{C.L.})\,, \tag{3.32}$$

obtained at the LAMPF laboratory /191/ by searching for secondary interactions of the decay electron-neutrino.

3.3.3. Limits on right-handed currents from inelastic neutrino-nucleon interactions

The reactions $\overset{(-)}{\nu}_\mu Fe \to \mu X$ have been analysed /192/ in the framework of a Lagrangian containing both V-A and V+A currents

$$\mathcal{L}^{CC} = \frac{G}{\sqrt{2}}\, \bar{\mu}\gamma_\alpha (1+\gamma_5)\, \nu_\mu \left[J^{V-A}_\alpha + \eta J^{V+A}_\alpha\right], \tag{3.33}$$

where η controls the relative strength of right-handed versus left-handed weak currents. Based on such an interaction form, the y-distributions become

$$\begin{aligned} \frac{d^2\sigma}{dx\,dy}(\nu_\mu Fe \to \mu^- X) &\sim q(x) + \eta^2 \bar{q}(x) + (1-y)^2 \left[\bar{q}(x) + \eta^2 q(x)\right] \\ &= q_L(x) + (1-y)^2\, q_R(x) \\ \frac{d^2\sigma}{dx\,dy}(\bar{\nu}_\mu Fe \to \mu^+ X) &\sim (1-y)^2 \left[q(x) + \eta^2 \bar{q}(x)\right] + \bar{q}(x) + \eta^2 q(x) \\ &= (1-y)^2\, q_L(x) + q_R(x) \end{aligned} \tag{3.34}$$

The different dependence on y for neutrino and antineutrino reactions has been used to determine experimentally the x-dependence of the two structure functions q_L and q_R. In the absence of right-handed currents, q_L and q_R represent the quark and antiquark structure functions respectively. It is found experimentally /192/ that $q_R(x) \ll q_L(x)$ at large x. This imposes an upper limit, at large x, on the sum of $\bar{q}(x)$ and $\eta^2 q(x)$. An upper limit on η^2 is thus obtained by setting $\bar{q}(x)$ to zero. In the experimental analysis one has made use of the inequality

$$\eta^2 \leq \left[\frac{d^2\sigma^{\bar{\nu}}}{dx\,dy} - (1-y)^2\, \frac{d^2\sigma^{\nu}}{dx\,dy}\right] \Big/ \left[\frac{d^2\sigma^{\nu}}{dx\,dy} - (1-y)^2\, \frac{d^2\sigma^{\bar{\nu}}}{dx\,dy}\right]$$

within the region $x > 0.5$ and $y > 0.66$, where the systematic error associated with the subtraction in the numerator is smallest. The result

$$\eta^2 < 0.009 \qquad (90\ \%\ \text{C.L.})\,, \tag{3.35}$$

obtained at a mean four-momentum transfer squared of $< Q^2 >= 33\ GeV^2/c^2$, limits the (W_L-W_R) mixing angle ς in left-right symmetric models as shown in Fig. 3.8 (solid lines), since for ς small, $\varsigma \approx \eta/(1 - M^2_{W_L}/M^2_{W_R})$. In contrast to the limits on ς imposed by the muon decay parameters, e.g. by the ρ parameter /161/ (dashed lines) and by the measurement of $\xi P_\mu \delta/\rho$ /97/ (dotted contour), this somewhat looser constraint on the mixing angle is independent from any assumption concerning the associated right-handed neutrino.

Likewise the chiral structure of charm-changing ($\Delta C = \pm 1$) charged currents has been analysed by studying the y-distribution of $\mu^+\mu^-$ events. Such opposite-sign dimuon events have been observed in neutrino and antineutrino interactions using electronic detectors /193-196/ as well as bubble chambers /197-202/, and have been interpreted as being due to the production and subsequent semileptonic decay of charmed mesons /283,204/

$$\begin{array}{l} \nu_\mu + N \to \mu^- + D^+ + X \\ \qquad\qquad\quad \big\lfloor \to \mu^+ + Y\,. \end{array} \tag{3.36}$$

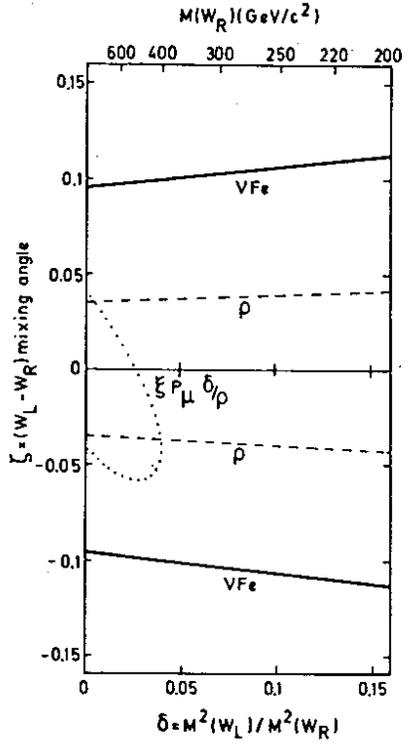

Fig. 3.8 Constraints on left-right symmetric models imposed by different experiments /97/.

In the quark-parton model the charm-producing processes are expected to be the following:

$$\begin{aligned} \nu_\mu d &\to \mu^- c \quad \sim \sin^2\Theta_C & \bar{\nu}_\mu \bar{d} &\to \mu^+ \bar{c} \quad \sim \sin^2\Theta_C \\ \nu_\mu s &\to \mu^- c \quad \sim \cos^2\Theta_C & \bar{\nu}_\mu \bar{s} &\to \mu^+ \bar{c} \quad \sim \cos^2\Theta_C \end{aligned} \tag{3.37}$$

The opposite-charged ("wrong-sign") second muon is due to

$$c \to \begin{cases} \mu^+ \nu_\mu s & \sim \cos^2\Theta_C \\ \mu^+ \nu_\mu d & \sim \sin^2\Theta_C \end{cases}, \qquad \bar{c} \to \begin{cases} \mu^- \bar{\nu}_\mu \bar{s} & \sim \cos^2\Theta_C \\ \mu^- \bar{\nu}_\mu \bar{d} & \sim \sin^2\Theta_C \end{cases}. \tag{3.38}$$

The charm origin of neutrino-induced opposite-sign dilepton events is by now fairly well established. Experimentally, it is supported by the observed small transverse momentum of the wrong-sign lepton relative to the hadron shower and by the strong enhancement at 180° of the angle between the projections of the two lepton momenta on a plane perpendicular to the neutrino direction in such events. Furthermore, the fraction of strange particle production is considerably higher than for single-muon charged-current events, in agreement with the GIM mechanism (Chap. 2.7).

The study of hadronic D decays gives evidence for the coexistence of vector and axialvector components in charm-changing charged currents since the D meson decays into states of opposite parity ($D^+ \to \bar{K}^0\pi^+$, $J^P = 0^+$ and $D^+ \to K^-\pi^+\pi^+$, $J^P = 0^-$ /205,206/). It remains to determine the chiral structure of this current.

In distinction to the single-muon cross sections, the charm-producing cross sections should be uniform in y, provided the current is pure V-A. The $(1-y)^2$ terms are absent because the interaction proceeds solely on quarks for neutrino collisions and solely on antiquarks for antineutrino collisions (3.37). Right-handed weak charm-changing currents would be characterized by $(1-y)^2$ dependences. The solid curves in Fig. 3.9 show the expected y_{vis} distributions of antineutrino-induced dimuon events /196,207/ for purely left-handed currents, taking acceptance and threshold effects /208/ into account. The dashed curve in Fig. 3.9a is the corresponding expectation for purely right-handed currents.

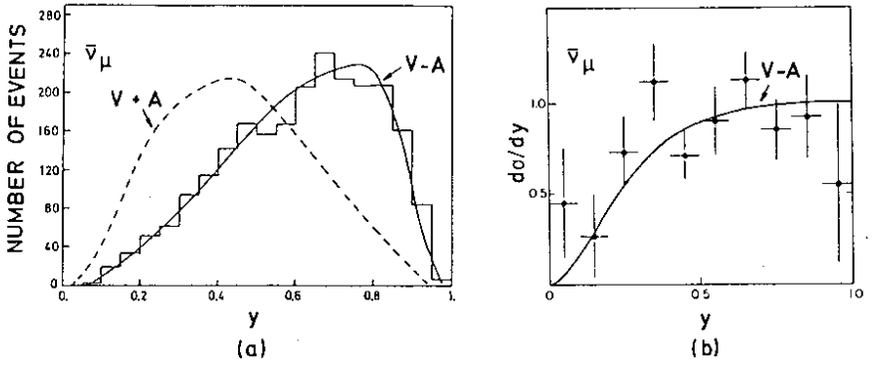

Fig. 3.9 y distributions of observed antineutrino dimuon events: (a) CDHS data /207/, (b) CHARM data /196/. The solid and dashed curves represent the V-A current and V+A current, respectively, for charm production.

The good agreement with V-A shows that only a small admixture of V+A coupling is allowed by the data. Assuming the interaction to have the form

$$\Delta\mathcal{L}_{CC}^{\Delta C=1} = \frac{G}{\sqrt{2}}\,\bar{\mu}\gamma_\alpha(1+\gamma_5)\nu_\mu\left[g_L J_\alpha^{\Delta C=1}(\text{V-A}) + g_R J_\alpha^{\Delta C=1}(\text{V+A})\right], \tag{3.39}$$

one gets quantitatively

$$\frac{g_R^2}{g_L^2+g_R^2} \begin{cases} = 0.15 \pm 0.10 & \text{(CHARM /196/)} \\ < 0.07 \quad (95\ \%\ \text{C.L.}) & \text{(CDHS /207/)}. \end{cases} \tag{3.40}$$

In conclusion, the experimental results on charged weak interactions at momentum transfers between 10 and 100 GeV^2/c^2 are well reproduced by an interaction form involving V and A currents only, combined to give dominantly left-handed coupling. This agrees well with the observed behaviour at low-momentum transfers accessible in decay processes.

4. NEUTRAL-CURRENT NEUTRINO INTERACTIONS

Since the discovery of the neutral weak current in the famous GARGAMELLE experiment /7/, many other neutrino experiments have established the existence of weak neutral-current interaction processes. It is tempting to proceed by analogy to the charge-changing weak interactions and to assume that the neutral-current interaction is also made-up of vector and axialvector currents as strongly suggested by gauge theories (Chap. 2). But nature may not always be so accommodating and the only proper way to solve the problem of the space-time structure of the weak neutral-current interaction is to determine, from experiment alone, a unique solution that could be a combination of V and A or something else.

A great deal of our understanding of charge-changing weak interactions comes from careful studies of weak decays in nuclei (Chap. 3). However, there is no opportunity to observe strangeness-conserving neutral currents in decay processes, since any decay which could occur through such currents would be overwhelmed - at these low energies - by electromagnetic processes. Therefore, one has to resort essentially to scattering experiments in order to reveal the structure of the weak neutral-current interactions.

4.1. Neutrino identity

It is generally believed that in neutrino-induced neutral-current processes

$$\nu_\mu N \to \nu' X, \qquad \bar{\nu}_\mu N \to \bar{\nu}' X \tag{4.1}$$

$$\nu_\mu e^- \to \nu' e^-, \qquad \bar{\nu}_\mu e^- \to \bar{\nu}' e^- \tag{4.2}$$

the neutral lepton in the final state is identical to the incident neutrino, where the identity may include a possible difference in helicity.

In general however, one cannot establish whether the final neutral lepton is completely or only partly identical with or completely different from the initial neutrino. But in several experimental situations, the possibility of a complete non-identity can be excluded.

Under the assumption that the neutral-current interaction is mediated by vector bosons, both the neutrino current and the non-neutrino neutral current in reactions (4.1) are necessarily Hermitian for identical ν and ν'. This implies that for kinematical configurations where a possible VA interference is required to vanish, any partial cross section has to be equal for neutrino and antineutrino semileptonic reactions /209/. Such configurations can be accomplished for exclusive reactions by going to $Q^2 \to 0$ for fixed invariant mass W of the final hadronic system, or $E_\nu \to \infty$ with W fixed, and for inclusive reactions by going to $\nu = Q^2/2ME_\nu \to 0$ or $y = 1 - E_{\nu'}/E_\nu \to 0$ /209,210/. Any deviation from the ν-$\bar{\nu}$ equality would either be evidence that incident and outgoing neutrinos are non-identical, if V and A interactions are assumed, or that non-diagonal scalar or tensor interactions contribute, if one assumes $\nu = \nu'$ (*neutrino identity*) /211/. To distinguish between these two interpretations, it is necessary to look for more direct evidence of possible S, P, T currents /26,27,42/, as discussed in the following.

Under the assumption that the neutral weak current is made-up of a linear combination of vector and axialvector covariants, the measurements

$$\left[\frac{R_{\bar{\nu}}}{R_\nu}\right]_{y=0}^{Fe-Target} = 0.95 \pm 0.15\ (\text{stat}) \pm 0.12\ (\text{syst}) \quad (\text{CDHS } /212/) \tag{4.3}$$

$$\left[\frac{d\sigma(\bar{\nu})}{dy} \Big/ \frac{d\sigma(\nu)}{dy}\right]_{y=0}^{I=0\ Target} = 1.16 \pm 0.14 \qquad \text{(CHARM /213/)} \qquad (4.4)$$

support the concept of neutrino identity within the experimental uncertainty. R_ν, $R_{\bar{\nu}}$ are the neutral- to charged-current cross-section ratios.

It is, in principle, possible to settle the question of neutrino identity by studying the scattering of electron-neutrinos or -antineutrinos on electrons

$$\nu_e e^- \rightarrow \nu' e^-, \qquad \bar{\nu}_e e^- \rightarrow \bar{\nu}' e^- \qquad (4.5)$$

where, differently from most neutral-current processes, both charged- and neutral-current contributions should be involved.

The unseen outgoing neutrino produced by the well-known charged current interaction will be a ν_e ($\bar{\nu}_e$), and not some new particle. Therefore, an experimental demonstration that neutral and charged current contributions do interfere will prove that, at least some of the time, the ν' ($\bar{\nu}'$) produced by the neutral-current interaction is also a ν_e ($\bar{\nu}_e$), and not some new particle /214/. At present, there is a reactor $\bar{\nu}_e e$-experiment /215/ that has already been completed. For $\nu_e e$-scattering, there are preliminary results from an experiment using neutrinos from the beam dump at LAMPF /216/, and also plans for measurements using neutrinos from decays of accelerated K_L^0's /217/. The results of the reactor experiment and the LAMPF experiment are of limited statistical significance, however consistent with interference being present.

Sehgal /218/ has pointed out that a measurement of the energy distribution of the recoil electron in low-energy $\bar{\nu}_e e$ scattering (4.5) should provide a precise test of neutrino identity. Allowing for the most general combination of V and A interactions, this distribution is expected to have the form /219/

$$\frac{d\sigma}{dE_e} = 2\frac{G^2 m_e}{\pi}\left[a + b\left(1 - \frac{E_e}{E_\nu}\right)^2 - c\frac{m_e E_e}{E_\nu^2}\right] \qquad (4.6)$$

where a, b, c are constants ($a, b \geq 0$) and E_e is the kinetic energy of the recoil electron. The c term, accessible only in low energy experiments because of its energy dependence, represents interference between interactions of opposite chirality /209/ and provides so a crucial test of neutrino identity. One can prove that for a situation where the state $\bar{\nu}'$ has an overlap with the state $\bar{\nu}_e$, i.e. when

$$0 \leq |< \bar{\nu}_e \mid \bar{\nu}' >| \leq 1\,, \qquad (4.7)$$

the coefficients a, b, and c must satisfy the relation

$$c^2 = a\{b - 1 + |< \bar{\nu}_e \mid \bar{\nu}' >|^2\}\,. \qquad (4.8)$$

Although this question has not been settled conclusively because of lack of data, it will be assumed in the following that in neutrino-induced neutral-current processes the outgoing neutral lepton is identical to the incident neutrino.

4.2. Helicity properties of the weak neutral current induced by neutrinos

Subsequently it is intended to discuss experimental observables from which one may determine which of the five possible covariants S, P, T, V, and A occur in neutrino-induced neutral-current interactions using electron and hadron targets, respectively. This implies essentially a study of the helicity structure of the weak leptonic current since V, A currents couple left-handed neutrinos always to left-handed neutrinos, while S, P, T currents couple left-handed neutrinos to right-handed neutrinos only (Chap. 3.1).

4.2.1. Indications from neutrino scattering on electrons

The purely leptonic interactions of neutrinos with electrons

$$\nu_e e^- \rightarrow \nu_e e^- \qquad (4.9)$$

$$\bar{\nu}_e e^- \rightarrow \bar{\nu}_e e^- \qquad (4.10)$$

$$\nu_\mu e^- \rightarrow \nu_\mu e^- \qquad (4.11)$$

$$\bar{\nu}_\mu e^- \rightarrow \bar{\nu}_\mu e^- \qquad (4.12)$$

are the simplest reactions to study the Lorentz structure of the neutral weak force. The electron is the only free point-like target existing in nature, and the main corrections to the zero-order diagram of the weak interaction are the well-known electromagnetic higher-order corrections.

For muon-neutrinos (antineutrinos) the elastic amplitudes are – to lowest order in weak interaction – due to neutral-current exchange in the t channel (Fig. 4.1 a), whereas for electron-neutrinos (antineutrinos) additional charged-current exchange in the crossed channels (Fig. 4.1 b,c) has to be taken into account.

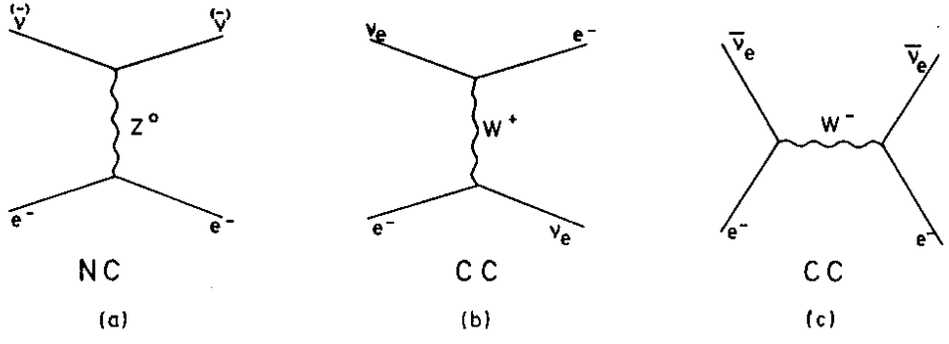

Fig. 4.1 Diagrams for neutrino-electron scattering.

The differential cross section for neutrino-electron scattering in terms of the dimensionless parameter ξ, the ratio of neutrino (antineutrino) laboratory energies, is given by /220/

$$\frac{d\sigma}{d\xi} = \frac{G^2 m_e E_\nu}{2\pi}\left[A + 2B\xi + C\xi^2 + \frac{m_e}{E_\nu}D(1-\xi)\right], \tag{4.13}$$

provided that one limits the exchange of angular momentum to zero and one in the t channel. The coefficients A, B, C, and D are related to the V, A, S, P, and T couplings:

$$\begin{aligned} A &= \frac{1}{2}\left\{(g_S+g_T)^2 + (g_P+g_T)^2 + 2(g_V+g_A)^2\right\} \\ B &= \frac{1}{2}\left\{2g_T^2 - g_S^2 - g_P^2\right\} \\ C &= \frac{1}{2}\left\{(g_S-g_T)^2 + (g_P-g_T)^2 + 2(g_V-g_A)^2\right\} \\ D &= \left(g_S^2 - g_T^2\right) + \left(g_A^2 - g_V^2\right), \end{aligned} \tag{4.14}$$

and energy conservation relates the parameter ξ to the inelasticity $y = E_e/E_\nu$ by

$$y + \xi = 1 + \frac{m_e}{E_\nu}, \tag{4.15}$$

where m_e denotes the electron mass.

Neutrino and antineutrino elastic cross sections are simply related by crossing properties, for instance, those of the electrons /220/. If time reversal invariance is assumed as suggested by experimental limits on electric dipole moments of atoms and molecules /221-223/, one gets

$$A^{\bar\nu} = C^\nu, \qquad B^{\bar\nu} = B^\nu, \qquad C^{\bar\nu} = A^\nu, \qquad D^{\bar\nu} = D^\nu. \tag{4.16}$$

The same four constants thus describe both neutrino and antineutrino scattering.

Therefore the distinction between neutrino and antineutrino cross sections is governed by the coefficients A and C, implying that for pure S, P and pure T currents neutrino and antineutrino cross sections are equal, and that the difference of the two cross sections has a definite energy dependence whatever interactions are present:

$$\frac{1}{E_\nu}\left(\frac{d\sigma^\nu}{d\xi} - \frac{d\sigma^{\bar\nu}}{d\xi}\right) \sim (1-\xi^2). \tag{4.17}$$

A violation of this relation would indicate that the present theory of weak interaction has to be revised /27/. At high energy ($E_\nu \gg m_e \rightarrow \xi \approx 1 - y$) the finite energy corrections (D terms) can be ignored:

$$\begin{aligned} \frac{d\sigma}{dy}\left(\nu_\mu e^- \rightarrow \nu_\mu e^-\right) &= \frac{G^2 m_e E_\nu}{2\pi}\left[A + 2B(1-y) + C(1-y)^2\right] \\ \frac{d\sigma}{dy}\left(\bar\nu_\mu e^- \rightarrow \bar\nu_\mu e^-\right) &= \frac{G^2 m_e E_\nu}{2\pi}\left[C + 2B(1-y) + A(1-y)^2\right]. \end{aligned} \tag{4.18}$$

These two y distributions are non-negative for any value of y in the physical region (0, 1). Taking into account the expressions (4.14) for A, B, and C one thus obtains the positivity constraint

$$B^2 \le AC, \tag{4.19}$$

from which bounds for the ratio of the total cross section can be derived (by integrating (4.18))

$$\begin{aligned} &\frac{\sqrt{7}-2}{\sqrt{7}+2} \le \frac{\sigma^{\bar\nu}}{\sigma^\nu} \le \frac{\sqrt{7}+2}{\sqrt{7}-2} \\ &(\simeq 0.14) \qquad\qquad (\simeq 7.19) \end{aligned} \tag{4.20}$$

These bounds reduce to

$$\frac{1}{3} \le \frac{\sigma^{\bar\nu}}{\sigma^\nu} \le 3 \tag{4.21}$$

in the case of vector and axialvector currents only (B = 0).

The two possibilities cannot be distinguished by means of experimental cross-section ratios /224,225/ since those are well covered by the more stringent V, A limits. Within the relatively large experimental uncertainties the cross-section ratio is even compatible with unity, as expected for any pure interaction (V, A, S, P, or T), since a difference in neutrino and antineutrino cross sections can only be caused by an interference between two interactions with different charge conjugation C, e.g. VA, ST or PT interference terms.

A non-vanishing B coefficient in the cross section (4.18) will be direct evidence for the presence of S, P, T in the neutral current. B = 0 is a necessary but not sufficient condition for the absence of S, P, T terms, since in this case the y distributions of high-energy νe-scattering are compatible with a pure V, A solution or with a pure S, P, T solution or an infinity of both types /26,27/ (*confusion theorem*). In the data of the Aachen-Padua Collaboration /224/ ($< E_\nu > \simeq 2\,GeV$) consistency of B with zero has been found from a combined fit to the neutrino and antineutrino cross sections.

The low-energy corrections (D terms), however, could be useful to disentangle the ambiguity due to the confusion theorem, provided that the incident beam energy is only of the order of a few MeV. If then the experimental data turn out to be compatible with B = 0, one gets some new information by determining the parameter D, since

(a) $D^2 \le AC$ for S, P, T, V, A,

(b) $D^2 = AC$ for V, A with identical neutrinos and

(c) $D^2 < AC$ for S, P, T

being present, provided that $AC \neq 0$ /220/. Unfortunately, a clean determination of the parameter D is very difficult.

Observation of an interference term between charged- and neutral-current interactions in $\overset{(-)}{\nu}_e e$-scattering would also help to resolve the ambiguity due to the confusion theorem, since both interactions won't interfere unless they contribute to the same helicity amplitudes. Unfortunately, the interactions of electron-neutrinos (antineutrinos) are rather poorly known. For a comparison of $\nu_e\,(\bar\nu_e)$ and $\nu_\mu\,(\bar\nu_\mu)$ scattering one has to assume that the $\overset{(-)}{\nu}_e e$ charged

current is purely V-A and that μ-e universality holds – a hypothesis not tested up to now for neutrinos (on the contrary there seems to exist a negative indication from the beam dump experiments /47/). A direct experimental test of the equality between the couplings of ν_e and ν_μ to the neutral weak boson(s) could be performed by comparing the cross sections for the processes $\nu_e N \to \nu_e X$ and $\nu_\mu N \to \nu_\mu X$.

The cross section σ for $\nu_e e$-scattering is expected to arise from diagrams as illustrated in Fig. 4.2, where the possibility is taken into consideration that several neutral weak bosons Z_i^0 could participate in the interaction.

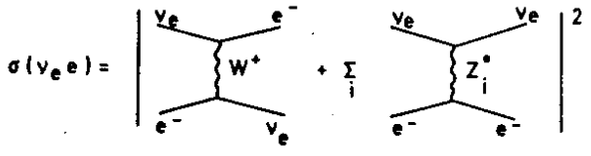

Fig. 4.2 Cross section σ for ν_ee-scattering as a sum over neutral and charged current diagrams. An arbitrary number of weak neutral bosons is assumed.

Eq. (4.13) applies equally well to elastic scattering of neutrinos (antineutrinos) of both families without any specific assumption concerning the weak charged current. But in order to compare $\overset{(-)}{\nu}_\mu e$- and $\overset{(-)}{\nu}_e e$-scattering, the discussed assumptions are needed, leading immediately to the following relations for the coupling constants:

$$\begin{aligned} g_V' &= g_V + 1, \\ g_A' &= g_A + 1, \\ g_j' &= g_j \quad \text{for j = S, P, T}. \end{aligned} \tag{4.22}$$

The coefficients A, B, C and D of the energy distributions are therefore related by

$$\begin{aligned} A^e &= A^\mu + 4(g_V + g_A) + 4 \\ B^e &= B^\mu \\ C^e &= C^\mu \\ D^e &= D^\mu + 2(g_A - g_V). \end{aligned} \tag{4.23}$$

The B and C coefficients of the differential cross sections are the same for both $\nu_\mu e$- and $\nu_e e$-scattering since they arise from neutral-current interactions only. Translating these two

equalities into relations between differential or total cross sections, one finds

$$\frac{\sigma(\nu_e e^-) - \sigma(\nu_\mu e^-)}{\sigma(\bar{\nu}_e e^-) - \sigma(\bar{\nu}_\mu e^-)} = 3. \tag{4.24}$$

This relation is valid, if μ-e universality holds, whatever interactions are present /220,226/.

The difference of cross sections involved in equation (4.24) provides a sensitive test for S, P, and T terms in the neutral-current interaction:

$$\Delta\sigma = \sigma_{\nu_e e} - \sigma_{\nu_\mu e} \leq \frac{G^2 m_e E_\nu}{2\pi}\left[4\sqrt{A^\mu} + 4\right]. \tag{4.25}$$

This turns into an equality for maximal neutral current - charged current interference, implying that the neutral current contains no S, P, or T contribution – provided that μ-e universality holds and that the $\nu_e e$ charged current has a pure V-A structure.

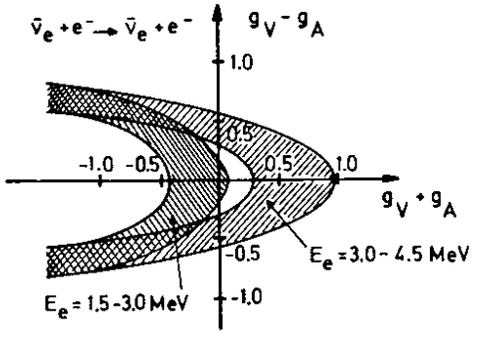

Fig. 4.3 Allowed range of (g_V+g_A) and (g_V-g_A) as determined from $\sigma(\bar{\nu}_e e)$. The shadowed regions correspond to the data from two different ranges of the electron recoil energy E_e /215/.

Corresponding to Fig. 4.2, the cross section for $\nu_e e$-scattering is given schematically by

$$\sigma(\nu_e e) \sim |C|^2 + |N|^2 + I, \tag{4.26}$$

where $|C|^2$ is the square of the charged-current amplitude and is known from muon decay, $|N|^2$ is the square of the neutral-current amplitude assumed to be known from ν_μ and $\bar{\nu}_\mu$ measurements, and I is a possible interference term /226/. An experimental demonstration that such an interference term is present, would prove that at least some of the time the neutral-current interaction preserves neutrino helicity as the charged current interaction does. This

would imply that at least a part of this interaction has V, A rather than S, P, T structure and furthermore that the left-handed electron participates in neutral weak interactions, because it is the left-handed electron that participates in the charged weak interactions. The only part of the neutral interaction which can interfere with the charged one is that involving the V-A neutral current of the electron. Therefore, $I \sim (g_V + g_A)$ is expected (Eq. 4.23). Since $(g_V + g_A) \sim (\sin^2\theta_W - 1/2)$ in $SU_2 \times U_1$ gauge models (Table 2.3), this implies $I < 0$ for the currently accepted values of $\sin^2\theta_W$.

The existing $\overset{(-)}{\nu}_e e$ results /215,216/ do not establish that the interference term is there. But if one assumes it to be present, then these data provide evidence that $I < 0$, as shown in Fig. 4.3 for the reactor data, where the only regions allowed by the two energy bins (Chap. 4.3.1.3) correspond to negative values of $(g_V + g_A)$.

4.2.2. Search for trident production

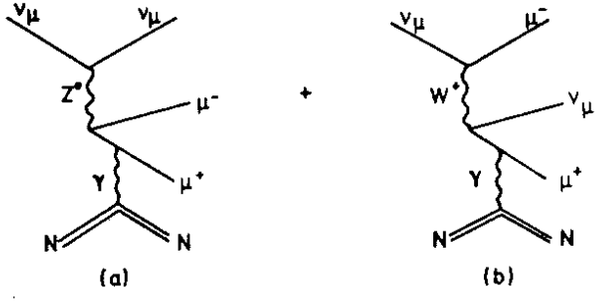

Fig. 4.4 Diagrams for neutrino trident production $\nu_\mu N \to \nu_\mu \mu^+ \mu^- N$ mediated by a neutral (a) resp. charged (b) vector boson.

Neutrino trident production /228/ is yet another way of revealing the space-time structure of the neutral weak force. The coherent lepton pair production by neutrinos in the Coulomb field of nuclei in the reactions

$$\begin{aligned} \overset{(-)}{\nu}_\mu N &\to \overset{(-)}{\nu}_\mu e^+ e^- N \\ \overset{(-)}{\nu}_e N &\to \overset{(-)}{\nu}_e \mu^+ \mu^- N, \end{aligned} \tag{4.27}$$

where the target nucleus participates as a whole, can only proceed via neutral-current exchange, whereas the trident production in

$$\overset{(-)}{\nu}_\mu N \to \overset{(-)}{\nu}_\mu \mu^+ \mu^- N \tag{4.28}$$

$$\overset{(-)}{\nu}_e N \to \overset{(-)}{\nu}_e e^+ e^- N \tag{4.29}$$

can be mediated both by neutral and charged currents and thus provides another possibility to study neutral current-charged current interferences (Fig. 4.4). With increasing experimental sensitivity, the reactions (4.28) could finally offer the possibility to investigate indirectly the processes $\overset{(-)}{\nu}_\mu \mu^- \to \overset{(-)}{\nu}_\mu \mu^-$ which are closely connected to $\overset{(-)}{\nu}_e e^- \to \overset{(-)}{\nu}_e e^-$.

The CHARM Collaboration has searched for neutrino trident production /229/. Out of 1.5×10^6 neutrino-induced and 1.8×10^6 antineutrino-induced charged-current events, candidates were selected with two muons with $p_\mu > 7$ GeV/c and without visible hadronic recoil ($E_H \leq 200$ MeV). Another signature for events due to reactions (4.28) is a low invariant $\mu^+\mu^-$ mass $W_{\mu^+\mu^-}$. Applying therefore a cut at $W_{\mu^+\mu^-} \leq 0.8$ GeV and subtracting possible background (due to semileptonic hadron decays), a signal of 1.7 ± 1.7 events could finally be attributed to coherent $\mu^+\mu^-$ pair production off the target nuclei ($CaCO_3$). From this, the coupling constant G_d of the diagonal four-fermion interactions (4.28) can be extracted

$$G_d = (0.75 \pm 0.40)\, G, \tag{4.30}$$

in agreement, within the very large error, with negative interference between the $W^\pm$ and Z^0 exchange diagrams as predicted by the standard model ($G_d = 0.77\, G$). This result points to a V, A structure of the neutral weak interaction although this conclusion suffers very much from lack of statistics. The result obtained imposes an upper limit on the diagonal leptonic coupling constant

$$G_d < 1.5\, G \qquad (90\ \%\ \text{C.L.}), \tag{4.31}$$

in agreement with a CDHS result /32/ of

$$G_d < 1.6\, G \qquad (90\ \%\ \text{C.L.}). \tag{4.32}$$

4.2.3. Expectations from low-energy neutrino physics

Low-energy neutrino physics with definite nuclear states may elucidate the space-time structure of the neutral weak interaction since nuclei are not subject to the confusion theorem /26,27/ discussed in Chap. 4.2.1 for νe-scattering. For energies of the order of some few MeV, the nucleons can be treated non-relativistically, implying that the Dirac spinors Ψ can be replaced by two-component spinors Φ (i.e. only the upper components of the nucleon fields Ψ remain). In the non-relativistic approximation, the Dirac covariants listed in Table 2.1, reduce to the form in Table 4.1 /2/.

In this approximation only two nuclear matrix elements remain, usually called Fermi and Gamow-Teller matrix element, respectively. Consequently nuclear transitions are called Fermi or Gamow-Teller transitions depending on whether the lepton pair is in a singlet state or in a triplet state. This determines the change of the nuclear spin as summarized in Table 4.2.

Table 4.1. Non-relativistic limit of the basic nuclear matrix elements.

Type	Relativistic expression	Non-relativistic approximation
S	$\bar{\Psi}_a \Psi_b$	$\Phi_a^+ \Phi_b$
V	$\bar{\Psi}_a \gamma^\mu \Psi_b$	$\delta_{\mu o} \Phi_a^+ \Phi_b$
T	$\bar{\Psi}_a \sigma^{\mu\nu} \Psi_b$	$\Phi_a^+ \sigma_j \Phi_b$ for $\mu = k \neq 0$; $\nu = 1 \neq 0$ 0 for μ or $\nu = 0$
A	$\bar{\Psi}_a \gamma^\mu \gamma_5 \Psi_b$	$-\Phi_a^+ \sigma_k \Phi_b$ for $\mu = k \neq 0$ 0 for $\mu = 0$
P	$\bar{\Psi}_a \gamma_5 \Psi_b$	0

Table 4.2. Couplings involved in Fermi and Gamow-Teller transitions.

Transition	Spin of lepton pair	Change of nuclear spin	Couplings involved
Fermi	0	0	S, V
Gamow-Teller	1	0, 1 ($0 \to 0$ forbidden)	T, A

In neutrino scattering, the behaviour of the helicity (no flip for V, A, flip for S, T) can strongly affect angular distributions, particularly when the target is a nucleus with specified angular momentum in its initial and final states /26/. Only S and V interactions are responsible for the pure Fermi transitions (Table 4.2):

$$\begin{aligned} \nu + {}^{20}Ne\,(0^+,\ I=0) &\to \nu + {}^{20}Ne\,(0^+,\ I=0) \\ \nu + {}^{22}Ne\,(0^+,\ I=1) &\to \nu + {}^{22}Ne\,(0^+,\ I=1)\,. \end{aligned} \tag{4.33}$$

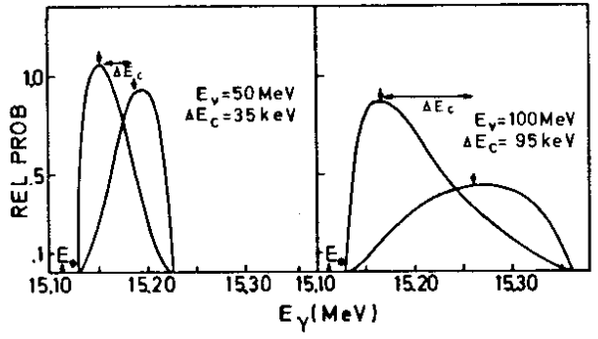

Fig. 4.5 Energy spectrum od photons emitted along the beam direction from the 15.11 MeV level of ^{12}C excited by inelastic scattering of 50 MeV (a) resp. 100 MeV (b) neutrinos. The spectrum peaked at the lower energy arises from the tensor interaction, the other from the axialvector interaction /26/.

The center-of-mass angular distribution

$$\frac{d\sigma}{d\Omega} \sim A_S^2\,(Q^2) \cdot (1 - \cos\Theta) + A_V^2\,(Q^2) \cdot (1 + \cos\Theta) \tag{4.34}$$

for these reactions may provide a handle to distinguish between S and V interactions by observing the nuclear recoil in the elastic scatterings (4.33). The isospin properties of the nuclear form factors A_S and A_V can be probed by comparing scattering from $^{20}Ne(0^+,\ I=0)$ with scattering from $^{22}Ne(0^+,\ I=1)$ /26/.

In a pure Gamow-Teller transition

$$\nu + {}^{12}C(0^+) \to \nu + {}^{12}C^*(1^+) \tag{4.35}$$

the helicity rule leads to the following center-of-mass angular distributions:

$$\frac{d\sigma}{d\Omega} \sim \alpha_A^2 \left\{ \begin{matrix} 0 & M=1 \\ 1+\cos\Theta & M=0 \\ 1-\cos\Theta & M=-1 \end{matrix} \right\} + \alpha_T^2 \left\{ \begin{matrix} 0 & M=1 \\ 1-\cos\Theta & M=0 \\ 1+\cos\Theta & M=-1 \end{matrix} \right\} \tag{4.36}$$

when the neutrino energy is not too high. α_A and α_T give the relative A and T couplings when the nucleus scatters into the magnetic substate M refered to the incident beam direction. The different angular distributions in the scattering process (4.35) lead to different γ-ray energy spectra in the subsequent radiative decay of the excited nucleus

$$^{12}C^*(1^+) \to {}^{12}C(0^+) + \gamma, \tag{4.37}$$

which should be measurable as shown in Fig. 4.5 for two different neutrino energies /26/.

The rule (Chap. 3.1) that the ν or $\bar{\nu}$ helicity will be preserved by any combination of V and A couplings and flipped by any combination of S, P, and T in scattering processes, implies that V and A will create only pairs consisting of a left-handed neutrino ν_L and a right-handed antineutrino $\bar{\nu}_R$ (or the experimental indistinguishable form $\nu_R\,\bar{\nu}_L$), whereas S, P, and T will create only pairs of the form $\nu_L\,\bar{\nu}_L$ or $\nu_R\,\bar{\nu}_R$ in decay processes. Therefore, the decay process

$$\pi^0 \rightarrow \nu\bar{\nu} \tag{4.38}$$

is forbidden by angular momentum conservation in the usual two-component neutrino theory but allowed by a pseudoscalar neutral density interaction with an estimated branching ratio relative to the $\gamma\gamma$-decay of about 3×10^{-8} /26/. This unusual decay mode might be looked for in

$$K^+ \rightarrow \pi^+\pi^0 \quad (\pi^0 \rightarrow \nu\bar{\nu}) \tag{4.39}$$

for which the signal would be a π^+ unaccompanied by other charged particles or photons. If the neutrinos are massless and couple via the S, P covariants, the $\gamma\gamma \rightarrow \nu\bar{\nu}$ amplitude could have a pole at the π or η mass, allowing an enormous conversion rate into neutrinos for temperatures of order $10^{11}\,^{\circ}K$, what could be of importance in various astrophysical phenomena /230/.

4.2.4. Study of high-energy semileptonic neutrino reactions

The most general local neutral-current interaction of neutrinos with hadrons can be written (Eq. 2.1 using Table 2.1) as

$$\begin{aligned}\mathcal{L} = \frac{G}{\sqrt{2}}\,\big[&\bar{\nu}\gamma_\alpha\,(C_V + C_V'\gamma_5)\,\nu V^\alpha + \bar{\nu}\gamma_\alpha\gamma_5\,(C_A + C_A'\gamma_5)\,\nu A^\alpha \\ &+ \bar{\nu}\,(C_S + C_S'\gamma_5)\,\nu S + \bar{\nu}\gamma_5\,(C_P + C_P'\gamma_5)\,\nu P \\ &+ \bar{\nu}\sigma_{\alpha\beta}\,(C_T + C_T'\gamma_5)\,\nu T^{\alpha\beta}\big]\,,\end{aligned} \tag{4.40}$$

where V^α, A^α, S, P and $T^{\alpha\beta}$ are the vector, axialvector, scalar, pseudoscalar, and tensor hadronic currents.

Neutrinos used in scattering experiments are always produced in charged-current reactions. Because of their V-A structure, these incident neutrinos (antineutrinos) are always left-handed (right-handed) (Chap. 3). If one thus replaces ν by $\nu_L = \frac{1}{2}(1+\gamma_5)\nu$ in each current $\bar{\nu}\Gamma\nu$, uses in addition the relations

$$\begin{aligned}&\bar{\nu}\nu_L = \bar{\nu}_R\nu_L, \quad \bar{\nu}\gamma_5\nu_L = \bar{\nu}_R\gamma_5\nu_L, \quad \bar{\nu}\sigma^{\alpha\beta}\nu_L = \bar{\nu}_R\sigma^{\alpha\beta}\nu_L \\ &\bar{\nu}\gamma^\alpha\nu_L = \bar{\nu}_L\gamma^\alpha\nu_L, \quad \bar{\nu}\gamma^\alpha\gamma_5\nu_L = \bar{\nu}_L\gamma^\alpha\nu_L,\end{aligned} \tag{4.41}$$

and absorbs the constants into the hadronic currents, a simpler form is obtained /231/:

$$\mathcal{L} = \frac{G}{\sqrt{2}}\,\big[\bar{\nu}_L\gamma_\alpha\nu_L\,(V^\alpha + A^\alpha) + \bar{\nu}_R\nu_L S + \bar{\nu}_R\gamma_5\nu_L P + \bar{\nu}_R\sigma_{\alpha\beta}\nu_L T^{\alpha\beta}\big]. \tag{4.42}$$

This reflects once more the fact that V and A currents couple left-handed neutrinos to left-handed neutrinos only, while S, P, and T currents couple left-handed neutrinos always to right-handed neutrinos, so that there is no interference possible between these different currents. Hence the V, A and S, P, T cross sections can be calculated separately.

4.2.4.1. Kinematics of neutrino-nucleon inclusive reactions

The neutrino-nucleon inclusive reaction

$$\nu + N \rightarrow l + X,$$

where l denotes the outgoing lepton ($l = \mu$, ν for charged-current and neutral-current processes, respectively) and X the hadronic part of the final state, can be characterized by three kinematic variables. Usually they are chosen to be s, Q^2, and ν or s, x, and y in the following notation:

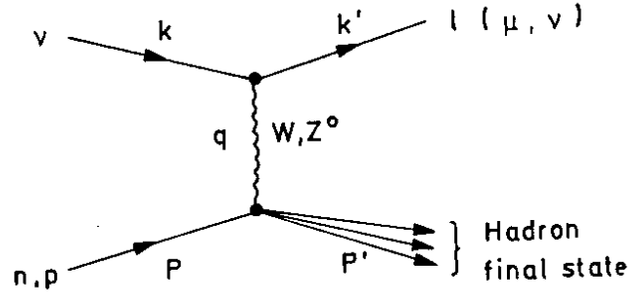

Fig. 4.6 Diagram of the neutrino-nucleon interaction.

$$
\begin{aligned}
\text{k, k', p, p'} &\equiv \text{four-momentum of } \nu,\ l,\ N,\ X \\
\text{s} &\equiv (\text{k}+\text{p})^2 \simeq 2\text{ME} \\
\text{E} &\equiv \text{energy of incident neutrino in lab frame} \\
\text{M} &\equiv \text{rest mass of nucleon} \\
\text{Q}^2 &\equiv -\text{q}^2 \equiv -(\text{k}-\text{k}')^2 \simeq 4\text{EE}'\sin^2\tfrac{\Theta}{2} \\
\text{E'} &\equiv \text{energy of outgoing lepton in lab frame} \\
\Theta &\equiv \text{lepton scattering angle in lab frame} \\
\nu &\equiv \text{p}\cdot\text{q}/\text{M} = \text{E} - \text{E'} = \text{E}_\text{H} - \text{M} \\
\text{E}_\text{H} &\equiv \text{hadron energy in lab frame} \\
\text{W}^2 &\equiv (\text{p}+\text{q})^2 = \text{M}^2 + 2\text{M}\nu - \text{Q}^2 \\
\text{x} &\equiv \text{Q}^2/2\text{M}\nu \\
\text{y} &\equiv \nu/\text{E}
\end{aligned}
\tag{4.43}
$$

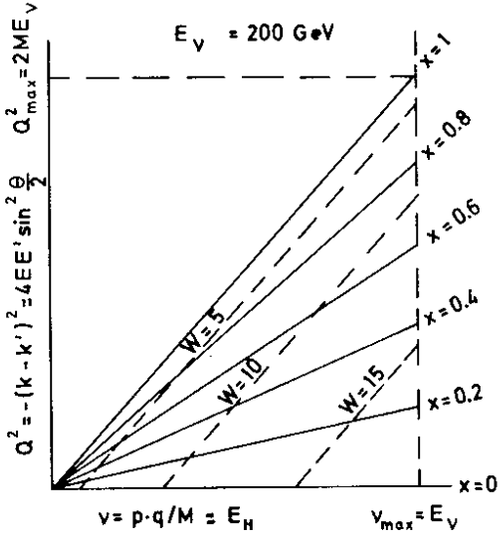

Fig. 4.7
Kinematic domain of neutrino-nucleon scattering Q^2-ν plot.

The kinematic domain probed in neutrino experiments is limited by the maximum neutrino energy, E, available. The physically allowed region in Q^2 and ν is given by the requirements: $Q^2 \leq Q^2_{max} = 2ME, \quad \nu \leq \nu_{max} = E, \quad$ and $Q^2 \leq 2M\nu$.

In the $Q^2 - \nu$ plot of Fig. 4.7 this corresponds to the triangular area which is limited by the elastic scattering line $Q^2 = 2M\nu$ ($W^2 = M^2$ or $x = 1$). Lines parallel to this line

indicate constant invariant mass W of the hadronic final state. Events of constant x are along lines originating at $\nu = Q^2 = 0$. The physically allowed domain in the x-y plot is given by

$$0 \leq x \leq 1, \text{ and}$$
$$0 \leq y \leq 1.$$

4.2.4.2. Inclusive VA cross sections

In the *Bjorken (or scaling) limit* /232/ (i.e. for high Q^2 and ν and thus necessarily large incident energy) the inclusive neutrino-nucleon cross sections in terms of the dimensionless variables x and y can be written as /233/

$$\frac{d^2\sigma^{\nu N,\bar{\nu}N}}{dx\,dy} = \frac{G^2M}{\pi}E\left[\frac{y^2}{2}2xF_1(x) + (1-y)\,F_2(x) \mp (y-\frac{y^2}{2})xF_3(x)\right], \tag{4.44}$$

where N presents an isoscalar target, i.e. a target with equal number of protons and neutrons. The three structure functions F_i are dimensionless functions of x and summarize the knowledge of the structure of the nucleon. In particular, $F_3(x)$ containing V, A interference decribes parity violation in weak interactions. The upper sign (-) of the interference term refers to neutrino-induced and the lower sign (+) to antineutrino-induced reactions. Integration over x and y yields the total cross sections

$$\sigma^{\nu N,\bar{\nu}N}_{tot} = \frac{G^2M}{\pi}E\int_0^1 F_2(x)\,dx \cdot \left\{\frac{1}{6}A + \frac{1}{2} \mp \frac{1}{3}B\right\} \tag{4.45}$$

rising linearly with the neutrino energy E. The parameters A and B are defined by

$$A = \frac{\int 2xF_1(x)\,dx}{\int F_2(x)\,dx} \qquad \text{and} \quad B = \frac{\int xF_3(x)\,dx}{\int F_2(x)\,dx}. \tag{4.46}$$

Since the cross sections (4.44) are non-negative for any value of x and y in the physical region (0,1), positivity constraints for the structure functions in the Bjorken limit can be derived

$$0 \leq |xF_3(x)| \leq 2xF_1(x) \leq F_2(x). \tag{4.47}$$

They can be translated into bounds for the ratio of the total (charged-current as well as neutral-current) cross sections

$$\frac{1}{3} \leq \frac{\sigma^{\bar{\nu}N}}{\sigma^{\nu N}} = \frac{3+A+2B}{3+A-2B} \leq 3. \tag{4.48}$$

Assuming the validity of the theoretical relation

$$2xF_1(x) = F_2(x) \tag{4.49}$$

suggested by Callan and Gross /234/ and predicted by the naive quark parton model with free spin 1/2 quarks, the double-differential cross section simplifies to

$$\frac{d^2\sigma^{\nu N,\bar{\nu}N}}{dx\,dy} = \frac{G^2M}{2\pi}E\left[\{F_2(x) \mp xF_3(x)\} + \{F_2(x) \pm xF_3(x)\}\,(1-y)^2\right]. \tag{4.50}$$

A violation of the *Callan-Gross relation*, i.e

$$R(x) = \frac{F_2(x) - 2xF_1(x)}{F_2(x)} \neq 0$$

as expected by quantum chromodynamics (QCD), would manifest itself as an extra term of the form

$$-\frac{R(x)}{2}y^2 \tag{4.51}$$

in the charged-current as well as neutral-current differential cross sections. From a fit to the neutral-current differential cross sections the CHARM Collaboration obtains

$$R = 0.10 \pm 0.10$$

in agreement with results obtained from charged-current interactions /173,235,236/. The evaluation using neutral-current events has the advantage of not being affected by radiative corrections, which play a major role in the analysis of charged-current events.

The earliest verifications of the scaling behaviour of the structure functions came at rather low energies (SLAC ep scattering and GARGAMELLE νN scattering). It was found that for $Q^2 \geq 2\ (GeV/c)^2$ the scaling hypothesis was valid at the 20 % level. This agreement could be extended to averaged data at lower Q^2 if x were replaced by an empirical parameter, $x' = Q^2/(2M\nu + a^2)$, with $a \leq 1$ GeV (*precocious scaling*).

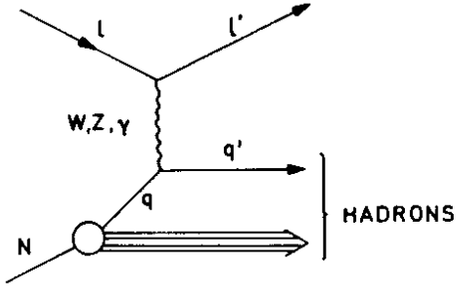

Fig. 4.8 Lepton-nucleon scattering in the simple QPM.

The scaling phenomenon has led to an interpretation of the structure of the nucleon as being composed of *point-like partons* of different types. In the *quark parton model* (QPM), where the partons are associated with the spin-$\frac{1}{2}$ quarks, the nucleons are assumed to be composed of three valence quarks which determine the quantum properties of the nucleon

and an infinite number of quark-antiquark pairs forming the so-called quark-antiquark sea. The quarks are assumed to be bound together by massless and chargeless gluons which do not interact weakly or electromagnetically.

Deep-inelastic scattering occurs when a lepton interacts with a quark or antiquark carrying the fraction x of the nucleon momentum. Because of the asymptotic freedom of QCD, at high Q^2 and ν a light quark can be considered in the zero approximation as a free and practically massless particle. After the scattering the partons rearrange themselves to form the observed final-state hadrons, as illustrated schematically in Fig. 4.8.

In this picture the inclusive cross section is the incoherent sum of all elementary parton cross sections

$$\frac{d^2\sigma}{dx\,dy} = \sum_i q_i(x) \left(\frac{d\sigma}{dy}\right)_i , \tag{4.52}$$

where the parton distribution functions $q_i(x)$, independent of Q^2 in the simple QPM approximation, specify the average number of partons of type i with a fractional momentum x. In the GIM four quark scheme /19/, the four quarks u, d, s, and c and their antiquarks have to be taken into account. Their momentum distribution functions in the proton are $xu^p(x)$, $xd^p(x)$, $xs^p(x)$, $xc^p(x)$, and $x\bar{u}^p(x)$, $x\bar{d}^p(x)$, $x\bar{s}^p(x)$, $x\bar{c}^p(x)$, where the flavour probability function $u^p(x) = q_u(x)$ is defined as the probability of finding a u quark in a proton at a given x.

For a SU_4-symmetric sea the four antiquark distributions are identical: $\bar{u}^p(x) = \bar{d}^p(x) = \bar{s}^p(x) = \bar{c}^p(x)$. Since s and c quarks exist only in the sea, one expects: $s^p(x) = \bar{s}^p(x)$ and $c^p(x) = \bar{c}^p(x)$. The quark distribution functions in the neutron and in the proton are related by isospin invariance (e.g. $u^n = d^p$, $s^n = s^p$).

The form of $(d\sigma/dy)_i$ follows simply from the spin-dependence of the elementary lepton-quark interaction, which is given by angular momentum conservation and the fact that both V and A currents preserve helicity. Therefore, the y-dependence of the lepton-quark scattering, where *both lepton and quark are left-handed or right-handed*, takes the simple form

$$\frac{d\sigma}{dy} = const \tag{4.53}$$

corresponding to an isotropic distribution in the center-of-mass frame. For the lepton-quark interaction, where *one particle is left-handed and the other is right-handed*,

$$\frac{d\sigma}{dy} \sim (1-y)^2 \tag{4.54}$$

is expected corresponding to a non-isotropic angular distribution of the scattered lepton $d\sigma/d\cos\Theta^{CM} \sim (1+\cos\Theta^{CM})^2$ with a suppression for 180° scattering in the center-of-mass system, remembering that $y = 1 - E'/E = \frac{1}{2}(1 - \cos\Theta^{CM})$ /237/.

In the quark-parton picture the structure functions are quark-momentum distribution functions in the nucleon and can be explicitly calculated /29/. In this framework the scaling behaviour of the structure functions states that for sufficiently large Q^2, such that the nucleon does not interact coherently, the structure of nucleons studied at different Q^2 is the same for constant x.

However, according to QCD, scaling is not absolute even for $Q^2 \to \infty$, $\nu \to \infty$, and $F_i(x)$ must be a logarithmic function of Q^2. This violation of scaling is due to the fact that quarks are not completely free and may emit bremsstrahlung gluons before being scattered, as illustrated in Fig. 4.9, so that the probe (γ , W, Z) of the hadron sees a smaller momentum in QCD than in the simple quark parton model.

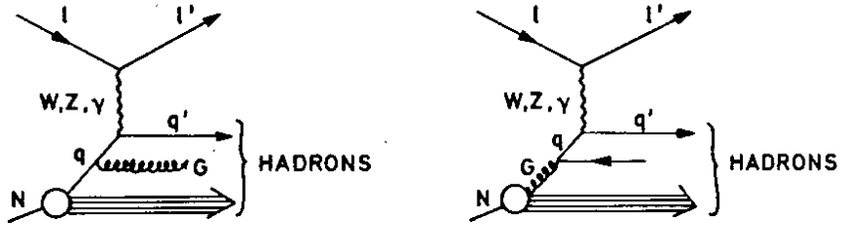

Fig. 4.9 QCD corrections to simple quark parton model (Fig. 4.8).

The quark momentum distribution is therefore shifted to a smaller x region. This results in a shrinkage (increase) of the quark momentum distribution for $x > 0.1 \sim 0.2$ ($x < 0.1 \sim 0.2$) and in an increase of the observed amount of sea quarks relative to the valence quarks as Q^2 increases, since there is more phase space for diagrams like Fig. 4.9 for larger Q^2. The parton distribution functions, and hence the structure functions, are thus expected to depend on Q^2 in addition to the x dependence.

QCD is incapable of predicting the shape of the parton distribution functions at a given momentum transfer Q_0^2. However, if the quark (and gluon) distribution functions are known for Q_0^2 then QCD predicts the variation with Q^2. Unfortunately, the theory does not give explicit analytic expressions for the Q^2 dependence of the parton x distributions themselves but for their moments

$$M_n^k(Q^2) = \int_0^1 x^{n-2} q_k(x, Q^2) dx. \tag{4.55}$$

The index $n \geq 2$ denotes the order of the moment and k stands for either valence, sea, charmed quarks, and gluons. In order to obtain the distributions themselves the inversion problem has to be solved. Buras and Gaemers /238/ have given an explicit functional form for the parton distributions $xq_k(x, Q^2)$, which satisfies the moment equations. Once the shape of the distributions at a low-Q^2 point, say at Q_0^2, is determined by fits to experimental data, the Q^2 evolution is provided by QCD depending on the value Λ, the free parameter of the theory, which determines the strength of the scaling violation.

Effects on the scaling behaviour of the structure functions, due to non-negligible quark masses compared with the momentum transfers accessible in neutrino processes, can be taken

into account by using the concept of *slow rescaling* /239,240/ which implies an appropriate redefinition of the scaling variable.

4.2.4.3. Inclusive SPT cross sections

For the S, P, T case as many as eight structure functions (neglecting the lepton mass and ignoring the structure functions arising from time-reversal violation) have to be introduced to parametrize the inclusive neutrino-nucleon cross sections. In analogy with Bjorken's scaling hypothesis for the V, A case, a scaling model for the S, P, T interactions is considered /231/. It is based on the hypothesis that for $\nu \to \infty$ and $Q^2 \to \infty$ such that x is finite, the structure functions should approach non-trivial limits depending only on the dimensionless variable x. In this scaling limit one gets (in an obvious notation)

$$\begin{aligned}\frac{d^2\sigma^{\nu N,\bar{\nu}N}}{dx\,dy} = \frac{G^2 M}{8\pi} E \big[& xy^2 \{F_{SS}(x) + F_{PP}(x)\} + 4\{x(2-y)^2 F_{TT}^{(1)}(x) \\ & + 4(1-y) F_{TT}^{(2)}(x) - 2x^2y^2 F_{TT}^{(3)}(x) + 2xy^2 F_{TT}^{(4)}(x)\} \\ & \pm 4xy(2-y)\{F_{ST}(x) + F_{PT}(x)\}\big].\end{aligned} \tag{4.56}$$

As expected from an interference between two interactions with different charge conjugation, the S-T and P-T interference terms change sign by going from neutrino to antineutrino reactions. This cross-section parametrization shows that S and/or P interactions would manifest themselves as a y^2 term, and S-T and/or P-T interferences as a $y(2-y)$ term, whereas the T interaction gives a more complicated quadratic in y.

However, it is by no means clear that the S, P, T interactions would obey this scaling. On the contrary, as Pakvasa and Rajasekaran /231/ pointed out, scaling will be violated in the S, P, T case if spin $\neq 1/2$ partons in the nucleon would participate in the neutral-current weak interactions. This is a peculiar feature of the S, P, T interactions since, in the case of V, A interactions, Bjorken scaling can be maintained for spin $\neq 1/2$ partons, too. Such a scaling break-down would manifest itself by cross sections rising faster than E or by y^3 terms in the y distributions.

By integrating Eq. (4.56) over x and y and exploiting the positivity properties of the structure functions, lower and upper bounds for the antineutrino-to-neutrino cross-section ratio $R \equiv \sigma^{\bar{\nu}N}/\sigma^{\nu N}$ can be derived:

$$\underset{(\simeq 0.14)}{\frac{\sqrt{7}-2}{\sqrt{7}+2}} \leq \frac{\sigma^{SPT}(\bar{\nu}N)}{\sigma^{SPT}(\nu N)} \leq \underset{(\simeq 7.19)}{\frac{\sqrt{7}+2}{\sqrt{7}-2}} \tag{4.57}$$

which is wider than in the V, A analog (4.48). So, if R falls outside the interval, 1/3 to 3, then there is evidence for S, P, T contributions, even with V and A present. But, as already mentioned, it turns out to be impossible to distinguish these two possibilities by means of the experimental cross-section ratios since those fall well inside the more stringent V, A limits.

To get any further, the eight scaled structure functions $F_{SS}, \ldots, F_{TT}^{(4)}$ have to be calculated. Relying just on the simple quark parton model, the tensor analogs of the Callan-Gross

relations are obtained /231,234/:

$$\begin{aligned} F_{TT}^{(1)}(x) &= F_{TT}^{(3)}(x) = 0 \\ F_{TT}^{(2)}(x) &= 2xF_{TT}^{(4)}(x)\,, \end{aligned} \tag{4.58}$$

so that the y-distribution for tensor interactions simplifies to $(2-y)^2$.

4.2.4.4. Confusion theorem

If the structure functions are evaluated in the quark-parton picture, the y-distributions for neutral-current neutrino (antineutrino)-nucleon interactions using isoscalar targets are obtained by integrating the double-differential cross sections (4.44) and (4.56) over x. They can be parametrized in the following manner /231/:

$$\begin{aligned} \frac{d\sigma^{\nu N}}{dy} &= \left(a + by + cy^2\right) \int \frac{G^2 ME}{16\pi}\, xQ(x)\, dx \\ \frac{d\sigma^{\bar{\nu} N}}{dy} &= \left(\bar{a} + \bar{b}y + \bar{c}y^2\right) \int \frac{G^2 ME}{16\pi}\, xQ(x)\, dx \end{aligned} \tag{4.59}$$

where $Q(x) = |u(x) + d(x)|/2$ in valence parton approximation. The six parameters involved in (4.59) are defined as

$$\begin{aligned} a = \bar{a} &= 2\left[\left(g_V + g_A\right)^2 + \left(g_V - g_A\right)^2\right] + 32g_T^2 \\ b &= -4\left(g_V - g_A\right)^2 - 32g_T^2 - 8g_T\left(g_S - g_P\right) \\ \bar{b} &= -4\left(g_V + g_A\right)^2 - 32g_T^2 + 8g_T\left(g_S - g_P\right) \\ c &= 2\left(g_V - g_A\right)^2 + 8g_T^2 + \left(g_S^2 + g_P^2\right) + 4g_T\left(g_S - g_P\right) \\ \bar{c} &= 2\left(g_V + g_A\right)^2 + 8g_T^2 + \left(g_S^2 + g_P^2\right) - 4g_T\left(g_S - g_P\right)\,. \end{aligned} \tag{4.60}$$

An examination of these equations shows that there are three relations among the six parameters, so that only three independent equations remain for the determination of the neutral-current coupling constants g_V, g_A, g_S, g_P, g_T:

$$\begin{aligned} a &= 4\left(g_V^2 + g_A^2\right) + 32g_T^2 \\ c + \bar{c} - a &= 2\left(g_S^2 + g_P^2\right) - 16g_T^2 \\ \bar{c} - c &= 8g_V g_A - 8g_T\left(g_S - g_P\right)\,. \end{aligned} \tag{4.61}$$

Therefore, the coupling constants for the five different interactions V, A, S, P, and T cannot be determined from the y-distributions. This is known as the *confusion theorem* /26,27,231/ which states that for inclusive cross sections any y-dependence which is possible for V, A couplings, is also possible for S, P, T currents.

Nevertheless there are certain y-dependences that cannot be simulated by V, A interactions. A rising y-distribution would be impossible for V, A unless scaling breaks down, since for any linear combination of V and A one expects

$$\begin{aligned} \frac{1}{E}\frac{d\sigma^{\nu N}}{dy} &\sim \left(g_V + g_A\right)^2 + \left(g_V - g_A\right)^2 (1-y)^2 \\ \frac{1}{E}\frac{d\sigma^{\bar{\nu} N}}{dy} &\sim \left(g_V + g_A\right)^2 (1-y)^2 + \left(g_V - g_A\right)^2\,, \end{aligned} \tag{4.62}$$

implying in particular equal cross sections for cases of pure V or pure A interactions.

If the current is a linear combination of S and P covariants,

$$\frac{1}{E}\frac{d\sigma^{\nu N}}{dy} = \frac{1}{E}\frac{d\sigma^{\bar{\nu} N}}{dy} \sim \left(g_S^2 + g_P^2\right) y^2\,, \tag{4.63}$$

is expected, and for a pure tensor current

$$\frac{1}{E}\frac{d\sigma^{\nu N}}{dy} = \frac{1}{E}\frac{d\sigma^{\bar{\nu} N}}{dy} \sim g_T^2 \left(1 - \frac{1}{2}y\right)^2\,. \tag{4.64}$$

More generally, if a y-distribution compatible with the expectations for V, A interactions (4.62) is measured, then the equation

$$c + \bar{c} - a = 0 \tag{4.65}$$

is a necessary, although not sufficient condition for the presence of V and A interactions only. On the other hand, a nonzero value for $c + \bar{c} - a$ is a sure indication of the presence of S, P, and/or T interactions.

There are astrophysical limits /241/ on possible weak neutral-tensor-current interactions which would give the neutrino dipole moments that permit it to couple directly to photons. Photons in an astrophysical plasma, with $Q^2 \neq 0$, could therefore decay into $\nu\bar{\nu}$ pairs. Such a mechanism may be relevant in stellar evolution where a transition from the high luminosity stage to the white dwarf stage takes place. However, a too high $\nu\bar{\nu}$ production rate due to the plasma-neutrino process implies that the cooling of white dwarfs would be too rapid, yielding a marked deficiency in the distribution of white dwarfs. The astrophysical cooling time infered from the distribution of white dwarfs sets the limit $g_T/G \leq \frac{1}{15}$ for the relative amount of the tensor-type coupling constant g_T.

If therefore a priori an absence of T contributions is assumed, the neutral-current differential cross sections may be parametrized as

$$\begin{aligned} \frac{d\sigma_{NC}^{\nu N}}{dy} &= A\left[(1-\alpha) + \alpha(1-y)^2\right] + By^2 \\ \frac{d\sigma_{NC}^{\bar{\nu} N}}{dy} &= A\left[\alpha + (1-\alpha)(1-y)^2\right] + By^2\,, \end{aligned} \tag{4.66}$$

where, according to Eqs. (4.62) and (4.63), $A \sim (g_V^2 + g_A^2)$ and $B \sim (g_S^2 + g_P^2)$. The two cross sections may just be added since there is no interference between S, P, T and V, A because of opposite helicities in the final state. The ratio B/A gives the relative proportions of S and/or P and V, A contributions.

From a simultaneous fit of Eqs. (4.66) to the experimental differential cross sections $d\sigma/dy$ corrected for resolution and acceptance (Fig. 4.10), the CHARM Collaboration /213/ quotes $B/A = -0.05 \pm 0.05$ implying thus

$$\frac{g_{SP}^2}{g_{VA}^2} \leq 0.03 \qquad (95\ \%\ \text{C.L.}), \tag{4.67}$$

where g_{SP}^2 and g_{VA}^2 are the S, P and V, A total coupling strengths. This is a considerable improvement upon the previous published limits /212,242-244/.

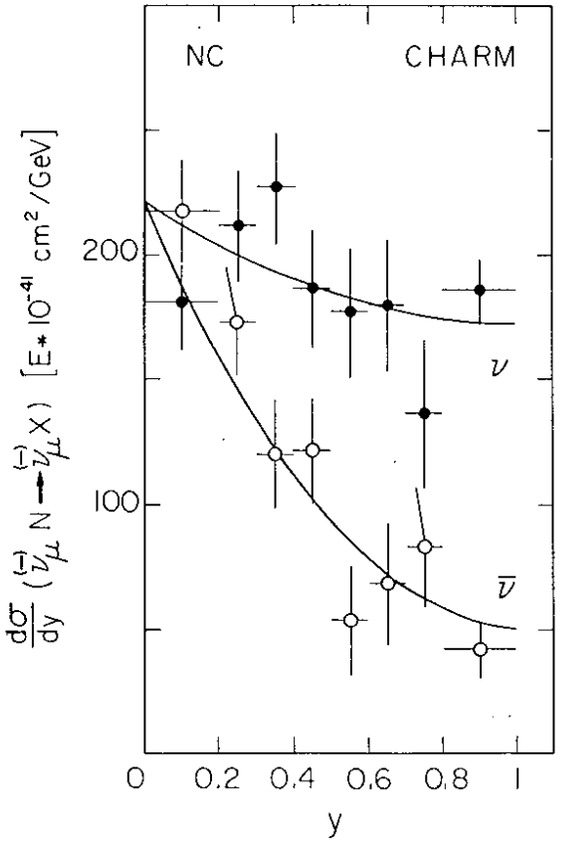

Fig. 4.10

Neutral-current differential cross sections, $d\sigma/dy$, after resolution unfolding and acceptance correction /213/. The curves correspond to the two-parameter fit of Eq. (4.66) for B = 0.

The confusion theorem in its original version /26,27,231/ established only that under the assumption of scaling any y-distribution of an inclusive cross section, which is compatible with V, A, is also compatible with S, P, T.

Lackner /28/ proved an even stronger version of this confusion theorem which states that S, P, T coupling can mimic more than only y-distributions of V, A cross sections, even if positivity constraints on the hadron tensor – determined essentially by the matrix elements of the weak hadronic currents between the initial and final hadronic states – are taken into account. It is found that the positivity domain of S, P, T contains that of V, A /28,245/. Hence, while V, A may not always be able to simulate S, P, T because the corresponding V, A tensor fails to be positive, S, P, T can always simulate V, A interactions. Nevertheless the positivity constraints are rather restrictive, so that appropriate additional constraints on S, P, T could make it impossible to simulate the corresponding V, A case /28/.

The Q^2-dependence of the hadronic tensor in the limit of $Q^2 \rightarrow 0$, for instance, does generally not impose such an appropriate constraint, so that by means of the behaviour of the differential cross section $d\sigma/dQ^2$ no discrimination between V, A and S, P, T coupling is possible /28/, although some special coupling ambiguities may be resolvable /211/.

4.2.4.5. Coherent π^0 production

In order to distinguish V, A from S, P, T experimentally, more information on the hadronic final state is needed, which may be provided by the study of appropriate exclusive channels. Here angular momentum conservation, for example, can lead to further restrictions on the hadronic tensor, which just rule out the only SPT hadron tensor compatible with the positivity constraints /28/.

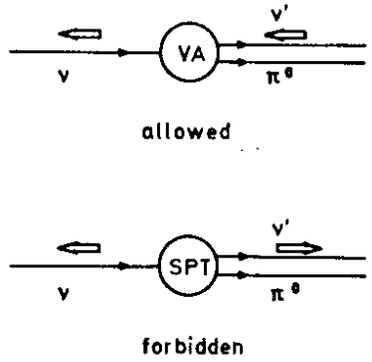

Fig. 4.11 Angular momentum configuration in coherent π^0 forward production by weak V, A resp. S, P, T currents /246/.

Coherent π^0 production on heavy nuclei

$$\nu_\mu + A \rightarrow \nu_\mu + A + \pi^0 \qquad (4.68)$$

may be a suitable process for this study /246/. In coherent pion production, responsible for the essential part of the small-angle pion production cross section, the nucleus A remains in its ground state. Therefore, neither the nucleus nor the 0^- boson, π, can take helicity from the neutral current. Hence, in exact forward production, the angular momentum conservation reduces to a conservation of the neutrino spin. This implies, that coherent π^0 production in forward direction is not allowed for S, P, T couplings which flip the neutrino helicity, whereas no suppression is expected for helicity preserving V, A currents (Fig. 4.11).

In fact, the pion can only couple to the isovector axialvector current /246/. The contribution of the vector current vanishes for forward neutrino scattering, because of CVC (hypothesis of conserved vector current), and is suppressed in general. Therefore, the process will be essentially parity-conserving. This leads to equal ν_μ and $\bar{\nu}_\mu$ cross sections.

Numerical calculations of the pion angular distributions, using the optical model approximation /246/, indicate a clear difference between S, P, T and V, A (Fig. 4.12 b, c) provided that the pion does not carry away nearly all the available energy (Fig. 4.12 a).

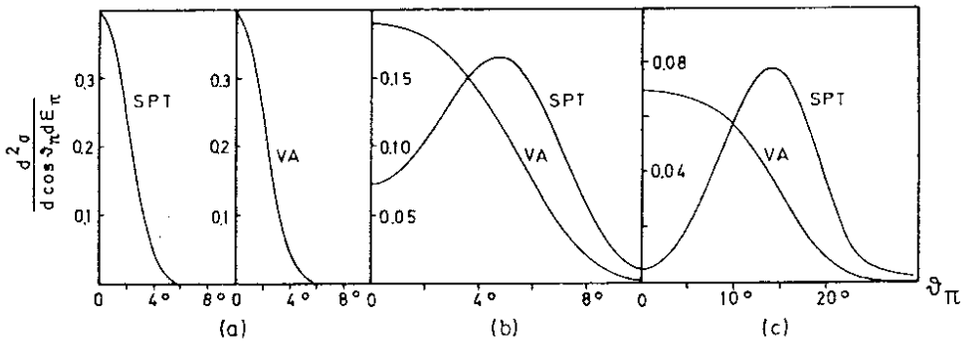

Fig. 4.12 The cross section $d^2\sigma/dE_\pi d\cos\vartheta_\pi$ for coherent π^0 production in arbitrary units as a function of ϑ_π. E_π = 2 GeV and E_ν = 2.05 GeV (a), E_ν = 2.3 GeV (b), and E_ν = 20 GeV (c) /246/.

The emission of the pion in forward direction ($\vartheta_\pi \approx 0$) implies in general a nearly forward scattering of the neutrino ($\vartheta_\nu \approx 0$), provided that the energy of the incident neutrino is significantly greater than the pion energy E_π. For S, P, T interactions however, forward scattering of the neutrino is forbidden by angular momentum conservation, implying thus a strong suppression of forward scattered pions. This relation between the scattering angle

of pion and neutrino, and thus this argumentation, is spoilt if the pion energy is not very different from the incident neutrino energy. In this case the neutrino can be scattered in all directions and still provide the small transverse momentum needed to balance the transverse momentum of the pion /246/.

To discriminate between V, A and S, P, T currents one thus has to measure the energy of the pion, its angular distribution and, in addition, the energy of the incident neutrino, i.e. such a study can only be performed in narrow-band beam experiments. Such experiments will thus presumably lack statistics since the total cross section for coherent π^0 production (4.68) is only a small fraction ($\sim$ 0.1 %) of the total neutrino cross section. But if one assumes that only vector and axialvector currents are present, already the experimental observation of coherent π^0 production provides valuable information about the V, A composition and isospin structure of the neutral weak current.

4.2.4.6. Production of vector mesons

Because of the special form of the S, P, T angular distribution (Fig. 4.12) due to the strong suppression in forward direction, a study of coherent π^0 production is not well-suited to exclude an additional S, P, T current hidden behind a V, A contribution. In the case of coherent π^0 production V, A interactions, if present, will always preponderate possible S, P, T interactions unless the coupling of the S, P, T currents is much stronger than the coupling of the axialvector current to produce a cross section of the same order of magnitude /246/.

From this point of view the study of coherent ρ^0 production

$$\nu_\mu + A \rightarrow \nu_\mu + A + \rho^0 \qquad (4.69)$$

at small momentum transfers, Q^2, seems to be more suitable for establishing a S, P, T contribution to the neutral current /246/. Since the ρ^0 has spin 1, angular momentum conservation leads to a suppression of ρ^0 production in forward direction for V, A couplings (assuming CVC), whereas the angular distribution of the ρ^0 is expected to be enhanced in forward direction if S, P, T couplings contribute. Therefore, ρ^0 production at $Q^2 = 0$ (i.e. forward scattered neutrino) is only possible for S, P, T currents or non-conserved vector currents. These two possibilities could be disentangled by means of the energy spectrum of the ρ^0 decay products which is different for different helicity states of the ρ^0 (ρ^0 carries helicity 0 if it is produced by V, A currents, and helicity -1 if S, P, T currents are responsible).

Quite generally, the experimental study of diffractive production of vector and/or axialvector mesons in charged-current /247/ and neutral-current interactions /248,249/ could help to reveal the space-time structure and isospin composition of the weak currents. In diffractive processes, characterized by momentum transfers (Q^2) of a few GeV^2/c^2 at the leptonic vertex and small momentum transfers (t) at the hadronic vertex (see Fig. 4.13), Pomeron exchange is expected to be the dominant exchange in the t channel.

The amplitudes for both the charged-current and neutral-current processes involve thus a matrix element of the weak current between the vacuum (or Pomeron) and the observed vector meson state, $< V |J_{weak}| 0 >$ /248/. This implies that the current J_{weak} has a component with quantum numbers identical to those of the vector meson. Therefore, diffractive production of vector and/or axialvector mesons can be an interesting tool to elucidate the isospin nature of the current and its V, A content. ρ^0 production, for example, will filter

out the isovector vector component of the neutral current , ω and Φ production its isoscalar vector component, and the observation of A_1 will be an indication of an isovector axialvector contribution. In the framework of the standard model, for instance, the electroweak mixing angle could be infered from the relative production of vector and axialvector mesons.

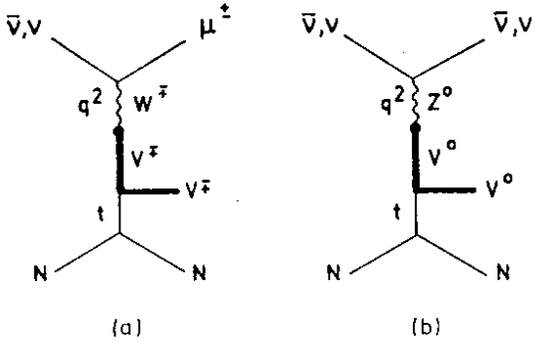

Fig. 4.13 Neutrino (antineutrino) elastic diffractive production of charged (a) and neutral (b) vector mesons V.

At present, there exist only upper limits /250/ or only indications /251/ for diffractive production of Φ and A_1 by neutral-current interactions, not in contradiction to the standard model. An experiment at FNAL /252/ has reported the observation of diffractive ρ^0 production by neutral currents in antineutrino reactions $\bar{\nu} N \rightarrow \bar{\nu} N \rho^0$. In the GWS model, the ratio of the cross section for this neutral-current process relative to that of $\bar{\nu} N \rightarrow \mu^+ N \rho^-$ is expected to be proportional to $1/2\alpha^2 = 1/2(1 - 2\sin^2\Theta_W)^2$, allowing thus the determination of the electroweak mixing angle. The result is $\alpha = 0.44 \pm 0.18$ implying thus $\sin^2\Theta_W = 0.28 \pm 0.09$.

Furthermore, the CDHS Collaboration /253/ found experimental evidence for the diffractive production of J/Ψ mesons in weak neutral-current reactions. The signal for J/Ψ production, seen in the $\mu^+\mu^-$ mass spectrum of neutrino-induced dimuon events with only small hadronic recoil, corresponds to the spectrum averaged cross section

$$\sigma_{diff}(\nu N \rightarrow \nu \Psi N) = (4.2 \pm 1.5)\, 10^{-41}\ cm^2/\text{nucleon}\,. \qquad (4.70)$$

This is in agreement with Z^0-gluon fusion models /254/ where vector and axialvector currents are supposed to contribute with equal weight. Vector dominance calculations /248,255/ predict a cross section an order of magnitude lower. However, as Sehgal /252/ pointed out, it remains to be understood why a fusion mechanism, involving the emission of a gluon from the nucleus (Fig. 4.14), should be relevant to a diffractive reaction in which the target is hardly excited.

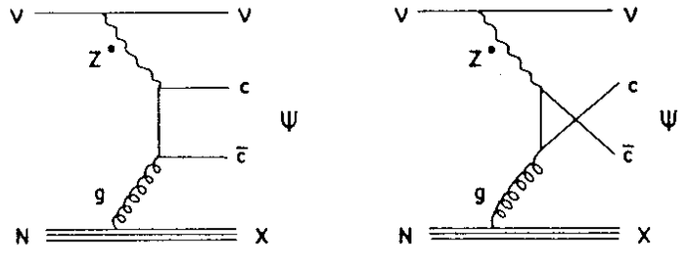

Fig. 4.14 Diagrams for Z^0-gluon (g) fusion mechanism of $c\bar{c}$ production.

4.2.4.7. Polarization phenomena

In order to settle the question of the existence or non-existence of S, P and T in weak neutral currents, measurements of the polarization of the baryons involved in neutrino-hadron inclusive or exclusive scattering may help. But a measurement of the initial nucleon polarization alone (i.e. target polarization) in inclusive neutrino and antineutrino reactions turns out to be not sufficient to resolve the VA/SPT ambiguity /256/. This is just a reflection of the fact that the transfer of helicity at the leptonic vertex, the essential difference between S, P, T and V, A, cannot be infered unambiguously from target polarization alone in inclusive processes.

Certainly, measurements of both target and recoil nucleon polarizations would be an interesting tool to disentangle the Lorentz structure of the currents /257/. However, such nucleon polarization experiments are difficult, if not impossible to perform. Fortunately, it can be shown /258/ that measurements of the final baryon polarizations alone in neutrino-baryon elastic and quasi-elastic scattering could help to reveal the space-time structure of the neutral weak force. Hence the reactions

$$l(\mathrm{k}) + B(\mathrm{p}) \rightarrow l'(\mathrm{k}') + B'(\mathrm{p}') \qquad (4.71)$$

are considered. Their kinematics are illustrated in Fig. 4.15. B and B' are the initial and final baryons, l and l' are the initial and final neutrinos (ν_μ or $\bar{\nu}_\mu$).

The laboratory-frame polarizations of the final baryon are defined with respect to the orthonormal vectors /259/

$$\vec{e}_{\mathrm{L}} = \frac{\vec{\mathrm{p}}'}{|\vec{\mathrm{p}}'|}\,, \qquad \vec{e}_{\mathrm{T}} = \frac{(\vec{\mathrm{p}}' \times \vec{\mathrm{k}}) \times \vec{\mathrm{p}}'}{|(\vec{\mathrm{p}}' \times \vec{\mathrm{k}}) \times \vec{\mathrm{p}}'|}\,, \qquad \vec{e}_{\mathrm{O}} = \frac{\vec{\mathrm{k}} \times \vec{\mathrm{p}}'}{|\vec{\mathrm{k}} \times \vec{\mathrm{p}}'|}\,, \qquad (4.72)$$

where L, T, and O refer to longitudinal, transverse and orthogonal, respectively (Fig. 4.15).

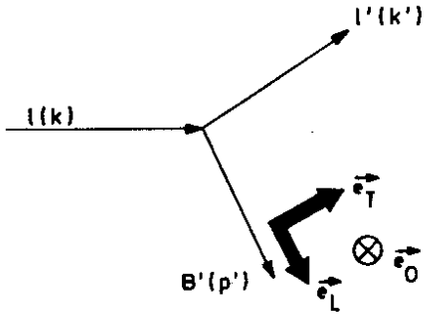

Fig. 4.15

Laboratory-frame polarizations $\vec{e}_L$, $\vec{e}_T$, $\vec{e}_O$ of the final baryons in reactions 1+B → 1'+B'.

Transverse and orthogonal polarizations of the final baryon, denoted as P_T and P_O, may be measured by observing the azimuthal asymmetries produced when the baryon rescatters via the strong interaction in the target material /260/. The longitudinal polarization P_L is hard to measure as it does not lead to rescattering asymmetries.

It has been shown /259/ that a non-zero result for P_O would imply not only time-reversal violation in the weak interactions but also, in the neutral-current case, either second-class currents or an off-diagonal coupling at the neutrino vertex (i.e. a change in neutrino type).

Neutrino-proton scattering at 0° in the center-of-mass (c.m.) frame implies that the final baryon will have average helicity -1, +1, or 0 if the hadronic current is V-A, V+A or pure V (or A), respectively. Since longitudinal polarization of the protons in the c.m. frame would appear as transverse polarization in the laboratory frame, one expects consistently a transverse polarization in the laboratory of $P_T(Q^2 = 0) = +1, -1$, or 0 for neutrino-induced as well as for antineutrino-induced reactions.

This has to be confronted with the neutrino-helicity flipping S, P, T case (Table 4.3), where angular momentum conservation at $Q^2 \equiv -(k-k')^2 = 0$ requires that the recoil baryon must have the same helicity in the c.m. frame as the final ν_μ or $\bar{\nu}_\mu$. Therefore, at 0° the final baryon has helicity ± 1 for $\nu_\mu p\,(\bar{\nu}_\mu p)$ scattering in the c.m. system which corresponds to $P_T(Q^2 = 0) = \mp 1$ in the laboratory /258/.

It is expected that the qualitative features of the $Q^2 = 0$ case, where the baryon has no recoil momentum at all, will be preserved for moderate momentum transfers ($Q^2 \simeq 0.5\ GeV^2/c^2$).

On the one hand, a measurement of the transverse polarization of the final baryon in neutrino-baryon elastic and quasi-elastic scattering could thus discriminate between pure V, A neutral currents and pure S, P, T interactions, although it might be necessary to measure the polarization in antineutrino-baryon scattering as well. Unfortunately, general admixtures of V, A with S, P, T – the only remaining conceivable possibility at the present experimental

knowledge – cannot be easily resolved by this method.

On the other hand, if the weak neutral force is assumed to contain only vector and axialvector components, a measurement of the transverse polarization of the recoil proton in $\nu_\mu p\,(\bar{\nu}_\mu p)$ elastic scattering could effectively discriminate between competing gauge theory models /259/.

Table 4.3. Transverse polarizations P_T of the final proton in the lab system for elastic $\nu_\mu p$ and $\bar{\nu}_\mu p$ scattering at zero-momentum transfer /259/.

Coupling	$P_T(Q^2=0)$ for $\nu_\mu p$	$P_T(Q^2=0)$ for $\bar{\nu}_\mu p$
V - A	+ 1	+ 1
V + A	- 1	- 1
V or A	0	0
S, P, T	- 1	+ 1

4.3. V, A composition of the neutral weak force

The presently available experimental results obtained in neutrino scattering experiments are – apart from the ambiguity problem caused by the confusion theorem – in quite good agreement with theoretical predictions based on the assumption that only vector and axialvector couplings contribute to the weak neutral current. This assumption is in addition strongly supported by the observation of electroweak interference effects in non-neutrino processes such as muon-hadron, electron-hadron and electron-positron reactions and the recent discovery of the $W^\pm$ and Z^0 particles which seem to have the required properties. However, small admixtures of S, P and T contributions can presently not be ruled out as will be discussed in the subsequent chapters.

Taking the result from the experiments as decisive for a pure V, A structure of the neutral-current interaction, the basic questions about the V, A composition and isospin structure of the neutral weak current remain to be answered.

4.3.1. Results from purely leptonic processes

The main goal of pursuing the study of neutrino scattering on electrons (4.9 - 4.12) is to determine the relative amount of vector and axialvector coupling of the leptonic weak neutral current. Here the ambiguities inherent in the use of hadronic targets disappear. Until now, however, the extremely low cross-section (~ 3 to 4 orders of magnitude smaller than the

Table 4.4. Summary of $\nu_\mu e^-$ scattering results

Experiment	$\nu_\mu e$ candidates	Background	σ/E (10^{-42}cm^2/GeV)
GGM CERN-PS /261/	1	0.3 ± 0.1	< 3 (90 % C.L.)
Aachen-Padua Counter Exp. (CERN-PS) /262/	32	20.5 ± 2.0	1.1 ± 0.6
GGM CERN-SPS /263/	9	0.5 ± 0.2	$2.4^{+1.2}_{-0.9}$
BNL-COL FNAL 15' /264/	11	0.5 ± 0.5	1.8 ± 0.8
VMNOP Counter Exp. (FNAL) /265/	46	12	1.4 ± 0.3
CHARM Counter Exp. (CERN-SPS) /266/	83 ± 16		1.9 ± 0.4 (stat) ± 0.4 (syst)
E734 Counter Exp. (BNL) /267/	51 ± 9		1.6 ± 0.29 (stat) ± 0.26 (syst)

Table 4.5. Summary of $\bar{\nu}_\mu e^-$ scattering results

Experiment	$\bar{\nu}_\mu e$ candidates	Background	σ/E (10^{-42}cm^2/GeV)
GGM CERN-PS /261/	3	0.4 ± 0.1	$1.0^{+2.1}_{-0.9}$
Aachen-Padua Counter Exp. (CERN-PS) /262/	17	7.4 ± 1.0	2.2 ± 1.0
GGM CERN-SPS /268/	0	< 0.03	< 2.7 (90 % C.L.)
FMMS FNAL 15' /269/	0	0.2 ± 0.2	< 2.1 (90 % C.L.)
BEBC-TST (CERN-SPS) /270/	1	0.5 ± 0.2	< 3.4 (90 % C.L.)
CHARM Counter Exp. (CERN-SPS) /266/	112 ± 21		1.5 ± 0.3 (stat) ± 0.4 (syst)
E734 Counter Exp. (BNL) /267/	59 ± 10		1.16 ± 0.20 (stat) ± 0.14 (syst)

total νN cross section because of the light target of mass m_e) has drastically limited the number of observed events, as illustrated in Tables 4.4 and 4.5.

There exist seven experiments /261-267/ which have published results on the $\nu_\mu e^- \to \nu_\mu e^-$ cross section. For $\bar{\nu}_\mu e^- \to \bar{\nu}_\mu e^-$ only four experiments /261,262,266,267/ have obtained a positive result, while three experiments /268-270/ have quoted upper limits near the expected level for the signal.

The experiments may be roughly divided into two categories: bubble chamber experiments which are very clean (background typically < 10%) but have low event rates, and counter experiments which are able to obtain moderately high event rates, but have significantly larger backgrounds /29/.

4.3.1.1. FNAL and BNL counter experiments

The most precise results on $\nu_\mu e$ ($\bar{\nu}_\mu e$) scattering have been obtained using fine-grain electronic calorimeters. As the target particle has a small mass, m_e, the final-state electron in νe elastic scattering is emitted in a narrow forward cone satisfying the relation

$$\Theta^2 = \frac{(E_\nu - E_e)}{E_\nu} \cdot \frac{2m_e}{E_e} \leq \frac{2m_e}{E_e}. \qquad (4.73)$$

This provides a signal peaking in the forward region, while the backgrounds have much broader angular distributions.

To select νe reactions it is thus necessary to identify isolated forward electromagnetic showers and to measure precisely their angle. The remaining backgrounds are then composed of $\overset{(-)}{\nu}_e$ quasi-elastic interactions, involving $e^\pm$ in the final-state, and $\overset{(-)}{\nu}_\mu$ neutral-current interactions, including coherent π^0 production. To determine the relative amount of these two background components it is important to be able to distinguish electrons from photons in some sample of data. This will be discussed in more detail in the next chapter, where the CHARM experiment is described.

The VPI-Maryland-NSF-Oxford-Peking (VMNOP) Collaboration /265/ extracted from a total of ~ 249 000 neutrino interactions observed at Fermilab in a high-angular-resolution electromagnetic shower detector (±5 mrad at 4 GeV and little energy dependence) with a fiducial target weight of 8.26 tons, a final sample of 313 events exhibiting isolated forward electromagnetic showers. Fig. 4.16 shows their angular distribution. Events with angles smaller than 10 mrad are candidates for $\nu_\mu e$ scattering; events with larger angles are assumed to represent the background, mainly due to quasi-elastic $\overset{(-)}{\nu}_e$ interactions. Extrapolating the background in the region $\Theta < 10$ mrad yields 34 events for the process $\nu_\mu e^- \to \nu_\mu e^-$. From this, a cross section of

$$\sigma(\nu_\mu e)/E_\nu = (1.40 \pm 0.30) \times 10^{-42}\ cm^2/\text{GeV}$$

has been evaluated, applying corrections for the electron detection efficiency (54 %), for the electron energy cut at 4 GeV and for the trigger efficiency for the monitor reactions ($\nu_\mu N \to \mu^- X$ and $\nu_\mu N \to \nu_\mu X$) /271/. The quoted error is statistical only.

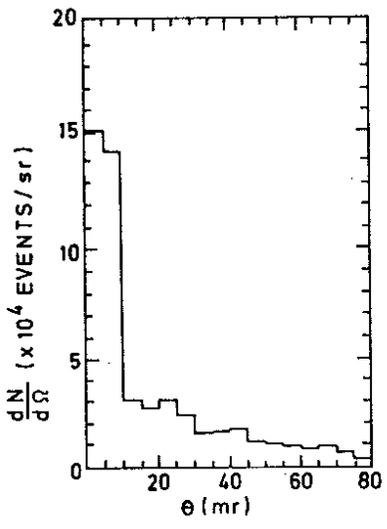

Fig. 4.16

Evidence for $\nu_\mu e$ scattering in the FNAL counter experiment /265/.

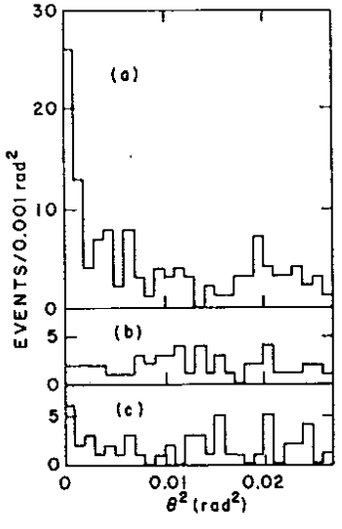

Fig. 4.17

Distribution in Θ^2 of showers which (a) are selected as e-candidates and (b) as γ-candidates by the e/γ algorithm. (c) distribution in Θ^2 of the γ-induced sample (E734 Coll. /267/).

A measurement with similar precision was reported recently by the E734 Collaboration /267/ using neutrinos (antineutrinos) of mean energy 1.5 (1.4) GeV from the Brookhaven National Laboratory alternating gradient synchrotron and a massive (75 tons fiducial target weight), predominantly active (> 90 %), high-resolution detector. It is composed of vertical planes of liquid scintillator and proportional drift tubes measuring the lateral positions. This set-up provides a measured angular resolution for electron showers of 16 mrad/$\sqrt{E_e}$, about half the kinematic limit (4.73) for elastic scattering. Out of $\sim 10^6$ neutrino and $\sim 2 \cdot 10^6$ antineutrino events a primary event sample of 316 (735) events has been selected with a single, clean electromagnetic shower at angle $\Theta \leq 0.18$ rad.

To separate electron and photon showers an algorithm based on the energy deposited in the first scintillator plane following the shower vertex and a minimized average of the pulse heights in the adjacent propotional drift tube cells was used. Fig. 4.17 shows the distribution in Θ^2 for isolated forward showers identified as electron showers (a) and photon showers (b). The energy of the selected showers is limited to the interval $210 \leq E_e \leq 2100$ MeV to reduce backgrounds. For comparison, the Θ^2 distribution for a control set of unambiguously recognized photon-showers is shown (Fig. 4.17c). The electron sample exhibits a clear peak in the forward region, while the photon distributions are flat in this region. The signal of 51 ± 9 electrons from $\nu_\mu e^- \rightarrow \nu_\mu e^-$ scattering, extracted from the Θ^2 distribution, can be translated into a cross section of

$$\sigma(\nu_\mu e)/E_\nu = \left[1.60 \pm 0.29\ (\text{stat}) \pm 0.26\ (\text{syst})\right] \times 10^{-42}\ cm^2/\text{GeV}\,.$$

For $\bar{\nu}_\mu e^- \rightarrow \bar{\nu}_\mu e^-$ scattering a cross section of

$$\sigma(\bar{\nu}_\mu e)/E_\nu = \left[1.16 \pm 0.20\ (\text{stat}) \pm 0.14\ (\text{syst})\right] \times 10^{-42}\ cm^2/\text{GeV}\,.$$

is quoted. The fully corrected ratio of the normalized cross sections for $\nu_\mu e$ and $\bar{\nu}_\mu e$ scattering yields the value

$$R = 1.38^{+0.40}_{-0.31}\ (\text{stat}) \pm 0.17\ (\text{syst})\,,$$

that determines the electroweak mixing angle to

$$\sin^2 \Theta_W = 0.209 \pm 0.029\ (\text{stat}) \pm 0.013\ (\text{syst})\,.$$

4.3.1.2. CHARM experiment

The CHARM Collaboration /266/ has measured the cross sections for the two reactions $\nu_\mu e^- \rightarrow \nu_\mu e^-$ and $\bar{\nu}_\mu e^- \rightarrow \bar{\nu}_\mu e^-$ using the same detector (with a fiducial target mass of 80 tons). The detector consists mostly of marble, has an average density $< \rho > \simeq 1.3\ g/cm^3$ and the average atomic number $< Z > \simeq 13$. The same criteria are used for the selection of neutrino and antineutrino events and the same cuts are applied. The ratio of the cross sections therefore determines the coupling constants of the leptonic weak neutral current with an experimental uncertainty which is smaller than in a measurement of a single cross section. In particular, many of the systematic errors tend to cancel out in the ratio.

Both the $\nu_\mu e$ and $\bar{\nu}_\mu e$ candidate events have been selected out of about 2 million neutrino and antineutrino interactions, respectively, by searching for isolated forward electromagnetic showers. The electron direction was determined by measuring the spatial distribution of the energy deposition of the shower in the calorimeter, using 1 cm wide streamer tubes, 3 cm wide proportional tubes and 15 cm wide scintillators. The apparatus measures the angle of the final-state electromagnetic shower with the resolution given in Table 4.6. For a part of the data /272/ the resolution is somewhat worse, since the detector was not fully equipped at that time.

Table 4.6. Measured angular resolution for electron showers

$E_{electron}$ (GeV)	5	7.5	10	15	20	30
$\sigma(\Theta)$ (mrad)	12.9	10.9	9.7	8.3	7.6	6.8

This resolution, $\sigma(\Theta) \sim 32$ mrad/$\sqrt{E_e/\text{GeV}}$, turns out to be sufficient to reject most of the background reactions which are expected to have a much wider angular distribution due to the kinematics of scattering on a heavy target mass (nucleon).

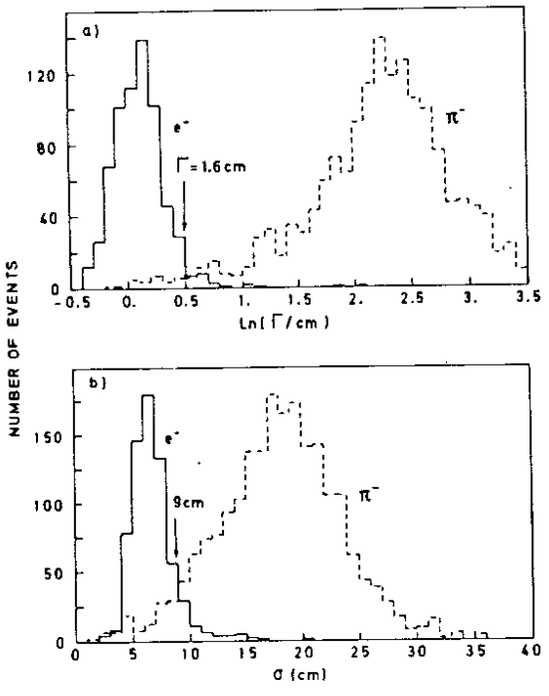

Fig. 4.18

Distributions of the width of 20 GeV electron and pion showers, (a) as measured by the scintillators and (b) as measured by the proportional tubes /266/.

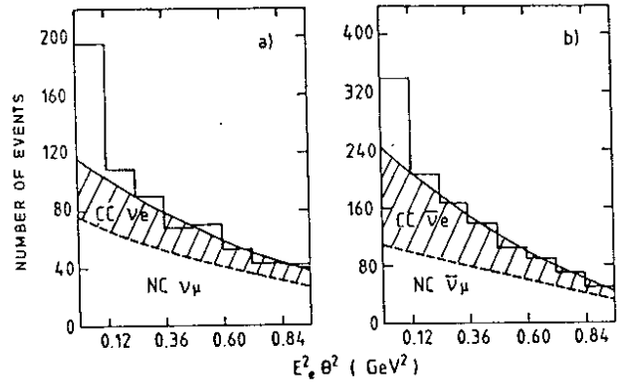

Fig. 4.19 Distribution of the selected events as a function of $E_e^2\theta^2$ (a) for neutrinos, (b) for antineutrinos (CHARM data) /266/. The dashed line shows the background due to neutral-current $\overset{(-)}{\nu}_\mu$ reactions, the shaded area is the background due to charged-current $\overset{(-)}{\nu}_e$ reactions.

Electromagnetic and hadronic showers are separated by the characteristic difference of their transverse energy profile. The results of measurements of the width of showers induced by electrons and pions are shown in Fig. 4.18. The lateral shower profile, as measured by the scintillator system, was used to calculate the width Γ of a Cauchy distribution fitted to the central part of the shower. A second parameter, σ, was determined by the rms width of the shower profiles as measured in a larger fiducial area by the proportional drift tubes. Correlations among the two width estimators are expected, as they measure both the same aspect of the shower. However, Γ parametrizes the width of the shower core, while σ is more sensitive to the tails of the shower profiles. Selecting events as indicated in the figure ($\Gamma < 1.6$ cm and $\sigma < 9$ cm) reduces the background due to semileptonic neutrino interactions by a factor of ~ 100.

The candidates for neutrino and antineutrino scattering on electrons have been searched for among events appearing as narrow showers (Γ and σ cuts), which is the characteristic of showers initiated by a single electron, photon, or π^0 /273/. Moreover, the angle Θ between the shower axis and the direction of the incoming neutrino beam was required to be smaller than 100 mrad. Only events with a shower energy E_e deposited in the calorimeter between 4 GeV and 30 GeV have been retained in the final sample, where the upper cut is applied to eliminate high-energy events due to elastic and quasi-elastic charged-current reactions induced by the ν_e ($\bar{\nu}_e$) component of the beam; the lower cut is applied to limit the energy dependence of the angular resolution for electron showers (Table 4.6). The $E_e^2\Theta^2$ distributions of the selected neutrino and antineutrino events are shown in Fig. 4.19. The $E_e^2\Theta^2$ variable was chosen because it emphasizes the different characteristics of the signal with respect to the background. A clear peak in the forward direction ($E_e^2\Theta^2 < 0.12\ GeV^2$) demonstrates a genuine $\overset{(-)}{\nu}_\mu e^- \rightarrow \overset{(-)}{\nu}_\mu e^-$ signal over a background which is assumed to be due to two sources:

(a) Elastic and quasi-elastic charged-current events induced by the ν_e and $\bar{\nu}_e$ contamination of the beam.

(b) Neutral-current events with γ and/or π^0 in the final state produced by coherent scattering of muon-neutrinos on nuclei.

The normalization of background (a) and (b) was obtained by a study of the energy deposition (E_F) in the first scintillator plane following the shower vertex.

As shown in Fig. 4.20, electromagnetic showers initiated by one or more photons tend to deposit in this scintillator plane an energy larger than one minimum ionizing particle (6 MeV), whilst a large fraction of the showers due to single electrons gives an energy deposition corresponding to one minimum ionizing particle.

The number of events attributed to background (a) is obtained from the number of events with $E_F < 8$ MeV in the region $0.12 < E_e^2\Theta^2 < 0.54\ GeV^2$ and from the known efficiency of this cut for elastic and quasi-elastic $\overset{(-)}{\nu}_e$-induced events. The remainder is attributed to background (b).

The shape of the two backgrounds has been studied carefully (Fig. 4.19). The $E_e^2\Theta^2$ distribution of background (a) has been determined by folding the measured $E_e^2\Theta^2$ distributions of elastic and quasielastic charged-current reactions induced by ν_μ and $\bar{\nu}_\mu$ with the measured electron energy and angular resolutions. The $E_e^2\Theta^2$ distribution of background (b) was calculated using a model for coherent π^0 production by neutrinos on nuclei /246/.

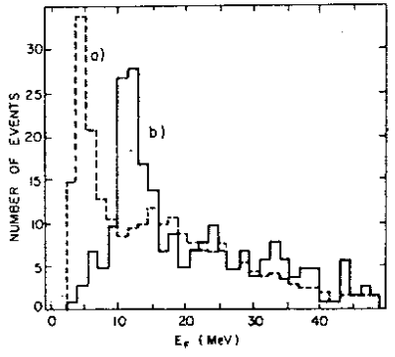

Fig. 4.20 Measured distributions of the energy deposition in the first scintillator plane following the shower vertex: (a) Showers induced by 15 GeV electrons traversing on the average half a radiation length. (b) Photon-induced showers produced by neutrino and antineutrino beams in a kinematic range where photon-induced showers due to coherent processes dominate ($7.5 < E_e < 17.5$ GeV, $E_e^2\Theta^2 > 0.54$ GeV^2). By Monte Carlo extrapolation, the contamination due to electron-induced showers is estimated to be 15% /266/.

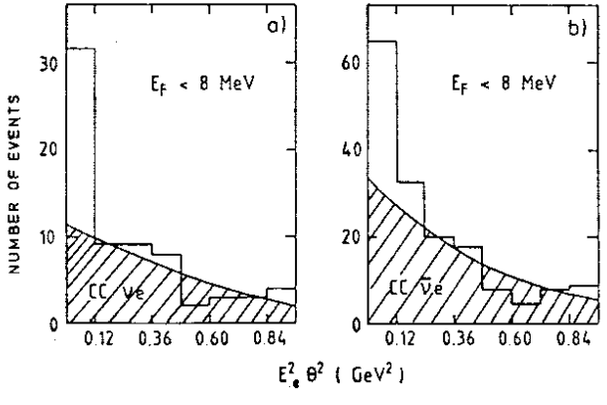

Fig. 4.21 $E_e^2\Theta^2$ distribution of the neutrino- (a) and antineutrino-induced (b) candidate events satisfying the additional criterion that the energy deposition in the first scintillator plane traversed by the showers is $E_F < 8$ MeV (CHARM data) /266/. In this case the background is only due to $\overset{(-)}{\nu}_e$ quasi-elastic scattering.

After subtraction of these backgrounds and correction for the contamination by wrong-kind neutrinos,(83 ± 16) events could be attributed to reaction $\nu_\mu e^- \to \nu_\mu e^-$ and (112 ± 21) events to reaction $\bar{\nu}_\mu e^- \to \bar{\nu}_\mu e^-$ assuming that the forward peaks are due to events with a single electron in the final state. This has been confirmed by employing an alternative method of analysing the data, which is selectively sensitive to electrons. It is based on the selection of events with one minimum ionizing particle close to the interaction vertex as expected for electron-induced showers (with reduced efficiency of course) in contrast to photon-induced showers. This is achieved by the requirement $E_F < 8$ MeV. The $E_e^2\Theta^2$ distributions for the neutrino and antineutrino events, selected by this method, are shown in Fig. 4.21.

Since the background induced by π^0's and/or γ's is cut by the requirement $E_F < 8$ MeV, the background can be subtracted by fitting the shape of the quasielastic $\overset{(-)}{\nu}_e$ background to the events outside the signal region ($E_e^2\Theta^2 > 0.12\ GeV^2$). The signals extracted by this procedure (24 ± 6 and 35 ± 9 events from the neutrino and antineutrino exposures, respectively) are in good agreement with the signals derived from the full sample of events, taking into account the different efficiencies for detecting electrons. This confirms the assumption that the forward peaks are due to events with a single electron in the final state.

The normalization of the (83 ± 16) $\nu_\mu e$ and (112 ± 21) $\bar{\nu}_\mu e$ events to the number of incoming neutrinos and antineutrinos, respectively, was done by making use of the known /274/ neutrino (antineutrino)-nucleon total cross section and the quasi-elastic charged-current $\nu_\mu N$ cross section. Correcting the observed $\nu_\mu e$ and $\bar{\nu}_\mu e$ events for acceptance and for the selection criteria, the following cross sections have been obtained:

$$\sigma(\nu_\mu e)/E_\nu = \left[1.9 \pm 0.4\ (\text{stat}) \pm 0.4\ (\text{syst})\right] \times 10^{-42}\ cm^2/\text{GeV}$$
$$\sigma(\bar{\nu}_\mu e)/E_{\bar{\nu}} = \left[1.5 \pm 0.3\ (\text{stat}) \pm 0.4\ (\text{syst})\right] \times 10^{-42}\ cm^2/\text{GeV}\,.$$

The systematic errors are due to uncertainties in the knowledge of the background, in the normalization procedure and in the efficiency in selecting electrons. They partially cancel in taking the ratio of the two rates, $R = \sigma(\nu_\mu e)/\sigma(\bar{\nu}_\mu e)$.

Within the framework of the $SU_2 \times U_1$ theory the two cross sections can be expressed in terms of the electroweak mixing angle, $\sin^2\Theta_W$, and the multiplying factor, ρ^2, equal to the ratio of the over-all strengths of neutral-current and charged-current couplings. It follows that the cross-section ratio R provides the most direct determination of the parameter $\sin^2\Theta_W$ without any hypothesis on the value of ρ:

$$R = \frac{\sigma(\nu_\mu e)}{\sigma(\bar{\nu}_\mu e)} = 3\,\frac{1 - 4\sin^2\Theta_W + (16/3)\sin^4\Theta_W}{1 - 4\sin^2\Theta_W + 16\sin^4\Theta_W} \qquad (4.74)$$

Fig. 4.22 shows the expected behaviour of the cross-section ratio R as a function of $\sin^2\Theta_W$. From this, one can extract

$$\sin^2\Theta_W = 0.215 \pm 0.032\ (\text{stat}) \pm 0.012\ (\text{syst})\,. \qquad (4.75)$$

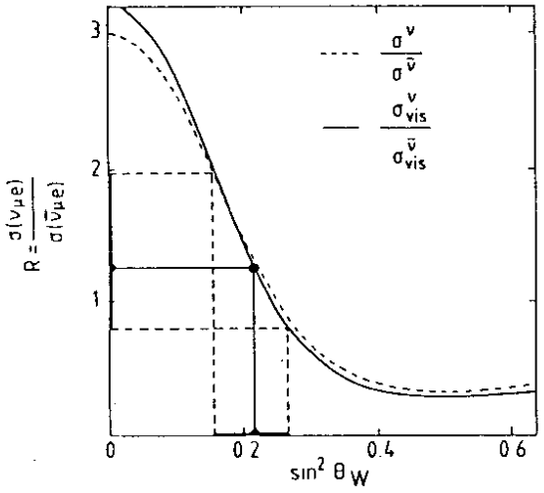

Fig. 4.22 Cross-section ratio R as a function of $\sin^2\theta_W$ compared to the expectation for full energy acceptance (dashed line) and for events in the energy range 7.5 to 30 GeV (full line) /266/.

The simultaneous measurements of R and $\sigma(\bar{\nu}_\mu e)$ allow a determination of ρ with the result

$$\rho = 1.09 \pm 0.09\ (\text{stat}) \pm 0.11\ (\text{syst}), \tag{4.76}$$

consistent with $\rho = 1$ as required by the standard model (Eqs. 2.30/2.31).

The measurements of $\nu_\mu e^- \to \nu_\mu e^-$ and $\bar{\nu}_\mu e^- \to \bar{\nu}_\mu e^-$ constrain the neutral-current coupling constants g_V^e and g_A^e

$$\frac{\sigma(\nu_\mu e)}{E_\nu} = \frac{2G^2 m_e}{3\pi}\left[g_V^{e^2} + g_V^e g_A^e + g_A^{e^2}\right] \tag{4.77}$$

$$\frac{\sigma(\bar{\nu}_\mu e)}{E_\nu} = \frac{2G^2 m_e}{3\pi}\left[g_V^{e^2} - g_V^e g_A^e + g_A^{e\,2}\right], \tag{4.78}$$

where Eqs. (4.18) have been integrated from y = 0 to y = 1, assuming only V, A components in formulae (4.14). Four values of the neutral-current coupling constants can be obtained from the measurements of R and $\sigma(\overset{(-)}{\nu}_\mu e)$, as shown in Fig. 4.23. These four solutions reflect the sign and vector-axialvector ambiguities in the couplings g_V^e and g_A^e. The sign ambiguity can be resolved by including data from reactor neutrinos.

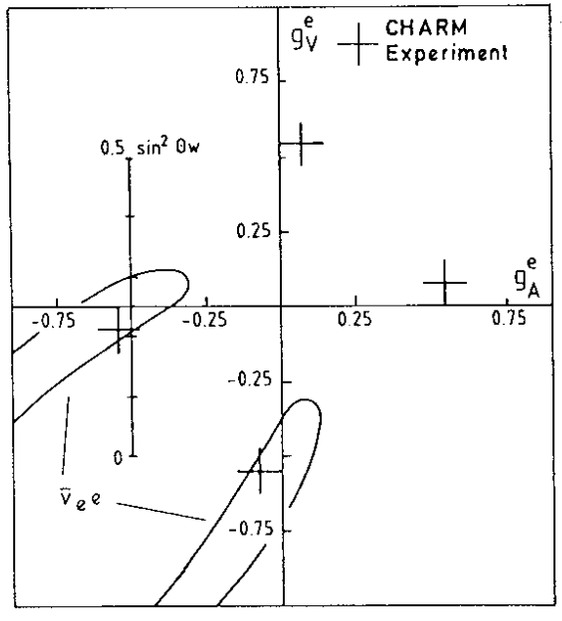

Fig. 4.23 g_A^e and g_V^e obtained from the measurement of R and of the $\nu_\mu e$ and $\bar{\nu}_\mu e$ cross sections. The 68% confidence limits from the measurement of the $\bar{\nu}_e e$ scattering cross section allow two solutions /266/.

4.3.1.3. $\bar{\nu}_e e$-scattering

The U.C.-Irvine (Savannah River) experiment /215/ on $\bar{\nu}_e e$ scattering presents separate cross sections for low (1.5 MeV $< E_e <$ 3.0 MeV) and high energy recoil electrons (3.0 MeV $< E_e <$ 4.5 MeV). The results are /276/:

$$\begin{aligned}\sigma(\bar{\nu}_e e,\ E_e > 3\ \text{MeV}) &= (1.86 \pm 0.48) \times 10^{-46}\ cm^2 \\ \sigma(\bar{\nu}_e e,\ E_e < 3\ \text{MeV}) &= (7.6 \pm 2.2) \times 10^{-46}\ cm^2.\end{aligned} \tag{4.79}$$

It has been pointed out by Avignone and Greenwood /276/ that these two results can be treated to some degree as independent experiments, since the background interferences in these two energy ranges are different.

The g_V^e, g_A^e dependence of the differential cross section for $\bar{\nu}_e e^- \to \bar{\nu}_e e^-$

$$\frac{d\sigma(\bar{\nu}_e e)}{dE_e} = \frac{G^2 m_e}{2\pi}\left[C^e + A^e\left(1 - \frac{E_e}{E_\nu}\right)^2 + D^e\,\frac{m_e E_e}{E_\nu^2}\right] \tag{4.80}$$

can be derived from Eqs. (4.14) assuming that only V and A currents contribute to the interaction and replacing g_V and g_A by $1 + g_V$ and $1 + g_A$, respectively. The "1" comes from

the charged-current contribution:

$$C^e = (g_V^e - g_A^e)^2$$
$$A^e = (2 + g_V^e + g_A^e)^2 \qquad (4.81)$$
$$D^e = (g_A^e - g_V^e)(2 + g_V^e + g_A^e) .$$

Different contibutions from integrals over the antineutrino spectrum lead to different numerical coefficients in Eq. (4.80) /276,277/:

$$\sigma(\bar{\nu}_e e,\, E_e > 3\ \text{MeV}) = F\left[0.1014\, C^e + 0.0053\, A^e + 0.0077\, D^e\right],$$
$$\sigma(\bar{\nu}_e e,\, E_e < 3\ \text{MeV}) = F\left[0.4008\, C^e + 0.0404\, A^e + 0.0373\, D^e\right], \qquad (4.82)$$

where $F = 43.0534 \times 10^{-46}\, cm^2$. The uncertainty in each coefficient is approximately 4 % /29/ and therefore negligible compared to the experimental uncertainties.

The $\bar{\nu}_e e$ data (4.79) define then bands (evaluated in ref. /275/) in the g_A^e-g_V^e plane. Because of the correction term D^e which is not negligible at reactor energies, the $\bar{\nu}_e e$ bands are slightly tilted with respect to the V-A axis (45° diagonal). As displayed in Fig. 4.23, the $\bar{\nu}_e e$ bands resolve the sign ambiguity but leave the vector-axialvector ambiguity intact. This ambiguity can experimentally only be resolved by combining the neutrino-electron results with other (essentially non-neutrino) results in a model-dependent way. It will be seen below that inclusion of the results on e^+e^- scattering or likewise the data on the asymmetry in polarized electron scattering uniquely selects the dominantly axialvector solution if factorization is assumed. A combined fit /266/ to the data ($\overset{(-)}{\nu}_\mu e$, $\bar{\nu}_e e$ and e^+e^-) selects a unique solution:

$$g_V^e = -0.08 \pm 0.07\ (\text{stat}) \pm 0.03\ (\text{syst})$$
$$g_A^e = -0.54 \pm 0.05\ (\text{stat}) \pm 0.06\ (\text{syst}), \qquad (4.83)$$

in excellent agreement with the standard model which, for $\sin^2\Theta_W = 0.22$, predicts (Table 2.3)

$$g_A^e = -0.5, \qquad g_V^e = -\frac{1}{2} + 2\sin^2\Theta_W = -0.06 .$$

The dominantly vector solution ($g_V \simeq -1/2$, $g_A \simeq 0$) which is experimentally ruled out if factorization holds, corresponds to a $SU_2 \times U_1$ model with e_R^- in a weak isospin doublet /29/.

4.3.1.4. Neutral current-charged current interference

The rection $\bar{\nu}_e e^- \rightarrow \bar{\nu}_e e^-$ (and $\nu_e e^- \rightarrow \nu_e e^-$) turns out to be of particular interest in studying the neutrino identity (Chap. 4.1) and resolving the VA/SPT ambiguity of the neutral-current space-time structure (Chap. 4.2.1). The most important thing to be learned from $\bar{\nu}_e e\,(\nu_e e)$ scattering is the sign of the neutral current-charged current interference in this reaction, depending on the sign of the coupling of the electron in the neutral current /214/. There is no other way of observing the absolute sign of the neutral current couplings of electrons and neutrinos in a model-independent way.

The various theories predict, with considerable agreement, destructive neutral current-charged current interference in $\overset{(-)}{\nu}_e e$-scattering. But one can think of models with two vector

bosons /214/ which reproduce almost all the results of the standard model but give constructive neutral current-charged current interference. In such models one boson couples to leptons and quarks exactly as in the GWS model while the other couples only to leptons with such a coupling strength that the sign of the interference term amplitude is reversed without changing its magnitude. Such models will yield a forward-backward asymmetry in $e^+e^- \rightarrow \mu^+\mu^-$ that is several times larger than the standard model prediction if μ-e universality holds.

Table 4.7. Cross sections for the $\bar{\nu}_e e^- \rightarrow \bar{\nu}_e e^-$ reactor experiment /215/ in units of σ_{V-A}, the pure charged-current cross section, compared with theoretical expectations /278/.

Case \ Electron energy	1.5 MeV < E_e < 3 MeV	3 MeV < E_e < 4.5 MeV
Destructive interference ($\sin^2\Theta_W = 1/4$)	0.85	1.1
Constructive interference	2.2	2.7
Incoherent interference	1.5	1.9
Experiment	0.87 ± 0.25	1.70 ± 0.44

In Table 4.7 the only published $\bar{\nu}_e e$-measurements /215/ are compared with the theoretical possibilities of destructive neutral current-charged current interference as predicted by the standard model for $\sin^2\Theta_W < 1/2$, or constructive interference allowed by models with at least two neutral bosons, or no coherent interference between charged and neutral currents applying to the situation that the outgoing neutrino in the neutral-current case is different from the incident one. Owing to the large errors in the experimental data, no definite answer can be given concerning the absence or presence of an interference term.

Taking into account the measured neutral-current cross sections $\sigma(\nu_\mu e)$ and $\sigma(\bar{\nu}_\mu e)$, the dominant term in $\sigma(\overset{(-)}{\nu}_e e)$ should be the charged-current contribution, followed by an expected ~ 50 % correction due to coherent neutral current-charged current interference, whereas the neutral-current term will amount to a ~ 5 % correction only. Therefore, if the charged-current contribution is assumed to be known from universality, $\sigma(\overset{(-)}{\nu}_e e)$ measurements of ~ 25 % accuracy would be sufficient to distinguish destructive from constructive interference, if coherent interference is assumed to be present. But greater precision, at the level of 10 - 15 % accuracy, would be necessary to prove that coherent interference occurs /214/.

In the LAMPF experiment /216/ neutrinos of intermediate energy have been produced by intense (a few hundreds of microamperes) proton beams which are dumped in a massive target, where the π^-'s are captured and the π^+'s generate three types of neutrinos:

$$\begin{array}{l} \pi^+ \rightarrow \mu^+ + \nu_\mu \\ \qquad\quad \hookrightarrow e^+ + \nu_e + \bar{\nu}_\mu \end{array} \tag{4.84}$$

The spectrum, as shown in Fig. 4.24, consists of a monoenergetic muon-type neutrino ν_μ (coming from a two-body decay), and of an electron-type neutrino ν_e and muon-type antineutrino $\bar{\nu}_\mu$, each with an energy spectrum characteristic of muon decay at rest, ranging from zero to 53 MeV.

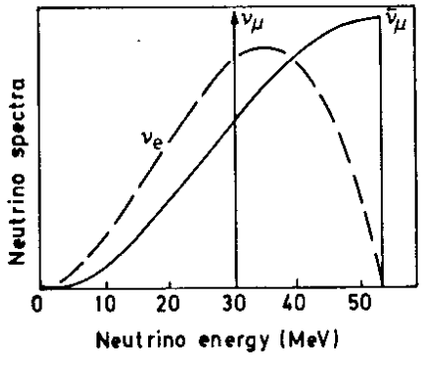

Fig. 4.24

The energy spectra of the neutrinos emitted from a beam dump /226/.

In this experiment 17.0 ± 7.4 events have been assigned to the reaction $\nu_e e^- \rightarrow \nu_e e^-$, giving a cross section of

$$\sigma(\nu_e e)/E_\nu = \left[10.6 \pm 4.6\ (\text{stat}) \pm 1.9\ (\text{syst})\right] \times 10^{-42}\ cm^2/\text{GeV}\,.$$

This value excludes a constructive interference of the charged- and neutral-current contributions, with a confidence level greater than 95 %. But negative interference as well as no interference is allowed. A more decisive result will be possible with improved statistics.

A possibility to study elastic $\nu_e e$ ($\bar{\nu}_e e$) scattering at high energy ($\sim$ 10 GeV) could be provided by the use of a $\overset{(-)}{\nu}_e$ enriched beam from the decay of accelerated K_L^0's. A selection of the semileptonic K_L^0 decays

$$K_L^0 \rightarrow \pi^-\, \mu^+\, \nu_\mu, \quad \pi^+\, \mu^-\, \bar{\nu}_\mu\,,$$

and

$$K_L^0 \rightarrow \pi^-\, e^+\, \nu_e, \quad \pi^+\, e^-\, \bar{\nu}_e\,,$$

yields a mixed neutrino beam of about 60 % ν_e and $\bar{\nu}_e$ and about 40 % ν_μ and $\bar{\nu}_\mu$, where both ν and $\bar{\nu}$ are produced with equal probability and have the same energy spectrum. The excess of $\overset{(-)}{\nu}_e$ is caused by the decay kinematics /279/. However, the beam intensity is expected to be low and there is no possibility to distinguish between $\overset{(-)}{\nu}_e$ and $\overset{(-)}{\nu}_\mu$. Therefore, the investigation of neutrino-electron elastic scattering will be limited to the measurement of the total cross section.

4.3.2. Results from neutrino-hadron scattering

Ideally the electroweak mixing angle is determined in purely leptonic reactions, which are free of hadronic corrections and uncertainties. Leptonic experiments, however, have not yet reached the desirable degree of accuracy (Chap. 4.3.1 and Chap. 7). One therefore considers semi-leptonic reactions and has then – because of the fact that hadrons are complex structures – to rely on a hadronic model to connect theoretical predictions and experimental reality.

Fortunately, the internal structure of the nucleons is now quite well known from the analysis of high-energy charged-current neutrino-nucleon and electron-nucleon reactions. The quark parton model turns out to be a very good approximation for the nucleon structure and all relevant deviations from it, such as scaling violation of the structure functions and the fraction and composition of the quark-antiquark sea as a function of Q^2, are reasonable well known (uncertainties from this sector are comparable or small compared to experimental errors of neutral-current studies). But serious theoretical and calculational difficulties still remain, e.g. in analysing exclusive pion production channels because of the existence of significant nuclear corrections and theoretical uncertainties short of reliable models of single and double pion production.

Nevertheless, the neutrino-hadron reactions are among the most essential factors in the analysis of neutral-current data. The methods /29,68,280-289/ commonly used to extract the neutral-current couplings determine the coupling constraints imposed by various sets of reactions separately, and obtain then a final allowed coupling region by taking the intersection of the regions allowed by individual sets of reactions. It has become widely customary to extract from the data the values of the various coupling constants defined by the general four-fermion Lagrangians in chapter 2.9. From a comparison of the behaviour of ν and $\bar{\nu}$ interactions the chiral structure of the quark currents may be infered, whereas searches for effects of isoscalar-isovector interference may finally reveal their isospin structure. The results are then compared with the predictions of the standard model. This strategy is also pursued in the following discussion.

4.3.2.1. Deep-inelastic scattering on isoscalar targets

The first important piece of information is obtained from data on neutrino and antineutrino inclusive scattering on isoscalar targets at high energy

$$\nu_\mu + N \rightarrow \nu_\mu + X, \qquad \bar{\nu}_\mu + N \rightarrow \bar{\nu}_\mu + X,$$

where N represents an isoscalar target. The measurements of the total cross sections from ν and $\bar{\nu}$ beams can be directly translated into a separate measurement of the left-handed (g_L)

and right-handed (g_R) coupling constants with

$$g_L^2 = \epsilon_L^2(u) + \epsilon_L^2(d)\,,$$
$$g_R^2 = \epsilon_R^2(u) + \epsilon_R^2(d)\,, \tag{4.85}$$

or, equivalently, in the framework of a $SU_2 \times U_1$ theory (Table 2.3), in which no specific value for the relative strength ρ of the neutral-current to charged-current coupling is assumed:

$$g_L^2 = \rho^2 \left(\frac{1}{2} - \sin^2\Theta_W + \frac{5}{9}\sin^4\Theta_W \right)$$
$$g_R^2 = \frac{5}{9}\rho^2 \sin^4\Theta_W. \tag{4.86}$$

In fact, the simplest parton model formalism in which the effects of QCD and the neutral-current coupling to s and c quarks are ignored, leads to

$$\sigma_{NC}(\nu N) = \frac{G^2 ME}{\pi} \int dx\, x \left\{ [u(x) + d(x)]\,[g_L^2 + \frac{1}{3}g_R^2] + [\bar{u}(x) + \bar{d}(x)]\,[\frac{1}{3}g_L^2 + g_R^2] + \ldots \right\},$$
$$\sigma_{NC}(\bar{\nu} N) = \frac{G^2 ME}{\pi} \int dx\, x \left\{ [u(x) + d(x)]\,[\frac{1}{3}g_L^2 + g_R^2] + [\bar{u}(x) + \bar{d}(x)]\,[g_L^2 + \frac{1}{3}g_R^2] + \ldots \right\},$$
$$\sigma_{CC}(\nu N) = \frac{G^2 ME}{\pi} \int dx\, x \left\{ [u(x) + d(x)] + \frac{1}{3}[\bar{u}(x) + \bar{d}(x)] + \ldots \right\}, \tag{4.87}$$
$$\sigma_{CC}(\bar{\nu} N) = \frac{G^2 ME}{\pi} \int dx\, x \left\{ \frac{1}{3}[u(x) + d(x)] + [\bar{u}(x) + \bar{d}(x)] + \ldots \right\},$$

integrating Eqs. (4.44) and assuming a pure V-A structure for the charged currents (i.e. $g_L = 1$, $g_R = 0$).

The values of the coupling constants are usually deduced from the ratios of the total cross sections from which the parton distributions drop out in the valence parton approximation. The most commonly used ratios and their Born approximation values are then

$$R_\nu \equiv \frac{\sigma_{NC}(\nu N)}{\sigma_{CC}(\nu N)} = g_L^2 + \frac{1}{3}g_R^2 = \frac{1}{2}\rho^2 \left(1 - 2\sin^2\Theta_W + \frac{40}{27}\sin^4\Theta_W \right) \tag{4.88}$$

$$R_{\bar{\nu}} \equiv \frac{\sigma_{NC}(\bar{\nu} N)}{\sigma_{CC}(\bar{\nu} N)} = g_L^2 + 3g_R^2 = \frac{1}{2}\rho^2 \left(1 - 2\sin^2\Theta_W + \frac{40}{9}\sin^4\Theta_W \right) \tag{4.89}$$

$$R_+ \equiv \frac{\sigma_{NC}(\nu N) + \sigma_{NC}(\bar{\nu} N)}{\sigma_{CC}(\nu N) + \sigma_{CC}(\bar{\nu} N)} = \frac{1}{4}\left(\alpha^2 + \beta^2 + \gamma^2 + \delta^2\right) = g_L^2 + g_R^2$$
$$= \rho^2 \left\{ \frac{1}{2} - \sin^2\Theta_W + \frac{10}{9}\sin^4\Theta_W \right\} \tag{4.90}$$

$$R_- \equiv \frac{\sigma_{NC}(\nu N) - \sigma_{NC}(\bar{\nu} N)}{\sigma_{CC}(\nu N) - \sigma_{CC}(\bar{\nu} N)} = \frac{1}{2}\left(\alpha\beta + \gamma\delta\right) = g_L^2 - g_R^2$$
$$= \rho^2 \left\{ \frac{1}{2} - \sin^2\Theta_W \right\}. \tag{4.91}$$

R_+ determines the overall-strength of the neutral-current interactions using the charged-current interactions as a reference standard, whereas Eq. (4.91), proposed by Paschos and Wolfenstein /290/, measures the VA interference of neutral-current interactions as can be seen most easily from Sakurai's notation.

This Paschos-Wolfenstein formula for $\sin^2\Theta_W$ in the GWS model is attractive theoretically in that it is almost independent of the structure functions and their scaling violations provided that they are equal in neutrino and antineutrino interactions. The main corrections to the formula involve the kinematic suppression of c (or s) quarks in charged-current interactions since relation (4.91) holds only if the charmed sea is negligible. However, these uncertainties arising from the hadronic model turn out to be small /291/, and will be reduced by future experiments determining the Kobayashi-Maskawa matrix elements (2.40) in a more refined way. A theoretical uncertainty of only 2 % due to hadronic corrections in the determination of the electroweak mixing angle seems to be feasible. However, R_- (and R_+) suffers from large experimental systematic effects due to the difficulty of normalizing neutrino and antineutrino fluxes since it involves a difference (sum) of cross sections that are measured with different spectra.

The ratios of cross sections, R_ν and $R_{\bar{\nu}}$, on the other hand, are free from systematic errors due to uncertainties in absolute flux determination. But the neutral-current parameters extracted from these ratios depend on knowing the shape of the neutrino spectrum since one has to correct for the fact that each experiment imposes a minimum hadron energy cut and a minimum muon-momentum cut to discriminate neutral-current events against hadronic background and to differentiate neutral-current events from charged-current events, respectively. In either case, the spectrum shape has to be known. Uncertainties arising from the hadronic model employed to correct the data will tend to cancel in taking the ratios.

The most useful ratio to abstract the value of $\sin^2\Theta_W$ is therefore R_ν since $\frac{dR_\nu}{d\sin^2\Theta_W} \simeq -0.67$ whereas $\frac{dR_{\bar{\nu}}}{d\sin^2\Theta_W} \simeq 0.02$ for $\sin^2\theta_W \sim 0.22$ and $\rho = 1$, so that R_ν is 30 times as sensitive to $\sin^2\Theta_W$ as $R_{\bar{\nu}}$.

Currently there exist essentially six high-energy experiments (i.e. $< E\nu > \geq 40$ GeV), performed by the HPWF (Harvard-Pennsylvania-Wisconsin-Fermilab) /242/, CITF (California Institute of Technology-Fermilab) /243/, CDHS /212,292/, ABCDLOS (Aachen-Bonn-CERN-Demokritos-London (I.C.)-Oxford-Saclay) /244/, CHARM /213,274/ and CCFRR (California Institute of Technology-Columbia-Fermilab-Rochester-Rockefeller) /293/ Collaborations, that have presented measurements of the cross section ratios (Table 4.8).

Table 4.8. Measurements of the cross-section ratios R_ν and $R_{\bar\nu}$ from high-energy experiments (i.e. $\langle E_\nu \rangle > 40$ GeV) studying ν and $\bar\nu$ inclusive scattering on (approximately) isoscalar targets and the neutral-current parameter $\sin^2\Theta_W$ (and ρ) of the GWS model extracted from these ratios. (E_{cut} denotes the hadron energy cut applied to the data. The first error quoted is the statistical one, the second the systematic one)

Experiment	Target	E_{cut} (GeV)	Cross-section ratio	$\sin^2\Theta$	ρ
HPWF /242/	CH_2	4	$R_\nu = 0.30 \pm 0.04$ b) $R_{\bar\nu} = 0.33 \pm 0.09$ b)	0.23 ± 0.06	1.0 a)
CITF /243/	Iron	12	$R_\nu = 0.28 \pm 0.03$ $R_{\bar\nu} = 0.35 \pm 0.11$	0.33 ± 0.07 d)	1.0 a)
CDHS /212,292/	Iron	10	$R_\nu = 0.301 \pm 0.007$ $R_{\bar\nu} = 0.363 \pm 0.015$	0.221 ± 0.030 e) 0.226 ± 0.012 e)	0.996 ± 0.026 1.0 a)
BEBC ABCDLOS /244/	H_2-Neon	15	$R_\nu = 0.345 \pm 0.015 \pm 0.009$ $R_{\bar\nu} = 0.364 \pm 0.029 \pm 0.009$	$0.182 \pm 0.020 \pm 0.012$ $0.170 \pm 0.030 \pm 0.010$ c)	1.0 a)
CHARM /213,274/	Marble	2	$R_\nu = 0.320 \pm 0.009 \pm 0.003$ $R_{\bar\nu} = 0.377 \pm 0.020 \pm 0.003$	0.247 ± 0.038 0.220 ± 0.014 0.230 ± 0.023 c)	1.027 ± 0.023 1.0 a)
CCFRR /293/	Iron	20	$R_+ = 0.319 \pm 0.007$ $R_- = 0.243 \pm 0.015$	0.234 ± 0.026 c) $0.242 \pm 0.011 \pm 0.005$ c)	0.991 ± 0.025 1.0 a)

a) Value fixed in calculation.

b) Numbers presented have been corrected for the energy cut (by the experimenters).

c) From the Paschos-Wolfenstein realtion, see Eq. (4.91)

d) Determined from an over-all fit including the observed distributions in hadron energy.

e) The results for $\sin^2\Theta_{\overline{MS}}(M_W)$ are given.

The low-energy experiments by GARGAMELLE /294/ ($< E_\nu > \simeq 2$ GeV) and other groups can be very helpful in studying a possible energy dependence. But the effect of the cut-off at low hadronic energy is more severe for these low-energy data compared to data taken in the 40 GeV domain. The R_ν and $R_{\bar\nu}$ values from GARGAMELLE ($R_\nu = 0.26 \pm 0.04$, $R_{\bar\nu} = 0.39 \pm 0.06$) and the R_+ and R_- values from the SKAT Collaboration ($R_+ = 0.33 \pm 0.03$, $R_- = 0.27 \pm 0.07$ /295/) show no significant difference from the high-energy values (Table 4.8). From these cross-section ratios $\sin^2\Theta_W = 0.32 \pm 0.05$ has been extracted assuming the energy to be below the charm threshold, in contrast to the analyses of the high-energy experiments.

In order to achieve measurements of at least moderately high precision, experiments with large statistics and good acceptance for final-state muons, if there are any, are necessary. If also differential cross sections are to be studied, narrow-band beam experiments, with the advantage of the known energy-radius relation, are almost indispensable. The over-all cross-section ratios, however, can be determined without major problems also in wide-band beam experiments.

Experimentally neutral-current events are differentiated from charged-current events on the basis of penetration: the muon in the charged-current event, $\nu_\mu + N \rightarrow \mu^- +$ anything, must penetrate through the calorimeter and beyond the hadron cascade, thus imposing a cut in $y = 1 - E_\mu/E_\nu$ (< 1). The fine spatial resolution of the CHARM calorimeter allows, like in bubble chamber experiments, the classification of events as neutral-current or charged-current candidates on an event-by-event basis, whereas for the high-density (CITF, CDHS, and CCFRR) detectors in general a statistical method, based on the total event length, is used to perform this event classification.

The thus selected events have then to be corrected for backgrounds and for various effects mixing neutral-current and charged-current events. Owing to the different methods of event classification and event selection, these corrections vary from experiment to experiment. Quite generally, the backgrounds for which corrections are needed are due to events induced by wrong-kind neutrinos or by the non-narrow-band component of the beam which is unavoidably present in narrow-band beam experiments. In addition, for bubble chamber experiments the background from neutron interactions has to be taken into account, though it can largely be reduced by suitable kinematic cuts.

Applying these primary corrections to the raw event numbers leads to the cross-section ratios listed in Table 4.8. Relating these values to the relative strength of the neutral-current to charged-current coupling ρ and the electroweak mixing angle $\sin^2\Theta_W$, or, in a model-independent analysis, to the chiral coupling constants ($\epsilon_L(u)$, $\epsilon_L(d)$, $\epsilon_R(u)$, and $\epsilon_R(d)$), requires theoretical analysis of deep-inelastic neutrino scattering, incorporating scaling violations predicted by QCD and sea-quark distributions. For illustration the order of magnitude of the theoretical uncertainties /292/ on $\sin^2\Theta_W$ is listed in Table 4.9.

Fig. 4.25 shows a comparison of the results of various experiments on R_ν and $R_{\bar\nu}$ with the expectation from the GWS model, based on a calculation /29/ which incorporates the effects of QCD, assuming $\Lambda = 0.47\,GeV$, $a_{\bar s} \sim \bar s/\bar u = 0.5$ and $r = \sigma(\bar\nu N \rightarrow \mu^+ X)/\sigma(\nu N \rightarrow \mu^- X) = 0.47$. For the theoretical prediction also the $E_{cut} > 2$ GeV cut of the CHARM experiment has been applied. The value of R_ν, and hence the best value for $\sin^2\Theta_W$, turns out to be affected very little by varying these parameters; $R_{\bar\nu}$ serves as a check on the model consistency, and is indeed sensitive to the values of $a_{\bar s}$ and r and to QCD effects.

Table 4.9. Order of magnitude of essential theoretical uncertainties in analysing neutral-current neutrino scattering /292/.

Source	$\Delta \sin^2 \Theta_W$
Ratio of antiquarks to valence quarks	± 0.001
Fraction of strange quarks	± 0.001
Fraction of charm quarks	± 0.001
Longitudinal structure function	± 0.002
Higher twist contributions	± 0.002

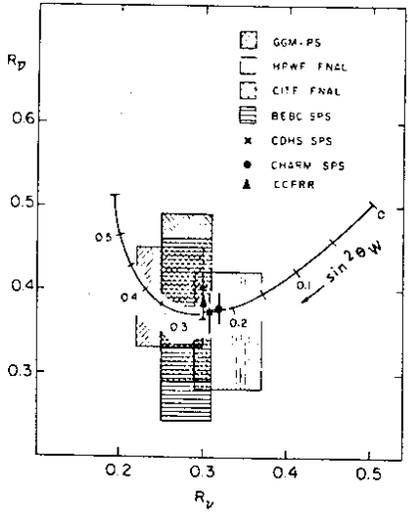

Fig. 4.25

Comparison of measurements of R_ν and $R_{\bar{\nu}}$ with the GWS model. The rectangles indicate the ± 1 σ limits. The data are taken with different cuts in shower energy E_H (the cuts are listed in Table 4.8). The curve is obtained for the CHARM conditions /274/ following the model calculations of ref. /26/, for different values of $\sin^2\theta_W$.

As can be seen from Table 4.8 and Fig. 4.25, all experiments are in reasonable agreement. A weighted average of most of these measurements gives within the context of the standard model /292/

$$\sin^2 \Theta_W = 1.006 \sin^2 \hat{\Theta}_W(M_W) = 0.224 \pm 0.007\ (\text{exp}) \pm 0.006\ (\text{theor}), \qquad (4.92)$$

where $\sin^2 \hat{\Theta}_W(M_W)$ is the $\overline{\text{MS}}$ definition of the renormalized quantity (which is convenient for grand unification).

Within the framework of a $SU_2 \times U_1$ gauge theory in which no specific value of the parameter ρ is assumed, a fit /29/ to most of the measurements in Table 4.8 yields:

$$\rho = 0.999 \pm 0.025, \qquad \sin^2 \Theta_W = 0.232 \pm 0.027. \qquad (4.93)$$

In a model-independent analysis the measurements of $R\nu$ and $R\bar{\nu}$ as well as the measurements of the y-distributions $\frac{d\sigma}{dy}(\nu N \to \nu X)$ and $\frac{d\sigma}{dy}(\bar{\nu} N \to \bar{\nu} X)$, determine the overall strength of the left- and right-handed couplings: $g_L = [\epsilon_L^2(u) + \epsilon_L^2(d)]^{1/2}$ and $g_R = [\epsilon_R^2(u) + \epsilon_R^2(d)]^{1/2}$, using the simplest parton model formalism, in which the QCD corrections, hadron energy cuts and neutral-current couplings to s and c quarks are ignored (Eqs. 4.88/4.89). The allowed regions of coupling constants are restricted by these determinations to two annuli in the $\epsilon_L(u)$-$\epsilon_L(d)$ and $\epsilon_R(u)$-$\epsilon_R(d)$ planes, respectively. The effects of QCD corrections, deviations from isoscalarity of the targets (i.e. neutron excess) and the coupling to s and c quarks, which have to be included in a detailed analysis, is to modify slightly the two annuli. Fig. 4.26 shows the restrictions imposed by $R\nu$ and $R_{\bar{\nu}}$ measurements used in the mentioned fit of Kim et al. /29/; they correspond to the values

$$g_L = 0.543 \pm 0.015, \qquad g_R = 0.172 \pm 0.027, \qquad (4.94)$$

demonstrating the existence of the right-handed coupling ($g_R^2 = 0.030 \pm 0.009$) with more than 99 % confidence. This is shown in Fig. 4.27 for the results of the CHARM experiment ($g_L^2 = 0.305 \pm 0.013$, and $g_R^2 = 0.036 \pm 0.013$) manifesting that this experiment alone extracts a non-zero value of g_R^2 with more than 90 % confidence without constraining the value of ρ /274/.

Within the context of the quark-parton model, the CHARM Collaboration /213/ has extracted the left- and right-handed couplings of the weak neutral current in addition from a simultaneous analysis of the differential cross sections $d\sigma/dy$ for events induced by both the neutral and charged-current interactions of neutrinos and antineutrinos. The values $g_L^2 = 0.32 \pm 0.02$ and $g_R^2 = 0.05 \pm 0.02$, obtained by necleting strange quark contributions, or equivalently the electroweak mixing angle $\sin^2 \Theta_W = 0.222 \pm 0.016$, obtained by assuming that the couplings of the u, d, and s quarks can all be described in terms of the GWS prescription, are consistent with the values extracted from the cross sections alone.

In the $\epsilon_L(u)$-$\epsilon_L(d)$ and $\epsilon_R(u)$-$\epsilon_R(d)$ plane the standard model limits the allowed region to a straight line segment, each on which corresponds to a different value of $\sin^2 \Theta_W$ (Fig. 4.26). Interpreting the chiral coupling constants (4.94) in the context of the standard model leads to the values for ρ and $\sin^2 \Theta_W$ quoted in (4.93).

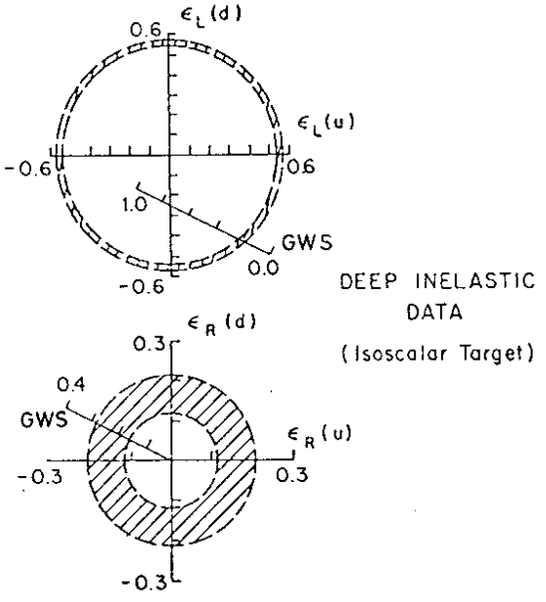

Fig. 4.26 Constraints imposed on the hadronic neutral-current couplings (90% confidence level) by the data on deep inelastic ν and $\bar{\nu}$ scattering on an isoscalar target /29/. The prediction of the GWS model is shown as a function of $\sin^2\Theta_W$.

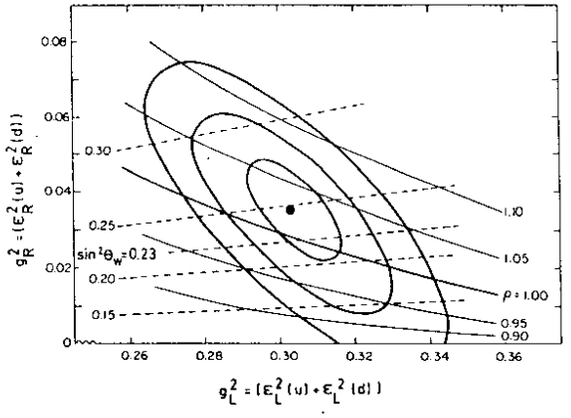

Fig. 4.27 Best fit and confidence limits of 39%, 87% and 99% on the chiral coupling constants as determined in the CHARM experiment /274/. The drawn curves are lines of constant ρ, and the dashed curves are lines of constant $\sin^2\Theta_W$.

It is possible to interpret the results (4.94) also within the framework of the left-right symmetric $SU_{2L} \times SU_{2R} \times U_1$ model (Chap. 2.8) since the chiral coupling constants g_L and g_R are determined by the three parameters $\eta_V = (\rho_L - \rho_{LR})$, $\eta_A = (\rho_L + \rho_{LR})$ and $\sin^2\Theta_W$ (Eq. 2.46), since all the coupling parameters, except h_{VV} and h_{AA}, are the same as in the standard model, modulo the factors η_V, η_A and $f_{PV} = (\rho_L - \rho_R)$ multiplying the vector, axialvector, and parity-violating coupling parameters, respectively /116/. Eliminating $\sin^2\Theta_W$, one obtains the allowed domain in the η_V-η_A plane /68/ shown in Fig. 4.28.

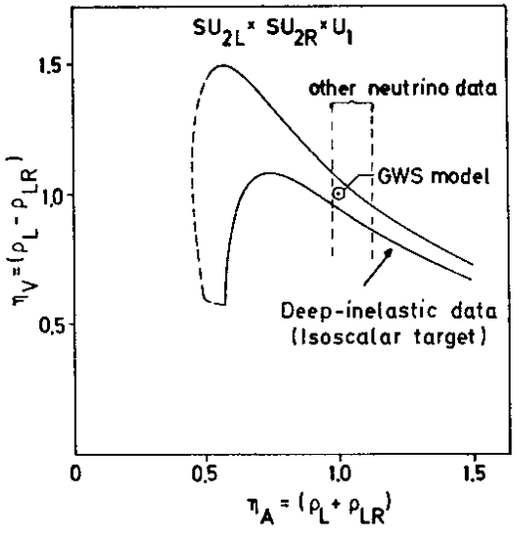

Fig. 4.28 Constraints imposed on parameters η_V, η_A of the $SU_{2L} \times SU_{2R} \times U_1$ model by the data on deep-inelastic ν and $\bar{\nu}$ scattering from an isoscalar target supplemented by other neutrino data (dashed lines) /68/.

The allowed region in the η_V-η_A plane by taking the intersection of the regions allowed by deep-inelastic neutrino scattering on isoscalar targets and other neutrino data, is compatible with $\eta_V = \eta_A = 1$, defining the standard model limit of the left-right symmetric model.

Usually, the correlations between left- and right-handed couplings are demonstrated by plotting the angle $\Theta_L = \arctan\{\epsilon_L(u)/\epsilon_L(d)\}$ vs. the angle $\Theta_R = \arctan\{\epsilon_R(u)/\epsilon_R(d)\}$ for the allowed regions. But deep-inelastic scattering data on isoscalar targets cannot provide any information on Θ_L and Θ_R. This is due to the fact that these data are only sensitive to $\epsilon_L^2(u) + \epsilon_L^2(d)$ and $\epsilon_R^2(u) + \epsilon_R^2(d)$ since no information about the isospin structure of the neutral current can be obtained. In order to determine the u and d coupling parameters separately and thus get information on the isospin of the neutral current, it is useful to study deep-inelastic scattering on neutrons and protons, π^+/π^- inclusive charge ratios, elastic scattering of ν and $\bar{\nu}$ on protons and single pion production.

4.3.2.2. Deep-inelastic scattering on neutron and proton targets

There are several measurements of deep-inelastic neutrino and antineutrino scattering on proton and neutron targets. Usually, the data are expressed in terms of the ratio of neutral-current to charged-current cross sections

$$R_\nu^p = \frac{\sigma(\nu p \to \nu X)}{\sigma(\nu p \to \mu^- X)}, \qquad R_{\bar\nu}^p = \frac{\sigma(\bar\nu p \to \bar\nu X)}{\sigma(\bar\nu p \to \mu^+ X)}, \tag{4.95}$$

and similarly for the ratios on neutrons, or in terms of neutral-current cross sections for neutron and proton targets

$$R_\nu^{n/p} = \frac{\sigma(\nu n \to \nu X)}{\sigma(\nu p \to \nu X)}, \qquad R_{\bar\nu}^{n/p} = \frac{\sigma(\bar\nu n \to \bar\nu X)}{\sigma(\bar\nu p \to \bar\nu X)}. \tag{4.96}$$

The presently available data are listed in Table 4.10. All the measurements have been obtained from bubble chamber experiments (BEBC, Fermilab 15-ft bubble chamber and GARGAMELLE). Therefore the sample of neutral-current candidates is contaminated by background due to i) the interaction of neutrons produced by neutrinos in front of the chamber and ii) unidentified charged-current events caused by non-trivial problems of muon identification (e.g. reduced muon efficiency at low muon momentum of the External Muon Identifier).

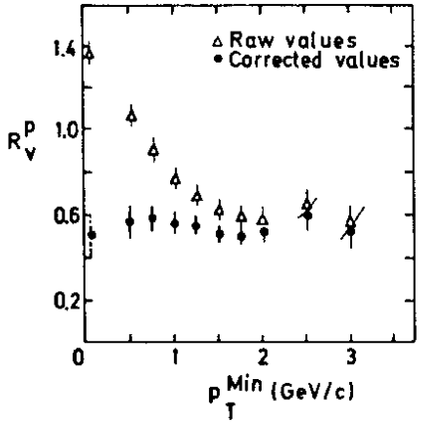

Fig. 4.29 Raw and corrected values of R_ν^p as a function of P_T^{Min}, the minimum transverse momentum of the reaction products with respect to the direction of the incident neutrinos, obtained by the ABCMO collaboration /296/.

Table 4.10. Measurements of the cross-section ratios R_ν^p, $R_{\bar\nu}^p$, $R_\nu^{n/p}$, and $R_{\bar\nu}^{n/p}$ from high-energy experiments studying deep-inelastic ν and $\bar\nu$ scattering on proton and neutron targets.

Experiment	Target	Cross-section ratio
ABCMO Collaboration /296/ (Aachen-Bonn-CERN-Munich-Oxford)	BEBC Hydrogen	$R_\nu^p = 0.51 \pm 0.04$
FNAL-Berkeley-Hawaii-Michigan Collaboration /297/	Fermilab 15-ft B.C. Hydrogen	$R_\nu^p = 0.48 \pm 0.17$
Bari-Birmingham-Brussels-London (U.C.)-E.P. Palaiseau-Rutherford-Saclay Collaboration /298/	BEBC Hydrogen (Track-Sensitive Target)	$R_\nu^p = 0.47 \pm 0.04$ $R_{\bar\nu}^p = 0.33 \pm 0.04$
ABBPPST Collaboration /299/ Amsterdam-Bergen-Bologna-Padua-Pisa-Saclay-Turin)	Deuterium	$R_\nu^p = 0.49 \pm 0.05$ $R_\nu^n = 0.25 \pm 0.02$ $R_{\bar\nu}^p = 0.26 \pm 0.04$ $R_{\bar\nu}^n = 0.57 \pm 0.09$
IMSTT Collaboration /300/ (Illinois-Maryland-Stony Brook-Tohoku-Tufts)	Fermilab 15-ft B.C. Deuterium	$R_\nu^p = 0.49 \pm 0.06$ $R_\nu^n = 0.22 \pm 0.03$ $R_\nu^{n/p} = 1.01 \pm 0.14$
ANL-Carnegie Mellon-Purdue Collaboration /301/	Fermilab 15-ft B.C. Hydrogen	$R_{\bar\nu}^p = 0.36 \pm 0.06$
Berkeley-CERN-Hawaii-Wisconsin Collaboration /302/	Fermilab 15-ft B.C. Hydrogen-Neon	$R_\nu^{n/p} = 1.22 \pm 0.35$
Aachen-Brussels-CERN-E.P. Palaiseau-Orsay-Padova Coll. /303/	GARGAMELLE Propane-Freon	$R_\nu^{n/p} = 0.76 \,^{+\,0.17}_{-\,0.15}$
FIIM Collaboration /304/ (Fermilab-IHEP-ITEP-Michigan)	Fermilab 15-ft B.C. Hydrogen-Neon	$R_{\bar\nu}^{n/p} = 0.64 \pm 0.18$

Both sources of background can be strongly reduced by a cut in the total transverse momentum of the reaction products relative to the beam direction. Fig. 4.29 shows the variation of the raw ratio R_ν^p, evaluated by the ABCMO Collaboration /296/, as a function of the detected transverse momentum and the result of corrections for the background effects.

A cut at 1.5 GeV/c is chosen to equalize the statistical error, which increases with increasing p_T, and the systematic uncertainty of the corrections, which is decreasing /271/. In addition quite high cuts ($\sim$ 5 - 15 GeV) in E_H, the hadronic energy, are applied. In order to examine the ratio of neutron to proton cross sections some experiments /302,304/ eliminate backgrounds from charged-current events by selecting only those events where all tracks interact. The events with target neutrons are separated from events with target protons by looking at the event charge, defined as the sum of the charges of the tracks at the primary vertex. But nuclear effects of the target nucleus smear the expected charge distributions (charge 0 for neutron events and charge 1 for proton events) considerably. Therefore, methods for unfolding the cross-section ratios from the smeared charge distribution have been developed, contributing considerably to the systematic uncertainties of the measurements.

The accuracy of the data is such that the simple parton model in valence parton approximation can be used - neglecting the effects of QCD and sea quarks - in developing the theoretical formalism to abstract the neutral-current coupling constants. The analysis of totally inclusive scattering on proton and neutron targets requires the input of the quantities

$$r = \frac{\int_0^1 xu(x)\,dx}{\int_0^1 xd(x)\,dx} \simeq 2 \tag{4.97}$$

and

$$\overset{(-)}{\xi} = \frac{\int dE_{\overset{(-)}{\nu}}\, E_{\overset{(-)}{\nu}} \Phi_{\overset{(-)}{\nu}} \int_a^1 dy\,(1-y)^2}{\int dE_{\overset{(-)}{\nu}}\, E_{\overset{(-)}{\nu}} \Phi_{\overset{(-)}{\nu}} \int_a^1 dy} \tag{4.98}$$

in order to take into consideration the effect of the hadron energy cut ($E_H > E_H^{cut}$). $\Phi_\nu(E_\nu)$ and $\Phi_{\bar\nu}(E_{\bar\nu})$ are the actual neutrino and antineutrino flux distributions of the experiments and $a(E_\nu) = E_H^{cut}/E_\nu$. For $E_H^{cut} = 0$ one gets $\xi\,(\bar\xi) = 1/3$, whereas for the experimental data in Table 4.10 $\xi\,(\bar\xi)$ is smaller (e.g. $\xi \simeq 0.21$ for /297,302/ and $\bar\xi = 0.13$ for /301,304/).

Then one has for the experimentally measured cross-section ratios the following expressions /29/:

$$R_\nu^p(\xi, r) = r\left[\epsilon_L^2(u) + \xi\epsilon_R^2(u)\right] + \left[\epsilon_L^2(d) + \xi\epsilon_R^2(d)\right] \tag{4.99}$$

$$R_{\bar\nu}^p(\bar\xi, r) = \left[\epsilon_R^2(u)/\bar\xi + \epsilon_L^2(u)\right] + \frac{1}{r}\left[\epsilon_R^2(d)/\bar\xi + \epsilon_L^2(d)\right] \tag{4.100}$$

$$R_\nu^{n/p}(\xi, r) = \frac{r\left[\epsilon_L^2(d) + \xi\epsilon_R^2(d)\right] + \left[\epsilon_L^2(u) + \xi\epsilon_R^2(u)\right]}{r\left[\epsilon_L^2(u) + \xi\epsilon_R^2(u)\right] + \left[\epsilon_L^2(d) + \xi\epsilon_R^2(d)\right]} \tag{4.101}$$

$$R_{\bar\nu}^{n/p}(\bar\xi, r) = \frac{r\left[\epsilon_R^2(d) + \bar\xi\epsilon_L^2(d)\right] + \left[\epsilon_R^2(u) + \bar\xi\epsilon_L^2(u)\right]}{r\left[\epsilon_R^2(u) + \bar\xi\epsilon_L^2(u)\right] + \left[\epsilon_R^2(d) + \bar\xi\epsilon_L^2(d)\right]}\,. \tag{4.102}$$

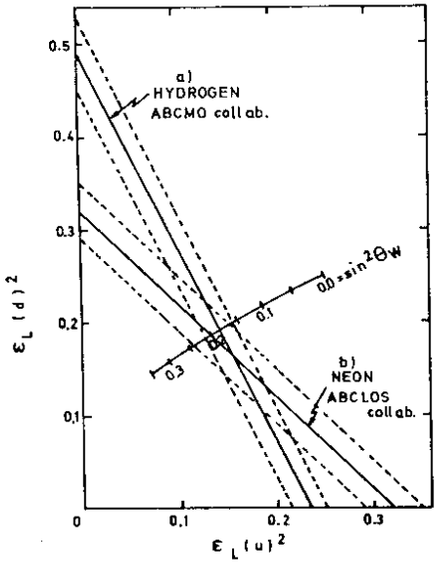

Fig. 4.30

Region of allowed values of left-handed chiral coupling parameters obtained from isoscalar data (line (b)) /244/ and from νp interactions (line (a)) /296/. The errors indicated by the dotted lines correspond to one standard deviation. Also shown is the prediction of the standard model as a function of $\sin^2\Theta_W$.

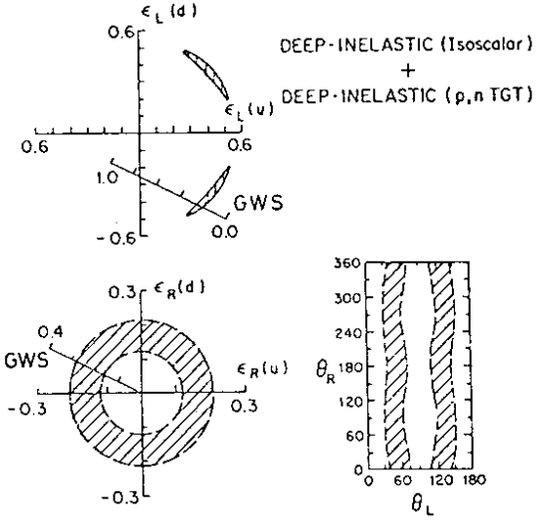

Fig. 4.31

Constraints imposed on the hadronic neutral-current couplings (90% confidence level) by the data on deep-inelastic ν, $\bar\nu$ scattering on both isoscalar and p, n targets /29/. The prediction of the GWS model is shown as a function of $\sin^2\Theta_W$.

In order to disentangle the u and d coupling parameters it is therefore useful to compare the scattering on an isoscalar target with that on protons. Studies of this type have provided some separation of $\epsilon_L^2(u)$ and $\epsilon_L^2(d)$. This is illustrated, for example, in Fig. 4.30 where values of R_ν measured in neon (ABCLOS Collaboration /244/) and R_ν^p measured in hydrogen (ABCMO Collaboration /296/) determine a region of allowed values of the left-handed chiral coupling constants. The ABBPPST Collaboration /299/ has measured neutral- and charged-current interactions of neutrinos and antineutrinos on protons and neutrons. From a combination of the ratios the neutral-current chiral coupling constants are extracted:

$$\epsilon_L^2(u) = 0.13 \pm 0.03\,, \qquad \epsilon_R^2(u) = 0.02 \pm 0.02\,,$$
$$\epsilon_L^2(d) = 0.19 \pm 0.03\,, \qquad \epsilon_R^2(d) = 0.00 \pm 0.02\,.$$

Using most of the data listed in Table 4.10, Kim et al. /29/ performed a fit to the parameters $\epsilon_L(u)$, $\epsilon_L(d)$, $\epsilon_R(u)$, and $\epsilon_R(d)$ constrained by (4.99 - 4.102). This results in a restriction of the regions in both the left-handed and right-handed coupling constant spaces, allowed by the data from isoscalar targets (Fig. 4.26), to those shown in Fig. 4.31. There is also a correlation between the allowed regions in the $\epsilon_L(u)$-$\epsilon_L(d)$ plane and the $\epsilon_R(u)$-$\epsilon_R(d)$ plane which is displayed as a shaded region in the Θ_L, Θ_R plot. Significant information is provided on Θ_L which measures the isospin of the left-handed coupling. Θ_R, however, which determines the isospin nature of the right-handed coupling, is still essentially undetermined.

4.3.2.3. Semi-inclusive pion production on isoscalar targets

The analysis of charge ratios of final-state pions produced in semi-inclusive reactions on isoscalar targets

$$\nu\,(\bar{\nu}) + N \rightarrow \nu\,(\bar{\nu}) + \pi^{\pm} + X\,, \qquad (4.103)$$

provides another way to disentangle the u and d coupling parameters. This analysis is based on the assumption that the composition of the hadronic system reflects in the "current fragmentation region" the composition of the quark beam produced in the primary neutrino-quark interaction /305/. The "current fragment pions" are defined as those going forward with respect to the momentum transfer, $\vec{q}$, from the lepton to the hadron system. This implies that the current fragment pions appear as leading pions in the forward hemisphere (positive rapidity) as seen from the Breit frame (defined by a Lorentz transformation along the direction of $\vec{q}$ with $\beta = E_H/|\vec{q}|$ /306/). But it is difficult to measure the vector $\vec{q}$ of neutral-current interactions. Fortunately, it turns out that the fragments of the target and the fragments of the current can also be distinguished by means of the fragmentation variable $z = E_\pi/E_H$, provided that the energy transfered to the hadron system, E_H, is not too small. (For $E_H \geq 1$ GeV and $z \geq 0.2 - 0.3$ most of the target fragments are cut out /306/).

As sketched in Fig. 4.32 for neutrinos, the charged- and neutral-current reactions on isoscalar targets create quark beams containing u and d quarks in different proportions as listed in Table 4.11 /305/.

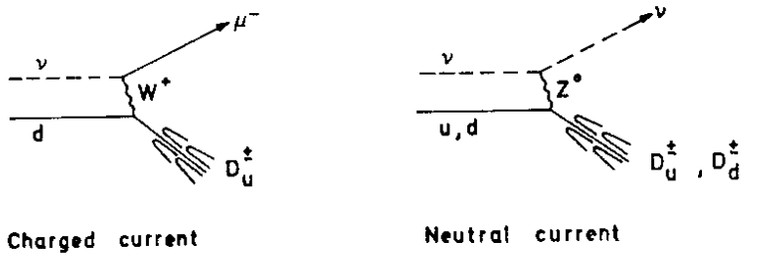

Fig. 4.32 Fragmentation of quarks struck by charged and neutral currents in neutrino reactions.

Table 4.11. Composition of the quark beam produced in the primary charged- and neutral-current $\nu(\bar{\nu})$-quark interaction.

Reaction		u : d
CC neutrino	$(\nu \rightarrow \mu^-)$	1 : 0
CC antineutrino	$(\bar{\nu} \rightarrow \mu^+)$	0 : 1
NC neutrino	$(\nu \rightarrow \nu)$	$(u_L^2 + \frac{1}{3}u_R^2) : (d_L^2 + \frac{1}{3}d_R^2)$
NC antineutrino	$(\bar{\nu} \rightarrow \bar{\nu})$	$(u_R^2 + \frac{1}{3}u_L^2) : (d_R^2 + \frac{1}{3}d_L^2)$

In the elementary processes (using valence parton approximation)

$$\nu_\mu + d \rightarrow \mu^- + u\,, \quad \bar{\nu}_\mu + u \rightarrow \mu^+ + d\,, \quad \overset{(-)}{\nu}_\mu + \left\{ \begin{matrix} u \\ d \end{matrix} \right\} \rightarrow \overset{(-)}{\nu}_\mu + \left\{ \begin{matrix} u \\ d \end{matrix} \right\},$$

a u-quark (d-quark) beam is produced in charged-current neutrino (antineutrino) interaction which then fragments into a pion characterized by a probability amplitude $D_u^\pi(z)$ $(D_d^\pi(z))$, the so-called fragmentation function. For neutral-current processes both quarks are involved - the right-handed quarks, however, are only one third as effective as the left-handed ones (because of $\int_0^1 (1-y)^2 dy = 1/3$).

Since isoscalar targets contain an equal amount of u and d quarks, an observed asymmetry between π^- und π^+ would provide information on the strength of the d quark interaction compared to that of the u quark. In the valence parton approximation one obtains for the charge ratios of final-state pions in $\nu\,(\bar{\nu})$ induced reactions on isoscalar targets /305,307-309/:

$$\left(\frac{\pi^+}{\pi^-}\right)_{\nu\to\nu} \equiv \frac{\sigma(\nu N \to \nu\pi^+ X)}{\sigma(\nu N \to \nu\pi^- X)} = \frac{\eta\left[\epsilon_L^2(u) + \xi\epsilon_R^2(u)\right] + \left[\epsilon_L^2(d) + \xi\epsilon_R^2(d)\right]}{\left[\epsilon_L^2(u) + \xi\epsilon_R^2(u)\right] + \eta\left[\epsilon_L^2(d) + \xi\epsilon_R^2(d)\right]} \tag{4.104}$$

$$\left(\frac{\pi^+}{\pi^-}\right)_{\bar{\nu}\to\bar{\nu}} \equiv \frac{\sigma(\bar{\nu} N \to \bar{\nu}\pi^+ X)}{\sigma(\bar{\nu} N \to \bar{\nu}\pi^- X)} = \frac{\eta\left[\bar{\xi}\epsilon_L^2(u) + \epsilon_R^2(u)\right] + \left[\bar{\xi}\epsilon_L^2(d) + \epsilon_R^2(d)\right]}{\left[\bar{\xi}\epsilon_L^2(u) + \epsilon_R^2(u)\right] + \eta\left[\bar{\xi}\epsilon_L^2(d) + \epsilon_R^2(d)\right]} \tag{4.105}$$

$$\left(\frac{\pi^+}{\pi^-}\right)_{\nu\to\mu^-} \equiv \frac{\sigma(\nu N \to \mu^-\pi^+ X)}{\sigma(\nu N \to \mu^-\pi^- X)} = \eta$$

$$\left(\frac{\pi^+}{\pi^-}\right)_{\bar{\nu}\to\mu^+} \equiv \frac{\sigma(\bar{\nu} N \to \mu^+\pi^+ X)}{\sigma(\bar{\nu} N \to \mu^+\pi^- X)} = \frac{1}{\eta}. \tag{4.106}$$

$$\eta = \frac{\int_{z_1}^{z_2} D_u^{\pi^+}(z)\,dz}{\int_{z_1}^{z_2} D_u^{\pi^-}(z)\,dz} \tag{4.107}$$

is the ratio of the probability for a u-quark to fragment into a π^+ to the probability for a u-quark to fragment into a π^- (carrying a fraction z of the total hadronic energy). The integral extends over the range of z values allowed in the actual experiment. Integrated fragmentation functions can be extracted from charged-current (Eqs. 4.106) and electroproduction experiments ($\eta \sim 3$ /305/).

Taking into account the cut in hadronic energy, E_H^{cut}, the factor 1/3 in Table 4.11 has to be replaced by ξ:

$$\xi = \frac{\int dE_\nu\, E_\nu \Phi_\nu \int_{a(E_\nu)}^1 (1-y)^2\,dy}{\int dE_\nu\, E_\nu \Phi_\nu \int_{a(E_\nu)}^1 dy} \tag{4.108}$$

where $a(E_\nu) = E_H^{cut}/E_\nu$ and $\Phi(E_\nu)$ and $\bar{\Phi}(E_{\bar{\nu}})$ are the fluxes for neutrinos and antineutrinos, respectively.

The presently available measurements of the π^+/π^- ratio for inclusive pion production are summarized in Table 4.12. All experiments were performed in heavy liquid bubble chambers. Thus corrections must be made for nuclear effects such as charge exchange reactions, which may occur before the pion leaves the complex nucleus and thus can affect the π^+/π^- ratio. For comparison of the observed ratios with the predictions of the quark parton model (4.104-4.106), one has to ensure that most of the pions used in the analysis come from the current fragmentation region. Therefore, rather stringent kinematical cuts (in E_H and z) have been applied which largely eliminate also the background from hadron-induced events. The uncertainty due to ambiguities in the $\pi/K/p$ separation for high-energy tracks has been resolved on a statistical basis by Monte Carlo calculations.

Table 4.12. Measurements of the ratios of π^+ and π^- produced in semi-inclusive ν and $\bar{\nu}$ reactions on isoscalar targets.

Experiment	Target	z Region	Charge ratios
GARGAMELLE /306/	Freon	$0.3 \leq z \leq 0.7$	$\left(\frac{\pi^+}{\pi^-}\right)_{\nu\to\nu} = 0.77 \pm 0.14$ $\left(\frac{\pi^+}{\pi^-}\right)_{\bar{\nu}\to\bar{\nu}} = 1.65 \pm 0.33$
Fermilab 15-ft B.C. FIIM Collab. /304/	Hydrogen-Neon	$0.4 < z < 0.9$	$\left(\frac{\pi^+}{\pi^-}\right)_{\nu\to\nu} = 1.27\ {}^{+\,0.36}_{-\,0.29}$ [a]
BEBC ABCDLOS Collab. (Aachen-Bonn-CERN-Demokritos-London (I.C.)-Oxford-Saclay) /310/	Hydrogen-Neon	$z > 0.3$	$\left(\frac{\pi^+}{\pi^-}\right)_{\nu\to\nu} = 0.69 \pm 0.22$ [b] $\left(\frac{\pi^+}{\pi^-}\right)_{\bar{\nu}\to\bar{\nu}} = 1.37 \pm 0.31$ [b]

a) Calculated from the measured ratio $\left(\frac{\pi^+}{\pi^+ + \pi^-}\right)_{\nu\to\nu} = 0.56 \pm 0.06$

b) Evaluated (by the experimenters) from the measured ratios $(h^+/h^-)_{\nu\to\nu} = 1.07 \pm 0.17$ and $(h^+/h^-)_{\bar{\nu}\to\bar{\nu}} = 1.54 \pm 0.45$ using isospin symmetry and charge conjugation to estimate the number of background protons and kaons in the final-state hadrons (h). Only statistical errors are quoted.

The fact that the ratios in Table 4.12 differ from each other (and from unity) is, without any model assumption, a demonstration that the weak neutral current is an isoscalar-isovector mixture /309/. A quantitative analysis /29/ based on Eqs. (4.104)-(4.106) and the inclusive constraints given by Eqs. (4.88) and (4.89) determines the squares of the chiral coupling constants completely. The solution is shown in Fig. 4.33.

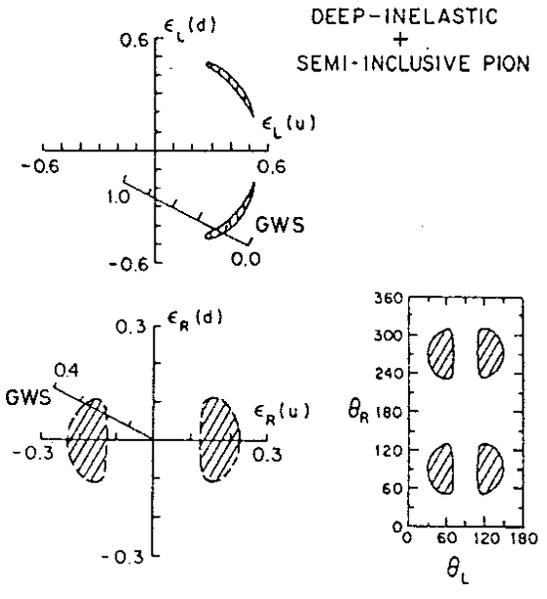

Fig. 4.33 Constraints imposed on the hadronic neutral-current couplings (90% confidence level) by the data on deep-inelastic ν, $\bar{\nu}$ scattering on an isoscalar target and measurements of the π^+/π^- ratio in semi-inclusive pion production /29/. The prediction of the standard model is shown as a function of $\sin^2\theta_W$.

The relative signs between the chiral couplings $\epsilon_L(u)$, $\epsilon_R(u)$, $\epsilon_L(d)$ and $\epsilon_R(d)$ still remain unmeasured in inclusive processes because of the incoherence assumption in the quark parton model, which implies that in high energy inelastic collisions, quarks of definite flavour and chirality act incoherently /68/. But a study of exclusive neutral-current channels provides independent constraints on the neutral-current couplings and allows finally to resolve these sign ambiguities left over from the analysis of inclusive and semi-inclusive measurements.

4.3.2.4. Exclusive neutrino channels

With four constants of unknown signs, sixteen (= 2^4)-fold ambiguities are expected. The incidental fact that $|\epsilon_R(d)| \simeq 0$ (Fig. 4.33) and the choice of the overall sign by taking $\epsilon_L(u) > 0$, reduce these sixteen-fold ambiguities then to two essential sign ambiguities, viz. those of $\epsilon_L(u) \cdot \epsilon_L(d)$ and $\epsilon_L(u) \cdot \epsilon_R(u)$. Using formulae (2.59) one obtains:

$$\epsilon_L(u)\cdot\epsilon_L(d) \sim \underbrace{(\gamma+\delta)^2}_{\substack{\text{Isoscalar}\\ \text{part}}} - \underbrace{(\alpha+\beta)^2}_{\substack{\text{Isovector}\\ \text{part}}} \tag{4.109}$$

$$\epsilon_L(u)\cdot\epsilon_R(u) \sim \underbrace{(\alpha+\gamma)^2}_{\substack{\text{Vector}\\ \text{part}}} - \underbrace{(\beta+\delta)^2}_{\substack{\text{Axialvector}\\ \text{part}}} . \tag{4.110}$$

The four possible solutions (Fig. 4.33), obtained by choosing the sign of $\epsilon_L(u) \cdot \epsilon_L(d)$ and $\epsilon_L(u) \cdot \epsilon_R(d)$, have rather distinct properties with respect to their isospin and vector/axialvector character (Table 4.13), so that a discrimination should be possible by studying special channels.

Table 4.13. Solutions allowed by inclusive and semi-inclusive data

Solution	Sign $\epsilon_L(u) \cdot \epsilon_L(d)$	Sign $\epsilon_L(u) \cdot \epsilon_R(u)$	Isospin Property	V,A Property
A	−	−	Isovector dominant	A dominant
B	−	+	" "	V dominant
C	+	−	Isoscalar dominant	V dominant
D	+	+	" "	A dominant

4.3.2.4.1. Elastic neutrino and antineutrino proton scattering

Elastic scattering experiments of neutrinos and antineutrinos on protons, $\nu p \to \nu p$ and $\bar{\nu} p \to \bar{\nu} p$, were of great help in resolving the solution ambiguities. There are now several measurements of the elastic cross sections normalized relative to the quasi-elastic reactions $\nu n \to \mu^- p$ and $\bar{\nu} p \to \mu^+ n$, respectively. The results for

$$R_\nu^{el} = \frac{\sigma(\nu p \to \nu p)}{\sigma(\nu n \to \mu^- p)}\,, \quad R_{\bar{\nu}}^{el} = \frac{\sigma(\bar{\nu} p \to \bar{\nu} p)}{\sigma(\bar{\nu} p \to \mu^+ n)}\,, \quad \text{and} \quad R_{NC} = \frac{\sigma(\bar{\nu} p \to \bar{\nu} p)}{\sigma(\nu p \to \nu p)} \tag{4.111}$$

are summarized in Table 4.14.

Table 4.14. Summary of neutrino-proton elastic scattering experiments

Experiment	R_{ν}^{el}	$R_{\bar{\nu}}^{el}$	R_{NC}	Q^2 Region (in GeV^2/c^2)
Columbia-Illinois-Rockefeller Collaboration (CIR) /311/	0.23 ± 0.09	-	-	$0.3 < Q^2 < 1.0$
Harvard-Pennsylvania-Wisconsin Collab. (HPW) /312/	0.11 ± 0.015	0.19 ± 0.035	0.41 ± 0.09	$0.4 \leq Q^2 \leq 0.9$
GARGAMELLE (Freon) /313/	0.12 ± 0.06	-	-	$0.3 \leq Q^2 \leq 1.0$
Aachen-Padua /314/	0.10 ± 0.03	-	-	$0.2 < Q^2 < 1.0$
Columbia-Illinois-Brookhaven Coll. (CIB)[a] /315/	0.11 ± 0.03	-	0.44 ± 0.12	$0.3 \leq Q^2 \leq 0.9$

[a] This experiment is a modification of the earlier CIR experiment.

The dominant background in elastic scattering experiments arises from elastic neutron-proton scattering $np \to pn$ with a topology identical to that of $\overset{(-)}{\nu} p \to \overset{(-)}{\nu} p$. By measuring the time of flight of events to differentiate neutron- from neutrino-induced reactions, this background can be reduced drastically /311,312/. Another source of background is single pion production by neutrinos (antineutrinos), in particular $\nu n \to \nu \pi^- p$ and $\nu p \to \nu p \pi^0$ where either the charged pion has such a low energy that it cannot be distinguished from the proton, or both photons from the neutral pion fail to convert in the detector. For a small fraction of $\nu n \to \nu n \pi^0$ and $\nu p \to \nu n \pi^+$ events the nucleon and pion energy deposition may simulate an apparent single proton. A potential systematic uncertainty arises also from the normalization of the elastic cross section to the observed rate for $\nu n \to \mu^- p$ ($\bar{\nu} p \to \mu^+ n$) which may be simulated – to a certain percentage – by the single pion channels $\nu n \to \mu^- p \pi^0$, $\nu p \to \mu^- p \pi^+$, $\nu n \to \mu^- n \pi^+$ ($\bar{\nu} p \to \mu^+ n \pi^0$, $\bar{\nu} n \to \mu^+ n \pi^-$, $\bar{\nu} p \to \mu^+ p \pi^-$).

The flux-averaged elastic cross section is sensitive to all four parameters of the neutral current (e.g. α , β , γ and δ) /316/:

$$\sigma(\overset{(-)}{\nu} p \to \overset{(-)}{\nu} p) = \frac{G^2}{8\pi} \left[a_E (\alpha + 3\gamma)^2 + a_M (\alpha + 0.56\gamma)^2 + a_A (\beta + \lambda\delta)^2 \overset{+}{(-)} a_I (\alpha + 0.56\gamma)(\beta + \lambda\delta) \right] . \tag{4.112}$$

The coefficients a_E, a_M, a_A and a_I are functions of the incident flux shape, the dipole mass parameters of the electric, magnetic and axial form factors and the Q^2 range available in a given experiment. The factor 0.56 ($= 3|1 + \kappa_p + \kappa_n|/|1 + \kappa_p - \kappa_n|$) comes from the isoscalar-isovector ratio where $\kappa_p = 1.79$ and $\kappa_n = -1.91$ are the proton and neutron anomalous magnetic moments, respectively. The ratio λ of the isoscalar to the isovector axialvector matrix elements is determined from SU_6 or the non-relativistic quark model to be $\lambda = 0.6$ ($\bar{s}s$ contribution is ignored). Another approach uses SU_3 symmetry (also ignoring $\bar{s}s$ contributions) giving $\lambda = (3F - D)/(F + D) = 0.44$ where F = 0.45 and D = 0.80 /317/. By assuming a Q^2-dependence of the form factors using CVC and the charged-current reaction $\nu n \to \mu^- p$, the integrated cross sections (4.112) have been calculated. In Fig. 4.34 R_{ν}^{el} and $R_{\bar{\nu}}^{el}$ from the HPW measurements (Table 4.14) are compared with these predictions using the dipol mass parameters $M_V = 0.84$ GeV and $M_A = 0.84$ GeV and 0.90 GeV, respectively /318/.

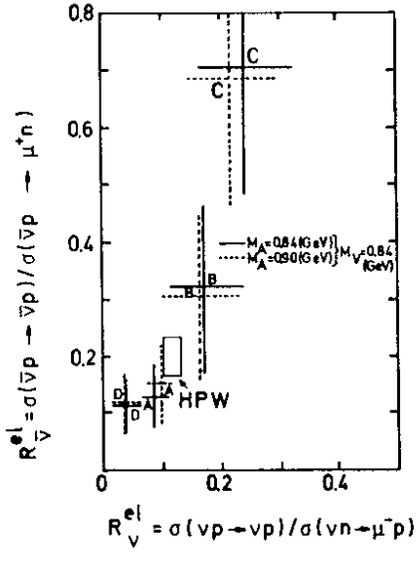

Fig. 4.34

Comparison of HPW data on $\nu p \to \nu p$ and $\bar{\nu} p \to \bar{\nu} p$ with various coupling constant solutions /312,318/.

It can be seen that the solutions (A,B) are favoured over (C,D) implying that the hadronic neutral current is dominantly isovector.

In another approach the Q^2-dependence of the differential cross section $d\sigma/dQ^2$ is exploited. The matrix element of the hadronic neutral current in elastic νp scattering takes the form /258,319/.

$$< f \,|J_\mu^H|\, i >= i\bar{u}(p_f)\left[\gamma_\mu F_1^N(Q^2) + i\sigma_{\mu\nu}q^\nu \frac{F_2^N(Q^2)}{2M} + \gamma_\mu\gamma_5 G_A(Q^2)\right] u(p_i)\,, \qquad (4.113)$$

where $q = p_f - p_i$ and $Q^2 = -q^2 > 0$. Here $u(p_i)$ and $u(p_f)$ are the initial and final nucleon wave functions. $F_1^N(Q^2)$, $F_2^N(Q^2)$ and $G_A(Q^2)$ are nucleon form factors which are real dimensionless functions of Q^2 and have the following clean prediction at $Q^2 = 0$:

$$G_E(0) = F_1^N(0) = \frac{1}{2}\left[\alpha + 3\gamma\right] \qquad (4.114)$$

$$G_M(0) = F_1^N(0) + F_2^N(0) = \frac{1}{2}\alpha\left[1 + \kappa_p - \kappa_n\right] + \frac{3}{2}\gamma\left[1 + \kappa_p + \kappa_n\right]$$

$$= \frac{4.7}{2}\left[\alpha + 0.56\gamma\right] \qquad (4.115)$$

$$G_A(0) = \frac{1}{2}\left(\frac{G_A}{G_V}\right)\left[\beta + \lambda\delta\right] = \frac{1.25}{2}\left[\beta + \lambda\delta\right] \qquad (4.116)$$

where $G_A/G_V = F + D = 1.25$. The factor 3 in (4.114) is due to the definition of the isovector and isoscalar currents which are $V_\mu^{(3)} = \frac{1}{2}(\bar{u}\gamma_\mu u - \bar{d}\gamma_\mu d)$ and $V_\mu^{(0)} = \frac{1}{3}(\bar{u}\gamma_\mu u + \bar{d}\gamma_\mu d)$ respectively /31/. The usual form factors G_E and G_M get only contributions from the vector currents while only axialvector currents contribute to G_A.

Unfortunately the differential cross sections $d\sigma/dQ^2$ are available for $Q^2 > 0.4\ GeV^2/c^2$ only since for $Q^2 \to 0$ the kinetic energy of the proton becomes zero and it cannot be seen. To determine the form factors a least-squares fit to the differential cross sections for both neutrino- and antineutrino-induced reactions has been performed. By extrapolating back to $Q^2 = 0$, one gets /312/ the values for the form factors listed in Table 4.15. They are compared with those values predicted by the various coupling constant solutions.

Clearly solution A ($\epsilon_L(u)\cdot\epsilon_R(u) < 0$) is favoured by the data. Fig. 4.35 shows the 68 % and 95 % confidence contours for $F_1^N(0)$ and $F_2^N(0)$, given that $G_A(0) = 0.615$, and compares them to the prediction of the standard model. With 95 % confidence, the model is consistent with $\sin^2\Theta_W$ between 0.205 and 0.33 /312/.

Table 4.15. Values of the elastic neutral-current form factors (Q^2=0) for solutions A, B, C, and D compared with the experimental results /312/.

Form Factor	Data[a]	Solution A	Solution B	Solution C	Solution D
$F_1^N(0)$	$-0.005^{+0.11}_{-0.15}$	- 0.12	0.62	- 1.46	0.75
$F_2^N(0)$	$0.86^{+0.12}_{-0.16}$	1.14	1.71	- 0.01	- 0.88
$G_A(0)$	0.615	0.615	0.29	0.01	0.32

[a] The experimenters quote /312/ two equally good fits, both with χ^2 = 9.7 for 7 degrees of freedom:

$F_1^N(0) = 0.30 \pm 0.11$, $F_2^N(0) = 0.67^{+0.12}_{-0.21}$, $G_A(0) = 0.56 \pm 0.03$ or

$F_1^N(0) = -0.30^{+0.10}_{-0.19}$, $F_2^N(0) = 1.2^{+0.22}_{-0.17}$, $G_A(0) = 0.57 \pm 0.03$.

The quoted values correspond to fits with $G_A(0)$ fixed to the value predicted by the standard model independent of the value of $\sin^2\Theta_W$.

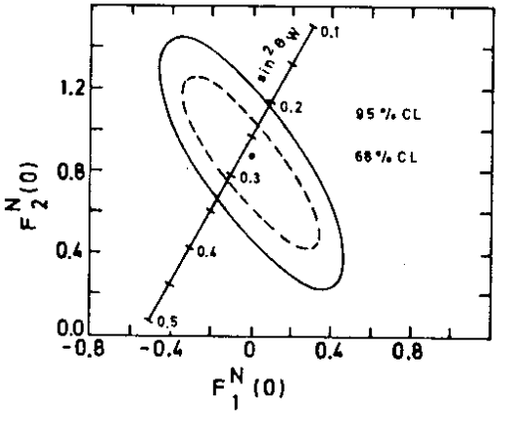

Fig. 4.35

Values of the neutral-current form factors $F_1^N(0)$, $F_2^N(0)$ allowed by a fit to the differential cross sections $d\sigma(\nu,\bar{\nu})/dQ^2$, for $G_A(0)$=0.615. The predictions of the standard model are superimposed (HPW data /312/).

4.3.2.4.2. Single pion production

The cleanest way to determine the isospin properties of the weak neutral current is to study neutral current induced single-pion production:

$$\nu p \to \nu p \pi^0 \qquad (\bar{\nu} p \to \bar{\nu} p \pi^0) \tag{4.117}$$

$$\nu n \to \nu n \pi^0 \qquad (\bar{\nu} n \to \bar{\nu} n \pi^0) \tag{4.118}$$

$$\nu p \to \nu n \pi^+ \qquad (\bar{\nu} p \to \bar{\nu} n \pi^+) \tag{4.119}$$

$$\nu n \to \nu p \pi^- \qquad (\bar{\nu} n \to \bar{\nu} p \pi^-). \tag{4.120}$$

The isospin decomposition of these channels (by neglecting a possible isotensor part which is not expected from the simplest gauge models based on $SU_2 \times U_1$ symmetry) is given by /321/

$$Ampl(\nu p \to \nu p \pi^0) = \frac{1}{3}(2A_3 + A_1) - \sqrt{\frac{1}{3}}\,S \tag{4.121}$$

$$Ampl(\nu n \to \nu n \pi^0) = \frac{1}{3}(2A_3 + A_1) + \sqrt{\frac{1}{3}}\,S \tag{4.122}$$

$$Ampl(\nu p \to \nu n \pi^+) = \frac{\sqrt{2}}{3}(A_3 - A_1) + \sqrt{\frac{2}{3}}\,S \tag{4.123}$$

$$Ampl(\nu n \to \nu p \pi^-) = \frac{\sqrt{2}}{3}(A_3 - A_1) - \sqrt{\frac{2}{3}}\,S. \tag{4.124}$$

Here A_3 and A_1 are the reduced matrix elements for production of I = 3/2 and I = 1/2 states by the isovector current, and S is the reduced matrix element of the isoscalar current inducing only a transitions to I = 1/2 states. From Eqs. (4.121) - (4.124) the sum rule

$$Ampl(\nu p \to \nu n \pi^+) - Ampl(\nu n \to \nu p \pi^-) = -\sqrt{2}\{Ampl(\nu p \to \nu p \pi^0) - Ampl(\nu n \to \nu n \pi^0)\} \tag{4.125}$$

can be derived giving rise to the inequality

$$\sqrt{\sigma(\nu p \to \nu n \pi^+)} \leq \sqrt{\sigma(\nu n \to \nu p \pi^-)} + \sqrt{2\sigma(\nu p \to \nu p \pi^0)} + \sqrt{2\sigma(\nu n \to \nu n \pi^0)}$$

and its permutations. They are all fulfilled experimentally.

The present experimental status of neutral-current induced weak single-pion production is summarized in Table 4.16. The data are preponderantly obtained on targets of complex nuclei, so that nuclear distortion effects (which can strongly affect the invariant mass distributions in their shape) may be important. Furthermore, nuclear reinteractions can lead to channel mixing, so that the observed ratios of π^+, π^- and π^0 can be different from those that would be produced on free nucleons. Such nuclear corrections can be taken into account using Monte Carlo simulation methods /321,330/ or a simple model of the reinteraction effects developed by Adler, Nussinov and Paschos /331/. The final number of events is strongly dependent on the adopted criteria which in general differ from one experiment to another.

Table 4.16. Summary of measurements concerning neutral-current induced weak single-pion production.

Cross-section ratio	Data	References
$\sigma(\nu p \to \nu p\pi^0)/\sigma(\nu p \to \nu n\pi^+)$	3.1 ± 2.1 1.65 ± 0.36	/320/ /321/
$\sigma(\nu p \to \nu p\pi^0)/\sigma(\nu p \to \mu^- p\pi^+)$	0.09 ± 0.05 0.23 ± 0.03	/322/ /321/
$\sigma(\nu p \to \nu n\pi^+)/\sigma(\nu p \to \mu^- p\pi^+)$	0.13 ± 0.04 0.15 ± 0.04	/322/ /321/
$\sigma(\nu n \to \nu p\pi^-)/\sigma(\nu n \to \mu^- n\pi^+)$	0.38 ± 0.11 0.32 ± 0.11	/323/ /321/
$\sigma(\nu n \to \nu p\pi^-)/\sigma(\nu p \to \mu^- p\pi^+)$	0.11 ± 0.02	/324/
$\sigma(\nu p \to \nu p\pi^0)$ $\sigma(\nu p \to \nu n\pi^+)$ $\sigma(\nu n \to \nu n\pi^0)$ $\sigma(\nu n \to \nu p\pi^-)$	297 ± 37 180 ± 31 177 ± 43 237 ± 59	/321/[a]
$\sigma(\bar{\nu} p \to \bar{\nu} p\pi^0)/\sigma(\bar{\nu} p \to \mu^+ n\pi^0)$ $\sigma(\bar{\nu} p \to \bar{\nu} n\pi^+)/\sigma(\bar{\nu} p \to \mu^+ n\pi^0)$ $\sigma(\bar{\nu} n \to \bar{\nu} n\pi^0)/\sigma(\bar{\nu} p \to \mu^+ n\pi^0)$ $\sigma(\bar{\nu} n \to \bar{\nu} p\pi^-)/\sigma(\bar{\nu} p \to \mu^+ n\pi^0)$	0.30 ± 0.14 0.54 ± 0.22 0.49 ± 0.21 0.41 ± 0.20	/325/
$\frac{\sigma(\nu p \to \nu p\pi^0)+\sigma(\nu n \to \nu n\pi^0)}{\sigma(\nu n \to \nu p\pi^-)}$	1.4 ± 0.2	/326/
$\frac{\sigma(\bar{\nu} p \to \bar{\nu} p\pi^0)+\sigma(\bar{\nu} n \to \bar{\nu} n\pi^0)}{\sigma(\bar{\nu} n \to \bar{\nu} p\pi^-)} = \bar{r}_1$	2.1 ± 0.4 $2.4\ ^{+\ 0.8}_{-\ 0.6}$	/326/ /327/[b]
$\frac{\sigma(\nu p \to \nu p\pi^0)+\sigma(\nu n \to \nu n\pi^0)}{2\sigma(\nu n \to \mu^- p\pi^0)} = R_0$	0.47 ± 0.06 0.45 ± 0.08 0.17 ± 0.04	/328/[b] /321/[b] /12,329/
$\frac{\sigma(\bar{\nu} p \to \bar{\nu} p\pi^0)+\sigma(\bar{\nu} n \to \bar{\nu} n\pi^0)}{2\sigma(\bar{\nu} p \to \mu^+ n\pi^0)} = \bar{R}_0$	0.62 ± 0.08 $0.57\ ^{+\ 0.11}_{-\ 0.10}$ 0.39 ± 0.18	/328/[b] /327/ /12,329/
$\frac{\sigma(\bar{\nu} p \to \bar{\nu} p\pi^0)+\sigma(\bar{\nu} n \to \bar{\nu} n\pi^0)}{\sigma(\nu p \to \nu p\pi^0)+\sigma(\nu n \to \nu n\pi^0)} = r_{NC}$	0.50 ± 0.09	/328/

[a] Cross sections are given in arbitrary units

[b] Corrected for nuclear effects

In analysing the data quantitatively a model is needed that contains both I = 1/2 and I = 3/2 amplitudes, and which is applicable to single-pion data up to an invariant $N\pi$ mass of $W \simeq 2$ GeV (the range of the present data). Several models have been proposed in the literature. The isobar models /333/ which differ in terms of the different coupling constants, form factors and so on, give a phenomenological description of the resonant part of the amplitude in those single-pion channels which are clearly dominated by a resonance (e.g. $\Delta(1234$ MeV) for the 3/2 amplitude). The model of Adler and co-workers /334/ is based on fixed momentum-transfer dispersion relations for the invariant amplitudes and includes all the multipoles which excite the $\Delta(1234$ MeV) resonance and which are dominant in the Born approximation. This model, designed basically for the region W $\leq$ 1.4 GeV, is able to predict the non-resonant and the resonant pion production amplitudes in good agreement with the weak-pion production data. Recent approaches to single-pion production mechanism by Fogli and Nardulli /332/ and by Rein and Sehgal /335/ extend the investigated invariant mass region far away from the $\Delta(1234$ MeV) region and include I = 1/2 resonant and non-resonant contributions. All the models are in good agreement with the charged and neutral current data (using the standard theory with $\sin^2\Theta_W = 0.22$), but differ in detail, particularly in the vector/axialvector decomposition of the cross sections. Applying such a model to the total information on pion production, one can obtain useful constraints on the neutral-current parameters. Quantitative analyses by Abbott and Barnett /336/ and by Monsay /337/ show a preference for solution A of Table 4.13 (i.e. $\epsilon_L(u)\cdot\epsilon_L(d) < 0$, $\epsilon_L(u)\cdot\epsilon_R(u) < 0$). This is confirmed by a more recent analysis /338/ of the neutral-current induced single-pion production data with the view of extracting the isoscalar couplings γ and δ. The following values are extracted:

$$\begin{array}{ll} \text{isovector couplings} & \alpha = 0.677^{+0.242}_{-0.452}, \quad \beta = 0.993^{+0.372}_{-0.453} \\ \text{isoscalar couplings} & \gamma = -0.202^{+0.077}_{-0.123}, \quad \delta = 0.007^{+0.103}_{-0.102}. \end{array} \tag{4.126}$$

A definite answer to the question whether the hadronic neutral current is pure isovector or pure isoscalar, can already be given by a qualitative analysis of the data listed in Table 4.16:

(1) If the neutral current is *pure isoscalar* ($A_3 = A_1 = 0$, $S \neq 0$), only I = 1/2 πN final states are possible. So the following cross-section ratios for reactions (4.117 - 4.120) are predicted:

$$\sigma(p\pi^0) : \sigma(n\pi^0) : \sigma(n\pi^+) : \sigma(p\pi^-) = 1 : 1 : 2 : 2. \tag{4.127}$$

A confidence level of $< 10^{-4}$ is obtained in testing the compatibility of this prediction with the GARGAMELLE data /321/. Such a current is also not favoured by the antineutrino cross sections /325/ and by the measurements of the π^0/π^- ratio for single pion production on a Freon target /326/

$$\frac{\sigma(\nu p \to \nu p\pi^0) + \sigma(\nu n \to \nu n\pi^0)}{\sigma(\nu n \to \nu p\pi^-)} = 1.4 \pm 0.2,$$
$$\frac{\sigma(\bar\nu p \to \bar\nu p\pi^0) + \sigma(\bar\nu n \to \bar\nu n\pi^0)}{\sigma(\bar\nu n \to \bar\nu p\pi^-)} = 2.1 \pm 0.4$$

which differ significantly from the ratio 0.9 expected for a purely isoscalar current.

(2) If the current is *pure isovector*, both I = 1/2 and I = 3/2 πN final states are possible. But, if the final πN system is dominated by the I = 3/2 A_3 amplitude ($A_3 \neq 0$, $A_1 \simeq S = 0$), one expects the ratios

$$\sigma(p\pi^0) : \sigma(n\pi^0) : \sigma(n\pi^+) : \sigma(p\pi^-) = 2 : 2 : 1 : 1. \tag{4.128}$$

The probability for this hypothesis tested against the cross sections /321/ is found to be $2 \cdot 10^{-2}$, so that one can conclude that this expectation is, although not incompatible, still very unlikely. This is confirmed by measurements of neutral-current two-pion production from nucleons in the BNL 7-ft. bubble chamber /31/, where the ratio

$$\frac{\sigma(\nu n \to \nu n\pi^+\pi^-)}{\sigma(\nu p \to \nu p\pi^+\pi^-)} = 0.51 \pm 0.10.$$

is expected to be one for a pure isovector current /339/.

(3) Evidence for an *isoscalar-isovector interference term* comes from the difference of the cross sections for the charge symmetric reactions measured by the GARGAMELLE Collaboration /321/ (in arbitrary units):

$$\sigma(p\pi^0) - \sigma(n\pi^0) = -C \cdot \Re S^*(A_3 + \frac{1}{2}A_1) = 120 \pm 60$$
$$\sigma(p\pi^-) - \sigma(n\pi^+) = -C \cdot \Re S^*(A_3 - A_1) = 57 \pm 66$$

giving $C \cdot \Re S^* A_3 = -99 \pm 46$ and $C \cdot \Re S^* A_1 = -42 \pm 59$ /321/. It thus indicates the existence of a non-vanishing isoscalar contribution at the level of two standard deviations. Further evidence for a mixed isospin structure of the hadronic neutral current comes from a measurement of the π^0/π^- ratio in antineutrino-induced reactions /327/

$$\frac{\sigma(\bar\nu p \to \bar\nu p\pi^0) + \sigma(\bar\nu n \to \bar\nu n\pi^0)}{\sigma(\bar\nu n \to \bar\nu p\pi^-)} = 2.4^{+0.8}_{-0.6},$$

where the values 1.1 and 4.4 are expected for a pure isoscalar and pure isovector interaction (with A_3 dominance) respectively, taking into account the different number of neutrons and protons in a Freon target (n/p = 1.22).

(4) A clear signal of Δ production has been seen in the reactions $\nu p \to \nu p\pi^0\,(\nu p\pi^-)$ and $\bar\nu p \to \bar\nu p\pi^0\,(\bar\nu p\pi^-)$. Figs. 4.36 and 4.37 show the differential cross sections for these processes plotted against the pion-nucleon mass.

The experimental results /321,327/ for these mass plots are quite rough because of nuclear distortion effects due to reinteractions and because of limited statistics, but they clearly show a strong excitation of the $\Delta(1234$ MeV) resonance. This indicates, at least qualitatively, that the hadronic neutral current has a large isovector component (solutions A and B in Table 4.13) and suggests strongly that $(\alpha+\beta)$ is dominant and thus $\epsilon_L(u)\cdot\epsilon_L(d) < 0$. The remaining V/A ambiguity can only be resolved by a quantitative analysis of the data using one of the mentioned pion-production models.

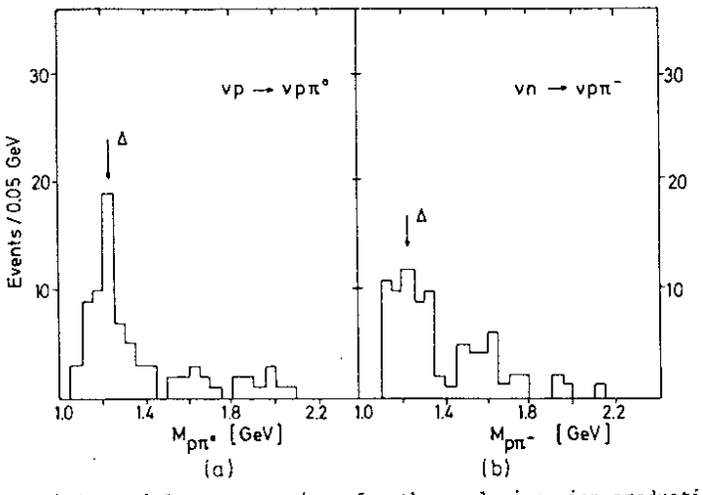

Fig. 4.36 Differential cross sections for the exclusive pion-production processes $\nu p \to \nu p\pi^0$ (a) and $\nu n \to \nu p\pi^-$ (b) plotted against the mass of the final-state $p\pi$ system /321/.

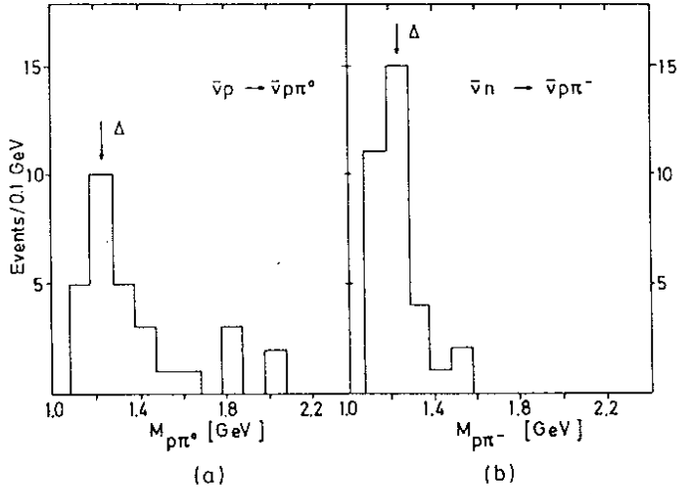

Fig. 4.37 Spectrum of invariant $p\pi^0$ (a) and $p\pi^-$ (b) masses in antineutrino-induced single-pion reactions /327/.

4.3.2.4.3. Antineutrino disintegration of the deuteron

A study of the neutrino (antineutrino) disintegration of the deuteron (Fig. 4.38)

$$\nu(\bar{\nu}) + d \to \nu(\bar{\nu}) + p + n \tag{4.129}$$

at intermediate neutrino energies (≤ 500 MeV) can help to elucidate the isospin and Lorentz character of the neutral weak current.

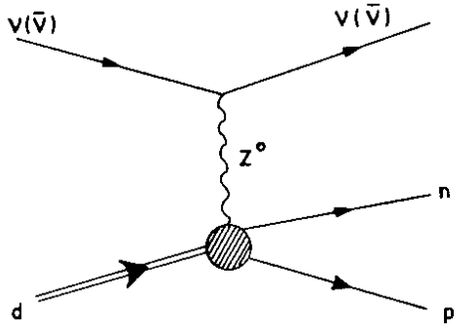

Fig. 4.38 Diagram for the neutrino (antineutrino) disintegration of the deuteron.

At and near the threshold ($E_\nu = 2.225\,MeV = E_b$ = binding energy of the deuteron) only a Gamow-Teller type transition is possible between nondiagonal (nondegenerated in energy) nuclear levels /340,341/. For the deuteron, this is caused by the isovector part of the axialvector current since near the threshold only the isospin-flip and spin-flip transition ${}^3S_1(I=0) \to {}^1S_0(I=1)$ is important. Therefore, neutrino disintegration of the deuteron near the threshold is sensitive only to the coupling parameter β of the neutral current and is thus, in the framework of the standard model, independent of the electroweak mixing angle. Away from the threshold, the forbidden transitions (i.e. the pure isoscalar V, A transition ${}^3S \to {}^1P$ and the pure isovector V, A transition ${}^3S \to {}^3P$) have to be taken into account. But they are not appreciable unless the incident neutrino energy is very high /340/.

A 4σ signal of the weak disintegration of the deuteron via a neutral current, $\bar{\nu}_e + d \to \bar{\nu}_e + p + n$, has been observed by an Irvine group /342/ using a well-shielded instrumented target of 268 kg D_20 exposed to an intense $\bar{\nu}_e$ flux of $2.5 \cdot 10^{13} cm^{-2} sec^{-1}$. The reaction was detected with use of only the product neutron as signature (via the reaction ${}^3He + n \to p + {}^3H + 764$ keV in ^{3}He-filled gas proportional counters). The measured cross section of $(3.8 \pm 0.9) \times 10^{-45} cm^2$, corresponds to

$$|\beta| = 0.9 \pm 0.1 \tag{4.130}$$

which has to be compared to $\beta = 0.92 \pm 0.14$ predicted for solution A and $\beta = 0.58 \pm 0.14$ expected for solution B, respectively. The experimental data are in excellent agreement with solution A and establish that

$$\epsilon_L(u) \cdot \epsilon_R(u) < 0\,, \tag{4.131}$$

while solution B is excluded at the level of approximately two standard deviations (solutions C and D are ruled out even more strongly).

4.3.2.4.4. Coherent π^0 production

The Aachen-Padova Collaboration /343/ has observed, in a spark chamber experiment at the CERN Proton Synchrotron (PS), a signal for π^0 production in a coherent interaction of the neutrino (antineutrino) with a complex nucleus as a whole:

$$\nu_\mu(\bar{\nu}_\mu) + Al^{27} \rightarrow \nu_\mu(\bar{\nu}_\mu) + Al^{27} + \pi^0. \tag{4.132}$$

As already pointed out /246,344/ (Chap. 4.2.4.5), this coherent process is dominated by the divergence of the isovector axialvector neutral current, and can be calculated using the PCAC theorem /345/. Thus the magnitude of the coherent π^0 cross section determines selectively the strength of this particular component of the hadronic current (parameter β in Sakurai's notation).

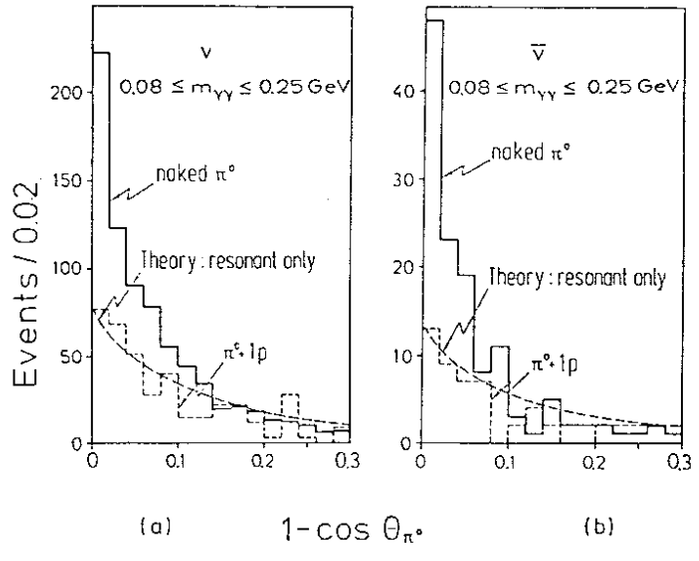

Fig. 4.39 Angular distributions of neutrino (a) and antineutrino (b) produced π^0's ($0.08\ \text{GeV} \leq m_{\gamma\gamma} \leq 0.25\ \text{GeV}$) compared with a prediction for resonant production /335/ and a control sample with visible proton recoil /343/.

The analysis is based on fully reconstructed 2γ events with no visible recoil. A resolution of $\sim$ 33 % is achieved for the 2γ invariant mass, and the π^0 can be reconstructed to $\sim \pm 45$ mrad in polar angle Θ_{π^0} and in azimuth. Figures 4.39 show the angular distributions of selected π^0 in both, neutrino and antineutrino interactions. These distributions exhibit clear forward peaks (for $\Theta_{\pi^0} \leq 16°$) as expected for π^0's produced in coherent interactions.

A control sample of π^0's accompanied by a visible proton recoil (essentially due to the reactions $\overset{(-)}{\nu}_\mu p \rightarrow \overset{(-)}{\nu}_\mu p\pi^0$) does not show a comparable sharp peak in forward direction. This behaviour agrees quite well with the theoretical prediction for the angular distributions of the incoherent background (dashed curves) coming from $\overset{(-)}{\nu}_\mu n \rightarrow \overset{(-)}{\nu}_\mu n\pi^0$ and $\overset{(-)}{\nu}_\mu p \rightarrow \overset{(-)}{\nu}_\mu p\pi^0$ events with no visible proton recoils. This calculation is based on the resonance model of Rein and Sehgal /335/, in which the final pion-nucleon system is treated as a superposition of I = 1/2 and I = 3/2 resonances using the relativistic quark model of Feynman, Kislinger and Ravndal /346/ to calculate the matrix elements.

The excess of naked π^0 in forward direction ($\Theta_{\pi^0} \leq 16°$) is attributed to coherent π^0 production, resulting in absolute cross sections /343/

$$\begin{aligned} \sigma_\nu^{\text{coh}} &= (29 \pm 10) \times 10^{-40}\ cm^2/Al^{27}\text{-nucleus} \\ \sigma_{\bar{\nu}}^{\text{coh}} &= (25 \pm 7) \times 10^{-40}\ cm^2/Al^{27}\text{-nucleus} \end{aligned} \tag{4.133}$$

where the error is statistical only. The observation that coherent π^0 production occurs with equal cross sections for neutrino and antineutrino (i.e. that coherent π^0 production is essentially a parity-conserving reaction) justifies the assumption that the vector contributions to these processes are negligible.

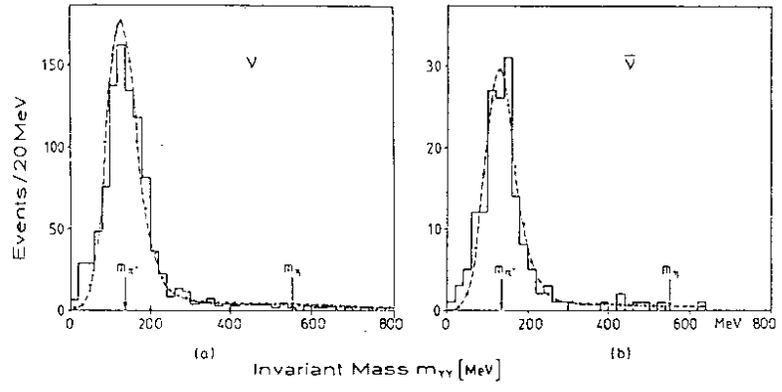

Fig. 4.40 Invariant mass distributions $m_{\gamma\gamma}$ of fully reconstructed 2 γ events produced by neutrinos (a) and antineutrinos (b), respectively /343/.

By comparing the Aachen-Padova results (4.133) with the theoretically expected absolute cross sections at $E_\nu = 2$ GeV /246,348/

$$\beta = 0.93 \pm 0.12 \tag{4.134}$$

is obtained in good agreement with the standard model prediction $\beta = 1$.

The absence of a η^0 signal in the 2γ events (Figures 4.40) imposes a limit on the isoscalar axialvector coupling parameter δ. Taking into account the difference of phase space and the $\eta^0 \to \gamma\gamma$ branching ratio (0.39), the limit on δ is /343/

$$\delta < 0.7 \qquad (90\ \%\ \text{C.L.})$$

which has to be compared with $\delta = 0$ as predicted by the standard model in lowest order.

A recent analysis /347/ of isolated electromagnetic showers in the GARGAMELLE Freon experiment extracts also absolute cross sections for coherent π^0 production which are compatible with the numbers given in (4.133).

The CHARM Collaboration /349/ has also carried out measurements of coherent π^0 production by ν_μ and $\bar{\nu}_\mu$ on nuclei in marble using the CHARM neutrino detector in the CERN-SPS neutrino wide band beam ($< E_\nu > \sim 31$ GeV and $< E_{\bar{\nu}} > \sim 24$ GeV). Out of $\sim 1.3 \times 10^6$ neutrino and $\sim 1.4 \times 10^6$ antineutrino interactions, respectively, $\sim 600\,\nu$ and $\sim 1300\,\bar{\nu}$ candidates for coherent π^0 production have been selected by following closely the procedure used in the analysis of $\overset{(-)}{\nu}_\mu e$ scattering (Chap. 4.3.1.2). Taking the background processes into account and correcting for the efficiencies, this results in

$$\begin{aligned} \sigma_\nu^{coh} &= (96 \pm 42) \times 10^{-40}\ cm^2/ \text{<nucleus in marble>} \\ \sigma_{\bar{\nu}}^{coh} &= (79 \pm 26) \times 10^{-40}\ cm^2/ \text{<nucleus in marble>} \end{aligned} \tag{4.135}$$

Comparing these experimental results to theoretical predictions /348/ one obtains the isovector axialvector neutral-current coupling constant

$$|\beta| = 1.08 \pm 0.24\,, \tag{4.136}$$

averaged over the neutrino and antineutrino results. The uncertainties of the theoretical calculation can partly be eliminated by comparing /349/ coherent π^0 production by neutral-current interactions observed in the CHARM experiment to coherent π^- production by charged-current interactions of antineutrinos measured in BEBC. Assuming $\rho = 1$ one finds

$$|\beta| = 1.10 \pm 0.23\,. \tag{4.137}$$

Finally it can be concluded that the study of coherent π^0 production favours again the solutions with $\epsilon_L(u) \cdot \epsilon_R(u) < 0$.

4.3.2.4.5. Diffractive neutrino reactions

The experimental study of diffractive production of vector and/or axialvector mesons in neutral-current interactions

$$\overset{(-)}{\nu} + N \to \overset{(-)}{\nu} + \rho^0(\omega,\varphi) + N, \qquad \overset{(-)}{\nu} + N \to \overset{(-)}{\nu} + A_1 + N \tag{4.138}$$

can provide additional information about the vector/axialvector and isoscalar/isovector ambiguities in the neutral-current sector (Chap. 4.2.4.6). The calculations performed to estimate the cross sections for reactions (4.138) are, unfortunately, highly model-dependent /248,249/. But if one compares the neutral-current reactions with their charged-current analogues, the model uncertainties cancel out /350/. One expects then:

$$\left.\frac{\sigma(\nu N \to \nu \rho^0 N)}{\sigma(\nu N \to \mu^- \rho^+ N)}\right|_{\text{diffractive}} = \frac{1}{2}\,\alpha^2 \tag{4.139}$$

$$\left.\frac{\sigma(\nu N \to \nu A_1 N)}{\sigma(\nu N \to \mu^- A_1^+ N)}\right|_{\text{diffractive}} = \frac{1}{2}\,\beta^2\,. \tag{4.140}$$

To resolve the ambiguities in inclusive and semi-inclusive data (Table 4.13) already a rough knowledge of diffractive processes is sufficient, since one only wants to know whether $|\alpha| > |\beta|$ or $|\alpha| < |\beta|$.

An experiment at Fermilab /252/ measured the cross-section ratio of diffractive ρ^0 production by neutral currents and ρ^- production by charged currents in antineutrino-induced reactions which is expected to be proportional to α^2 (Eq. 4.139). The result is $|\alpha| = 0.44 \pm 0.18$. It fulfills the relation $|\alpha| < |\beta|$ when $|\beta|$ is taken from another analysis. Therefore, diffractive production of vector mesons favours once more the solutions with $\epsilon_L(u) \cdot \epsilon_R(u) < 0$ (i.e. solutions A and C in Table 4.13).

4.3.2.5. Determination of hadronic weak neutral current

All the experimental data together offer a high degree of redundancy. They single out solution A (i.e. $\epsilon_L(u) \cdot \epsilon_L(d) < 0$ and $\epsilon_L(u) \cdot \epsilon_R(u) < 0$) as the favoured solution. Thus the hadronic weak neutral current is determined to be dominantly isovector-axialvector. One finds (within errors) a single set of coupling constants, both in left-handed and right-handed space (Fig. 4.41). Both solutions are consistent with the constraint imposed by the standard model (Table 4.17) and both correspond to the same value of $\sin^2\Theta_W = (0.2 - 0.25)$ which, on the other hand, is consistent with that obtained from the purely leptonic reactions (Chap. 4.3.1).

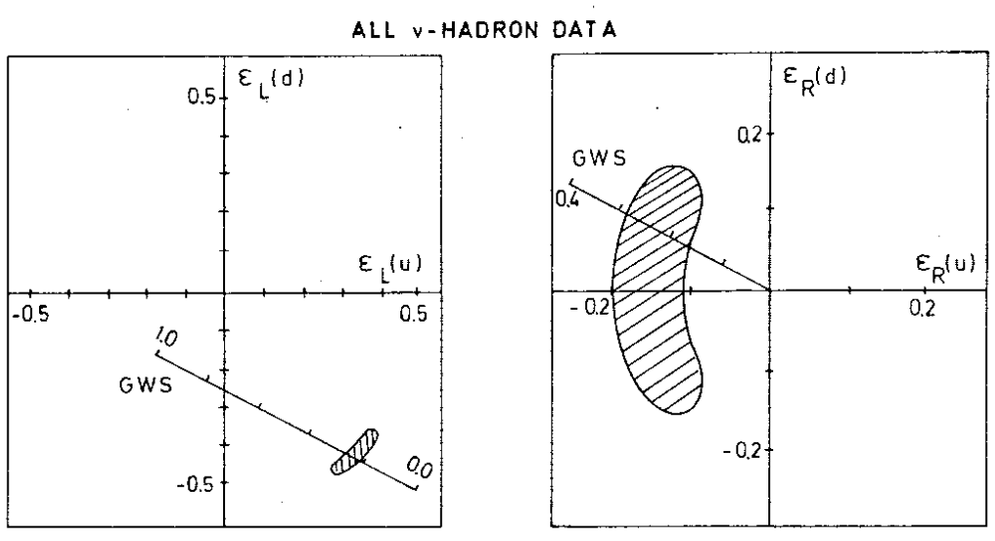

Fig. 4.41 Constraints imposed on the hadronic neutral-current couplings (90% confidence level) by a simultaneous fit to the inclusive and semi-inclusive ν, $\bar{\nu}$ - hadron data discussed above. Only the shaded region is allowed by exclusive neutral-current ν, $\bar{\nu}$ data /281/. The prediction of the standard model is shown as a function of $\sin^2\Theta_W$.

Table 4.17. Summary of quark couplings determined by a fit to the $\nu,\bar{\nu}$-hadron data /281/. The number in brackets are the predictions from the standard model with $\sin^2\Theta_W = 0.22$.

$\varepsilon_L(u) = 0.344 \pm 0.026$ (0.353)	$\alpha = 0.533 \pm 0.037$ (0.560)
$\varepsilon_L(d) = -0.419 \pm 0.022$ (-0.427)	$\beta = 0.992 \pm 0.037$ (1.0)
$\varepsilon_R(u) = -0.153 \pm 0.022$ (-0.147)	$\gamma = -0.152 \pm 0.089$ (-0.147)
$\varepsilon_R(d) = 0.076 \pm 0.041$ (0.073)	$\delta = 0.002 \pm 0.049$ (0)
$\Theta_L = 140.6^\circ \pm 3.6^\circ$ (140°)	$\Theta_R = 296.4 \pm 14.2$ (296°)

5. WEAK NEUTRAL CURRENTS IN MUON-QUARK SCATTERING

Muon-induced weak neutral currents are expected in the standard model. At the energies presently available the weak interaction is overwhelmed by the electromagnetic one. But their interference may be used to get information about the properties of the neutral weak force. One of the aims of high-intensity deep-inelastic muon scattering experiments is thus to determine, by measuring possible interference effects, the parameters of the muon-quark interaction Lagrangian

$$\mathcal{L}_{NC}^{\mu q} = \frac{G}{\sqrt{2}}\Big[\bar{\mu}\gamma_\alpha\left(C_V^\mu + C_V'^\mu\gamma_5\right)\mu\cdot\bar{q}_i\gamma^\alpha q_i + \bar{\mu}\gamma_\alpha\gamma_5\left(C_A^\mu + C_A'^\mu\gamma_5\right)\mu\cdot\bar{q}_i\gamma^\alpha\gamma_5 q_i$$
$$+\bar{\mu}\left(C_S^\mu + C_S'^\mu\gamma_5\right)\mu\cdot\bar{q}_i q_i + \bar{\mu}\gamma_5\left(C_P^\mu + C_P'^\mu\gamma_5\right)\mu\cdot\bar{q}_i\gamma_5 q_i \qquad (5.1)$$
$$+\bar{\mu}\sigma_{\alpha\beta}\left(C_T^\mu + C_T'^\mu\gamma_5\right)\mu\cdot\bar{q}_i\sigma^{\alpha\beta}q_i\Big],$$

where μ and q_i are muon field and i^{th} quark field, respectively. C_i^μ and $C_i'^\mu$ are the V, A, S, P, T-type coupling constants constrained by $C_S'^\mu = C_P'^\mu = C_T'^\mu = 0$ if CP conservation of the weak current is assumed.

The determination of the muon couplings is of fundamental interest for neutral-current μ-e universality, for the single Z-boson hypothesis (Chap. 2.9), for the existence of right-handed currents and of muon-induced parity violation /351/.

5.1. Study of S, P, T-type neutral weak currents

Deep-inelastic muon scattering offers in principle a possibility to discriminate directly between V, A and S, P, T contributions to weak neutral-current interactions by measuring helicity correlations between initial and final state muons.

In the rest frame of the pion positive (negative) muons, originating from $\pi \to \mu\nu$ decays, are always left (right)-handed: μ_L^+, μ_R^-. By using a high-energy beam of pions as a source of muons, the helicity remains negative (positive) for those muons emitted forward. Muons emitted backward will have a positive (negative) helicity if the pion velocity in the laboratory system is larger than the muon velocity in the pion rest system, $\beta_\pi > \beta_\mu^*$. In general the helicity λ of the muons is a function of the decay angle Θ_μ^* in the pion rest system /42/

$$\lambda = \mp\frac{\cos\Theta_\mu^* + (\beta_\mu^*/\beta_\pi)}{1 + (\beta_\mu^*/\beta_\pi)\cos\Theta_\mu^*}, \qquad (5.2)$$

where the upper and lower sign applies to π^+ and π^-, respectively. The helicity can thus be selected by momentum analysis of the decay muons. Muons with momentum $p_\mu \simeq p_\pi$ and $p_\mu \simeq (m_\mu/m_\pi)^2 p_\pi$ - corresponding to $\cos\Theta_\mu^* = +1$ and -1 - have helicity $\lambda_{\mu^+(\mu^-)} = -1\,(+1)$ and $\lambda_{\mu^+(\mu^-)} = +1\,(-1)$, respectively, in the limit of $\beta_\pi \to 1$.

The helicity of the final state muons could then be measured using the parity-violating decay of stopped muons as helicity analyser, in complete analogy to the charged-current polarization experiment /181,182/ described in section 3.3.1.

The scattering of longitudinally polarized muons can proceed by electromagnetic and weak interactions (Fig. 5.1). The V, A coupling types of weak interaction can interfere with the electromagnetic interaction since both preserve the muon helicity, whereas S, P, T-type coupling interactions interfere with each other and change the helicity of the muon. Possible S, P, and T contributions could thus be detected by measuring the final-state muon helicity.

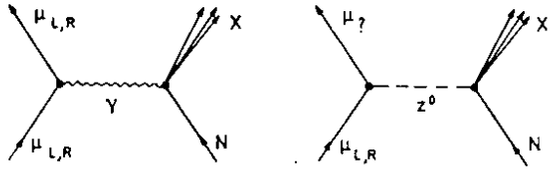

Fig. 5.1 Feynman diagrams in muon scattering.

Since the ratio of the helicity-changing cross section of muon scattering on a nucleon to the helicity-preserving cross section /352/

$$\frac{\sigma(\mu_L N \to \mu_R X)}{\sigma(\mu_L N \to \mu_L X)} = \frac{\sigma(\mu_R N \to \mu_L X)}{\sigma(\mu_R N \to \mu_R X)} = \frac{\sum_i f_i(x)\left[2(C_S^{\mu^2} + C_P^{\mu^2})a_1 + C_T^{\mu}(C_S^{\mu} + C_P^{\mu})a_2 + C_T^{\mu^2}a_3\right]}{\sum_i f_i(x)\left[(e^2/Q^2)e_{q_i}\right]^2 64\,(s-m_\mu^2)^2\left[1+(1-y)^2\right]} \tag{5.3}$$

(neglecting the V, A weak interactions in the helicity-preserving cross section) has a Q^4-dependence, experiments carried out at high Q^2 (square of the momentum transfer between the muon and the struck quark) would be very sensitive to small helicity-flip amplitudes. s is the total energy squared in the center-of-mass system, e_{q_i} is the charge of the ith quark (i=u, d, s,...) and $f_i(x)$ is the probability of finding a quark of type i with fractional longitudinal momentum $x = Q^2/2M\nu$ in the nucleon. The a_i's are functions of the inelasticity $y = \nu/E_\mu^{in} = 1 - E_\mu^{out}/E_\mu^{in}$ /352/:

$$\begin{aligned} a_1 &= 16\,(s-m_\mu^2)^2 y^2 + 32 m_\mu^2 (s-m_\mu^2)\, y \\ a_2 &= -256\,(s-m_\mu^2)^2 y(1-\frac{1}{2}y) \\ a_3 &= 1024\Big[(s-m_\mu^2)^2(1-y+\frac{1}{4}y^2) - m_\mu^2\frac{1}{2}(s-m_\mu^2)\,y\Big]. \end{aligned} \tag{5.4}$$

The experimental requirements needed to study the polarization of scattered muons in deep-inelastic muon scattering have been examined /353/ for the high-intensity muon beams at CERN and Fermilab Tevatron (where Q^2 can reach up to $\sim 600\ GeV^2/c^2$), with intent to elucidate the Lorentz structure of the neutral weak current in the manner discussed above.

5.2. Parity-violation asymmetries

In deep-inelastic muon scattering parity-violating neutral-current effects are expected to be of the order of

$$\frac{A_{em}\cdot A_{weak}}{|A_{em}|^2 + |A_{weak}|^2} \simeq \frac{A_{weak}}{A_{em}} \simeq \frac{G/\sqrt{2}}{2\pi\alpha/Q^2} = \kappa = 1.79\times 10^{-4}\,Q^2\ (\text{in } GeV^2/c^2) \tag{5.5}$$

resulting from the interference of (dominant) one-photon exchange (amplitude A_{em}) with Z-boson exchange (amplitude A_{weak}) /14,354/. Possible helicity-flip amplitudes are neglected. At $Q^2 = 200\ GeV^2/c^2$ one expects therefore about 3 % effects.

For a given magnitude of beam helicity λ there exist three independent cross section asymmetries /351/ whose observation would manifest such expected interference effects. Varying the beam polarization and keeping the charge of the muons fixed gives two parity-violation asymmetries (which are of the type measured at the SLAC experiment described in Chap. 6.1):

$$A^{\pm} = \frac{d\sigma^{\pm}(\lambda_1) - d\sigma^{\pm}(\lambda_2)}{d\sigma^{\pm}(\lambda_1) + d\sigma^{\pm}(\lambda_2)} = -\kappa\,\frac{(\lambda_1-\lambda_2)}{2}\left[\pm g_A^{\mu} V(x) + g_V^{\mu} A(x) g(y)\right], \tag{5.6}$$

with

$$g(y) = \frac{1-(1-y)^2}{1+(1-y)^2}. \tag{5.7}$$

g_V^{μ} and g_A^{μ} denote the vector and axialvector coupling of the muon, respectively, by rewriting the Lagrangian (5.1) in the form

$$\mathcal{L}_{NC,VA}^{\mu q} = \frac{G}{\sqrt{2}}\left[\bar{\mu}\gamma_\alpha\left(g_V^{\mu} + g_A^{\mu}\gamma_5\right)\mu\cdot\bar{q}_i\gamma^\alpha\left(g_V^{i} + g_A^{i}\gamma_5\right)q_i\right] \tag{5.8}$$

for V, A contributions only. V(x) and A(x) are ratios of structure functions which for isoscalar targets reduce to constants in the framework of the quark parton model (even if the quark distributions depend on Q^2):

$$\begin{aligned} V &= \frac{6}{5}(2g_V^u - g_V^d) \\ A &= \frac{6}{5}(g_A^d - 2g_A^u), \end{aligned} \tag{5.9}$$

where g_V^i, g_A^i are the vector and axialvector couplings of the quarks (i = u, d) which in Sakurai's notation /31/ read:

$$\begin{aligned} g_V^u &= \frac{1}{2}(\tilde{\alpha}+\tilde{\gamma}), \qquad & g_A^u &= \frac{1}{2}(\tilde{\beta}+\tilde{\delta}) \\ g_V^d &= \frac{1}{2}(-\tilde{\alpha}+\tilde{\gamma}), \qquad & g_A^d &= \frac{1}{2}(-\tilde{\beta}+\tilde{\delta}). \end{aligned} \tag{5.10}$$

Inserting (5.9) in (5.8) one obtains

$$\begin{aligned} V &= \frac{3}{5}(3\tilde{\alpha}+\tilde{\gamma}) \\ A &= -\frac{3}{5}(3\tilde{\beta}+\tilde{\delta}) \end{aligned} \tag{5.11}$$

implying enhanced isovector ($\tilde{\alpha}, \tilde{\beta}$) over isoscalar current contributions ($\tilde{\gamma}, \tilde{\delta}$) to the asymmetries (5.6).

The only experiment to study these partity-violation asymmetries with muons was performed at Serpukhov /355/ using longitudinally polarized μ-beams ($\lambda_1 \simeq -\lambda_2$) with average muon momenta of 21 GeV/c. No statistically significant dependence of the μN cross section on the longitudinal polarization of the muons has been found in this relatively low Q^2-domain (Fig. 5.2). The magnitude of this cross-section asymmetry is given by

$$A^- = (-4 \pm 6) \times 10^{-3} < Q^2/(GeV^2/c^2) > .$$

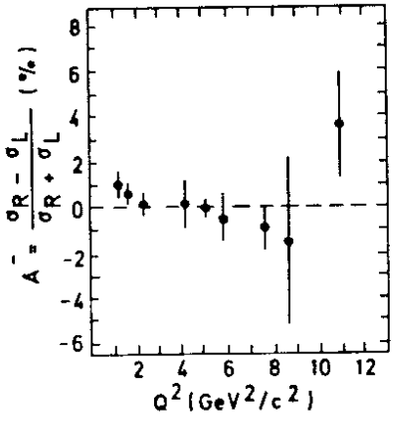

Fig. 5.2 Dependence of the parity-violation asymmetry $A^- = [\sigma^-(\lambda>0) - \sigma^-(\lambda<0)]/[\sigma^-(\lambda>0) + \sigma^-(\lambda<0)]$ on the average momentum transfer squared, Q^2 /354/.

5.3. Beam-conjugation asymmetry

Variation of both the beam charge and the helicity defines a third asymmetry

$$B(\lambda_1, \lambda_2) = \frac{d\sigma^+(\lambda_1) - d\sigma^-(\lambda_2)}{d\sigma^+(\lambda_1) + d\sigma^-(\lambda_2)} \tag{5.12}$$

which is equal to

$$B(\lambda_1, \lambda_2) = -\kappa \left[g_A^\mu A(x) g(y) + \frac{\lambda_1 - \lambda_2}{2} g_V^\mu A(x) g(y) - \frac{\lambda_1 + \lambda_2}{2} g_A^\mu V(x) \right] \tag{5.13}$$

taking into account only one-photon and one-Z^0 exchange graphs /351/. This asymmetry is predominantly due to the parity-conserving $A_{lepton} \cdot A_{quark}$ interaction while the asymmetries $A^\pm$ (Eq. 5.6) primarily explore the parity-violating $A_{lepton} \cdot V_{quark}$ interaction.

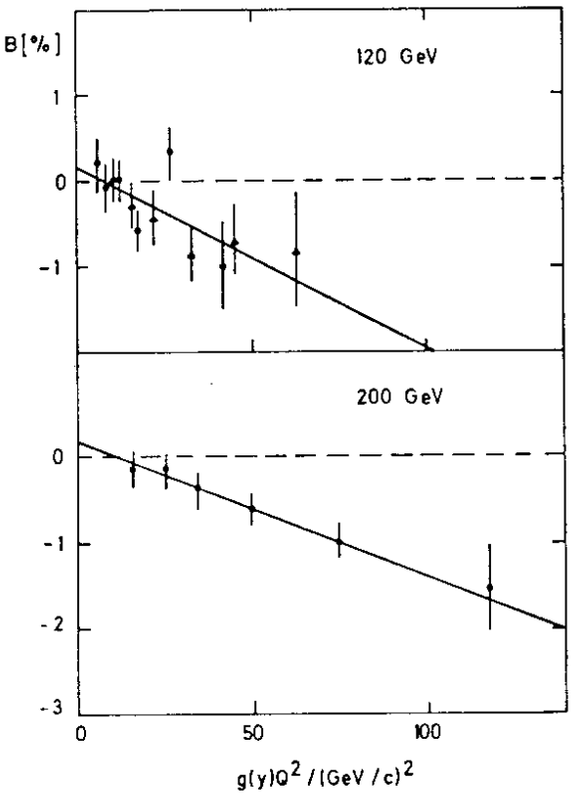

Fig. 5.3 Measured B asymmetry after radiative corrections at 120 GeV and 200 GeV beam energy as a function of $g(y)Q^2$ /355/. For the 120 GeV data, circles represent data with Q^2>15 GeV^2/c^2 and triangles data with Q^2>25 GeV^2/c^2. For the 200 GeV data a higher Q^2-cut (Q^2>40 GeV^2/c^2) has been applied. Solid lines are straight line fits to the data.

The Bologna-CERN-Dubna-Munich-Saclay (BCDMS) Collaboration has studied /356/ deep-inelastic scattering of polarized muons on nucleons

$$\mu_R^- + C \rightarrow \mu^- + X$$
$$\mu_L^+ + C \rightarrow \mu^+ + X$$

at two energies 120 and 200 GeV using an isoscalar target (carbon). This experiment has established a statistically significant beam-conjugation asymmetry

$$B = \frac{d\sigma^+(-\lambda) - d\sigma^-(\lambda)}{d\sigma^+(-\lambda) + d\sigma^-(\lambda)} = -\kappa (g_A^\mu - \lambda g_V^\mu) A(x) g(y) \tag{5.14}$$

by reversing simultaneously both the charge and the helicity of the muon ($|\lambda| \sim 0.81$ at 200 GeV and $|\lambda| \sim 0.66$ at 120 GeV). Figs. 5.3 show the measured asymmetries for the two beam energies as a function of $g(y)Q^2$. The data have been corrected for higher-order electromagnetic and weak-electromagnetic effects /357/. The following values for the slope b of the B asymmetry are obtained

$$b = \left[-0.147 \pm 0.037\,(\text{stat}) \pm 0.02\,(\text{syst})\right] \times 10^{-3}\ (GeV/c)^{-2} \quad \text{at 200 GeV}$$

$$b = \left[-0.174 \pm 0.075\,(\text{stat}) \pm 0.03\,(\text{syst})\right] \times 10^{-3}\ (GeV/c)^{-2} \quad \text{at 120 GeV}$$

by fitting the two data samples independently to $B = a + b\,g(y)\,Q^2$.

The general gauge theory couplings of the muon, allowing for left- and right-handed weak isospin multiplets, can (Eqs. 2.36) be expressed as

$$\begin{aligned} g_V^\mu &= \rho\left[T_3^L + T_3^R - 2\sin^2\Theta_W Q_\mu\right] \\ g_A^\mu &= \rho\left[T_3^L - T_3^R\right], \end{aligned} \tag{5.15}$$

where Q_μ is the charge of the muon and ρ denotes the ratio of the over-all strengths of neutral- and charged-current couplings.

These couplings are related to the slope b of the B asymmetry by

$$b = \rho\left[T_3^L(\lambda - 1) + T_3^R(\lambda + 1) + 2\lambda\sin^2\Theta_W\right]\frac{G}{\sqrt{2}}\frac{1}{2\pi\alpha}A(x), \tag{5.16}$$

where the fact that μ^+ (μ^-) have negative (positive) helicity has been taken into account. This shows that the experimentally prefered helicity $\lambda \approx 1$ implies sensitivity of b to the right-handed muon coupling and to $\sin^2\Theta_W$. Therefore, the experimental results for the slope parameter b can be used either to determine the electroweak mixing angle in the framework of the standard model ($T_3^L = -1/2$, $T_3^R = 0$, $\rho = 1$) giving /356/

$$\sin^2\Theta_W = 0.23 \pm 0.07\,(\text{stat}) \pm 0.04\,(\text{syst}), \tag{5.17}$$

or to determine the right-handed weak charge T_3^R of the muon assuming $\sin^2\Theta_W = 0.23$ and $T_3^L = -1/2$. One finds

$$T_3^R = 0.00 \pm 0.06\,(\text{stat}) \pm 0.04\,(\text{syst}). \tag{5.18}$$

This result rules out a weak-isospin doublet of the form

$$\begin{pmatrix} M^0 \\ \mu^- \end{pmatrix}_R$$

where M^0 is a heavy neutral lepton with no mass restriction.

The BCDMS Collaboration /356/ was moreover able to extract the weak-electromagnetic interference structure function $xG_3(x)$ by measuring the beam-conjugation asymmetry B as a function of x:

$$B = \kappa\,(g_A^\mu - \lambda g_V^\mu)\,\frac{xG_3(x)}{F_2(x)}\,g(y). \tag{5.19}$$

For high x where effects of the sea-quark contribution can be neglected, one finds

$$\frac{xG_3}{F_2} = \frac{2\,(g_A^u Q_u + g_A^d Q_d)}{Q_u^2 + Q_d^2} \tag{5.20}$$

which in the standard model is equal to $\frac{9}{5}$. Q_i is the charge of the quark i (= u,d). Experimentally one finds for the ratio (5.20) a value of 1.87 ± 0.25 (stat) ± 0.24 (syst). This measurement can be used to impose constraints on the chiral coupling constants $\epsilon_R(u)$ and $\epsilon_R(d)$, if factorization is assumed and the left-handed coupling constants are taken from other experiments /358/. It excludes regions in the $\epsilon_R(u)$-$\epsilon_R(d)$ plane as shown in Fig. 5.4.

Eq. (5.16) makes clear that the quantities $\sin^2\Theta_W$, ρ, and T_3^R can be determined simultaneously provided that the experiment can be performed at different values of the beam helicity λ.

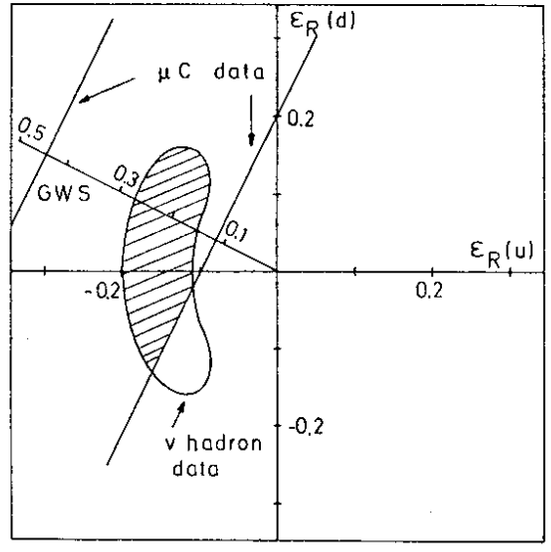

Fig. 5.4 Allowed regions (at 90% C.L.) for the right-handed neutral-current couplings by a simultaneous fit to all neutrino-hadron data. The constraints given by the muon-carbon scattering experiments are shown, using the left-handed coupling constants from other experiments as input /358/. The prediction of the standard model is given as a function of $\sin^2\Theta_W$.

6. WEAK NEUTRAL CURRENTS IN ELECTRON-QUARK SCATTERING

Substantial progress has been made in determining the neutral-current couplings by the study of interactions of electrons with hadrons (ultimately with quarks) as revealed in optical transitions of heavy atoms and in inelastic scattering of polarized electrons on deuterons (historically the most decisive experiment in eliminating various alternatives to the standard model).

These non-neutrino reactions can be used to distinguish V, A couplings from alternative coupling types. The observed neutrino-antineutrino cross-section differences (Chap. 4), for example, can be explained in both V, A and S, P, T current pictures. In the V, A coupling case the presence of such cross-section differences (implying the presence of V, A interference effects) is in general accompanied by parity-violating neutral-current effects in processes in which neutrinos are not involved. For S, P, T type couplings neutrino and antineutrino cross-sections can also differ since both even (S and P) and odd (T) charge conjugation pieces are present. But there would not be neutral-current induced parity-violating effects in non-neutrino reactions, since a CP-conserving S, P, T Lagrangian is still parity-conserving. In multiboson models neutrino-antineutrino inequalities are also possible /359/ for a strictly parity-conserving neutral force (e.g. VV + AA type) which, however, would not induce parity-violating neutral-current effects in non-neutrino processes. This may illustrate the importance of non-neutrino experiments such as μq, eq experiments in answering some very basic questions about the neutral weak interaction and in confirming some of the results extracted from neutrino physics, respectively.

The electron-quark neutral-current interaction can be divided into a parity-conserving part containing $V_{lepton} \cdot V_{quark}$ and $A_{lepton} \cdot A_{quark}$ terms and a parity-violating part, described by the Lagrangian (2.63), containing $A_{lepton} \cdot V_{quark}$ and $V_{lepton} \cdot A_{quark}$ terms. At low Q^2 ($\leq 10^4\ GeV^2/c^2$) the effect of parity-conserving neutral-current interactions is expected to be completely overwhelmed by the much stronger electromagnetic interactions. But parity-violating neutral-current interactions may be detected by looking for the dependence of experimental observables on pseudoscalars as, for instance, the electron or photon helicity. Such parity-violating effects of the order $\sim 10^{-4}Q^2$ (Eq. 5.5) are expected to arise from the interference between the γ-exchange and Z^0-exchange diagrams (Fig. 6.1).

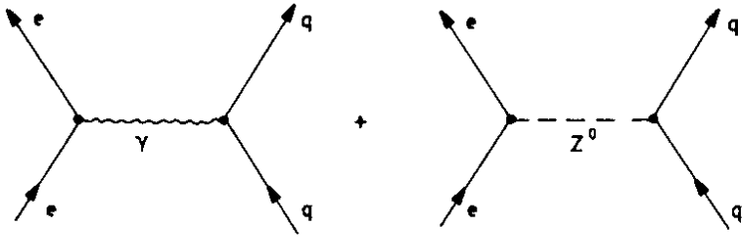

Fig. 6.1 Weak-electromagnetic interference in electron-quark interaction.

6.1. Scattering of polarized electrons on deuterons

In this experiment performed at SLAC /40,41/ the parity-violating cross section asymmetry

$$A(x,y,Q^2) = \frac{d\sigma_{e_R D} - d\sigma_{e_L D}}{d\sigma_{e_R D} + d\sigma_{e_L D}} \tag{6.1}$$

for the scattering of right-handed and left-handed electrons on deuterium

$$e^-_{L,R} + D \rightarrow e^- + X \tag{6.2}$$

was measured. Here $-Q^2$ is the virtual photon mass squared, x is the Bjorken variable and $y = (E - E')/E$, where E and E' are the initial and final electron energies in the lab frame. The average momentum transfer was $< Q^2 >= 1.6\ GeV^2/c^2$, and the inelasticity region $0.15 \leq y \leq 0.36$ was covered.

The dependence of A on x, y and Q^2 is of the form

$$A(x,y,Q^2) = Q^2 \left[a_1(x) + a_2(x) \frac{1-(1-y)^2}{1+(1-y)^2} \right]. \tag{6.3}$$

a_1, a_2 are proportional to the interference of the weak and electromagnetic amplitudes. a_1 is proportional to the axial coupling of the electron times the vector coupling of the quarks, while a_2 is proportional to the vector coupling of the electron times the axial coupling of the quarks. A calculation by Cahn and Gilman /360/ leads to

$$\begin{aligned} a_1 &\sim A_{electron} \cdot V_{quark} = A_1 \left[2C_{1u} - C_{1d} \right] = \frac{1}{2} A_1 \left[3\tilde{\alpha} + \tilde{\gamma} \right] \\ a_2 &\sim V_{electron} \cdot A_{quark} = A_1 \left[2C_{2u} - C_{2d} \right] = \frac{1}{2} A_1 \left[3\tilde{\beta} + \tilde{\delta} \right] \end{aligned} \tag{6.4}$$

neglecting antiquarks as well as heavy quarks (valence parton approximation). The constant A_1 is given by

$$A_1 = \frac{3G}{10\pi\alpha\sqrt{2}} = 1.08 \times 10^{-4}\ (\mathrm{Gev/c})^{-2}. \tag{6.5}$$

Corrections due to sea quark effects, violations of the already discussed Callan-Gross relation /234/ ($R = \sigma_L/\sigma_T \neq 0$), logarithmic scaling violation, coherence between diagrams in which Z^0 and γ scatter from different quarks and higher-order weak effects appear to be small. They add up to a ~ 7 % theoretical uncertainty in the coefficients a_1 and a_2 /29/.

The first experiment /40/ was performed at $y \simeq 0.21$ with $< Q^2 > \simeq 1.6\ GeV^2/c^2$ and $< x > \simeq 0.15$. A significant asymmetry

$$A/Q^2 = (-9.5 \pm 1.6) \times 10^{-5}\ (GeV/c)^{-2}, \tag{6.6}$$

was found. This is compatible with the $10^{-4}Q^2$ rule from Eq.(5.5), where maximal interference between the weak and electromagnetic amplitudes is assumed. It demonstrates the V, A character of the neutral weak interaction for the same reason that observation of neutral current-charged current interferences in $\overset{(-)}{\nu}_e$ e scattering would do so. In both cases the interaction with which the neutral-current term interferes, preserves the electron helicity. There

is no interference unless the neutral-current interaction does the same which requires that it is mainly V, A. Small admixtures of S, P and T contributions, however, are much harder to rule out.

By changing the inelasticity y it is possible to determine /41/ the magnitude of a_1 and a_2 separately, with the result shown in Fig. 6.2:

$$\begin{aligned} a_1 &= (-9.7 \pm 2.6) \times 10^{-5}\ (GeV/c)^{-2} \\ a_2 &= (4.9 \pm 8.1) \times 10^{-5}\ (GeV/c)^{-2}\,, \end{aligned} \tag{6.7}$$

or in terms of the coupling parameters

$$\begin{aligned} \tilde{\alpha} + \tilde{\gamma}/3 &= -0.60 \pm 0.16\,, \quad C_{1u} - C_{1d}/2 = -0.45 \pm 0.12 \\ \tilde{\beta} + \tilde{\delta}/3 &= 0.31 \pm 0.51\,, \quad C_{2u} - C_{2d}/2 = 0.23 \pm 0.38\,. \end{aligned} \tag{6.8}$$

The best determined quantity /31/ is the linear combination

$$(\tilde{\alpha} + \tilde{\gamma}/3) + 0.25(\tilde{\beta} + \tilde{\delta}/3) = -0.53 \pm 0.05. \tag{6.9}$$

The errors in the relations (6.7/6.8) are highly correlated as demonstrated in Fig. 6.3. It turns out that the $A_{electron} \cdot V_{quark}$ interactions are much stronger than the $V_{electron} \cdot A_{quark}$ interactions (compatible with zero), in contradiction with the hybrid model /360/ in which the axialvector coupling of the electron vanishes identically. This model which assumes a weak-isospin doublet of the form $\begin{pmatrix} N^0 \\ e^- \end{pmatrix}_R$ - N^0 being a heavy neutral lepton with no mass restrictions - appears to be ruled out by the SLAC data (best fit has a χ^2 probability of only $6 \cdot 10^{-4}$).

By analysing the data in the framework of the GWS model (Table 2.3) one finds /29/

$$\rho = 1.74 \pm 0.36, \qquad \sin^2\Theta_W = 0.293^{+0.033}_{-0.100}, \tag{6.10}$$

or /41/

$$\sin^2\Theta_W = 0.224 \pm 0.012\ (\text{stat}) \pm 0.008\ (\text{syst}) \tag{6.11}$$

using the standard model ($\rho = 1$), respectively.

The SLAC asymmetry experiment succeeded only in determining particular linear combinations (Eqs. 6.8) of the four coupling constants $\tilde{\alpha}, \tilde{\beta}, \tilde{\gamma}, \tilde{\delta}$ or $C_{1u}, C_{2u}, C_{1d}, C_{2d}$, respectively. For a complete and separate determination of all four parameters additional experiments are needed. Measurements of an electron-proton inclusive cross section asymmetry with longitudinally polarized electrons could help, since a proton target provides a different mixture of quarks and is expected to give a different asymmetry than deuterium /360/. So far, however, the asymmetry on protons has only been measured for a fixed y value /40/. It yields

$$A/Q^2 = (-9.7 \pm 2.7) \times 10^{-5}\ (GeV/c)^{-2}, \tag{6.12}$$

where the error contains both statistical and systematic uncertainties.

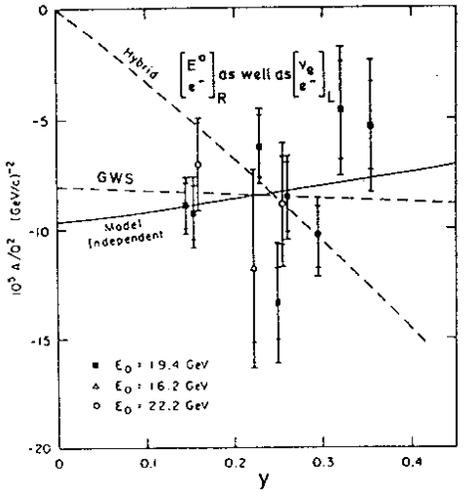

Fig. 6.2 The y dependence of the asymmetry A between the cross section of right-handed and left-handed polarized electrons on deuterons /41/. The data are compared with the standard model and the Hybrid model. In each case $\sin^2\Theta_W$ has been adjusted to minimize χ^2.

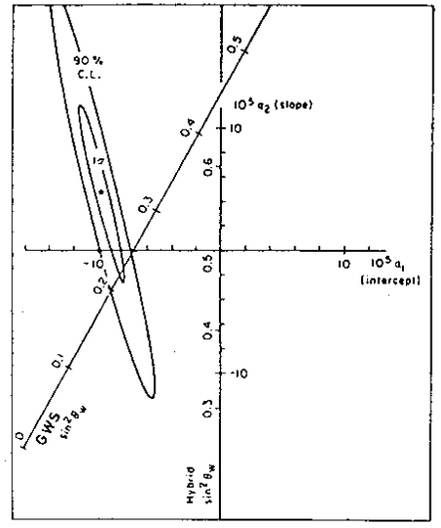

Fig. 6.3 Determination of a_1 (intercept) and a_2 (slope) in inelastic electron-deuteron scattering /41/.

Additional information can, in principle, be obtained by studies of parity-violating effects in elastic ep, eD and e-nucleus scattering at moderate energies /31/ and in optical transitions between atomic levels.

6.2. Parity violation in atoms

In atomic physics Q^2 is of order r^{-2}, where r is the atomic radius, $r^{-2} \sim (m_e/137)^2$. This implies parity-violating effects of order 10^{-15} due to weak-electromagnetic interferences. Fortunately these effects can be greatly enhanced by working with heavy (high Z) atoms /361/. From the two possible contributions $A_{electron} \cdot V_{quark}$ and $V_{electron} \cdot A_{quark}$ to the parity-violating part of the interaction then only the first alternative (corresponding to the SLAC asymmetry at $y = 0$) is dominant and produces a detectable effect /362/. In fact the vector charges of all quarks in the nucleus (a huge number in a heavy atom) add up coherently. On the other hand, the axialvector couplings to quarks which correspond to charge times spin, give a negligible effect because the nucleus spin is small and different quarks with the same charge add up with different signs according to their spins. Thus, in heavy atoms the measurement of parity violation determines a quantity, called the weak charge Q_W. It is given by the vector coupling of u quarks times the number of u quarks in the nucleus plus the same quantity for d quarks:

$$Q_W = -\left[(\tilde{\gamma} + \tilde{\alpha})\, N_u + (\tilde{\gamma} - \tilde{\alpha})\, N_d\right]. \tag{6.13}$$

Since there are two u (d) quarks and one d (u) quark inside the proton (neutron) one gets

$$\begin{aligned} Q_W &= -\left[(\tilde{\gamma} + \tilde{\alpha})\,(2Z + N) + (\tilde{\gamma} - \tilde{\alpha})\,(Z + 2N)\right] \\ &= -\left[\tilde{\alpha}\,(Z - N) + 3\tilde{\gamma}\,(Z + N)\right], \end{aligned} \tag{6.14}$$

where Z and N are the number of protons and neutrons in the nucleus.

The parity-violating lepton-quark interaction is described by a short-range effective Hamiltonian /361/

$$H_{PV} \sim Q_W \frac{\vec{\sigma}_e \cdot \vec{p}_e}{m_e}\, \delta(\vec{r}), \tag{6.15}$$

where $\vec{\sigma}_e$, $\vec{p}_e$, and m_e refer to the spin, momentum and mass of the electron. Therefore the parity-violating effects are largely enhanced for atoms with high Z, since the weak charge Q_W gives a factor of Z (Eq. 6.14). An additional factor of Z arises from the proportionality of H_{PV} to the electron momentum operator, since the velocity of the valence electron is known to scale like Z /31/. Furthermore the parity-violating matrix element depends on $|\Psi|^2$ of the valence electron evaluated at the origin; this varies like Z if screening is taken into account. Altogether one thus gains a factor Z^3 which, for example, for bismuth amounts to $\sim 5.7 \cdot 10^5$.

The Hamiltonian (6.15) can mix atomic levels with opposite parities. The atomic levels are no longer expected to be pure eigenstates of parity. Instead one may have

$$|n, P>' = |n, P> + \sum_{n'} \delta_{nP,n'S} |n', S>, \tag{6.16}$$

where $|n, P>'$ is the energy eigenstate for the system. $|n, P>$ and $|n', S>$ are the parity eigenstates. The mixing parameter is then given by /363/:

$$\delta_{nP,n'S} = \frac{<n', S|H_{PV}|n, P>}{E_{nP} - E_{n'S}}. \tag{6.17}$$

Consequently radiative transitions are expected to violate parity. In fact it is the interference between the parity-conserving magnetic (M1 - connecting two P states) and parity-violating electric (E1 - connecting P and S states) dipol transitions in atoms that is sensitive to the photon handedness. Such an interference will manifest itself in observable left-right asymmetry effects. This exhibits an additional possibility to enhance parity-violating effects. The expected tiny amount of E1 transition will not be completely masked by the normally much stronger M1 transition, if a transition is chosen where the parity-conserving transition is suppressed as in the so-called forbidden M1 transitions. One can gain a factor of order 10^4 in this way.

Another possibility /31/ to enhance parity-violating effects follows from formula (6.17). The parity mixing parameter δ can be enlarged by choosing a level with an almost degenerate opposite-parity level nearby and by subjecting in addition the atom to an external magnetic field in order to achieve crossing of some of the hyperfine sublevels. This will make the energy denominator in Eq. (6.17) small. This technique can be used in experiments with hydrogen or deuterium, where the $nS_{1/2}$ and $nP_{1/2}$ levels of opposite parity are nearly degenerate. It results in a mixing effect of the parity-violating Hamiltonian which is by a factor of order 10^4 greater than in other atoms. Experiments along this line are now in progress at Seattle /364/, Yale /365/, Zurich /366/ and Michigan /367/, where the first results /368/ constrain the C_{2p} parameter characterizing the $V_{electron} \cdot A_{proton}$ interaction to: $C_{2p} = -\frac{1.25}{2}(\tilde{\beta} + 0.6\tilde{\delta}) < 620$. It shows that the sensitivity is several orders of magnitude from providing a test of electroweak theory.

Most proposed experiments, and the ones that have actually been carried out, involve the interaction of photons with atoms where the helicity of the photon is used as pseudoscalar quantity to investigate the expected handedness of the atoms, i.e. their non-invariance under space reflection. Essentially two different experimental techniques exploit the photon helicity to search for parity-violating effects in heavy atoms.

One approach originally proposed by Bouchiat and Bouchiat /369/ involves the observation of resonance absorption of circularly polarized photons by a heavy atom such as Cesium or Thallium. The so-called circular dichroism is measured by comparing the cross sections for left-handed ($\vec{s} \cdot \vec{p} = -1$) and right-handed photons ($\vec{s} \cdot \vec{p} = +1$)

$$\delta = \frac{\sigma_R - \sigma_L}{\sigma_R + \sigma_L} = \frac{2\Im\left[\mathcal{E}_1^{PV} \cdot \mathcal{M}_1\right]}{|\mathcal{M}_1|^2 + \left|\mathcal{E}_1^{PV}\right|^2} \simeq 2\Im\mathcal{E}_1^{PV}/\mathcal{M}_1, \tag{6.18}$$

where $\mathcal{M}_1$ is the M1 amplitude and $\mathcal{E}_1^{PV}$ the parity-violating E1 amplitude. Any difference between the cross sections must be due to parity violations in atoms.

But instead of studying the interference between $\mathcal{E}_1^{PV}$ and $\mathcal{M}_1$ directly by measuring circular dichroism, it is experimentally easier to look for an interference between $\mathcal{E}_1^{PV}$ and a known parity-conserving Stark-induced E1 amplitude $\mathcal{E}_1^{ind}$, caused by a static electric field E_0. This results in an atomic polarization $\vec{P}$ which is proportional to the circular polarization $\vec{\sigma}_{in} \cdot \vec{k}_{in}$ of the incoming photons and to $\Im\mathcal{E}_1^{PV}/\mathcal{E}_1^{ind} \sim \Im\mathcal{E}_1^{PV}/\beta$, where β characterizes the vector part of the Stark-induced electric dipole. $\vec{P}$ is directed perpendicular to both $\vec{E}_0$ and $\vec{k}_{in}$ /370/. The presence of $\vec{P}$ leads to circular polarization in fluorescence observed along $\vec{E}_0 \times \vec{k}_{in}$. The actual pseudoscalar quantity detected is $(\vec{\sigma}_{in} \cdot \vec{k}_{in})(\vec{k}_{in} \times \vec{E}_0 \cdot \vec{k}_{out})(\vec{\sigma}_{out} \cdot \vec{k}_{out})$.

Table 6.1. Experimental results on parity violations in atomic physics /377/. The predictions are averages of recent theoretical estimates.

Experiment		Result	Predictions
Bismuth, λ = 6476 Å		$\left[10^8 \ \mathrm{Im}\ E_1^{PV}/M_1\right]$	
Novosibirsk	(1979) /378/	-20.2 ± 2.7	$-12.5 \ ^{+\ 3.5}_{-\ 2.5}$ /381-384/
Oxford	(1984) /377/	$-\ 9.3 \pm 1.5$	
Moscow	(1984) /377/	$-\ 7.8 \pm 1.8$	
Bismuth, λ = 8757 Å			
Seattle	(1980) /379/	-10.4 ± 1.7	-10 ± 2.5 /381-383/
Lead, λ = 1.28 μm			
Seattle	(1983) /380/	$-\ 9.9 \pm 2.5$	-13 ± 2 /383,385/
Thallium		$\left[\mathrm{Im}\ E_1^{PV}/\beta\right]$ in mV/cm	
Berkeley	(1981) /371/	$-1.80 \ ^{+\ 0.65}_{-\ 0.60}$	-1.15 ± 0.35 /386-388/
Berkeley	(1984) /371/	-1.73 ± 0.33	
Cesium			
Paris	(1982) /373/	-1.34 ± 0.33	-1.61 ± 0.2 /389-391/
Paris	(1984) /374/	-1.78 ± 0.38	

Experiments of this kind have been performed in Berkeley /371,372/ using the $6\,^2P_{1/2} - 7\,^2P_{1/2}$ transition in Thallium and Paris /373,374/ utilizing the $6S - 7P$ transition of Cesium, where a parity-violating effect of ~ 5 standard deviations has been found (Table 6.1).

An alternative way /375,376/ to search for parity violation in atoms uses the Lorentz relation between the index of refraction $n_\pm$ of a medium with N atoms per unit volume and the forward scattering amplitude $f_\pm(\omega)$ of right-handed (+) and left-handed (-) photons at energy ω :

$$n_\pm = 1 + \frac{2\pi}{\omega^2} N f_\pm(\omega) . \tag{6.19}$$

Near the resonance line the forward scattering amplitude is given /31/ by

$$f_\pm = - \frac{\omega^2 \left[|M_1|^2 \pm 2\Re \left(\mathcal{E}_1^{PV} M_1 \right) \right]}{\omega - \omega_0 + i\Gamma/2} , \tag{6.20}$$

where ω_0 denotes the resonance energy and Γ the width of the line. If n_+ and n_- are different, then linearly polarized light which is a superposition of the two opposite circular polarizations, will have its plane of polarization rotated by a tiny amount when traversing the medium of these atoms. Close to a M1 transition the rotation angle is given by

$$\Phi_{PV} \sim \frac{l}{\lambda} R \quad \text{with } R = \frac{\Re \mathcal{E}_1^{PV}}{M_1} , \tag{6.21}$$

where λ is the wave-length and l is the path length traversed /370/. The ratio R, the so-called rotation parameter, is the quantity that is usually quoted in the various optical rotation experiments. The attenuation of the photon beam due to absorption of light limits the path length (to a few times the absorption length l_0) and thus the attainable rotation angle.

All groups following this approach to study parity non-conservation effects in atoms have used Bismuth atoms. The optical activity of Bismuth vapour was investigated in the region of the allowed M1 transitions $6p^3\,^4S_{3/2} \rightarrow 6p^3\,^2D_{5/2}$ at $\lambda = 6476$ Å (Oxford /377/, Novosibirsk /378/ and Moscow /377/) and $6p^3\,^4S_{3/2} \rightarrow 6p^3\,^2D_{3/2}$ at $\lambda = 8757$ Å (Seattle /379/). The same method was used to search for parity-violating effects in atomic lead /380/ utilizing the 1.28 μm $^3P_0 \rightarrow {}^3P_1$ transition. The results are listed in Table 6.1 and compared with theoretical predictions based on the standard model.

The status of atomic parity experiments has had a rather confusing history and some of the discrepancies between the older and newer measurements are still not completely understood. But it can be seen that the experimental situation gives now a clear confirmation of the standard model predictions.

6.3. Limits on parity-violating scalar-type neutral-current interactions

The observations of parity violation in atoms and in the SLAC eD experiment imply that the relevant neutral-current interaction must have vector and axialvector components because of its interference with the electromagnetic interaction. Limits on dipole moments of atoms and molecules can now be used to impose constraints on still possible parity-violating scalar-type interactions.

Parity-violating S, P, T electron-nucleon interactions which must violate time-reversal invariance as well /392/, can give rise to electric dipole moment effects in atoms and molecules. This is in contrast to V, A interactions /221/ where no static electric dipole moment can be induced but only non-diagonal transition eletric dipole moments between states of the same parity.

In the non-relativistic limit which eliminates the pseudoscalar interaction, the Hamiltonian H_S and H_T, describing S and T interactions respectively, may be written /222/ in the effective operator form:

$$H_S^{eff} = -\frac{d_S}{J}\,\vec{J}\cdot\vec{E}, \qquad H_T^{eff} = -\frac{d_T}{I}\,\vec{I}\cdot\vec{E}, \tag{6.22}$$

where J is the angular momentum of the electrons in the shell, I the nuclear spin and $\vec{E}$ is the externally applied electric field. The electric dipole constants d_S and d_T are proportional to the scalar and tensor coupling constants g_S and g_T, respectively, with a proportionality factor depending on the particular atomic or molecular state. Therefore an experiment sensitive to H_S requires an atom or molecule with non-zero electronic angular momentum (e.g. $5p^5 6s\,^3P_2$ metastable state of Xe /393/), whereas an experiment sensitive to H_T requires non-zero nuclear spin (e.g. J = 1 rotational state of TlF /394/). The experimental limits on the electric dipole moments ($a_0 \equiv$ Bohr radius), e.g.

$$|d_S(\mathrm{Xe})| \leq 4\cdot 10^{-14}\, e a_0 \qquad (90\ \%\ \mathrm{C.L.}) \quad /393/$$
$$|d_T(\mathrm{TlF})| \leq 1\cdot 10^{-12}\, e a_0 \qquad (90\ \%\ \mathrm{C.L.}) \quad /394/$$

can be translated into experimental limits (at 90 % confidence level) on the scalar and tensor coupling constants g_S and g_T by comparing them with the theoretical expressions for d_S(Xe) and d_T(TlF) which one gets by evaluating H_S and H_T in the appropriate atomic and molecular states /222,223/:

$$\begin{aligned} |g_S| &\leq 3\cdot 10^{-4} \\ |g_T| &\leq 4\cdot 10^{-6}. \end{aligned} \tag{6.23}$$

Using the experimental limit on the electric dipole moment of the Cesium atom /395/, an upper limit of the same order of magnitude has been evaluated /221/ for the effective coupling of weak interactions involving the product of an electronic pseudoscalar and a hadronic scalar neutral current.

The effective coupling constants appropriate to S, P, T neutral-current interactions are therefore at least three orders of magnitude smaller than the Fermi constant, provided that so-called second-rank currents can be excluded. This restriction is due to the fact that the essential conclusion, that parity-violating S, P, T interactions violate also time-reversal invariance (and give so rise to electric dipole moment effects), is not quite correct if one allows for non-diagonal structures of the hadronic currents, i.e. if several different quark fields with the same strangeness and charge are allowed. Experimental tests for the presence of such second-rank currents by studying neutrino-hadron scattering, can be found in Ref. /211/. With the presently available statistics, however, such tests are of no significance.

6.4. Determination of the parity-violating coupling constants

A comparison of the SLAC measurements (Chap. 6.1) with the measurements of the atomic parity experiments (Chap. 6.2) provides further information about the relative strength and phase of the V and A components of the parity-violating electron-quark interaction. This can be done best by using the concept of weak charge (Eq. 6.14) which for the heavy atom (Cs, Tl, Bi) experiments is given by

$$\begin{aligned} Q_W^{Cs}(N,Z) &= Q_W(78,55) &&= 23\,\tilde{\alpha} - 399\,\tilde{\gamma} \\ Q_W^{Tl}(N,Z) &= Q_W(123,81) &&= 42\,\tilde{\alpha} - 612\,\tilde{\gamma} \\ Q_W^{Bi}(N,Z) &= Q_W(126,83) &&= 43\,\tilde{\alpha} - 627\,\tilde{\gamma}. \end{aligned} \tag{6.24}$$

The linear combinations of $\tilde{\alpha}$ and $\tilde{\gamma}$ measured by the SLAC experiment (Eq. 6.8) and the heavy atom experiments are almost orthogonal. This provides a model-independent way to determine $\tilde{\alpha}$ (enhanced in the SLAC experiment) and $\tilde{\gamma}$ (enhanced in the atomic parity experiments) separately (Fig. 6.4).

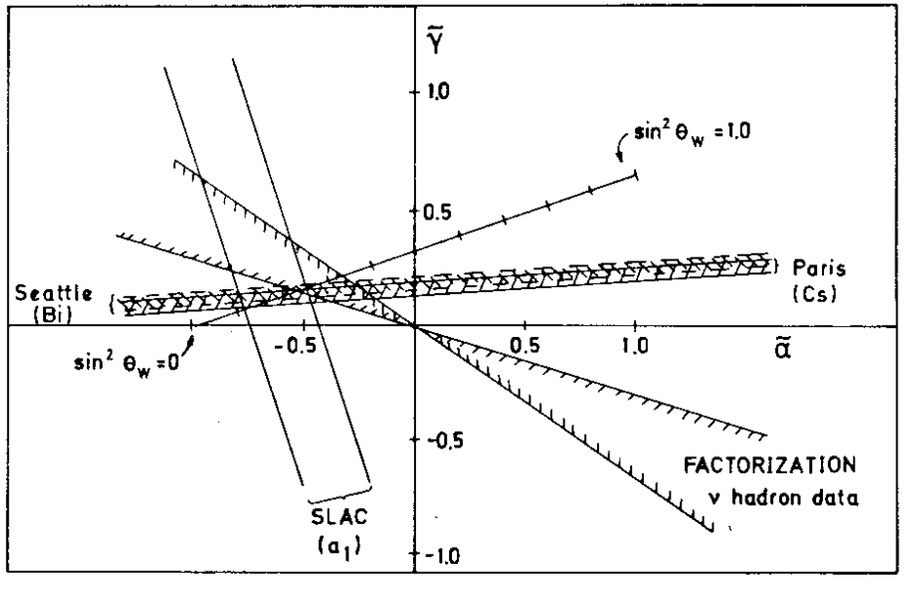

Fig. 6.4 Region of $\tilde{\alpha}$ and $\tilde{\gamma}$ allowed (at 68% confidence level) by i) the SLAC eD experiment, ii) the Berkeley and Seattle atomic physics experiments, and iii) ν-hadron scattering (assuming factorization) /31/.

In drawing the atomic physics bands of Fig. 6.4 the results of two different experimental methods have been used. In terms of Q_W the Seattle result for the rotation parameter R gives /31/

$$Q_W^{Bi} = -115 \pm 19\,, \tag{6.25}$$

and the circular dichroism observed in the Paris Cesium experiment /377/ implies

$$Q_W^{Tl} = -66.5 \pm 7.2\ (\text{stat}) \pm 5.1\ (\text{syst}) \pm 10\ (\text{atomic physics})\,. \tag{6.26}$$

Eqs. (6.25) and (6.26) combined with Eqs. (6.24) contrain $\tilde{\alpha}$ and $\tilde{\gamma}$ to the regions indicated in the figure. The intersection of the atomic physics band and the one determined by the intercept a_1 measured in the SLAC eD experiment determines uniquely $\tilde{\alpha}$ and $\tilde{\gamma}$, the parameters of the $A_{electron} \cdot V_{quark}$ interactions, including the signs. From Fig. 6.4 one reads

$$\begin{aligned} \tilde{\alpha} &= -0.65 \pm 0.17 \\ \tilde{\gamma} &= +0.14 \pm 0.05\,. \end{aligned} \tag{6.27}$$

If a single vector boson mediates the e-hadron and ν-hadron interactions, then the factorization relation (2.60) imposes constraints on $\tilde{\alpha}$ and $\tilde{\gamma}$ from measurements of the ν-hadron coupling constants (Table 4.17). The allowed region is shown in Fig. 6.4, too. One sees that the intersection of the SLAC a_1-asymmetry band and the atomic physics band lies within the region allowed by factorization. Clearly the result is consistent with the standard model and a value of $\sin^2\Theta_W \simeq 0.22$.

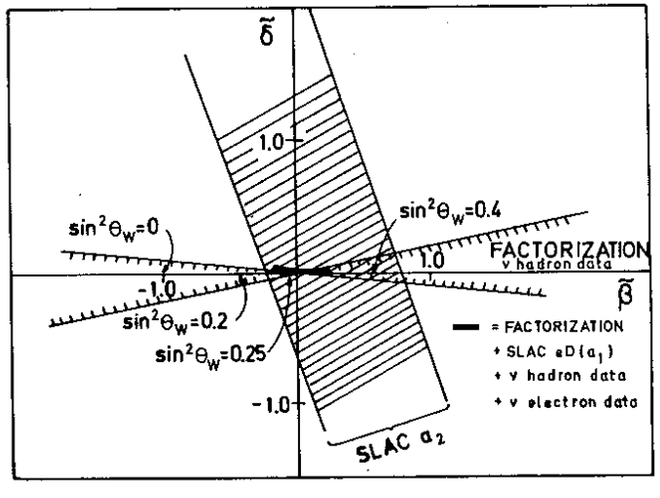

Fig. 6.5 Region $\tilde{\beta}$ and $\tilde{\delta}$ allowed by i) the SLAC eD experiment, ii) ν-hadron scattering (assuming factorization) and iii) a simultaneous fit to the ν-hadron, ν_e, and eD results (assuming factorization) /55/.

Unfortunately a similar isoscalar ($\tilde{\delta}$)-isovector ($\tilde{\beta}$) separation is not available for the $V_{electron} \cdot A_{quark}$ interactions. For this a measurement of the SLAC asymmetry on protons with x close to one is needed or a not less difficult atomic parity experiment with hydrogen and deuterium. But if factorization ($\tilde{\delta}/\tilde{\beta} = \delta/\beta$) is assumed, one can determine the regions in the $\tilde{\beta}$-$\tilde{\delta}$ plane allowed separately by Eq. (6.8) for the slope measured in the SLAC eD experiment and by the ν-hadron data (Fig. 6.5). Also shown is the region allowed by a simultaneous fit /31/ to the eD, νe and ν-hadron data assuming factorization:

$$\begin{Bmatrix} \tilde{\beta} \\ \tilde{\delta} \end{Bmatrix} = \begin{Bmatrix} \beta \\ \delta \end{Bmatrix} \frac{g_V^e}{g_A^e} \frac{(\tilde{\alpha} + \tilde{\gamma}/3)}{(\alpha + \gamma/3)}\,. \tag{6.28}$$

Both $\tilde{\beta}$ and $\tilde{\delta}$ are vanishingly small. From Ref. /31/ one gets

$$\begin{aligned} \tilde{\beta} &= 0.06 \pm 0.21 \qquad (-0.12) \\ \tilde{\delta} &= 0.00 \pm 0.02 \qquad (0)\,, \end{aligned} \tag{6.29}$$

where the values in brackets are the standard model predictions for $\sin^2\Theta_W = 0.22$.

The SLAC asymmetry measurement provides a further test of factorization which is displayed in Fig. 6.6, where the eD measurements taken together with the ν-hadron data and the assumption of a single intermediate boson (Eq. 2.69) restrict the possible g_V^e- g_A^e domain. It turns out that factorization is valid provided the vector-axialvector ambiguity is resolved in favour of an axialvector dominant solution.

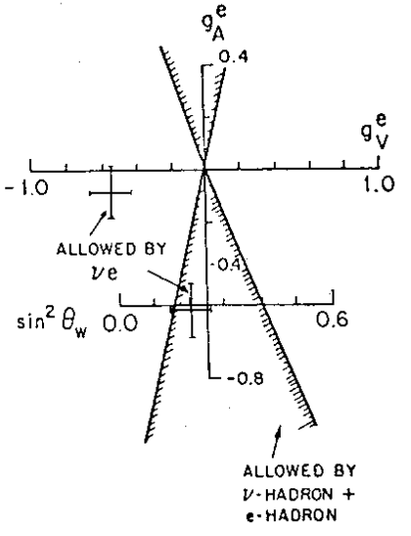

Fig. 6.6

Region of leptonic coupling constants g_V^e and g_A^e allowed (at 90% C.L.) by a fit to the measurements of $\nu_\mu e \to \nu_\mu e$, $\bar{\nu}_\mu e \to \bar{\nu}_\mu e$ and $\bar{\nu}_e e \to \bar{\nu}_e e$. Also shown is the region allowed by the data on neutrino quark and electron quark scattering, assuming factorization /29/.

Since the signs of the couplings in the ν-e sector (by interference with the charged-current contribution in $\bar{\nu}_e e$ scattering) and in the e-q sector are fixed (because of interference with electromagnetism), the factorization hypothesis predicts the signs of the couplings in the ν-quark sector. They turn out to correspond to the solution with $\epsilon_L(u) > 0$ (because the $\nu\bar{\nu} \to \nu\bar{\nu}$ amplitude is positive: $\epsilon_\nu^2 = 2g_A(\alpha + \gamma/3)/(\tilde{\alpha} + \tilde{\gamma}/3) = 0.86 \pm 0.28$ /31/).

The Bernabéu-Jarlskog relations (Eqs. 2.70/71) which must equal zero in any $SU_2 \times U_1$ model with the canonical values for the weak isospin of the left-handed fermions, can also be checked. One obtains

$$2\epsilon_\nu^2 - (\alpha + \beta) + 3(\gamma + \delta) = 0.03 \pm 0.31$$

$$2(g_V^\epsilon + g_A^\epsilon) + (\alpha + \beta) + 3(\gamma + \delta) = -0.17 \pm 0.35\,,$$

and similarly for the Sidhu relation (Eq. 2.72)

$$(\alpha - \beta) + 3(\gamma - \delta) + 2(g_V^\epsilon - g_A^\epsilon) = -0.001 \pm 0.350$$

compatible with zero as expected if the GWS model is correct.

7. WEAK NEUTRAL CURRENT EFFECTS IN e^+e^- ANNIHILATIONS

The discussed lepton-lepton (νe) and lepton-quark (νq, μq and eq) scattering experiments are characterized by relatively low space-like momentum transfers between 10^{-11} and 10^2 GeV^2/c^2. They indicate a parity-violating neutral current with contributions from vector and axialvector currents. In short, everything agrees quite well with expectations based on the standard model.

The operation of the PETRA (1978) and PEP (1980) electron-positron storage rings opened up a new kinematic region - with time-like momentum transfers of 10^3 GeV^2/c^2 - for the study of weak neutral-current effects in e^+e^- annihilations. Large weak-electromagnetic interference effects ($10^{-4}Q^2 \sim 0.1$) are expected. Moreover, the pair production of leptons and quarks, neglecting fragmentation, provides a very clean way of testing electroweak theories since no internal structure of projectile or target enters the interpretation of the results.

7.1. Observable electroweak effects in e^+e^- scattering

The fermion-pair production processes $e^+e^- \to f\bar{f}$, where the $f\bar{f}$ pair stands for either a lepton pair (e^+e^-, $\mu^+\mu^-$ and $\tau^+\tau^-$) or quark-antiquark pairs, can proceed via one-photon exchange and via Z^0 exchange (Fig. 7.1) in the s channel. The interference of the one-photon exchange amplitude with the weak amplitude gives rise to a number of effects in $e^+e^- \to f\bar{f}$ processes. For Bhabha scattering ($e^+e^- \to e^+e^-$) the neutral current appears in both the s channel and t channel; thus the momentum transfer can be time-like as well as space-like.

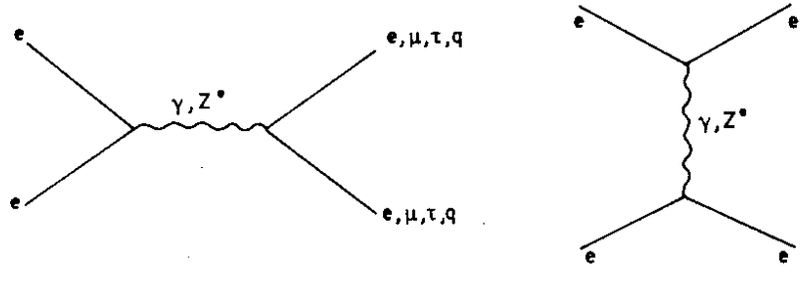

Fig. 7.1 Lowest order weak and electromagnetic contributions to $e^+e^- \to f\bar{f}$.

For $Q^2 \ll M_Z^2$ the most general Lagrangian /392/ which describes fermion-pair production in e^+e^- annihilations (e.g. $e^+e^- \to \mu^+\mu^-$) is given by

$$\mathcal{L}^{e\mu} = e\left[\bar{e}\gamma_\mu e + \bar{\mu}\gamma_\mu\mu\right]A_\mu + \frac{G}{\sqrt{2}}\sum_i \left[\bar{\mu}\Gamma_i\mu\right]\left[\bar{e}\Gamma_i(C_i + C_i'\gamma_5)e\right], \qquad (7.1)$$

including both the usual electromagnetic and the weak interaction. Hermiticity requires that the five coupling constants C_i (i = V, A, S, P, T) and also C'_V and C'_A are real and that C'_S, C'_P and C'_T are imaginary or vanish, respectively, if time-reversal invariance holds in addition. The matrices Γ_i can be found in Tab. 2.1. The relationship between the coupling parameters defined above and those introduced in Chap. 2 (Eq. 2.79) is

$$\left[C_V, C'_V, C'_A, C_A\right] = 2\left[-h_{VV}, h_{VA}, h_{AV}, -h_{AA}\right]. \tag{7.2}$$

If e^+e^- annihilation into fermion pairs proceeds only via s-channel exchange, the different transfer of helicity at the leptonic vertex for S, P, T and V, A currents implies that both the initial and final states involve particles of like helicity for S, P, T interactions and particles of opposite helicity for electromagnetism and V, A interactions. For Bhabha scattering (s-channel as well as t-channel exchange), however, V and A interactions contribute also when both the initial and final states contain particles of like helicity /68/.

It is therefore obvious that a knowledge of the helicity of the incident leptons and/or produced fermions could help to reveal the space-time structure of the neutral currents. The polarization of produced muons, for example, could be deduced from the observation of parity-violating decays $\mu \to e\nu\bar{\nu}$ (Chap. 3.3.1), whereas the τ helicity in τ-pair production ($e^+e^- \to \tau^+\tau^-$) may be infered from the two-body decay mode $\tau \to \nu_\tau\pi$ which favours emission of ν_τ in direction of the τ helicity owing to helicity conservation.

The idea to test the neutral-current structure in polarized colliding beam experiments /392,396/ is supported by the fact that transversally polarized beams are naturally obtained in storage rings due to a tiny spin dependence of synchrotron radiation /397,398/. Theoretically a polarization of about 92 % can be achieved but several depolarizing effects come into play to limit the realistic final value. The transverse polarization can be rotated into a longitudinal polarization with usual spin precession in a magnetic field /399/. This operation, however, requires strong bending magnets next to the beam crossing and the experiment, being thus a possible source for synchrotron radiation background. Furthermore, since both e^- and e^+ beams move in opposite directions in the same magnetic field and since their initial transverse polarizations are opposite, the only configurations which are possible in a single ring are those in which both electron and positron have like helicity $e^-_R e^+_R$ or $e^-_L e^+_L$ /400/ forbidden for electromagnetism and weak V, A interactions.

7.1.1. Muon and tau pair production

If the e^- and e^+ beams have transverse polarizations S^- and S^+ (either positive or negative), respectively, along a common direction $\hat{v}$, then the differential cross section for reaction $e^+e^- \to \mu^+\mu^-$, $\tau^+\tau^-$ is given by /392/

$$\frac{d\sigma}{d\Omega} = \frac{\alpha^2}{4s}\left[(1 - 4\frac{G/\sqrt{2}}{e^2/s}h_{VV})(1 + \cos^2\Theta + S^-S^+\sin^2\Theta\cos 2\Phi) - 8\frac{G/\sqrt{2}}{e^2/s}h_{AA}\cos\Theta\right] \tag{7.3}$$

where $\alpha \equiv e^2/4\pi$. The azimuthal angle Φ between $\hat{v}$ and the fermion-pair production plane is defined so that $\sin\Phi = \hat{v}\cdot\hat{n}$ and $\cos\Phi = \hat{v}\cdot\hat{n}'$, where $\hat{n} \equiv \vec{k}_{e^-} \times \vec{k}_l / \left|\vec{k}_{e^-} \times \vec{k}_l\right|$ is the normal to the production plane and $\hat{n}' \equiv \hat{n} \times \vec{k}_{e^-} / \left|\hat{n} \times \vec{k}_{e^-}\right|$; $\vec{k}_l$ ($=\vec{k}_\mu$, $\vec{k}_\tau$) is the momentum of the final-state particle in the c.m. frame.

The average $\frac{1}{2}[d\sigma(\Theta,\Phi) + d\sigma(\pi-\Theta,\Phi)]$ is deviating from the 1/s behaviour expected from one-photon exchange (QED) by an energy-dependent shift in counting rate. This deviation from the QED cross section measures h_{VV} :

$$\frac{\Delta\sigma}{\sigma_{QED}} = -\frac{G}{\sqrt{2}\pi\alpha}h_{VV}s, \tag{7.4}$$

where $\sigma_{QED} = \frac{4}{3}\pi\alpha^2/s$ + radiative corrections and $G/\sqrt{2}\pi\alpha \simeq 3.5 \times 10^{-4}\ GeV^{-2}$. The presence of a weak neutral current will thus not produce large deviations from the QED cross section for $s \ll M_Z^2$ (~ 0.3 % at PETRA energies $\sqrt{s} \sim 34$ GeV).

The angular distribution of μ^- (τ^-) with respect to the incident e^- is expected to be forward-backward asymmetric. The fractional asymmetry

$$A = \frac{d\sigma(\Theta,\Phi) - d\sigma(\pi-\Theta,\Phi)}{d\sigma(\Theta,\Phi) + d\sigma(\pi-\Theta,\Phi)} = \frac{G}{\sqrt{2}\pi\alpha}h_{AA}s\left(\frac{2\cos\Theta}{1+\cos^2\Theta + S^-S^+\sin^2\Theta\cos 2\Phi}\right) \tag{7.5}$$

is determined by the neutral-current coupling constant h_{AA}. The integrated asymmetry between forward (F) and backward hemispheres (B) is

$$< A_{FB} > \equiv \frac{F - B}{F + B} \simeq -\frac{3}{4}\frac{G}{\sqrt{2}\pi\alpha}h_{AA}s, \tag{7.6}$$

thus predicting a substantial effect (~ 10 % at PETRA energies).

If $P_l(l^+)$ denotes the longitudinal fermion polarization ($l^+ = \mu^+, \tau^+$), $P_n(l^+)$ and $P_\perp(l^+)$ the transverse l^+ polarizations along $\hat{n}$ and $\hat{n} \times \vec{k}_{l^+} / |\hat{n} + k_{l^+}|$, respectively, one expects /392/

$$P_l(l^+) = \frac{G}{\sqrt{2}\pi\alpha}s\left(h_{AV} + \frac{2h_{VA}\cos\Theta}{1+\cos^2\Theta + S^-S^+\sin^2\Theta\cos 2\Phi}\right) \tag{7.7}$$

$$\begin{aligned} P_n(l^+) = {} & \frac{G}{2\sqrt{2}\pi\alpha}s\frac{1}{1+\cos^2\Theta + S^-S^+\sin^2\Theta\cos 2\Phi} \\ & \times\left\{\left(S^+ - S^-\right)\left[\sin\Phi(C_P + 2C_T\cos\Theta) - \cos\Phi\cos\Theta\, i\left(-C'_S + 2C'_T\cos\Theta\right)\right]\right. \\ & \left. + \left(S^+ + S^-\right)\left[\sin\Phi\cos\Theta(C_S - 2C_T\cos\Theta) + \cos\Phi\, i\left(C'_P + 2C'_T\cos\Theta\right)\right]\right\} \end{aligned} \tag{7.8}$$

$$\begin{aligned} P_\perp(l^+) = {} & \frac{G}{2\sqrt{2}\pi\alpha}s\frac{1}{1+\cos^2\Theta + S^-S^+\sin^2\Theta\cos 2\Phi} \\ & \times\left\{\left(S^+ - S^-\right)\left[-\cos\Phi\cos\Theta(C_P + 2C_T\cos\Theta) - \sin\Phi\, i\left(-C'_S + 2C'_T\cos\Theta\right)\right]\right. \\ & \left. + \left(S^+ + S^-\right)\left[-\cos\Phi(C_S - 2C_T\cos\Theta) + \sin\Phi\cos\Theta\, i\left(C'_P + 2C'_T\cos\Theta\right)\right]\right\} \end{aligned} \tag{7.9}$$

This shows that the observation of a transversely polarized μ (τ) produced in e^+e^- annihilations is a clean signal for the presence of S, P, T couplings, whereas the observation of longitudinally polarized μ (τ) indicates the presence of parity-violating neutral currents from V, A coupling type. The experimental situation, however, is complicated by the fact that some of the physical phenomena can also be induced by higher-order electromagnetism. But it can be shown /392/ that higher-order electromagnetic contributions to the transverse polarizations $P_\perp$ and P_n vanish at high energies.

If it finally will be possible to have longitudinally polarized beams, the parity-violating asymmetry

$$H = \frac{d\sigma(e_L^- e_R^+) - d\sigma(e_R^- e_L^+)}{d\sigma(e_L^- e_R^+) + d\sigma(e_R^- e_L^+)} = \frac{G}{\sqrt{2}\pi\alpha}\left(h_{VA} + \frac{2h_{AV}\cos\Theta}{1+\cos^2\Theta}\right) \tag{7.10}$$

could be measured. This expression applies also if only one of the beams is longitudinally polarized and the other unpolarized or transversely polarized. The measurement of H is thus also possible in storage rings with a single ring. The coupling parameters h_{VA} and h_{AV} could then be extracted from such measurements.

The formulae (7.3) - (7.10) ignore finite Z mass effects due to the Z boson propagator. If s is still small but not completely negligible compared to M_Z^2, one can correct for these effects by multiplying the prediction by $M_Z^2/(M_Z^2 - s)$ /31/. This results in an enhancement of the electroweak effects. The prediction for the asymmetry $< A_{FB} >$, for instance, changes from -6.6 % to -7.5 % at s = 1000 GeV^2 and M_Z = 90 GeV.

Observation of the discussed electroweak effects (Eqs. 7.3 - 7.10) may finally allow to extract all 10 structure constants C_i and C_i' involved in weak neutral-current interactions. They would then provide tests for parity violation (i.e. the presence of C_i' coefficients), time-reversal non-invariance (i.e. the presence of C_S', C_P' or C_T') and the break-down of μ-e universality (i.e. violation of the relations $h_{VA} = h_{AV}$ and $C_P' = C_S'$) /392/.

7.1.2. Electron pair production

A formula analogous to (7.3) can be derived for Bhabha scattering $e^+e^- \to e^+e^-$ by taking into consideration that the scattering amplitude consists of a time-like and a space-like part. For unpolarized beams ($S^+ = S^- = 0$) one has /68,401/:

$$\frac{d\sigma}{d\cos\Theta} = \left(\frac{d\sigma}{d\cos\Theta}\right)_{e.m.} + \left(\frac{d\sigma}{d\cos\Theta}\right)_{int.} + \left(\frac{d\sigma}{d\cos\Theta}\right)_{weak} \tag{7.11}$$

where

$$\left(\frac{d\sigma}{d\cos\Theta}\right)_{e.m.} = \frac{\pi\alpha^2}{s}\left[\left(1+\frac{s}{t}\right)^2\left(\frac{1+\cos\Theta}{2}\right)^2 + \left(\frac{1-\cos\Theta}{2}\right)^2 + \left(\frac{s}{t}\right)^2\right]$$
$$= \frac{\pi\alpha^2}{2s}\left[\frac{3+\cos^2\Theta}{1-\cos\Theta}\right]^2 \tag{7.12}$$

$$\left(\frac{d\sigma}{d\cos\Theta}\right)_{int.} = -\frac{\pi\alpha^2}{s}\left[\left(1+\frac{s}{t}\right)^2\eta(s)\,2(h_{VV}+h_{AA})\left(\frac{1+\cos\Theta}{2}\right)^2\right.$$
$$\left. + \eta(s)(h_{VV}-h_{AA})\left(\frac{1-\cos\Theta}{2}\right)^2 + \left(\frac{s}{t}\right)^2\eta(t)(h_{VV}-h_{AA})\right] \tag{7.13}$$

with

$$\eta(s) = \frac{G}{\sqrt{2}\pi\alpha}s, \quad \eta(t) = \frac{G}{\sqrt{2}\pi\alpha}t, \quad \frac{s}{t} = \frac{-2}{1-\cos\Theta}. \tag{7.14}$$

Comparison between Eq. (7.12) and (7.13) shows that the weak-electromagnetic interference causes a slight distortion of the angular distribution of Bhabha scattering which depends

on the vector (h_{VV}) and axialvector coupling constants (h_{AA}). The Eqs. (7.12-7.14) show that the electromagnetic contribution to the cross section is proportional to $\frac{\alpha^2}{s}$ and that the interference term is proportional to αG. The weak part behaves like $G^2 s$ and is thus negligible at the present available energies. Since the size of the interference term relative to the QED contribution is of order $\frac{G}{\alpha}s$ and rises with s, one must measure at the highest possible energies in order to enhance the electroweak interference.

7.1.3. Quark pair production

The study of weak-electromagnetic interference in the production of $q\bar{q}$ pairs in e^+e^- annihilations is a unique situation. All quarks are involved (not only u and d quarks as in neutrino scattering experiments) provided it is kinematically possible, and therefore weak couplings of all quarks can be determined in principle. Hadronic jets produced in

$$e^+e^- \to q\bar{q} \;\big\}\; \text{hadron jets} \tag{7.15}$$

are more copiously produced than $\mu^+\mu^-$ pairs by a factor $R \sim 3.9$ (for five flavours and QCD corrections applied) and the quark production asymmetries - inversely proportional to the quark charges (7.21) - are larger than muonic asymmetries by a factor of 1.5 (3) for u, c (d, s, b) quarks /402/. However, the analysis of possible quark-jet asymmetries is model-dependent due to its dependence on the particular quark-fragmentation model which is used to relate the quark asymmetries to the experimentally observable jet asymmetries. In spite of the experimental difficulty to identify unambiguously the quark and antiquark jets on an event-by-event basis and to define properly the jet axes, results on quark asymmetries have recently been published.

The normalized cross section for the production of a quark pair $q\bar{q}$ can be written /403/ as

$$R_f = \frac{\sigma(e^+e^- \to \gamma, Z^0 \to q_f\bar{q}_f)}{\sigma_P}$$
$$= 3\left[Q_f^2 - 8Q_f g_V^e g_V^f \chi + 16\left(g_V^{e^2} + g_A^{e^2}\right)\left(g_V^{f^2} + g_A^{f^2}\right)\chi'\right], \tag{7.16}$$

where $\sigma_P = 4\pi\alpha^2/3s$ is the point-like QED cross section for $e^+e^- \to \mu^+\mu^-$. Q_f is the charge of the quark f, g_V^e and g_A^e are the weak vector and axialvector coupling constants of the electron and g_V^f, g_A^f are those of the quark f. The factor 3 stands for the number of colours.

The 3 terms in (7.16) represent the photon term, γ-Z^0 interference term and pure Z^0 term, respectively. One sets $\chi = sgP(s)$ and $\chi' = s^2g^2P'(s)$, where $g \equiv G/(8\sqrt{2}\pi\alpha) \simeq 4.4 \cdot 10^{-5}\ GeV^{-2}$. P(s) is the propagator term for the γ-Z^0 interference (taking into account the Z^0-width effects)

$$P(s) = \left[\left(\frac{s}{M_Z^2} - 1\right) + \frac{\Gamma_Z^2}{s - M_Z^2}\right]^{-1} \tag{7.17}$$

and P'(s) for the pure Z^o exchange

$$P'(s) = \left[\left(\frac{s}{M_Z^2} - 1\right)^2 + \frac{\Gamma_Z^2}{M_Z^2}\right]^{-1}. \tag{7.18}$$

In the quark parton model the total normalized cross section is given by the incoherent sum over all final state quarks including corrections for gluon contributions /404/

$$R = \sum_f R_f \left[1 + \frac{\alpha_s}{\pi} + C_2 \frac{\alpha_s^2}{\pi^2} + \cdots\right], \tag{7.19}$$

where α_s (Eq. 2.43) is the coupling constant of the strong interaction. It has been measured to be 0.18 at $\sqrt{s} \simeq 33$ GeV /405/ and changes slowly with energy. C_2 is the strength of the second order gluon diagrams and depends on the renormalization scheme used

$$\begin{aligned} C_2 &= 7.35 - 0.442 N_f \quad /406/, \\ C_2 &= 1.98 - 0.115 N_f \quad /407/, \\ C_2 &= 0.739 N_f - 4.637 \quad /408/, \end{aligned} \tag{7.20}$$

where N_f is the number of flavours contributing.

In the framework of the GWS model g_V^f and g_V^f are functions of $\sin^2\Theta_W$ (Eq. 2.36). The total cross section is thus expected to have a mild dependence on that parameter (Θ_W also comes in the propagator terms through M_Z). Therefore, if QCD corrections are believed to be known exactly, one can write the total normalized cross section as a function of $\sin^2\Theta_W$. Fig. 7.2 /409/ shows the dependence of R on $\sin^2\Theta_W$ for different values of s, the center-of-mass energy squared.

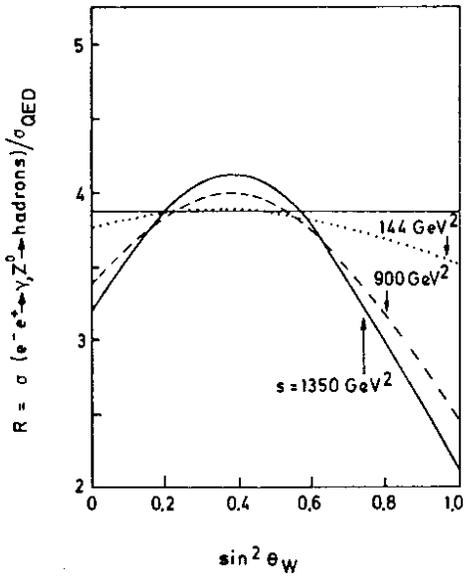

Fig. 7.2
Variation of the total cross section R with s and $\sin^2\Theta_W$ as predicted by the standard model. The horizontal line at R = 3.87 corresponds to γ exchange only /409/.

For small energies, where $\chi, \chi' \ll 1$, the ratio of quark to muon integrated asymmetry is given by /402/

$$\frac{< A_{q_f \bar{q}_f} >}{< A_{\mu^+\mu^-} >} = \frac{g_A^f (8 g_V^\mu g_V^f \chi - Q_f)}{g_A^\mu (8 g_V^{\mu^2} \chi + 1)} \cdot \frac{1 + 8 g_V^{\mu^2} \chi + 16 (g_V^{\mu^2} + g_A^{\mu^2}) \chi'}{Q_f^2 - 8 Q_f g_V^\mu g_V^f \chi + 16 (g_V^{\mu^2} + g_A^{\mu^2})(g_V^{f^2} + g_A^{f^2}) \chi'}$$

$$\xrightarrow{\chi,\chi' \ll 1} -\frac{g_A^f}{g_A^\mu} \cdot \frac{1}{Q_f} = \begin{cases} 1.5 & \text{for u, c} \\ 3 & \text{for d, s, b.} \end{cases} \tag{7.21}$$

The presence of the neutral current will lead to a change in $R \sim 1$ % and is expected to be responsible for quark production asymmetries $A_{d,s,b} \sim -0.30$ and $A_{u,c} \sim -0.15$.

7.1.4. Polarized Møller scattering $e^-e^- \to e^-e^-$

A study of neutral-current effects in Møller scattering processes $e^-e^- \to e^-e^-$ /410/ would provide another way of testing electroweak models /411-414/. It requires a machine such as the proposed Single Loop Collider (SLC) at SLAC ($\sqrt{s} \simeq 100$ GeV) with electrons in both beams and the possibility of polarizing these beams longitudinally.

There are four diagrams (two γ and two Z^0 exchange diagrams, respectively) for the Møller scattering process - two (t channel) direct graphs and two (u channel) cross graphs (Fig. 7.3) which are required by the Pauli exclusion principle.

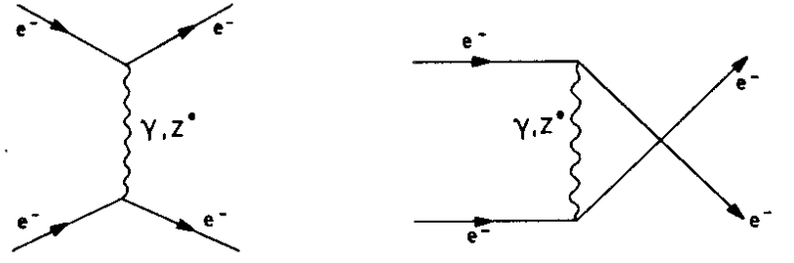

Fig. 7.3 Lowest order weak and electromagnetic contributions to electron-electron scattering.

Unlike the $e^+e^- \to \mu^+\mu^-$ process, there is no forward-backward asymmetry for the $e^-e^- \to e^-e^-$ process with unpolarized beams since the initial particles are identical (no annihilation contribution) /414/. One has therefore to use polarized beams. The differential

scattering cross section for longitudinally polarized electron beams is /415/:

$$\frac{d\sigma_{\lambda_1\lambda_2}}{d\Omega} = \frac{s\alpha^2}{2}\left[\frac{1}{t_1}+\frac{1}{t_2}+4(\rho_1+\rho_2)(g_V^e+g_A^e)^2\right]^2 + \frac{s(1+\cos\Theta)^2}{2}\left[\frac{1}{t_1}+4\rho_1\left(g_V^{e^2}-g_A^{e^2}\right)\right]^2 + \frac{s(1-\cos\Theta)^2}{2}\left[\frac{1}{t_2}+4\rho_2\left(g_V^{e^2}-g_A^{e^2}\right)\right]^2 \tag{7.22}$$

with the definitions

$$t_1 = \frac{s(1-\cos\Theta)}{2}, \quad t_2 = \frac{s(1+\cos\Theta)}{2}$$
$$\rho_1 = \frac{1}{t_1+M_Z^2}\cdot\frac{1}{4\pi\alpha}, \quad \rho_2 = \frac{1}{t_2+M_Z^2}\cdot\frac{1}{4\pi\alpha}. \tag{7.23}$$

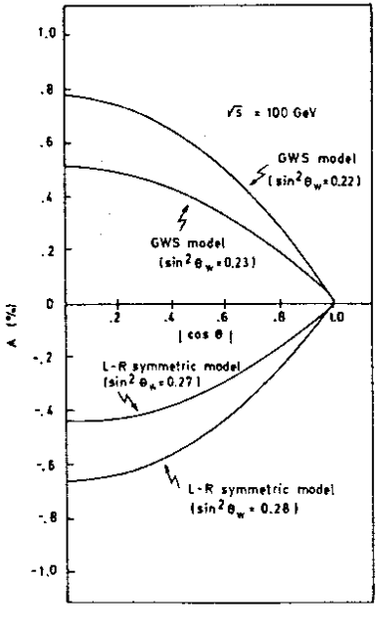

Fig. 7.4

Parity-violating asymmetry as a function of $|\cos\Theta|$ for $e^-e^- \to e^-e^-$ in the GWS model ($\sin^2\Theta_W = 0.22$ and 0.23) and in a left-right symmetric model ($\sin^2\Theta_W = 0.27$ and 0.28) /414/. Θ is the center-of-mass scattering angle.

The parity-violating asymmetry for the case of initially longitudinally polarized beams and unobserved final state polarizations is then given by

$$A \equiv \frac{d\sigma_{++}-d\sigma_{--}}{d\sigma_{++}+d\sigma_{--}} = \frac{32 g_V^e g_A^e(\rho_1+\rho_2)\left[\frac{1}{t_1}+\frac{1}{t_2}+4(\rho_1+\rho_2)\left(g_V^{e^2}+g_A^{e^2}\right)\right]}{\left\{2\left[\left(\frac{1}{t_1}+\frac{1}{t_2}+4(\rho_1+\rho_2)\left(g_V^{e^2}+g_A^{e^2}\right)\right)^2+64(\rho_1+\rho_2)^2 g_V^{e^2} g_A^{e^2}\right] + \frac{(1+\cos\Theta)^2}{2}\left[\frac{1}{t_1}+4\rho_1\left(g_V^{e^2}-g_A^{e^2}\right)\right]^2 + \frac{(1-\cos\Theta)^2}{2}\left[\frac{1}{t_2}+4\rho_2\left(g_V^{e^2}-g_A^{e^2}\right)\right]^2\right\}}, \tag{7.24}$$

where $++$ $(--)$ means the electron helicities $\lambda_1 = \lambda_2 = +1\,(-1)$.

Fig. 7.4 shows A as a function of $|\cos\Theta|$ predicted by two different models /414/: the standard model ($\sin^2\Theta_W = 0.22$ and 0.23) and a left-right symmetric model ($\sin^2\Theta_W = 0.27$ and 0.28). As $|\cos\Theta| \to 1$, for all values of $\sqrt{s}$ one gets the pure QED result alone since these regions are dominated by the photon u and t channel poles. Both models predict roughly the same magnitude for A (which has its maximum value at $\Theta = 90^0$) but opposite sign. This could be used to distinguish both models. But unlike the muon asymmetry in e^+e^- annihilations, the parity-violating asymmetry in Møller scattering is expected to be small even when $\sqrt{s} \simeq M_Z$.

7.2. Experimental results

Measurements /418/ of electroweak effects in high-energy electron-positron collisions come from the five PETRA experiments CELLO /419/, JADE /420/, MARK J /421/, PLUTO /422/ and TASSO /423/ and from the PEP experiments HRS /424/, MAC /425/, MARK II /426/ and TPC /427/.

The PETRA experiments have collected most of their data in the center-of-mass energy range 30 - 37 GeV ($< \sqrt{s} > \sim 34.5$ GeV). Smaller amounts of data have also been collected in the energy ranges 12 - 14 and 22 - 25 GeV and recently 39 - 46.8 GeV. The PEP experiments have collected their events at $\sqrt{s} = 29$ GeV.

All the detectors use similar techniques, viz. large volume magnetic solenoids which enclose charged particle tracking chambers and are surrounded by electromagnetic calorimeters, muon identifiers, etc. Detailed descriptions of the individual detectors can be found somewhere else /419-427/.

7.2.1. Radiative corrections

For the data discussed in the following both PETRA and PEP operated with unpolarized electron and positron beams. Since moreover the final-state fermion polarization has not been measured, all observed neutral-current effects are intrinsically parity conserving and may therefore be simulated by higher-order QED graphs. Figs. 7.5 show the muon graphs contributing up to order α^3 to the purely electromagnetic process.

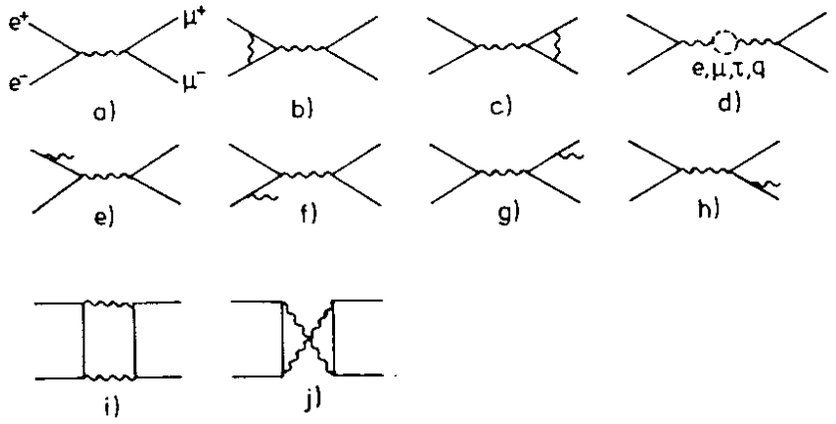

Fig. 7.5 Higher-order QED diagrams contributing to muon pair production /428/.

These higher-order corrections contribute to the fermion-pair production cross sections and produce a forward-backward asymmetry by interference of C-odd graphs (such as Figs. 7.5 a, b and d-f) and C-even graphs (such as Figs. 7.5 g-j). In order to extract the neutral-current information one has thus to subtract the QED radiative correction which, in principle, is calculable /429/. The magnitude of this correction depends on the experimental conditions. The QED contribution to the muon pair asymmetry, for example, is small ($\sim +1.5$ %) compared to the expected asymmetry of ~ -10 % at $\sqrt{s} = 34.5$ GeV from electroweak origin.

In extracting electroweak effects in principle higher orders have to be taken into account also for the Z^0 exchange graph. But the modification of the forward-backward asymmetry is still expected to be small at PETRA and PEP energies /430/. In the following the QED contribution will always be subtracted, whereas the radiative correction to the weak diagram will not be applied to the results.

7.2.2. Elektroweak effects in muon pair production

It has become traditional to parametrize possible departures from QED predictions in lepton pair production by introducing form factors

$$F_s(Q^2) = 1 \mp \frac{Q^2}{Q^2 - \Lambda_{s\pm}^2}$$
$$F_t(s) = 1 \mp \frac{s}{s - \Lambda_{t\pm}^2} \qquad (7.25)$$

in the time-like and the space-like region, respectively, which modify lepton vertices or propagators.

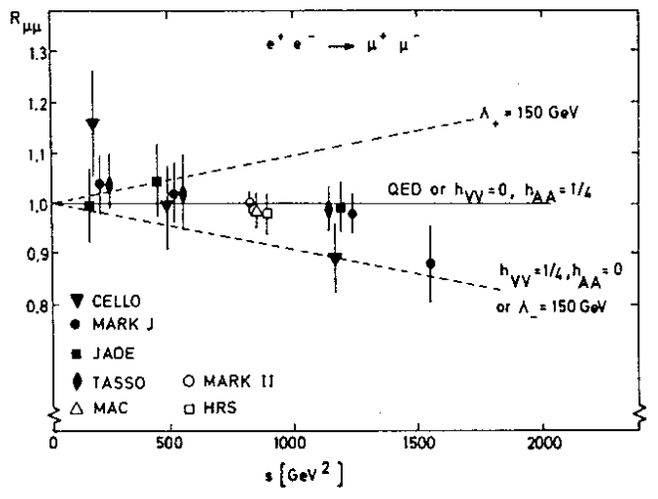

Fig. 7.6 Ratio, $R_{\mu\mu}$, of total measured μ-pair cross section to the QED point-like cross section /418/.

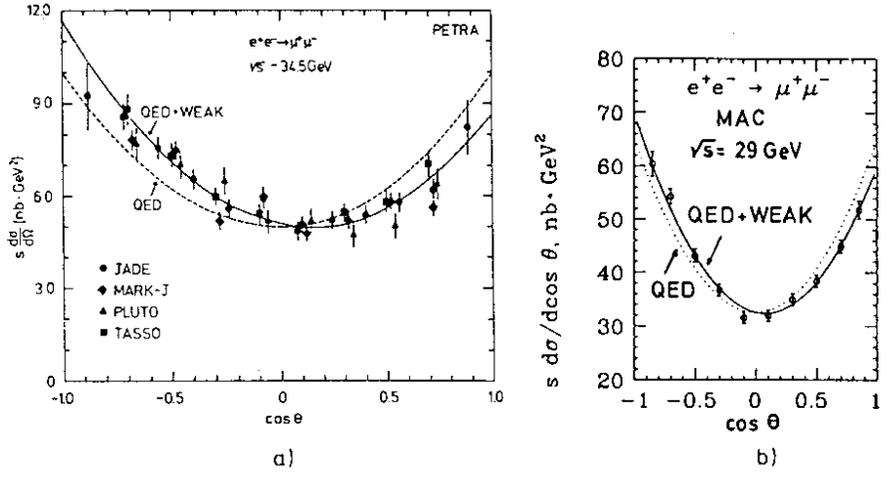

Fig. 7.7 Differential cross sections for muon pair production measured by (a) the PETRA experiments and (b) the PEP experiment MAC /418/.

If $\Lambda_\pm^2 \gg s$ one gets for muon pair production

$$\sigma_{\mu\mu} = \sigma_{QED}\,|F_e(t)|^2 \simeq \sigma_{QED}\left(1 \pm \frac{2s}{\Lambda_\pm^2}\right) \tag{7.26}$$

assuming $\Lambda_e = \Lambda_t = \Lambda$ for simplicity. This leads to

$$\frac{\sigma_{\mu\mu} - \sigma_{QED}}{\sigma_{QED}} = R_{\mu\mu} - 1 \simeq \pm 2s/\Lambda_\pm \tag{7.27}$$

which by comparison with Eq. (7.4) shows that a lower limit on Λ_- implies an upper limit on h_{VV}, as shown in Fig. 7.6. The experiments obtain lower limits for Λ_- around 150 GeV at the 95 % confidence level, which correspond to upper limits on h_{VV} around 1/4.

Furthermore, the forward-backward asymmetry in the angular distribution of the reaction $e^+e^- \to \mu^+\mu^-$, which is sensitive to h_{AA} (Eqs. 7.5/7.6), has been measured at PETRA and PEP. In Figs. 7.7 a and b the angular distributions of four PETRA experiments and the PEP experiment MAC, respectively, are displayed. Possible systematic errors of the angular asymmetries are found to be ≤ 1 %. The dotted lines show the symmetric prediction by QED, where only the normalization has been fitted. The full lines represent the QED plus fitted weak neutral-current contributions. A clear preference for this non-symmetric form is observed. The combined muon pair asymmetries /418/ seen at PETRA ($\sqrt{s} \sim 34.5$ GeV) and PEP ($\sqrt{s} = 29$ GeV) are

$$\begin{aligned} < A_{\mu\mu}^{PETRA} > &= (-10.8 \pm 1.1)\ \% \\ < A_{\mu\mu}^{PEP} > &= (-6.3 \pm 0.9)\ \%, \end{aligned} \tag{7.28}$$

in good agreement with the values expected from the standard model, - 9.4 % and - 6.3 %, respectively. Such averaged values are of course only meaningful if the systematic errors of the individual experiments are small.

The PETRA experiments also took data at lower (12 - 14 GeV and 22 - 25 GeV) and higher energies (39 - 46.8 GeV) which turn out to be in good agreement with the standard model predictions. The energy dependence of the integrated forward-backward asymmetry is displayed in Fig. 7.8 and compared with GWS model predictions allowing for different Z^0 masses in the Z boson propagator term which modifies formula (7.6) to

$$< A_{FB} > \simeq -\frac{3}{4}\frac{G}{\sqrt{2}\pi\alpha}\, h_{AA} s \cdot \frac{M_Z^2}{M_Z^2 - s}\,.$$

This propagator effect can be used to derive an unfortunately not yet very stringent limit on the Z^0 mass from the measured asymmetries, assuming that $h_{AA} = 1/4$ and $\rho = 1$ as in the standard model. The combined PETRA and PEP results lead then to $61 < M_Z < 130$ GeV at the 95 % confidence level /418/. This is consistent with the UA1 and UA2 measurements /20/.

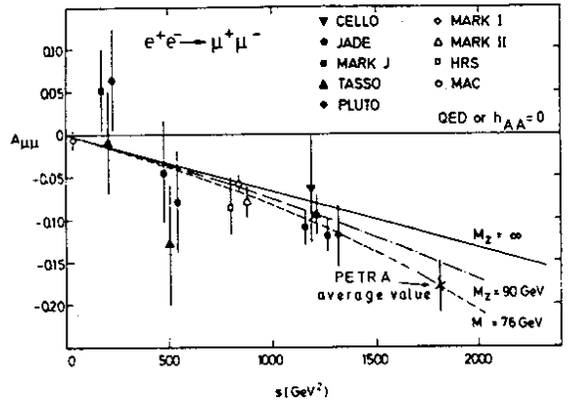

Fig. 7.8 Integrated forward-backward asymmetry $<A_{\mu\mu}>$ for muon pair production as a function of s. The curves represent theoretical expectations for different Z^0 masses /418/.

Assuming $\rho = 1$ and $M_Z = 93$ GeV on the other hand, the axialvector coupling constant h_{AA} can be extracted /418/ from the measured asymmetries

$$h_{AA}^{\mu\mu} = g_A^e g_A^\mu = 0.266 \pm 0.020\,. \tag{7.29}$$

Giving up lepton universality for a moment this leads to

$$g_A^\mu = -0.53 \pm 0.04 \tag{7.30}$$

for the standard model value $g_A^e = -1/2$.

By using Eqs. (2.19) A_{FB} can be rewritten as

$$< A_{FB} > \simeq -\frac{3}{8}\frac{h_{AA}}{\sin^2\Theta_W \cos^2\Theta_W}\frac{s}{M_Z^2 - s}\,.$$

If one assumes that the weak isospin assignments in the standard theory are correct (i.e. $g_A^e \cdot g_A^\mu = \frac{1}{4}$), A_{FB} determines $\sin^2\Theta_W$ and the Z^0 mass. The result of a fit to all muon pair production data is given in Fig. 7.9. It is compared /358/ to the limits imposed by the neutrino-electron scattering data which have been analyzed in an analogous way by determining the parameters $\sin^2\Theta_W$ and ρ simultaneously. Using the observed Z^0 mass one obtains /418/

$$\sin^2\Theta_W = 0.18 \pm 0.02\,.$$

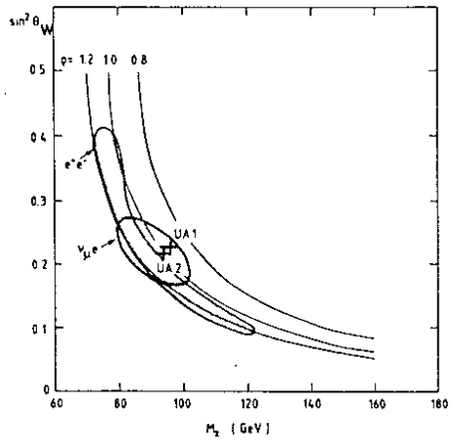

Fig. 7.9 Allowed regions (at 68% C.L.) in the $\sin^2\Theta_W - M_Z$ plane obtained from: a) a combined fit to all $e^+e^- \to \mu^+\mu^-$ data /418/ and b) the combined CHARM results on $\nu_\mu e$ and $\bar{\nu}_\mu e$ scattering /266/. The contours are compared to the mass measurements of UA1 and UA2 /20/. Curves of constant ρ are indicated /358/ (ρ = 1 for the standard model).

7.2.3. Elektroweak effects in τ-pair production

Since τ's decay before they enter the detector ($l_\tau = (3.4 \pm 0.7) \times 10^{-13}$ s /431/) and the decay neutrinos leave the detector unobserved, event selection and background rejection is more difficult in the analysis of τ-pairs than in that of μ-pairs. Some groups have restricted their analysis to special decay modes of the τ. This accounts for the smaller statistics.

Fig. 7.10 shows the behaviour of the total cross-section ratio for τ-pair production, $R_{\tau\tau} = \sigma_{\tau\tau}/\sigma_{QED}$, as a function of s. As for the muon data the total cross section agrees with the QED prediction implying thus agreement with the standard model, too (i.e. $h_{VV} = \left[-1/2 + 2\sin^2\Theta_W\right]^2$ must be small according to Eq. 7.4).

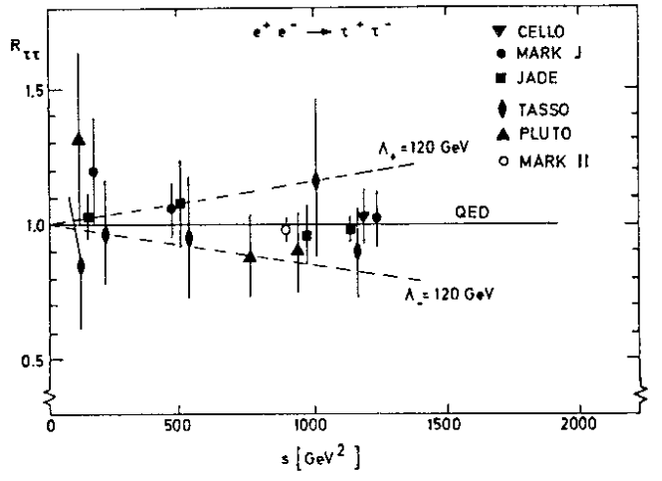

Fig. 7.10 Total cross-section ratio for τ-pair production to the QED cross section as a function of s /418/.

The τ-pair angular distributions measured by the PETRA experiments and the PEP experiment MAC are shown in Figs. 7.11 a and b, respectively, together with the symmetric QED fits (dotted curves) and asymmetric electroweak predictions (full curves). The tau pair asymmetries seen at PETRA and PEP /358,418/ are

$$< A_{\tau\tau} >= \begin{cases} (-6.6 \pm 1.4)\% & \sqrt{s} = 29.0 \text{ GeV} \quad \text{MAC} \\ (-4.2 \pm 2.0)\% & \sqrt{s} = 29.0 \text{ GeV} \quad \text{MARK II} \\ (-7.7 \pm 1.9)\% & \sqrt{s} \sim 34.5 \text{ GeV} \quad \text{PETRA combined data} \\ (-16.7 \pm 9.0)\% & \sqrt{s} \sim 42.5 \text{ GeV} \quad \text{CELLO}. \end{cases} \tag{7.31}$$

These measured asymmetries are compatible with the standard model predictions ($M_Z \simeq$ 90 GeV) as shown in Fig. 7.12 for the results of each group. At present, however, the τ-pair data cannot be used to limit the Z^0 mass to a finite value.

For $\rho = 1$ and $M_Z = 93$ GeV the axialvector coupling strength can be extracted from (7.31). One finds /358/

$$h^{\tau\tau}_{AA} = g^e_A g^\tau_A = 0.222 \pm 0.031\,, \tag{7.32}$$

implying thus

$$g^\tau_A = -0.44 \pm 0.06\,, \tag{7.33}$$

if g^e_A is set to its standard model value, -1/2, and if one allows for violation of lepton universality.

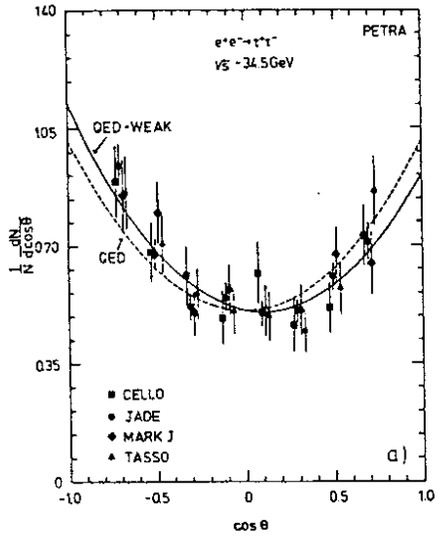

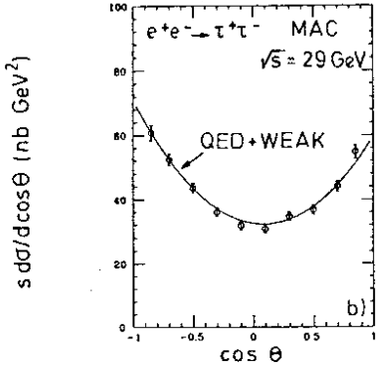

Fig. 7.11

Angular distributions of τ-pairs for (a) PETRA experiments and (b) the PEP experiment MAC /418/.

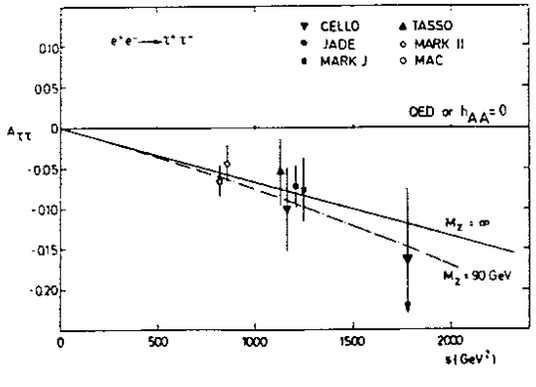

Fig. 7.12

Integrated forward-backward asymmetry $\langle A_{\tau\tau} \rangle$ for τ-pair production as a function of s /418/.

7.2.4. Elektroweak effects in Bhabha scattering

The elastic scattering reaction $e^+e^- \rightarrow e^+e^-$ is complicated by the existence of additional t-channel exchanges. Weak interaction effects are negligible at small scattering angles since the extra γ-exchange diagram produces a large increase in the cross section particularly in the forward direction. Measurements at large scattering angles, however, can be used to study neutral current effects. The QED normalized angular distributions of Bhabha scattering are shown /418/ in Figs. 7.13 for two PETRA experiments (TASSO, MARK J) and the PEP experiment MAC together with the best fits for a variation of the standard model parameter $\sin^2 \Theta_W$.

Since Bhabha events contain only electrons and positrons, these angular distributions determine directly (Eqs. 7.11-14) the vector $(g_V^{e^2})$ and axialvector coupling constant $(g_A^{e^2})$ of the electron, if $\rho = 1$ is assumed. The MAC experiment /418/, for instance, finds the following, of course correlated values for these coupling constants:

$$\begin{aligned} h_{VV} &= g_V^{e^2} = 0.09 \pm 0.14 \\ h_{AA} &= g_A^{e^2} = 0.33 \pm 0.24 \,. \end{aligned} \tag{7.34}$$

Assuming lepton universality, $M_Z = 93$ GeV and $\rho = 1$ the information from the individual leptonic channels can be added to impose more stringent contraints on the coupling constants and the electroweak mixing angle, respectively /418/:

$$\begin{aligned} h_{VV} &= -0.01 \pm 0.03 \qquad (0.004) \\ h_{AA} &= 0.27 \pm 0.03 \qquad (0.25) \\ \sin^2 \Theta_W &= 0.25 \pm 0.05 \,, \end{aligned} \tag{7.35}$$

where the values in parentheses are the standard model predictions for $\sin^2 \Theta_W = 0.23$.

One can use the constraint on h_{VV} to put restrictions on theories of the type $SU_2 \times U_1 \times G$ which lead to neutral-current interactions of the form of Eq. (2.51) with a richer boson structure (Chap. 2.8). As such extensions of the $SU_2 \times U_1$ model modify the vector coupling parameter

$$h_{VV} \rightarrow h_{VV} + 4C \,, \tag{7.36}$$

the result (7.35) implies

$$C < 0.007 \qquad (95\ \%\ C.L.) \,.$$

The normalized difference between the actual theory and the standard theory integrated over all energies is equal to 16 C (Eq. 2.52). Therefore, this limit on C implies that the actual theory of weak interactions is within $\sim$ 89 % of the standard model. The magnitude of C is on the other hand determined by the mass spectra of the bosons in the different models. In view of this interpretation Fig. 7.14 shows the limits placed by measurements (MARK J /434/) on the parameter space (M_{Z_1}, M_{Z_2}) for a $SU_2 \times U_1 \times U_1$ /21/ and a $SU_2 \times U_1 \times SU_2$ model /22/, respectively.

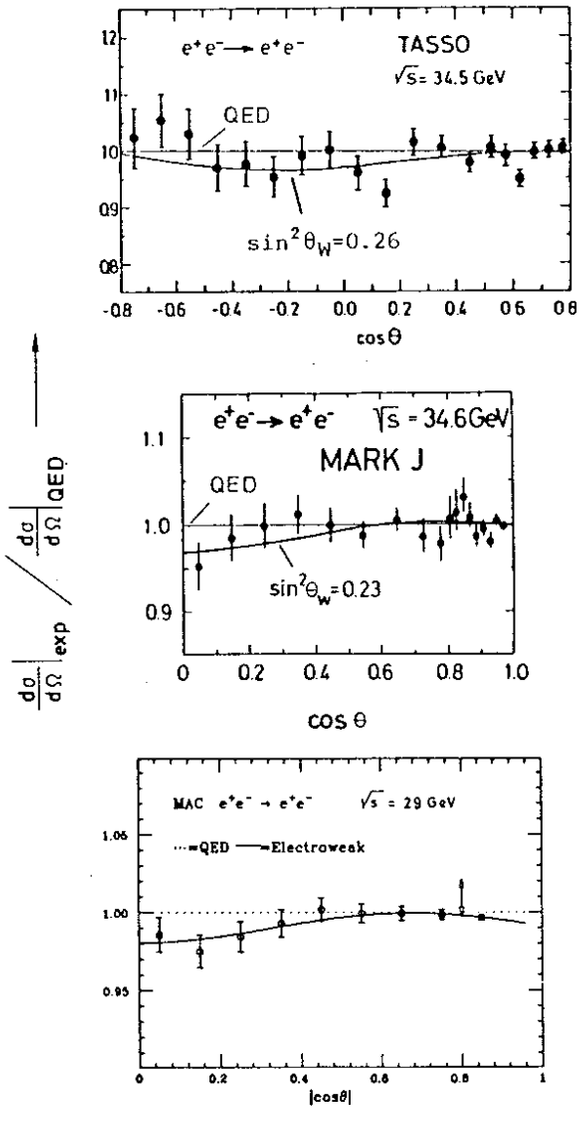

Fig. 7.13 Differential cross section for Bhabha production normalized by the QED cross section measured by TASSO, MARK J and MAC /418,432/.

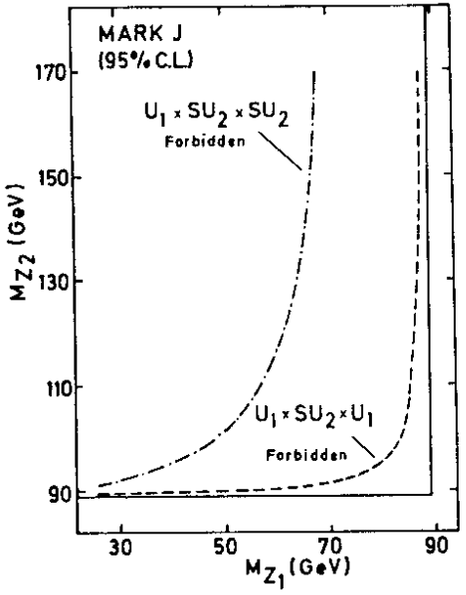

Fig. 7.14 Excluded mass range of the two neutral bosons Z_1 and Z_2 from MARK J /434/ for the extended gauge models $SU_2 \times U_1 \times U_1$ and $SU_2 \times U_1 \times SU_2$.

7.2.5. Elektroweak effects in quark pair production

In the quark parton model hadron production in e^+e^- annihilations proceeds via a quark-antiquark pair $q_f\bar{q}_f$ (Chap. 7.1.3). At present center-of-mass energies the five quark flavours u, d, s, c and b contribute. Since the neutral time-like current (Fig. 7.1), electromagnetic or weak, couples directly to the quark-antiquark pair, the rate for pair production of heavy quarks - if kinematically possible - is expected to be equal to that for pair production of lighter quarks, if one corrects for the quark charges. Therefore, the study of electroweak effects in e^+e^- annihilations offers the unique possibility of testing the couplings of the Z^0 to the heavy quarks. This cannot easily be done in lepton-hadron scattering which is dominated by light quarks.

7.2.5.1. Total hadronic cross section

The presence of a neutral current causes an energy dependence of the total hadronic cross section predicted by the quark parton model as can be seen from Eq. (7.16). However, substantial effects (~ 6 %) are also expected by first and second order QCD (Eq. 7.19) which give rise to an additional energy dependence ($\sim ln\sqrt{s}$) of the hadronic cross section due to contributions from gluon bremsstrahlung graphs. Both effects have to be disentangled.

The energy dependence of the cross-section ratio measured by the PETRA experiment JADE /433/ is shown in Figs. 7.15 and compared to the predictions of the simple quark parton model (dashed line) and QCD including electroweak interference (full line for $\sin^2\Theta_W = 0.23$ and $\alpha_s = 0.20$), respectively.

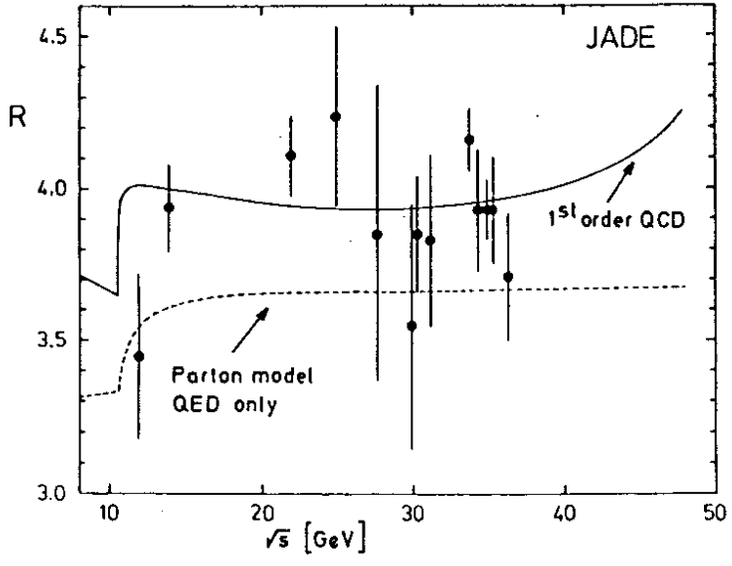

Fig. 7.15 The ratio R compared to predictions of the standard model with $\sin^2\Theta = 0.23$ and $a_s = 0.20$ (full line). The dotted curve is the expectation of the quark parton model.

The value of $\sin^2\Theta_W$ is obtained by fixing α_s, the coupling constant of the strong interaction, and fitting the cross-section ratios over the energy range with $\sin^2\Theta_W$ free. The precision of

$$\sin^2\Theta_W = \begin{cases} 0.28^{+0.08}_{-0.05} & \text{(MARK J)} \\ 0.23 \pm 0.05 & \text{(JADE)} \\ 0.30^{+0.23}_{-0.07} & \text{(TASSO)} \end{cases}$$

determined /433/ in this way is not yet comparable to those of fixed target experiments. But these measurements, which test the standard theory in the region of high Q^2, show that none of the quarks has an unexpected large vector coupling strength (Eq. 7.16) since the contribution of the heavy quarks to the ratio R is just as important as that of the u and d quarks.

7.2.5.2. Quark pair asymmetries

The axialvector couplings of the quarks can be determined by measuring the forward-backward angular asymmetry $A_{q\bar{q}}$ (Eq. 7.21) in the reaction $e^+e^- \rightarrow q\bar{q} \rightarrow 2$ hadron jets. For this both the charge and flavour have to be tagged, restricting thus so far the study of charge asymmetries in quark pair production to the heavy quarks c and b.

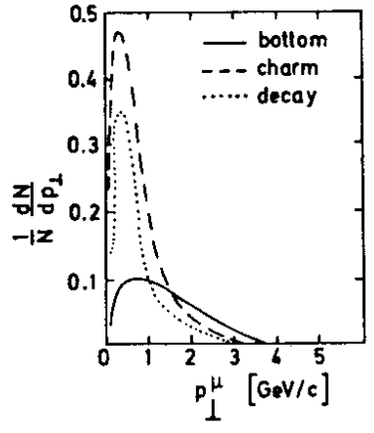

Fig. 7.16

Transverse momentum distributions for muons from c and b decay and decay background /434/.

One method to tag primary heavy quark events exploits the fact that the semileptonic decay of c and b quarks produces a muon of relatively large transverse momentum, $p_\perp^\mu$, relative to the jet axis. The Monte Carlo muon $p_\perp^\mu$ distributions from primary weak c and b decays as well as from hadronic punch through and decay backgrounds are shown in Fig.7.16 /434/. One sees that it is impossible to separate pure c and b quark samples by a $p_\perp^\mu$ cut. But by applying appropriate $p_\perp^\mu$ cuts to the prompt leptons one can select samples of events enriched with primary c and b quarks, respectively. Other cuts (e.g. in the momentum distribution, in the thrust distribution, etc.) further enhance the b/c content in the event sample. The remaining contaminations affect the measured asymmetries because a μ^- identifies a b or $\bar{c}$ and a μ^+ identifies a $\bar{b}$ or c primary quark. The results extracted from recently observed quark pair asymmetries /418/ become therefore model dependent. They turn out to be in good agreement with the standard model couplings.

The forward-backward asymmetry in $c\bar{c}$ production can also be studied in that way that the c quark tagging is done by the reconstruction of the D^* mass /418/. The D^* meson formation is the largest fraction of the c fragmentation. The primary D^* mesons can be identified by means of the decay chain

$$D^* \rightarrow D^0 + \pi$$
$$\longrightarrow K^- \pi^+$$

with a small Q value. The angular distribution of D^* production in the reaction $e^+e^- \rightarrow D^* X$, as measured by the TASSO detector /418/, is shown in Fig. 7.17.

At $\sqrt{s} \sim 34.5$ GeV the c-quark asymmetry /435/ is -14.2 ± 5.2 (stat) % (-14 %) averaged over all PETRA results, whereas the PETRA average of the b-quark asymmetry yields -23.5 ± 5.5 (stat) % (-25 %); the predictions of the standard model are quoted in parentheses. Within the errors the PEP results /435/ agree also with the theoretical predictions. Assuming that the electron weak axialvector coupling constant $g_A^e = -\frac{1}{2}$ as given by the standard theory, the quark coupling constants g_A^c and g_A^b can be extracted from these measured

asymmetries:

$$g_A^c = \begin{cases} 0.50 \pm 0.20 & \text{(PETRA)} \\ 0.60 \pm 0.15 & \text{(PEP)} \end{cases} \qquad g_A^b = \begin{cases} -0.47 \pm 0.11 & \text{(PETRA)} \\ -0.57 \pm 0.12 & \text{(PEP).} \end{cases} \tag{7.37}$$

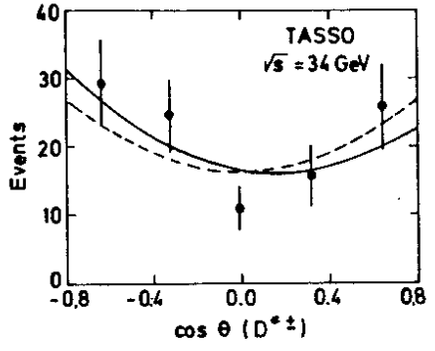

Fig. 7.17
Differential cross section for D^* production in $e^+e^- \to D^*X$ measured by TASSO at PETRA /418/.

7.3. Tests on generation universality

The standard model assumes that fermions of the same charge couple with the same strength to the neutral vector boson independent of the fermion generation. The lepton and quark vector and axialvector coupling constants predicted by the GWS model are listed in Table 7.2 (assuming $\rho = 1$), applying Eqs. (2.36) to the representations of the leptons and quarks defined in (2.10) and (2.11), respectively.

Table 7.2. Standard model definitions of vector and axialvector coupling constants for leptons and quarks.

	Q	g_A	g_V
ν_e, ν_μ, ν_τ	0	1/2	1/2
e, μ, τ	- 1	- 1/2	$- 1/2 + 2 \sin^2\Theta_W$
u, c, t	2/3	1/2	$1/2 - 4/3 \sin^2\Theta_W$
d, s, b	- 1/3	- 1/2	$- 1/2 + 2/3 \sin^2\Theta_W$

The basis for this generation universality of the GWS model is provided by the GIM mechanism /19/ which implies that the weak hadronic neutral current is, by construction, flavour-conserving. Within this context the question of universality of the neutral-current coupling for the different generations of fermions can be studied experimentally by searching for small deviations from flavour conservation of the neutral current.

7.3.1. Limits on flavour-changing neutral currents

Studies of strange particle decays and production put quite stringent limits on the existence of strangeness-changing neutral currents (Chap. 2.7) /86,436/.

The search for "wrong-sign" muons in inclusive neutrino reactions has given a stringent limit /437/ on the cross section of the charm-changing reaction $\nu_\mu u \to \nu_\mu c$, where the c quark in turn decays semileptonically, $c \to s\mu^+\nu_\mu$. This results in a wrong-sign muon:

$$\frac{\sigma(\nu_\mu N \to \nu_\mu C)}{\sigma(\nu_\mu N \to \nu_\mu X)} < 0.026 \qquad (90\ \%\ \text{C.L.}). \tag{7.38}$$

The ITEP-FNAL-IHEP-Michigan Collaboration /438/ quotes a corresponding limit for charmed particle production in antineutrino-nucleon neutral-current interactions, where the recognition signature used was e^+ decay of the charmed particle, $C \to e^+\nu_e X$:

$$\frac{\sigma(\bar\nu_\mu N \to \bar\nu_\mu C)}{\sigma(\bar\nu_\mu N \to \bar\nu_\mu X)} < 0.04 \qquad (90\ \%\ \text{C.L.}). \tag{7.39}$$

Charm-changing neutral currents have also been searched for in the decay of charmed particles produced in charged-current neutrino reactions. One obtains /439/

$$\frac{\Gamma(C \to e^+e^- X)}{\Gamma(C \to e^+\nu X)} < 0.02 \qquad (90\ \%\ \text{C.L.}). \tag{7.40}$$

Further contraints on the amount of $c \leftrightarrow u$ transitions can be provided by a search for D^0-$\bar D^0$ mixing due to their neutral-current decay /440/. Such a mixing would lead to final states of D^0D^0 or $\bar D^0\bar D^0$ and hence to events with two leptons of equal charge from their semileptonic decays (in the quark parton model D^0 is a $c\bar u$ state). In the energy range 3.72 GeV $< E_{cm} <$ 4.14 GeV an upper limit for D^0-$\bar D^0$ mixing has been determined in the reaction $e^+e^- \to e^\pm e^\pm X$:

$$\frac{N(e^+e^+) + N(e^-e^-)}{N(e^+e^+) + N(e^-e^-) + N(e^+e^-)} < 0.05 \qquad (90\ \%\ \text{C.L.}). \tag{7.41}$$

From the search for "wrong" sign K's (from a D^0 a single S=-1 kaon is expected with amplitude $\cos^2\Theta_C$, since $c \to sl^+\nu_l \sim \cos\Theta_C$) in $e^+e^- \to D^{*+} + \ldots$, $D^{*+} \to K^+$ or K^- /441/ and $e^+e^- \to D^0K^\pm + \ldots$ /442/ the MARK II Collaboration at SPEAR obtained an upper limit on $D^0\bar D^0$ mixing. This can be translated /443/ in an upper limit on the coupling strength of charm-changing neutral currents of

$$g_{NC}^{\Delta C \neq 0} \leq 10^{-7}\, G. \tag{7.42}$$

The CLEO group /444/ at CESR has set an upper limit on the neutral-current transition $b \leftrightarrow d$ (s) by studying e^+e^- events with two leptons in the final state. Such events are expected from the semileptonic decay of both the B and $\bar{B}$ and, if flavour-changing neutral currents exist, from the decay $B \rightarrow l^+l^-X$. The numbers of observed dilepton events turn out to be consistent with the assumption that they arise only from semileptonic B, $\bar{B}$ decays. From this an upper limit on b-changing neutral-current B decays can be extracted:

$$\text{Branching ratio } (B \rightarrow l^+l^-X) \leq 0.74\,\% \qquad (90\,\%\ C.L.). \tag{7.43}$$

Within the context of the GIM mechanism these limits imply quite stringent constraints on the generation universality of the neutral-current couplings.

7.3.2. Universality of the neutral-current couplings

The generation universality has furthermore to be established in a model-independent way manifesting that really all fermions of the same charge couple in the same way to the Z^0 boson. There are new experimental results that confirm this hypothesis.

i) From the asymmetries measured in e^+e^- scattering the axialvector coupling constants g_A^e (Eq. 7.34), g_A^μ (Eq. 7.30) and g_A^τ (Eq. 7.33) have been extracted, confirming e-μ-τ universality within the errors.
The fact that the QED predictions for the integrated muon pair and tau pair cross section agree with the data (Figs. 7.6 and 7.10) implies that g_V^μ and g_V^τ are small, as expected in the standard model ($g_V^\mu = g_V^\tau = -0.04$ for $\sin^2\Theta_W = 0.23$).
Combining /351,445/ the e^+e^- results with data from other experiments that involve e and μ couplings (viz. polarized eD scattering, $\mu^\pm C$ and $\overset{(-)}{\nu}_\mu e$ scattering) vector and axialvector couplings are obtained which confirm e-μ universality:

$$\begin{aligned} g_V^e &= 0.02 \pm 0.06\,, & g_V^\mu &= -0.05 \pm 0.16\,, \\ g_A^e &= -0.54 \pm 0.03\,, & g_A^\mu &= -0.51 \pm 0.05\,. \end{aligned} \tag{7.44}$$

ii) From a comparative study of the y distribution of both neutral-current and charged-current neutrino and antineutrino interactions on nucleons (Fig. 7.18) the CHARM Collaboration /213/ has extracted a contribution from the neutral-current coupling of strange quarks present in the $s\bar{s}$ sea. The coupling strength, when compared with that of the d quark, is

$$\frac{g_s^2}{g_d^2} = \frac{\epsilon_L^2(s) + \epsilon_R^2(s)}{\epsilon_L^2(d) + \epsilon_R^2(d)} = 1.39 \pm 0.43 \tag{7.45}$$

consistent with GIM symmetry which predicts unity (Table 7.2).

iii) The CDHS experiment /253/ has observed diffractive J/Ψ production in neutral-current neutrino-nucleon interactions (Chap. 4.2.4.6). The $\mu^+\mu^-$ mass spectrum of the dimuon events produced in $\nu_\mu Fe \rightarrow \mu^+\mu^- X$ reactions is shown in Fig. 7.19. The peak at 3.1 GeV is interpreted as the creation of the $c\bar{c}$ bound state J/Ψ produced through Z^0 and gluon fusion /254/.

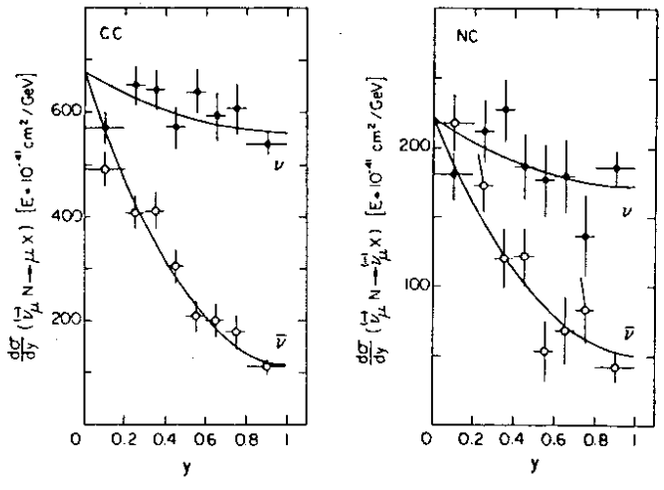

Fig. 7.18 Inelasticity distribution of ν_μ- and $\bar{\nu}_\mu$-induced charged and neutral current events in the CHARM detector /213/.

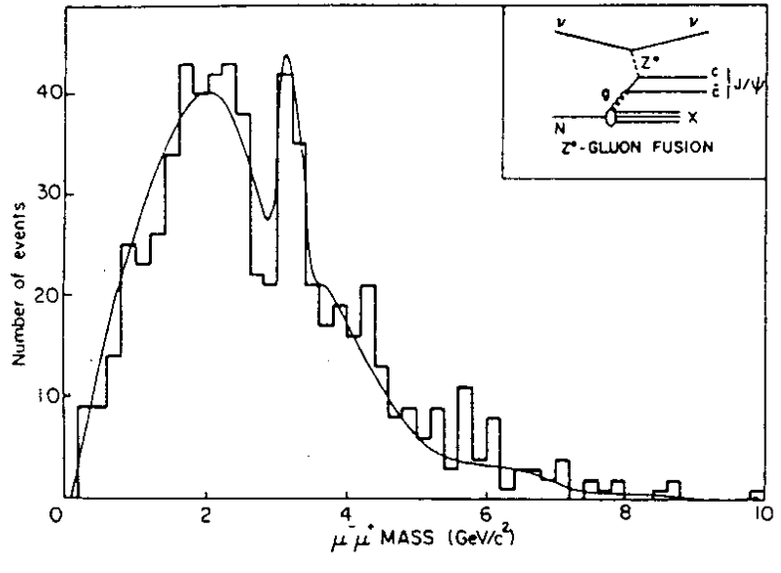

Fig. 7.19 Invariant $\mu^+\mu^-$ mass of neutrino dimuon events with only small hadronic recoil /253/.

Comparing the cross section for the diffractive process $\nu_\mu + N \to \nu_\mu + N + J/\Psi$ with that of $\mu + N \to \mu + N + J/\Psi$, and assuming the Z-gluon fusion mechanism also for the muon-induced events one gets an estimate of the neutral-current coupling strength of charmed quarks /252/:

$$\frac{g_c^2}{g_u^2} = \frac{\epsilon_L^2(c) + \epsilon_R^2(c)}{\epsilon_L^2(u) + \epsilon_R^2(u)} = 2.1 \pm 1.0 \qquad (7.46)$$

compatible with that expected from universality (Table 7.2).

iv) The total hadronic cross section in e^+e^- annihilation, $\sigma(e^+e^- \to q\bar{q} \to \text{hadrons})$, to which the c and b quarks contribute with almost one half total weight, is essentially sensitive to the vector coupling of the quarks (Chap. 7.1.3). One finds that in these data the weak vector couplings are consistent in strength with those measured in lepton-nucleon scattering which is dominated by light quarks.
The results of quark pair asymmetries sensitive to the axialvector couplings of the quarks are confined at the moment to the heavy b and c quarks for which charge and flavour tagging techniques have been developed (Chap.7.2.5.2). The coupling constants extracted from the data (Eqs. 7.37) agree quite well with the predictions of the standard model (Table 7.2) although the errors are still large.

In summarizing it can be concluded that the direct experimental study of the generation universality of the neutral-current couplings confirms its validity already suggested - within the context of the GWS model – by the stringent limits on flavour-changing neutral currents (Chap. 7.3.1).

7.4. Factorization test in the leptonic sector

The factorization hypothesis (Chap. 2.9) allows to convert the coupling parameters h_{VV} and h_{AA} extracted from e^+e^- annihilation data into the coupling constants g_V^e and g_A^e determined in neutrino-electron scattering (Fig. 7.20). For that purpose the model-dependent parameter c_ν (Eqs. 2.67) characterizing the strength of elastic $\nu\nu$ scattering must be known. This constant c_ν is one in a large class of gauge models. Furthermore by combining neutrino-electron scattering with neutrino-hadron and parity-violating electron-deuteron scattering one can show that c_ν^2 is one to an accuracy of ~ 15 % (Chap. 6.4). In evaluating (7.30) and (7.33) $c_\nu^2 = 1$ has been assumed.

But factorization can be studied in purely leptonic reactions alone /444/ by deducing from Eqs. (2.67) the ratio

$$h_{VV}/h_{AA} = g_V^{e^2}/g_A^{e^2}. \qquad (7.47)$$

Then, by the experimental fact that h_{VV} is vanishingly small whereas h_{AA} is sizeable (Eqs. 7.35), the axialvector dominant solution in neutrino-electron scattering ($g_A^{e^2} \gg g_V^{e^2}$) is conclusively selected (Fig. 7.20), in agreement with the result already obtained by comparing the νe scattering data with neutrino hadron and electron-hadron data (Fig. 6.6).

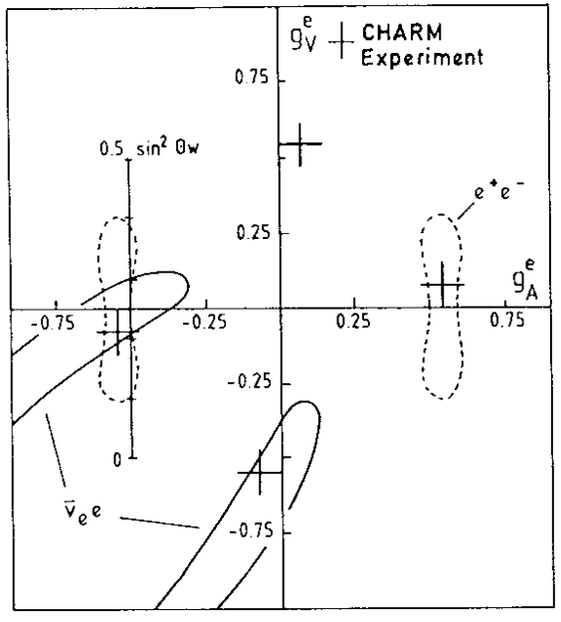

Fig. 7.20 Constraints imposed in the g_V^e, g_A^e space by various leptonic reactions /266/. The shaded area is selected by factorization.

8. SUMMARY OF NEUTRAL-CURRENT PROCESSES

Assuming that the weak currents are arbitrary mixtures of V and A - a very reasonable working hypothesis in view of the data discussed above - model-independent analyses of the neutral-current data at low energies (s, $Q^2 \ll M_Z^2$) have been performed. They aim to determine the measurable, a priori independent parameters needed to describe the neutral-current processes phenomenologically and then to confront them with model predictions. For this the neutral-current interaction is written in form of a current-current interaction with a certain number of coupling parameters which characterize the space-time and isospin structure of the currents. To proceed further it is necessary to exploit the hypothesis that all neutral-current interactions are mediated by a single Z boson (factorization hypothesis).

Analyses of this type /29,31,68,447/ covering a very wide range of reactions, particles and momentum transfers have extracted the neutral-current parameters listed in Table 8.1. The agreement with the expectations of the standard model is excellent.

The data have also been analysed in terms of the standard model. In order to test the theory it must be shown that all experiments (ν, $\bar{\nu}$, e^+e^-, eN, μN, $M_{W/Z}$) can be described by the same value of $\sin^2\Theta_W$. If possible, this should be done to an accuracy which tests the second order corrections so as to establish the standard theory as a renormalizable theory and to distinguish it from other models with the same first order low-energy predictions /446/. Applying the process-dependent electroweak radiative corrections (W and Z propagator corrections, vertex corrections, two W exchange, real bremsstrahlung etc.), one extracts $\sin^2\Theta_W$ as listed in Table 8.2. All existing results are in quite good agreement with each other. From a global analysis /447/ of all data available in 1981 one obtained

$$\sin^2\Theta_W = 0.217 \pm 0.014 . \qquad (8.1)$$

Using this value the mass of the Z^0 is predicted to $M_Z = (93.8^{+2.4}_{-2.2})$ GeV in excellent agreement with the combined UA1 and UA2 result $M_Z = (93.0 \pm 2.0)$ GeV /448/. However, to make a significant distinction between the first order (leading to $M_Z = (89^{+2.2}_{-2.0})$ GeV) and second order predictions of M_Z, the present uncertainty in $\sin^2\Theta_W$ should be improved by a factor of at least 3. In order to achieve such a precision both the statistical and the systematic errors have to be reduced. In deep-inelastic neutrino-nucleon scattering both improvements could be obtained with a quadrupole-focused neutrino beam providing high intensity (anti)neutrino fluxes with a high average neutrino energy and low backgrounds. Using this type of beam and deriving $\sin^2\Theta_W$ from the Paschos-Wolfenstein relation (Eq. 4.91), for example, a total (experimental and theoretical) uncertainty of ± 0.005 in $\sin^2\Theta_W$ seems to be achievable in semileptonic weak neutral-current interactions /449/.

The most direct determination of $\sin^2\Theta_W$ in the leptonic sector is provided by the measurement of the cross section ratio $R = \sigma(\nu_\mu e)/\sigma(\bar{\nu}_\mu e)$ (Eq. 4.74). By using the fine-grain calorimeter proposed by the CHARM II Collaboration /450/, there seems to be no obstacle in measuring this ratio R to ± 0.05 corresponding to an uncertainty of ± 0.005 in $\sin^2\Theta_W$. This would reduce the error on the predicted Z^0 mass to 0.7 GeV, allowing thus a decisive test of the underlying electroweak gauge theory.

Table 8.1. Empirical status of neutral-current couplings. The number in brackets are the expectations of the standard model with $\sin^2\Theta_W = 0.22$.

Neutrino-Quark Scattering			
$\varepsilon_L(u)$ =	0.344 ± 0.026 (0.353)	α =	0.533 ± 0.037 (0.560)
$\varepsilon_L(d)$ =	-0.419 ± 0.022 (-0.427)	β =	0.992 ± 0.037 (1)
$\varepsilon_R(u)$ =	-0.153 ± 0.022 (-0.153)	γ =	-0.152 ± 0.089 (-0.147)
$\varepsilon_R(d)$ =	0.076 ± 0.041 (0.073)	δ =	0.002 ± 0.049 (0)
Neutrino-Electron Scattering			
g_V^e =	0.02 ± 0.06 (-0.060)	g_A^e =	-0.54 ± 0.03 (-0.500)
Electron-Quark Scattering			
$\tilde{\alpha}$ =	-0.65 ± 0.17 (-0.560)	$\tilde{\gamma}$ =	0.14 ± 0.05 (0.147)
$\tilde{\beta}$ =	0.06 ± 0.21 (-0.120)	$\tilde{\delta}$ =	0.00 ± 0.02 (0)
Electron-Positron Scattering			
h_{VV} =	0.002 ± 0.005 (0.004)	h_{VA} =	0.02 ± 0.02 (0.030)
h_{AA} =	0.27 ± 0.03 (0.250)		

Table 8.2. Measurements of $\sin^2\Theta_W$ from a variety of reactions. Where appropriate the results are quoted with radiative corrections.

Reaction	$\sin^2\Theta_W$	Typical Q^2 $[\mathrm{GeV}^2]$
$\overset{(-)}{\nu}N \to \overset{(-)}{\nu}X$ /292/	$0.223 \pm 0.007(\mathrm{exp}) \pm 0.006(\mathrm{theor})$	10^2–10^3
$\overset{(-)}{\nu}p \to \overset{(-)}{\nu}p$ /358/	0.26 ± 0.04	10^0
$\overset{(-)}{\nu}e \to \overset{(-)}{\nu}e$ /266/	$0.22 \pm 0.03(\mathrm{stat}) \pm 0.01(\mathrm{syst})$	10^{-2}
e D asymmetries /358/	$0.215 \pm 0.015(\mathrm{stat}) \pm 0.005(\mathrm{syst})$	10^0
μ N asymmetries /351/	$0.23 \pm 0.07(\mathrm{stat}) \pm 0.04(\mathrm{syst})$	10^2
atomic parity /377/	$0.205 \pm 0.035(\mathrm{stat}) \pm 0.025(\mathrm{syst})$	10^{-11}
e^+e^- /418/	0.18 ± 0.02	10^3
W, Z /20,446/	0.22 ± 0.01	10^4
world-average /447/	0.217 ± 0.014	

In grand unified theories (GUTS) in which the strong, weak and electromagnetic interactions are embedded in a larger underlying gauge theory, the arbitrary parameter in the standard theory, $\sin^2\Theta_W$, is predictable. In the SU_5 model /25/, for example, one finds

$$\sin^2\hat{\Theta}_W(M_W) = 0.216 \pm 0.004(N_H - 1) + 0.006\ln(0.1\,\mathrm{GeV}/\Lambda_{\overline{\mathrm{MS}}}). \tag{8.2}$$

For $\Lambda_{\overline{\mathrm{MS}}} \simeq 0.1$ GeV and $N_H \leq 4$ (number of Higgs doublets) this prediction is in very good agreement with the experimental values ($\sin^2\Theta_W = 1.006\sin^2\hat{\Theta}_W(M_W)$ if one defines $\sin^2\Theta_W = 1 - M_W^2/M_Z^2$). For this reason as well a precise measurement of $\sin^2\Theta_W$ is of great interest.

In order to check the usual assumption of the standard model that all the Higgs scalars belong to weak isodoublets, the data have also been analysed in two-parameter models. In addition to $\sin^2\Theta_W$, in these models ρ is a free parameter which describes the relative

strength of the neutral and charged current interactions. The ρ values /358/ extracted from the different processes

$$\rho = \begin{cases} 1.01 \pm 0.02 & \text{semileptonic } \overset{(-)}{\nu} \text{ scattering} \\ 1.09 \pm 0.14 & \overset{(-)}{\nu}_\mu e \text{ scattering} \\ 1.17 \pm 0.09 & e^+e^- \to \mu^+\mu^- \\ 1.00 \pm 0.04 & M_W,\, M_Z \end{cases}$$

are in excellent agreement with each other and with the standard model ($\rho = 1$). In particular, all data are still compatible with the 1981 world average /447/

$$\rho = 1.02 \pm 0.02\,, \quad \sin^2\Theta_W = 0.238 \pm 0.030\,. \tag{8.3}$$

This value of ρ indicates that the data are quite consistent with a Higgs doublet structure, i.e. the absence of any other multiplets for Higgs scalars. In addition, the result has implications on a possible existence of heavy fermions (Chap. 2.8, Eq. 2.45). With the assumption that $\rho = 1$ before renormalization effects, then the upper limit on ρ implies an upper limit on any heavy fermion of 300 GeV, assuming that its partner is massless.

Since the discovery of the $W^\pm$ and the Z^0 /20/, alternative models to the standard electroweak theory seem to be strongly restricted /448/ because of the very impressive agreement between the data and the standard model predictions. Similarly the generalized global SU_2 current-current interaction model of Bjorken /23/, where discrete weak quanta need not exist, is already ruled out. The fact that the unification condition has to hold in the phenomenological γ-W^0 mixing model of Hung and Sakurai /24/ in order to satisfy experimental observation and theoretical prediction, implies furthermore that also this approach is no longer a real alternative /448/.

If both M_W and M_Z are as predicted by the standard model, also theories with enlarged gauge groups $SU_2 \times U_1 \times G$ /21,22/ (Chap. 2.8) implying a richer boson structure are in trouble. From the e^+e^- data (Chap. 7) one knows already that the effect of these alternatives in the low-energy range must be very small (Eq. 7.36).

However, left-right symmetric models/116/ involving two W (viz. W_L and W_R) and two Z bosons (Z_1^0, Z_2^0) cannot be ruled out at the present, provided that $M_{Z_1^0}$ is identical to M_Z of the standard model. Dramatic differences between this class of models and the standard model are expected to show up only at energies far above the first (lower) Z boson mass /31/. From the low-energy data Sehgal /68/ extracted the neutral-current parameters which describe left-right symmetric models (Eq. 2.46):

$$\begin{aligned} \sin^2\Theta_W &= 0.22 \pm 0.02 \\ \rho_L &= 1.0 \pm 0.06 \\ \rho_R &= 0.1 \pm 0.1 \\ \rho_{LR} &= 0.05 \pm 0.06 \end{aligned} \tag{8.4}$$

constraining the weak boson masses to

$$\begin{aligned} 87\ \mathrm{GeV} < M_{Z_1^0} &< 90\ \mathrm{GeV} \\ 230\ \mathrm{GeV} < M_{Z_2^0} &< \infty\,. \end{aligned} \tag{8.5}$$

9. CONCLUSIONS

A variety of weak neutral- and charged-current phenomena covering an enormously wide range of energy and momentum transfer has been reviewed: from relatively low space-like $Q^2 \sim 10^{-11}\ GeV^2$ in radiative atomic transitions and $10^{-6}\ GeV^2$ in decay processes of elementary particles to $Q^2 \sim 10^2\ GeV^2$ in neutrino-induced reactions and recently to time-like momentum transfers exceeding $10^3\ GeV^2$ in electron-positron storage ring experiments.

All experimental results concerning weak charged currents are well reproduced by a V-A structure of the interaction and mixing angles as given by the Cabibbo theory /3/ or by its six flavour generalization by Kobayashi and Maskawa /4/, respectively. A lot of progress has been made in determining or restricting the elements of the flavour mixing Kobayashi-Maskawa matrix /97/. Despite of the good agreement between data and V-A theory predictions, right-handed (V+A) currents and/or S, P, T currents at the level of 10 % cannot be ruled out by the results extracted from decay process and neutrino scattering experiments at the present. The discovery /20/ of the $W^{\pm}$ particles, which have the properties of the predicted mediators of the weak charged-current interactions, favours however the standard weak interaction theory that implies V-A charged currents. This is supported by the fact that the electroweak mixing angle $\sin^2\Theta_W$ determined from the W mass is compatible - within the experimental errors - with the values obtained from low-energy neutral-current experiments.

Since the discovery of neutral-current weak interactions in 1973 /7-10/ a large number of different experiments has been performed in order to reveal their space-time structure. Nevertheless, up to now there is only limited information available concerning the question whether the final-state lepton in neutrino scattering processes is identical to the incident neutrino (neutrino identity), and whether their helicities are the same (absence of S, P, T). Further higher statistic $\overset{(-)}{\nu}_e e$ scattering experiments using $\overset{(-)}{\nu}_e$ enriched beams (e.g. at LAMPF) may provide some answers to these questions by the study of the interference between neutral-current and charged-current contributions. The experimental fact that the electroweak mixing angle determined in neutrino scattering processes - where helicity-flipping S, P, T interactions may contribute - is in excellent agreement with the one extracted from weak-electromagnetic interference in electron-hadron and e^+e^- scattering - where scalar interactions cannot contribute - suggests that scalar neutral-current couplings are quite small /68/. This suggests that the neutral weak interactions are of the V, A type like the charged ones as assumed in electroweak theories.

The cross sections for inclusive neutrino-hadron and (both reactor and accelerator) neutrino-lepton scattering processes are in very good agreement with the standard model predictions. But they are invariant under interchange of vector and axialvector currents so that, in principle, an alternative form of the weak neutral current could exist. This vector-axialvector ambiguity has been resolved in studying both exclusive neutrino reactions and, assuming factorization, non-neutrino processes such as: the left-right asymmetry in polarized electron-nucleon inelastic scattering, the beam-conjugation asymmetry in deep-inelastic muon scattering and also the forward-backward asymmetry in $e^+e^- \rightarrow \mu^+\mu^-$, $\tau^+\tau^-$ and $q\bar{q}$. All experiments together demonstrate that the weak neutral current is not purely V-A but has, in contrast to the weak charged currents, a significant right-handed part as predicted in models which unify weak and electromagnetic interactions.

In particular, all experimental results are well reproduced by the one-parameter standard

$SU_2 \times U_1$ model /15-18/, with $\sin^2\Theta_W = 0.217 \pm 0.014$ /447/. The parameter ρ, the ratio of the squares of the intrinsic neutral-current and charged-current couplings, is found to be 1.02 ± 0.02. This is in good agreement with the standard model where ρ equals 1 in lowest order as a consequence of the choice of the Higgs representation (only one Higgs doublet). The question of how many Higgs doublets there are, what masses the physical scalars that survive the Higgs mechanism have and so on, can only be settled experimentally. Settling the questions concerning the Higgs sector is presumably one of the most important tasks of future high-energy physics experiments.

The success of the standard model is quite significant since the selective power of the data is quite high now. This is proved by the failure of a large number of alternative models that have primarily been proposed to explain apparent disagreements between the standard model and some experimental observations, which have all been proven wrong by now. Since the discovery of $W^{\pm}$ and Z^0 in $p\bar{p}$ collider experiments /20/, alternative models are even stronger restricted because of the very impressive agreement between the data and the standard model predictions. No equally simple alternative to the standard model appears to survive at present. One should however not forget that also the standard electroweak model for three generations contains 17 arbitrary parameters (24 if one allows the neutrino to have masses): the 3 model parameters e, G, and $\sin^2\Theta_W$, the Higgs mass, 10 parameters from the quark mass matrix (6 masses, 3 mixing angles and one CP violating phase), and 3 charged lepton masses (with massive neutrinos one must add 3 neutrino masses, 3 lepton mixing angles and one phase). If the number of Higgs doublets or the number of generations are larger, the number of free parameters can grow to a significantly higher number.

Among these 17 (or 24) parameters the electroweak mixing angle, $\sin^2\Theta_W$, has been of greatest interest. Also future low-energy experiments /449-451/ aim to measure this parameter with high precision since an accurate value of $\sin^2\Theta_W$ is needed to distinguish significantly between the first and second order predictions of the W and Z masses. This will then allow a decisive test of the underlying electroweak gauge theory by comparing the predictions with the W and Z mass measurements.

ACKNOWLEDGMENTS

It is a pleasure for me to express appreciations to my colleagues in the CHARM Collaboration: F. Bergsma, J. Dorenbusch, M. Jonker and F. Udo (Amsterdam); J. V. Allaby, U. Amaldi, G. Barbiellini, V. Blobel, G. Cocconi, W. Flegel, W. Kozanecki, L. Lanceri, K. H. Mess, M. Metcalf, J. Meyer, C. Nieuwenhuis, R. S. Orr, J. Panman, C. Santoni, F. Schneider, A. M. Wetherell and K. Winter (CERN); I. Abt, J. Aspiazu, T. Bauche, A. Büngener, F. W. Büsser, H. Daumann, H. Grote, T. Hebbeker, P. Heine, B. Kröger, E. Metz, F. Niebergall, K. H. Ranitzsch, P. Schütt, P. Stähelin (Hamburg); P. Gorbunov, E. Grigoriev, V. Kaftanov, V. Khovansky and A. Rosanov (Moscow); A. Baroncelli, L. Barone, B. Borgia, C. Bosio, A. Capone, U. Dore, F. Ferroni, E. Longo, L. Luminari, P. Monacelli, F. de Notaristefani, P. Pistilli, L. Tortora and V. Valente (Rome).

Special thanks go to Prof. F. W. Büsser and Prof. P. Stähelin for many valuable suggestions, steady encouragement and a careful reading of this manuscript. I am also deeply indebted to Prof. H. Joos and Prof. K. Winter for interesting discussions and helpful comments. Furthermore, I thank Mrs. C. Harder and Mrs. M. Schmidt for their patient typing of the manuscript and especially Mrs. B. Lohl for the careful processing of the figures and reproductions. Finally, I thank Dr. P.-K. Schilling for his help in setting this manuscript with the typesetting system TEX.

REFERENCES

1. E. Fermi, Nuovo Cimento **11** (1934), 1; Z. Phys. **88** (1934), 161.

2. For introductions to weak charged-current interactions see, for example:
T. D. Lee and C. S. Wu, Ann. Rev. Nucl. Sci. **15** (1965), 381;
R. E. Marshak, Riazuddin and C. P. Ryan, *Theory of Weak Interactions in Particle Physics*, Wiley, New York (1969);
S. Gasiorowicz, *Elementary Particle Physics*, Wiley, New York (1966);
G. Källén, *Elementary Particle Physics*, Addison-Wesley Pub. Comp. Inc., Reading (1964).

3. N. Cabibbo, Phys. Rev. Lett. **10** (1963), 531.

4. M. Kobayashi and T. Maskawa, Progr. Theoret. Phys. **49** (1973), 652.

5. P. Langacker, Phys. Rep. **72** (1981), 185.

6. P. W. Higgs, Phys. Rev. Lett. **12** (1964), 132;
T. Englert and R. Brout, Phys. Rev. Lett. **13** (1964), 321;
G. S. Guralnik, C. R. Hagen and T. Kibble, Phys. Rev. Lett. **13** (1965), 585;
P. W. Higgs, Phys. Rev. **145** (1966), 1156;
G. 't Hooft, Nucl. Phys. **B33** (1971), 173;
B. W. Lee and J. Zinn-Justin, Phys. Rev. **D5** (1972), 3121; Phys. Rev. **D5** (1972), 3137; Phys. Rev. **D5** (1972), 3155;
G. 't Hooft and M. Veltman, Nucl. Phys. **B44** (1972), 189.

7. F. J. Hasert *et al.*, Phys. Lett. **46B** (1973), 121.

8. F. J. Hasert *et al.*, Phys. Lett. **46B** (1973), 138.

9. A. Benvenuti *et al.*, Phys. Rev. Lett. **32** (1974), 800.

10. B. C. Barish *et al.*, Phys. Rev. Lett. **34** (1975), 538.

11. S. J. Barish *et al.*, Phys. Rev. Lett. **33** (1974), 448.

12. W. Lee *et al.*, Phys. Rev. Lett. **38** (1977), 202.

13. S. A. Bludman, Nuovo Cimento **9** (1958), 433.

14. Y. B. Zel'dovich, JETP **9** (1959), 682.

15. S. L. Glashow, Nucl. Phys. **22** (1961), 579.

16. A. Salam and J. C. Ward, Phys. Lett. **13** (1964), 168.

17. S. Weinberg, Phys. Lett. **19** (1967), 1264; Phys. Rev. **D5** (1972), 1412.

18. A. Salam, *Elementary Particle Theory*, ed. N. Svartholm, Almquist and Wiksells, Stockholm (1969), p. 367.

19. S. L. Glashow, J. Iliopoulos and L. Maiani, Phys. Rev. **D2** (1970), 1285.

20. UA1 Collaboration: G. Arnison *et al.*, Phys. Lett. **122B** (1983), 103;
Phys. Lett. **126B** (1983), 398;
UA2 Collaboration: M. Banner *et al.*, Phys. Lett. **122B** (1983), 476;
UA2 Collaboration: P. Bagnaia *et al.*, Phys. Lett. **129B** (1983), 130.

21. E. H. de Groot, G. J. Gounaris and D. Schildknecht, Phys. Lett. **85B** (1979), 399;
Phys. Lett. **90B** (1980), 427; Z. Phys. **5** (1980), 127.

22. V. Barger, W. Y. Keung and E. Ma, Phys. Rev. Lett. **44** (1980), 1169;
Phys. Rev. **D22** (1980), 727; Phys. Lett. **94B** (1980), 377.

23. J. D. Bjorken, *Ben Lee Memorial International Conference on Parity Non-Conservation, Weak Neutral Currents and Gauge Theories*, eds. D. B. Cline and F. E. Mills (1977), p. 701, Harwood Academic Pub., London - Chur;
J. D. Bjorken, Phys. Rev. **D19** (1979), 335.

24. P. Q. Hung and J. J. Sakurai, Nucl. Phys. **B143** (1978), 81.

25. H. Georgi and S. L. Glashow, Phys. Rev. Lett. **32** (1974), 438;
H. Georgi, H. Quinn and S. Weinberg, Phys. Rev. Lett. **33** (1974), 451;
A. J. Buras, J. Ellis, M. K. Gaillard and D. V. Nanopoulos, Nucl. Phys. **B135** (1978), 66.

26. B. Kayser *et al.*, Phys. Lett. **52B** (1974), 385.

27. R. L. Kingsley *et al.*, Phys. Rev. **D10** (1974), 2216.

28. K. S. Lackner, Nucl. Phys. **B153** (1979), 505.

29. J. E. Kim, P. Langacker, M. Levine and H. H. Williams, Rev. Mod. Phys. **53** (1980), 211.

30. J. J. Sakurai, *Proceedings of the International Conference on Neutrino Physics and Astrophysics*, Maui (Hawaii), eds. R. J. Cence, E. Ma and A. Roberts, **Vol. II** (1981), p. 457.

31. P. Q. Hung and J. J. Sakurai, Ann. Rev. Nucl. Part. Sci. **31** (1981), 375.

32. F. W. Büsser, *Proceedings of the International Conference on Neutrino Physics and Astrophysics*, Maui (Hawaii), eds. R. J. Cence, E. Ma and A. Roberts, **Vol. II** (1981), p. 351.

33. F. W. Büsser, Acta Physica Austriaca Suppl. **XXII** (1980), 139.

34. M. M. Nagels *et al.*, Nucl. Phys. **B147** (1979), 189.

35. The metric and Dirac matrix conventions (except for the sign of γ_5) used are those of
J. D. Bjorken and S. D. Drell, *Relativistic Quantum Mechanics*, Mc Graw-Hill Book Co., New York (1964).

36. R. E. Shrock and Ling-Lie Wang, Phys. Rev. Lett. **41** (1978), 1692.

37. C. H. Llewellyn-Smith, Phys. Rep. **3** (1972), 261.

38. H. Fritzsch and P. Minkowski, Phys. Rep. **73** (1981), 67.

39. H. C. Lee and K. W. Cheng, Lecture Notes in Physics **144** (1981), p. 353, Springer-Verlag.

40. C. Y. Prescott *et al.*, Phys. Lett. **77B** (1978), 347.

41. C. Y. Prescott *et al.*, Phys. Lett. **84B** (1979), 524.

42. K. Winter, Phys. Lett. **67B** (1977), 236.

43. B. Kayser, Phys. Rev. **D15** (1977), 3407.

44. L. Wolfenstein, *Proceedings of the 1975 International Symposium on Lepton and Photon Interactions at High Energies*, Stanford, California, ed W. T. Kirk (1976), p. 613.

45. F. Nezrick and F. Reines, Phys. Rev. **142** (1966), 852;
F. Reines, H. W. Sobel and E. Pasierb, Phys. Rev. Lett. **45** (1980), 1307.

46. J. N. Bahcall, Phys. Rev. Lett. **12** (1964), 300;
R. Davis, Jr., Phys. Rev. Lett. **12** (1964), 303;
R. Davis, Jr., D. S. Harmer and K. C. Hoffmann, Phys. Rev. Lett. **20** (1968), 1205;
J. N. Bahcall, Rev. Mod. Phys. **50** (1978), 881;
R. Davis, Jr., *Proceedings of the Brookhaven Solar Neutrino Conference*, BNL 50879 **1** (1978), p. 1;
B. T. Cleveland, R. Davis and J. K. Rowley, *Proceedings of the Workshop on Weak Interactions as Probes of Unification*, Blacksburg, USA (1980), p. 322;
Proceedings of the Mini-Conference on Neutrino Mass, Telemark, Wisconsin, USA (1980), p. 38;
J. N. Bahcall, *Proceedings of the International Conference on Neutrino Physics and Astrophysics*, Maui (Hawaii), eds. R. J. Cence, E. Ma and A. Roberts, **Vol. I** (1981), p. 1.

47. BEBC Collaboration: P. Fritze *et al.*, Phys. Lett. **96B** (1980), 427;
CHARM Collaboration: M. Jonker *et al.*, Phys. Lett. **96B** (1980), 435;
CDHS Collaboration: H. Abramowicz *et al.*, Z. Phys. **C13** (1982), 179;
V. Khovansky, *Proceedings of the International Europhysics Conference on High Energy Physics*, Brighton (UK), eds. J. Guy and C. Costain (1983), p. 792, Rutherford Appleton Laboratory, Chilton, Didcot.

48. S. M. Bilenky and B. Pontecorvo, Phys. Rep. **41C** (1978), 225.

49. M. Akano, Nuovo Cimento **64A** (1981), 201;
M. Akano, Lett. Nuovo Cimento **33** (1982), 331.

50. W. Kummer and G. Segrè, Nucl. Phys. **64** (1965), 585;
D. A. Dicus, G. Segrè and V. L. Teplitz, Phys. Rev. **D13** (1976), 3092.

51. E. Abers and B. W. Lee, Phys. Rep. **9C** (1973), 1.

52. M. A. B. Bég and A. Sirlin, Ann. Rev. Nucl. Science **24** (1974), 379.

53. S. Weinberg, Rev. Mod. Phys. **46** (1974), 255.

54. H. Fritzsch and P. Minkowski, Phys. Rev. **73** (1981), 67.

55. J. J. Sakurai, *Topical Conference on Particle Physics*, Hawaii, eds. S. Pakvasa and S. F. Tuan, **Vol. 2** (1980), p. 815.

56. P. Becher, M. Böhm and H. Joos, *Eichtheorien der starken und elektroschwachen Wechselwirkung*, Teubner Studienbücher Physik, B. G. Teubner (1981), Stuttgart.

57. L. Jauneau, Preprint, Orsay LAL 82/34 (1982).

58. T. W. Donnelly and R. D. Peccei, Phys. Rep. **50** (1979), 1.

59. A. Silverman, *Proceedings of the 10 th International Symposium on Lepton and Photon Interactions at High Energies*, Bonn, ed. W. Pfeil (1981), p. 138.

60. S. Yamada, *Proceedings of the International Symposium on Lepton and Photon Interactions at High Energies*, Cornell, Ithaca, eds. D. G. Cassel and D. L. Kreinick (1983), p. 525.

61. UA1 Collaboration: G. Arnison *et al.*, Phys. Lett. **147B** (1984), 493.

62. H. Leutwyler, Nucl. Phys. **B76** (1974), 413.

63. P. Langacker, Phys. Rev. **D20** (1979), 2983.

64. P. Langacker and H. Pagels, Phys. Rev. **D19** (1979), 2070.

65. S. Weinberg, *Festschrift for I. I. Rabi*, ed. L. Motz (1977), New York Acad. Sci..

66. C. A. Dominguez, Phys. Rev. Lett. **41** (1978), 605; Phys. Lett. **86B** (1979), 171.

67. C. N. Yang and R. Mills, Phys. Rev. **96** (1954), 191.

68. L. M. Sehgal, Preprint, Aachen PITHA 80/17 (1980);
L. M. Sehgal, Preprint, Aachen PITHA 84/03 (1984).

71. W. Marciano and A. Sirlin, Phys. Rev. **D22** (1980), 2695.

72. S. Sakakibara, Phys. Rev. **D24** (1981), 1149.

73. M. Veltman, Phys. Lett. **91B** (1980), 95.

74. F. Antonelli, M. Consoli and G. Corbo, Phys. Lett. **91B** (1980), 90.

75. M. Marciano, Phys. Rev. **D20** (1979), 274.

76. M. Gell-Mann, Phys. Lett. **8** (1964), 214.

77. G. Zweig, Preprint CERN-TH-401 (1964).

78. O. W. Greenberg, Ann. Rev. Nucl. Sci **28** (1978), 327.

79. F. Sciulli, *High-Energy Physics in the Einstein Centennial Year*, eds. A. Perlmutter, F. Krausz and L. F. Scott (1979), p. 1, Plenum Press, New York and London.

80. K. Berkelman, *High-Energy Physics in the Einstein Centennial Year*, eds. A. Perlmutter, F. Krausz and L. F. Scott (1979), p. 31, Plenum Press, New York and London.

81. F. E. Close, *An Introduction to Quarks and Partons*, Academic Press, London – New York – San Francisco (1979).

82. H. Fritzsch and M. Gell-Mann, *XVI International Conference on High Energy Physics*, NAL, Batavia, **Vol. 2** (1972), p. 135.

83. H. Fritzsch, M. Gell-Mann and H. Leutwyler, Phys. Lett. **47B** (1973), 365.

84. S. Weinberg, Phys. Rev. Lett. **31** (1973), 494.

85. S. Weinberg, Phys. Rev. **D8** (1973), 4482.

86. J. M. Gaillard, M. K. Gaillard and F. Vannucci, *Weak Interaction*, eds. M. K. Gaillard and M. Nikolic (1977), p. 61, Paris. See references therein.

87. S. Pakvasa and H. Sugawara, Phys. Rev. **D14** (1976), 305.

88. L. Maiani, Phys. Lett. **62B** (1976), 183.

89. B. Winstein, *Proceedings of the XIth International Conference on Neutrino Physics and Astrophysics*, Nordkirchen, eds. K. Kleinknecht and E. A. Paschos (1984), p. 627. See references therein.

90. P. Langacker, *Proceedings of the XXII International Conference on High Energy Physics*, Leipzig, eds. A. Meyer and E. Wieczorek, **Vol. II** (1984), p. 215. See references therein.

91. L. Wolfenstein, Phys. Lett. **13** (1964), 562;
S. Barr and P. Langacker, Phys. Rev. Lett. **42** (1979), 1654;
M. A. B. Bég and H.-S. Tsao, Phys. Rev. Lett. **41** (1978), 278.

92. L.-F. Li and L. Wolfenstein, Phys. Rev. **D21** (1980), 178.

93. T. D. Lee, Phys. Rep. **9C** (1974), 143.

94. S. Weinberg, Phys. Rev. Lett. **37** (1976), 657.

95. A. A. Amselm and D. I. D'Yakonov, Nucl. Phys. **B145** (1978), 271.

96. R. N. Mohapatra and J. C. Pati, Phys. Rev. **D8** (1973), 2317; Phys. Rev. **D11** (1975), 566;
R. N. Mohapatra and D. P. Sidhu, Phys. Rev. **D17** (1978), 1876.

97. M. Strovink, *Proceedings of the XIth International Conference on Neutrino Physics and Astrophysics*, Nordkirchen, eds. K. Kleinknecht and E. A. Paschos (1984), p. 699;
K. Kleinknecht, Preprint, University Dortmund UNIDO 84/282 (1984);
K. Kleinknecht, *Proceedings of Europhysics Study Conference on Flavour Mixing in Weak Interactions*, Erice (Italy) (1984);
C. Jarlskog, *4th Topical Workshop on Proton Antiproton Collider Physics*, Berne, Switzerland (1984).

98. M. A. B. Bég and A. Sirlin, Preprint, Rockefeller University Report Number RU 82/B/21 (1982).

99. P. D. Gall, *Proceedings of the XIth International Conference on Neutrino Physics and Astrophysics*, Nordkirchen, eds. K. Kleinknecht and E. A. Paschos (1984), p. 193.

100. L. Wolfenstein, *Proceedings of the XIth International Conference on Neutrino Physics and Astrophysics*, Nordkirchen, eds. K. Kleinknecht and E. A. Paschos, p. 730.

101. V. A. Lubimov, *Proceedings of the XXII International Conference on High Energy Physics*, Leipzig, A. Meyer and E. Wieczorek, **Vol. II** (1984), p. 108.

102. UA1 Collaboration G. Arnison *et al.*, Phys. Lett. **122B** (1983), 398;
Phys. Lett. **135B** (1984), 250;
UA2 Collaboration P. Bagnaia *et al.*, Phys. Lett. **129B** (1983), 130.

103. UA1 Collaboration G. Arnison *et al.*, Phys. Lett. **139B** (1984), 115.

104. UA2 Collaboration P. Bagnaia *et al.*, Phys. Lett. **139B** (1984), 105.

105. D. V. Nanopoulos, *Proceedings of the XXII International Conference on High Energy Physics*, Leipzig, A. Meyer and E. Wieczorek, **Vol. II** (1984), p. 36.

106. R. Klanner, *Proceedings of the XXII International Conference on High Energy Physics*, Leipzig, eds. A. Meyer and E. Wieczorek, **Vol. II** (1984), p. 201.

107. H. Terazawa, *Proceedings of the XXII International Conference on High Energy Physics*, Leipzig, eds. A. Meyer and E. Wieczorek, **Vol. I** (1984), p. 63.

108. For reviews see:
P. Fayet and S. Ferrara, Phys. Rep. **32C** (1977), 249;
C. Kounnas, A. Masiero, D. V. Nanopoulos and K. A. Olive, *International School for Advanced Studies Lecture Series*, No. 2 (1984), World Scient. Publ. Comp..

109. G. Steigman, D. N. Schramm and J. E. Gunn, Phys. Lett. **66B** (1977), 202;
J. Yang, D. N. Schramm, G. Steigman and R. T. Rood, Ap. J. **227** (1979), 697.

110. D. J. Gross and F. Wilczek, Phys. Rev. Lett. **30** (1973), 1343;
Phys. Rev. **D8** (1973), 3633; Phys. Rev. **D9** (1974), 980;
H. D. Pollitzer, Phys. Rev. Lett. **30** (1973), 1346; Phys. Rep. **14C** (1974), 129.

111. M. Veltman, Nucl. Phys. **B123** (1977), 89;
M. S. Chanowitz, M. A. Furman and I. Hinchliffe, Phys. Lett. **78B** (1978), 285.

112. G. Altarelli, Preprint CERN-TH.3983/84 (1984).

113. R. M. Barnett, Phys. Rev. **D11** (1975), 3246;
F. Gursey and P. Sikivie, Phys. Rev. Lett. **36** (1976), 775.

114. R. M. Barnett, Phys. Rev. **D14** (1976), 2990.

115. H. Fritzsch, M. Gell-Mann and P. Minkowski, Phys. Lett. **59B** (1975), 256;
S. Pakvasa, W. A. Simmons and S. F. Tuan, Phys. Rev. Lett. **35** (1975), 703;
F. A. Wilczek, A. Zee, R. L. Kingsley and S. Treiman, Phys. Rev. **D12** (1975), 2768.

116. J. Pati and A. Salam, Phys. Rev. **D10** (1974), 275;
H. Fritzsch and P. Minkowski, Nucl. Phys. **B103** (1976), 61;
M. A. Bég *et al.*, Phys. Rev. Lett. **38** (1977), 1252;
R. N. Mohapatra and D. P. Sidhu, Phys. Rev. Lett. **38** (1977), 667;
I. Liede, J. Maalampi and M. Roos, Nucl. Phys. **B146** (1978), 157;
T. G. Rizzo, Phys. Rev. **D21** (1980), 1214;
D. P. Sidhu, Phys. Rev. **D22** (1980), 1158;
J. K. Bajaj and G. Rajasekaran, Phys. Lett. **93B** (1980), 461;
For a recent review, see:;
G. Senjanovic, Preprint, Virginia Polytechnic VPI-HEP-84/2 (1984).

117. G. Beall, M. Bander and A. Soni, Phys. Rev. Lett. **48** (1982), 848.

118. G. J. Gounaris and D. Schildknecht, Z. Phys. **C12** (1982), 57;
D. Schildknecht, Preprint, Bielefeld BI-TP 81/12 (1981).

119. S. Yamada, *Proceedings of the XXII International Conference on High Energy Physics*, Leipzig, eds. A. Meyer and E. Wieczorek, **Vol. I** (1984), p. 72.

120. J. J. Sakurai, *Proceedings of the International Conference on Neutrino Physics and Astrophysics*, Baksan Valley, USSR **2** (1977), p. 242.

121. P. Q. Hung and J. J. Sakurai, Phys. Lett. **69B** (1977), 323;
P. Q. Hung and J. J. Sakurai, Phys. Lett. **88B** (1979), 91;
G. Ecker, Nucl. Phys. **B151** (1979), 147.

122. S. G. Wojcicki, *Annual Meeting of the Division of the Particle and Fields of the APS*, Santa Cruz, eds. C. A. Heusch and W. T. Kirk (1981), p. 316.

123. J. Bernabeú and C. Jarlskog, Phys. Lett. **69B** (1977), 71.

124. D. P. Sidhu, Phys. Lett. **87B** (1979), 67.

125. M. Gell-Mann and R. P. Feynman, Phys. Rev. **109** (1958), 193;
J. J. Sakurai, Nuovo Cimento **7** (1958), 649;
E. C. G. Sudarshan and R. E. Marshak, Phys. Rev. **109** (1958), 1860.

126. C. S. Wu *et al.*, Phys. Rev. **105** (1957), 1413.

127. R. Garwin *et al.*, Phys. Rev. **105** (1957), 1415.

128. H. Frauenfelder *et al.*, Phys. Rev. **106** (1957), 386.

129. M. Goldhaber *et al.*, Phys. Rev. **109** (1958), 1015.

130. L. Landau, Nucl. Phys. **3** (1957), 127.

131. T. D. Lee and C. N. Yang, Phys. Rev. **105** (1957), 1671.

132. A. Salam, Nuovo Cimento **5** (1957), 299.

133. See review article by
H.Frauenfelder and R. Steffen, *Alpha, Beta and Gamma Spectroscopy*,
ed. K. Siegbahn (1964), North – Holland Publ. Comp., Amsterdam.

134. H. F. Schopper, *Weak Interactions and Nuclear Beta Decay*, Amsterdam (1966).

135. H. Sato, Phys. Rev. Lett. **45** (1980), 1997;
J. Chakrabarti, M. Popović and R. N. Mohapatra, Phys. Rev. **D21** (1980), 3212;
I. Bars and M. Günaydin, Phys. Rev. Lett. **45** (1980), 859;
J. Maalampi and K. Enqvist, Phys. Lett. **97B** (1980), 62.

136. K. Enqvist *et al.*, Preprint Series in Theoretical Physics, Helsinki HU-TFT-81-18 (1981).

137. P. Schacht, *Proceedings of the XXII International Conference on High Energy Physics*, Leipzig, eds. A. Meyer and E. Wieczorek, **Vol. I** (1984), p. 196;
P. Franzini, *Proceedings of the XXII International Conference on High Energy Physics*, Leipzig, eds. A. Meyer and E. Wieczorek, **Vol. I** (1984), p. 205.

138. S. Weinberg, Phys. Rev. Lett. **36** (1976), 294;
A. D. Linde, JETP Lett. **23** (1976), 64;
J. Ellis, M. K. Gaillard, D. V. Nanopoulos and C. T. Sachrajda, Phys. Lett. **83B** (1979), 339;
J. Ellis, M. K. Gaillard and D. V. Nanopoulos, Nucl. Phys. **B106** (1976), 292.

139. K. Mursula, Report Series in Physics, University of Helsinki HU-P-D38 (1983).

140. E. Di Capua *et al.*, Phys. Rev. **B133** (1964), 1333.

141. S. E. Derenzo, Phys. Rev. **181** (1969), 1854.

142. W. B. Hermannsfeldt *et al.*, Phys. Rev. Lett. **1** (1958), 61.

143. M. T. Burgy *et al.*, Phys. Rev. **120** (1960), 1829.

144. H.Frauenfelder and R. Steffen, *Alpha, Beta and Gamma Ray Spectroscopy*,
ed. K. Siegbahn, **Vol. 2** (1965), p. 1431, North – Holland Publ. Comp., Amsterdam.

145. F. W. J. Koks and J. van Klinken, Nucl. Phys. **A272** (1976), 61.

146. F. P. Calaprice *et al.*, Phys. Rev. Lett. **35** (1975), 1566.

147. B. R. Holstein and S. B. Treiman, Phys. Rev. **D16** (1977), 2369.

148. J. van Klinken, Nucl. Phys. **75** (1966), 145;
J. van Klinken *et al.*, Phys. Rev. Lett. **50** (1983), 94.

149. H. Paul, Nucl. Phys. **A154** (1970), 160.

150. H. Brandle *et al.*, Phys. Rev. Lett. **40** (1978), 306.

151. P. Lebrun *et al.*, Phys. Rev. Lett. **40** (1978), 302.

152. J. C. Hardy and T. Towner, Nucl. Phys. **A254** (1975), 221.

153. F. Scheck, Phys. Rep. **44** (1978), 187.

154. S. E. Derenzo, Phys. Rev. **181** (1969), 1854.

155. J. Egger, Nucl. Phys. **A335** (1980), 87.

156. H. M. Steiner, *Proceedings of the XXII International Conference on High Energy Physics*, Leipzig, eds. A. Meyer and E. Wieczorek, **Vol. I** (1984), p. 208;
J. Carr *et al.*, Phys. Rev. Lett. **51** (1983), 627.

157. G. Bardin *et al.*, Phys. Lett. **137B** (1984), 135.

158. K. L. Giovanetti *et al.*, Phys. Rev. **D29** (1984), 343.

159. F. Corriveau *et al.*, Phys. Lett. **129B** (1983), 260.

160. F. Scheck, *Proceedings of the 10th International Conference on Particles and Nuclei*, Heidelberg, Germany, eds. B. Povh and G. Zu Putlitz (1984), p. 487C, North-Holland Publ. Comp., Amsterdam. See references therein.

161. Review of Particle Properties, Phys. Lett. **111B** (1982), 1;
references to the individual experiments are given there.

162. V. V. Akhmanov *et al.*, Sov. J. Nucl. Phys. **6** (1968), 230;
D. A. Bryman *et al.*, Phys. Rev. Lett. **50** (1983), 7.

163. F. Corriveau *et al.*, Phys. Rev. **D24** (1981), 2004.

164. G. Flügge, Z. Phys. **C2** (1979), 121.

165. T. Fazzini *et al.*, Phys. Rev. Lett. **1** (1958), 247.

166. D. Bryman and C. Picciotto, Phys. Rev. **D11** (1975), 1337.

167. L. Simons *et al.*, Nucl. Phys. **A395** (1983), 413.

168. D. R. Botterill *et al.*, Phys. Rev. Lett. **19** (1967), 982.

169. R. S. Hayano *et al.*, Phys. Rev. Lett. **52** (1984), 329.

170. K. Mursula, M. Roos and F. Scheck, Nucl. Phys. **B129** (1983), 321;
K. Mursula and F. Scheck, Preprint, Mainz MZ-TH/08 (1984).

171. T. Goldman and W. J. Wilson, Phys. Rev. **D15** (1977), 709.

172. P. C. Bosetti *et al.*, Nucl. Phys. **B142** (1978), 1.

173. H. de Groot *et al.*, Z. Phys. **C1** (1979), 143.

174. M. Jonker *et al.*, Phys. Lett. **109B** (1982), 133;
H. Grote, Ph. D. Thesis, Hamburg (1981), unpublished;
J. Panman, Ph. D. Thesis, Amsterdam (1981), unpublished.

175. T. P. Cheng and Wu-Ki Tung, Phys. Rev. **D3** (1971), 733.

176. C. A. Coombes *et al.*, Phys. Rev. **108** (1957), 1348.

177. G. Backenstoss *et al.*, Phys. Rev. Lett. **6** (1961), 415.

178. M. Holder *et al.*, Nucl. Inst. Meth. **148** (1978), 235; Nucl. Inst. Meth. **151** (1978), 69.

179. A. N. Diddens *et al.*, Nucl. Inst. Meth. **178** (1980), 27.

180. E. Metz, Ph. D. Thesis, Hamburg (1982), unpublished.

181. M. Jonker *et al.*, Phys. Lett. **86B** (1979), 229.

182. M. Jonker *et al.*, Z. Phys. **C17** (1983), 211.

183. F. W. Bullock, *Proceedings of Neutrino 79, International Conference on Neutrinos, Weak Interactions and Cosmology*, Bergen, eds. A. Haatuft and C. Jarlskog **Vol. 1** (1979), p. 398.

184. C. Jarlskog, Lett. Nuovo Cimento **4** (1970), 377.

185. M. K. Gaillard, *SPSC Workshop on Neutrino Physics*, CERN/SPSC 78-153 (1978), p. 71.

186. N. Armenise *et al.*, Phys. Lett. **84B** (1979), 137.

187. M. Jonker *et al.*, Phys. Lett. **93B** (1980), 203.

188. F. Bergsma *et al.*, Phys. Lett. **122B** (1983), 465.

189. J. Maalampi, K. Mursula and M. Roos, Nucl. Phys. **B207** (1982), 233.

190. G. Feinberg and S. Weinberg, Phys. Rev. Lett. **6** (1961), 381.

191. S. E. Willis *et al.*, Phys. Rev. Lett. **44** (1980), 522; Phys. Rev. Lett. **45** (1980), 1370.

192. H. Abramowicz *et al.*, Z. Phys. **C12** (1982), 225.

193. A. Benvenuti *et al.*, Phys. Rev. Lett. **34** (1975), 419; Phys. Rev. Lett. **35** (1975), 1199;
Phys. Rev. Lett. **41** (1978), 1204.

194. B. C. Barish *et al.*, Phys. Rev. Lett. **36** (1976), 939; Phys. Rev. Lett. **39** (1977), 981.

195. M. Holder *et al.*, Phys. Lett. **69B** (1977), 377.

196. M. Jonker *et al.*, Phys. Lett. **107B** (1981), 241.

197. J. Blietschau *et al.*, Phys. Lett. **59B** (1975), 361; Phys. Lett. **60B** (1976), 207.

198. P. C. Bosetti *et al.*, Phys. Lett. **73B** (1978), 380.

199. J. von Krogh *et al.*, Phys. Rev. Lett. **36** (1976), 710.

200. P. C. Bosetti *et al.*, Phys. Rev. Lett. **38** (1977), 1248.

201. C. Baltay *et al.*, Phys. Rev. Lett. **39** (1977), 62.

202. N. Armenise *et al.*, Phys. Lett. **86B** (1979), 115; Phys. Lett. **94B** (1980), 527.

203. R. Odorico and V. Roberto, Nucl. Phys. **B136** (1978), 333.

204. V. Roberto, Z. Phys. **C2** (1979), 315.

205. R. H. Schindler *et al.*, Phys. Rev. **D24** (1981), 78.

206. I. Peruzzi *et al.*, Phys. Rev. Lett. **39** (1977), 1301.

207. H. Abramowicz *et al.*, Z. Phys. **C15** (1982), 19.

208. R. Brock, Phys. Rev. Lett. **44** (1980), 1027.

209. J. J. Sakurai, *International Summer Institute on Theoretical Particle Physics in Hamburg*, Lecture Notes in Physics **56** (1975), p. 258, Springer-Verlag.

210. L. Wolfenstein, Nucl. Phys. **B91** (1975), 95.

211. R. L. Kingsley *et al.*, Phys. Rev. **D11** (1975), 1043.

212. M. Holder *et al.*, Phys. Lett. **72B** (1977), 254.

213. M. Jonker *et al.*, Phys. Lett. **102B** (1981), 67.

214. B. Kayser *et al.*, Phys. Rev. **D20** (1979), 87.

215. F. Reines, H. Gurr and H. Sobel, Phys. Rev. Lett. **37** (1976), 315.

216. K. C. Wang, *Proceedings of the XIth International Conference on Neutrino Physics and Astrophysics*, Nordkirchen, eds. K. Kleinknecht and E. A. Paschos (1984), p. 322.

217. A. P. Bugorsky *et al.*, Preprint, Serpukov IHEP 80-37 (1980);
A. A. Borisov *et al.*, Proposal for a Neutrino Calorimeter, SERP-P-136 (1978).

218. L. M. Sehgal, Phys. Lett. **55B** (1975), 205.

219. G. 't Hooft, Phys. Lett. **37B** (1971), 195;
D. Yu. Bardin, S. M. Bilenky and B. Pontecorvo, Phys. Lett. **32B** (1970), 68.

220. M. Gourdin, *Proceedings of the International Neutrino Conference*, Aachen, eds. H. Faissner, H. Reithler and P. Zerwas (1976), p. 234, Vieweg, Braunschweig.

221. C. Bouchiat, Phys. Lett. **57B** (1975), 284.

222. E. A. Hinds, C. E. Loving and P. G. H. Sandars, Phys. Lett. **62B** (1976), 97.

223. B. A. Dzuba, V. V. Flambaum and P. G. Silvestrov, Preprint, Novosibirsk 84-130 (1984).

224. G. Puglierin, *Proceedings of the Topical Conference on Neutrino Physics at Accelerators*, Oxford, eds. A. G. Michette and P. B. Renton (1978), p. 279.

225. F. Bergsma *et al.*, Phys. Lett. **117B** (1982), 272.

226. B. Kayser, *Proceedings of Neutrinos-78*, Purdue, ed. E. C. Fowler (1978), p. 979.

227. G. V. Dass and P. Ram Babu, Phys. Lett. **85B** (1979), 75.

228. W. Chyz *et al.*, Nuovo Cimento **34** (1964), 404;
R. W. Brown *et al.*, Phys. Rev. **D6** (1972), 3273;
K. Fujikawa, Phys. Rev. **D8** (1978), 1623.

229. F. Bergsma *et al.*, Phys. Lett. **122B** (1983), 185.

230. E. Fischback *et al.*, Phys. Rev. **D13** (1976), 1523.

231. S. Pakvasa and G. Rajasekaran, Phys. Rev. **D12** (1975), 113.

232. J. D. Bjorken, Phys. Rev. **179** (1969), 1547.

233. L. B. Okun, *Leptons and Quarks*, North-Holland Pub. Comp. (1982), Amsterdam – New York – Oxford.

234. C. Callan and D. J. Gross, Phys. Rev. Lett. **22** (1969), 156.

235. P. C. Bosetti *et al.*, Phys. Lett. **70B** (1977), 273.

236. A. Bodek *et al.*, Phys. Rev. **D20** (1979), 1471.

237. J. Wotschack, Ph. D. Thesis, Heidelberg (1978), unpublished.

238. A. J. Buras and K. J. F. Gaemers, Nucl. Phys. **B132** (1978), 249.

239. H. Georgi and H. D. Politzer, Phys. Rev. **D14** (1976), 1829;
R. M. Barnett, Phys. Rev. Lett. **36** (1976), 1163; Phys. Rev. **D14** (1976), 70.

240. A. J. Buras and K. J. F. Gaemers, Phys. Lett. **71B** (1977), 106;
I. Hinchliffe and C. H. Llewellyn Smith, Nucl. Phys. **B128** (1977), 93.

241. J.J. Sakurai, *Proceedings of the 11th Rencontre de Moriond*, ed. J Tran Thanh Van, **Vol. II** (1976), p. 299;
P. Sutherland *et al.*, Phys. Rev. **D13** (1976), 2700.

242. P. Wanderer *et al.*, Phys. Rev. **D17** (1978), 1679.

243. F. S. Merritt *et al.*, Phys. Rev. **D17** (1978), 2199.

244. H. Deden *et al.*, Nucl. Phys. **B149** (1979), 1;
P. C. Bosetti *et al.*, Nucl. Phys. **B217** (1983), 1.

245. C. F. Cho and M. Gourdin, Nucl. Phys. **B112** (1976), 365.

246. K. S. Lackner, Nucl. Phys. **B153** (1979), 526.

247. C. A. Piketty and L. Stodolsky, Nucl. Phys. **B15** (1970), 571.

248. M. K. Gaillard, S. A. Jackson and D. V. Nanopoulos, Nucl. Phys. **B102** (1976), 326.

249. A. Bartl, H. Fraas and W. Majerotto, Phys. Rev. **D16** (1977), 2124.

250. J. Bell *et al.*, Phys. Rev. Lett. **40** (1978), 1226.

251. C. Longuemare and C. Pascaud, Preprint, Orsay LAL-81/14 (1981).

252. L. M. Sehgal, *Proceedings of the 21st International Conference on High Energy Physics*, Paris, eds. P. Petiau and M. Porneuf (1982), p. C3-22. See references therein.

253. H. Abramowicz *et al.*, Phys. Lett. **109B** (1982), 115.

254. J. P. Leveille and T. Weiler, Nucl. Phys. **B147** (1979), 147;
M. Glück and E. Reya, Phys. Lett. **79B** (1978), 453; Phys. Lett. **83B** (1979), 98;
V. Barger, W. Y. Keung and R. J. N. Phillips, Phys. Lett. **91B** (1980), 253;
Phys. Lett. **91B** (1980), 179.

255. J. H. Kühn and R. Rückl, Phys. Lett. **95B** (1980), 431.

256. C. F. Cho and M. Gourdin, Nucl. Phys. **B112** (1976), 365.

257. C. F. Cho and M. Gourdin, Nucl. Phys. **B112** (1976), 387.

258. E. Fischbach *et al.*, Phys. Rev. **D15** (1977), 97.

259. J. E. Kim, P. Langacker and S. Sarkar, Phys. Rev. **D18** (1978), 123;
Proceedings of Neutrinos 78, Purdue, ed. E. C. Fowler (1978), p. 979.

260. L. Wolfenstein, Phys. Rev. **96** (1954), 1654.

261. J. Blietschau *et al.*, Nucl. Phys. **B114** (1976), 189; Phys. Lett. **73B** (1978), 232.

262. H. Faissner *et al.*, Phys. Rev. Lett. **41** (1978), 213.

263. N. Armenise *et al.*, Phys. Lett. **86B** (1979), 225.

264. A. M. Cnops *et al.*, Phys. Rev. Lett. **41** (1978), 357.

265. R. H. Heisterberg *et al.*, Phys. Rev. Lett. **44** (1980), 635.

266. M. Jonker *et al.*, Phys. Lett. **105B** (1981), 242;
F. Bergsma *et al.*, Phys. Lett. **117B** (1982), 272; Phys. Lett. **147B** (1984), 481.

267. L. A. Ahrens *et al.*, Phys. Rev. Lett. **51** (1983), 1514; Phys. Rev. Lett. **54** (1985), 18;
M. J. Murtagh, *Proceedings of the XIth International Conference on Neutrino Physics and Astrophysics*, Nordkirchen, eds. K. Kleinknecht and E. A. Paschos (1984), p. 290.

268. D. Bertrand *et al.*, Phys. Lett. **84B** (1979), 354.

269. J. P. Berge *et al.*, Phys. Lett. **84B** (1979), 357.

270. N. Armenise *et al.*, Phys. Lett. **81B** (1979), 385.

271. K. Winter, *Proceedings of the International Symposium on Lepton and Photon Interactions at High Energies*, FNAL, Batavia (Illinois), eds. T. B. W. Kirk and H. D. I. Abarbanel (1979), p. 258.

272. M. Jonker, Ph. D. Thesis, Amsterdam (1983), unpublished.

273. M. Jonker *et al.*, Nucl. Inst. Meth. **200** (1982), 183.

274. M. Jonker *et al.*, Phys. Lett. **99B** (1981), 265.

275. W. Krenz, Preprint, Aachen PITHA 82/26 (1982).

276. F. T. Avignone and Z. D. Greenwood, Phys. Rev. **D16** (1977), 2383.

277. I. Liede, J. Maalampi and M. Roos, Nucl. Phys. **B146** (1978), 157.

278. S. P. Rosen, *High Energy Physics in the Einstein Centennial Year*, eds. A. Perlmutter, F. Krausz and L. F. Scott (1979), p. 175, Plenum Press, New York and London.

279. T. Riemann, H. E. Ryseck and M. Walter, Z. Phys. **C8** (1981), 245.

280. BEBC-TST Collaboration: B. Jongejans *et al.*, CERN/SPSC 83-28 (1983).

281. L. F. Abbott and R. M. Barnett, Phys. Rev. **D18** (1978), 3214.

282. L. F. Abbott and R. M. Barnett, Phys. Rev. Lett. **40** (1978), 1303.

283. M. Roos and I. Liede, Phys. Lett. **82B** (1979), 89.

284. L. F. Abbott and R. M. Barnett, Phys. Rev. **D19** (1979), 3230.

285. R. E. Hendrick and L.-F. Li, Phys. Rev. **D19** (1979), 779.

286. M. Claudson, E. A. Paschos and L. R. Sulak, Phys. Rev. **D19** (1979), 1373.

287. E. A. Paschos, Phys. Rev. **D19** (1979), 83.

288. V. S. Mathur and T. Rizzo, Phys. Rev. **D19** (1979), 309.

289. R. E. Hendrick, Phys. Rev. **D20** (1979), 2965.

290. E. A. Paschos and L. Wolfenstein, Phys. Rev. **D7** (1973), 91.

291. E. A. Paschos and M. Wirbel, Nucl. Phys. **B194** (1982), 189;
E. A. Paschos, Preprint, Dortmund DO-TH 80/12 (1980).

292. C. Geweniger, *Proceedings of the XIth International Conference on Neutrino Physics and Astrophysics*, Nordkirchen, eds. K. Kleinknecht and E. A. Paschos (1984), p. 265.

293. P. G. Reutens, *Proceedings of the XIth International Conference on Neutrino Physics and Astrophysics*, Nordkirchen, eds. K. Kleinknecht and E. A. Paschos (1984), p. 256.

294. J. Blietschau *et al.*, Nucl. Phys. **B118** (1977), 218.

295. R. Nahnhauer, *Proceedings of the XXII International Conference on High Energy Physics*, Leipzig, eds. A. Meyer and E. Wieczorek, **Vol. I** (1984), p. 233.

296. J. Blietschau *et al.*, Phys. Lett. **88B** (1979), 381.

297. F. A. Harris *et al.*, Phys. Rev. Lett. **39** (1977), 437.

298. N. Armenise *et al.*, Phys. Lett. **122B** (1983), 448;
J. Moreels *et al.*, Phys. Lett. **138B** (1984), 230.

299. D.Allasia *et al.*, Phys. Lett. **133B** (1983), 129.

300. T. Kafka *et al.*, Phys. Rev. Lett. **48** (1982), 910.

301. M. Derrick *et al.*, Phys. Rev. **D18** (1978), 7;
D. D. Carmony *et al.*, Phys. Rev. **D26** (1982), 2965.

302. J. Marriner, University of California Ph. D. Thesis, Lawrence Berkeley Laboratory Report LBL-6438 (1977).

303. M. Pohl *et al.*, Phys. Lett. **79B** (1978), 501.

304. B. P. Roe, *Proceedings of Neutrino 79, International Conference on Neutrinos, Weak Interactions and Cosmology*, Bergen, eds. A. Haatuft and C. Jarlskog, **Vol. 2** (1979), p. 592.

305. L. M. Sehgal, *Proceedings of the International Symposium on Lepton and Photon Interactions at High Energies*, Hamburg, ed. F. Gutbrod (1977), p. 873.

306. H. Kluttig, J. G. Morfín and W. Van Doninck, Phys. Lett. **71B** (1977), 446.

307. P. Q. Hung, Phys. Lett. **69B** (1977), 216.

308. J. Okada and S. Pakvasa, Nucl. Phys. **B112** (1976), 400.

309. L. M. Sehgal, Phys. Lett. **71B** (1977), 99.

310. H. Deden, *Proceedings of Neutrino 79, International Conference on Neutrinos, Weak Interactions and Cosmology*, Bergen, eds. A. Haatuft and C. Jarlskog **Vol. 2** (1979), p. 397.

311. W. Lee *et al.*, Phys. Rev. Lett. **37** (1976), 186.

312. D. Cline *et al.*, Phys. Rev. Lett. **37** (1976), 252; Phys. Rev. Lett. **37** (1976), 648;
A. Entenberg *et al.*, Phys. Rev. Lett. **42** (1979), 1198;
W. Kozanecki, Ph. D. Thesis, Harward (1978);
J. Horstkotte *et al.*, Phys. Rev. **D25** (1982), 2743.

313. M. Pohl *et al.*, Phys. Lett. **72B** (1978), 489.

314. H. Faissner *et al.*, Phys. Rev. **D21** (1980), 555.

315. P. Coteus *et al.*, Phys. Rev. **D24** (1981), 1420.

316. P. Q. Hung and J. J. Sakurai, Phys. Lett. **72B** (1977), 208.

317. P. Q. Hung, Phys. Rev. **D17** (1978), 1893;
L. Wolfenstein, Phys. Rev. D19 (1979), 3450.

318. P. Langacker and S. Sidhu, *Proceedings of Neutrinos-78*, Purdue, ed. E. C. Fowler (1978), p. C 74.

319. E. Fischbach *et al.*, Phys. Rev. Lett. **37** (1976), 582.

320. S. J. Barish *et al.*, Phys. Rev. Lett. **33** (1974), 448.

321. W. Krenz *et al.*, Nucl. Phys. **B135** (1978), 45.

322. M. Derrick *et al.*, Phys. Rev. **D23** (1981), 569.

323. P. Schreiner, *Proceedings of the International Neutrino Conference*, Aachen, eds. H. Faissner, H. Reithler and P. Zerwas (1976), p. 333, Vieweg, Braunschweig.

324. M. Derrick *et al.*, Phys. Lett. **92B** (1980), 363.

325. M. Paty, *Proceedings of the International Symposium on Lepton and Photon Interactions at High Energies*, FNAL, Batavia (Illinois), eds. T. B. W. Kirk and H. D. I. Abarbanel (1979).

326. G. H. Bertrand Coremans *et al.*, Phys. Lett. **61B** (1976), 207.

327. O. Erriques *et al.*, Phys. Lett. **73B** (1978), 350.

328. T. Hand, *Proceedings of the International Neutrino Conference*, Aachen, eds. H. Faissner, H. Reithler and P. Zerwas (1976), p. 278, Vieweg, Braunschweig;
H. Faissner *et al.*, Phys. Lett. **68B** (1977), 377.

329. W. Lee, *Proceedings of the International Neutrino Conference*, Aachen, eds. H. Faissner, H. Reithler and P. Zerwas (1976), p. 319, Vieweg, Braunschweig.

330. M. Pohl, Ph. D. Thesis, Aachen (1979), unpublished.

331. S. L. Adler, S. Nussinov and E. A. Paschos, Phys. Rev. **D9** (1974), 2125;
S. L. Adler, Phys. Rev. **D9** (1974), 2144.

332. G. L. Fogli and G. Nardulli. Nucl. Phys. **B160** (1979), 116; Nucl. Phys. **B165** (1980), 162.

333. S. M. Berman and M. Veltman, Nuovo Cimento **38** (1965), 993;
C. H. Albright and S. L. Liu, Phys. Rev. **140B** (1965), 748;
C. W. Kim, Nuovo Cimento **37** (1965), 142;
P. Salin, Nuovo Cimento **48A** (1967), 506;
C. H. Llewellyn Smith, Phys. Rep. **3C** (1972), 261.

334. S. L. Adler, Ann. Phys. 50 (1968), 189; Phys. Rev. **D9** (1974), 229;
Phys. Rev. **D12** (1975), 2644; Phys. Rev. **D13** (1976), 1216.

335. D. Rein and L. M. Sehgal, Ann. Phys. **133** (1981), 79.

336. L. F. Abbott and R. M. Barnett, Phys. Rev. **D18** (1978), 3214.

337. L. Monsay, Phys. Rev. **D18** (1978), 2277.

338. G. L. Fogli, Nucl. Phys. **B207** (1982), 322.

339. S. A. Adjei, D. A. Dicus and V. L. Teplitz, Phys. Rev. **D23** (1981), 672.

340. A. Ali and C. A. Dominguez, Phys. Rev. **D12** (1975), 3673.

341. T. W. Donnelly *et al.*, Phys. Lett. **49B** (1974), 8.

342. E. Pasierb *et al.*, Phys. Rev. Lett. **43** (1979), 96.

343. H. Faissner *et al.*, Phys. Lett. **125B** (1983), 230.

344. O. Nachtmann, Nucl. Phys. **B22** (1970), 385.

345. S. L. Adler, Phys. Rev. **B135** (1964), 963.

346. R. P. Feynman, M. Kislinger and F. Ravndal, Phys. Rev. **D3** (1970), 270.

347. E. Isiksal, D. Rein and J. G. Morfín, Phys. Rev. Lett. **52** (1984), 1096.

348. D. Rein and L. M. Sehgal, Phys. Lett. **104B** (1981), 394; Nucl. Phys. **B223** (1983), 29.

349. H. Daumann, Ph. D. Thesis, Hamburg (1984), unpublished;
F.Bergsma *et al.*, to be published in Phys. Lett. (1985). See references therein.

350. P. Q. Hung and J. J. Sakurai, Phys. Lett. **63B** (1976), 295.

351. M. Klein and T. Riemann, Phys. Lett. **76B** (1978), 79;
M. Klein, *XV International School of Elementary Particle Physics*, Kupari (Yugoslavia) (1979);
M. Klein, T. Riemann and I. A. Savin, Phys. Lett. **85B** (1979), 385;
M. Klein, Preprint, Berlin-Zeuthen PHE 84-01 (1984).

352. Wu Chi-Min, Phys. Lett. **89B** (1980), 218.

353. K. W. Chen, Preprint, Ref. EP-CERN (1980).

354. E. Derman, Phys. Rev. **D7** (1973), 2755;
S. M. Berman and J. R. Primack, Phys. Rev. **D9** (1974), 2171.

355. Yu. B. Bushnin *et al.*, Phys. Lett. **64B** (1976), 102.

356. A. Argento *et al.*, Phys. Lett. **120B** (1983), 245; Phys. Lett. **140B** (1984), 142.

357. D. Yu. Bardin *et al.*, Nucl. Phys. **B197** (1982), 1.

358. J. Panman, *Proceedings of the XIth International Conference on Neutrino Physics and Astrophysics*, Nordkirchen, eds. K. Kleinknecht and E. A. Paschos (1984), p. 741.

359. H. Fritzsch and P. Minkowski, Nucl. Phys. **B103** (1976), 61.

360. R. N. Cahn and F. J. Gilman, Phys. Rev. **D17** (1978), 1313.

361. M. A. Bouchiat and C. C. Bouchiat, Phys. Lett. **48B** (1974), 111.

362. J. Bernabéu and C. Jarlskog, Nuovo Cimento **38A** (1977), 295.

363. G. Feinberg, *Ben Lee Memorial International Conference on Parity Non Conservation, Weak Neutral Currents and Gauge Theories*, eds. D. B. Cline and F. E. Mills (1977), p. 131, Harwood Academic Pub., London - Chur.

364. T. A. Trainor, *Proceedings of the International Workshop on Neutral Current Interactions in Atoms*, Cargèse, Corsica, France (1979), p. 231.

365. E. A. Hinds, *Proceedings of the International Workshop on Neutral Current Interactions in Atoms*, Cargèse, Corsica, France (1979), p. 256.

366. R. T. Robiscoe, *Proceedings of the International Workshop on Neutral Current Interactions in Atoms*, Cargèse, Corsica, France (1979), p. 275.

367. C. E. Wieman, *Proceedings of the International Workshop on Neutral Current Interactions in Atoms*, Cargèse, Corsica, France (1979), p. 213.

368. L. P. Lévy and W. L. Williams, Phys. Rev. Lett. **48** (1982), 607.

369. M. A. Bouchiat and C. C. Bouchiat, J. de Physique. **35** (1974), 899.

370. P. G. H. Sandars, *Proceedings of the International Symposium on Lepton and Photon Interactions at High Energies*, Hamburg, ed. F. Gutbrod (1977), p. 599.

371. P. Bucksbaum, E. Commins and L. Hunter, Phys. Rev. Lett. **46** (1981), 640.

372. P. S. Drell and E. D. Commins, Preprint, University of California, Berkeley (1984).

373. M. A. Bouchiat, J. Guena, L. Hunter and and L. Pottier, Phys. Lett. **117B** (1982), 358;
Phys. Lett. **121B** (1983), 456.

374. M. A. Bouchiat, J. Guena, L. Pottier and L. Hunter, Phys. Lett. **134B** (1984), 463.

375. I. B. Khriplovich, JETP Lett. **20** (1974), 315.

376. E. N. Fortson, Bull. Am.Phys. Soc. **20** (1975), 491.

377. C.-A. Piketty, *Proceedings of the XIth International Conference on Neutrino Physics and Astrophysics*, Nordkirchen, eds. K. Kleinknecht and E. A. Paschos (1984), p. 308.

378. L. M. Barkov and M. S. Zolotorev, Phys.Lett. **85B** (1979), 308.

379. J. H. Hollister *et al.*, Phys. Rev. Lett. **46** (1981), 643.

380. T. P. Emmons, J. M. Reeves and E. N. Fortson, Phys. Rev. Lett. **51** (1983), 2089.

381. V. N. Novikov, O. P. Sushkov and I. B. Khriplovich, Sov. Phys. JETP **44** (1976), 872;
O. P. Sushov, V. V. Flambaum and I. B. Khriplovich, *Report at the Conference on the Theory of Atoms and Molecules*, Vilnius (1979).

382. M. J. Harris, C. E. Loving and P. G. H. Sandars, J. of Phys. **11B** (1978), L749;
P. G. H. Sandars, Phys. Scr. **284** (1980), 21.

383. E. M. Henley, M. Klapisch and L. Wilets, Phys. Rev. Lett. **39** (1977), 994;
L. Wilets, *Proceedings of Neutrinos-78*, Purdue, ed. E. C. Fowler (1978), p. 437;
A. M. Martensson, E. M. Henley and L. Wilets, Phys. Rev. **A24** (1981), 308.

384. D. B. Saak'an, I. I. Sobelman and E. A. Yukov, Preprint, Lebedev Physical Institute No. 64 (1980).

385. S. L. Carter and H. P. Kelly, Phys. Rev. Lett. **42** (1979), 966.

386. O. P. Sushkov, V. V. Flambaum and I. B. Khriplovich, JETP Lett. **24** (1976), 502.

387. D. V. Neuffer and E. Commins, Phys. Rev. **A16** (1977), 844.

388. B. P. Das *et al.*, Phys. Rev. Lett. **49** (1982), 32.

389. C. Bouchiat *et al.*, Nucl. Phys. **B221** (1983), 68.

390. B. P. Das *et al.*, Preprint, State University of New York (Albany, NY) (1982).

391. V. A. Dzuba *et al.*, Preprint, Institute of Nuclear Physics of Novosibirsk, USSR (1984).

392. B. Kayser, S. P. Rosen and E. Fischbach, Phys. Rev. **D11** (1975), 2547.

393. M. A. Player and P. G. H. Sandars, J. of Phys. **B3** (1970), 1620.

394. G. Harrison, P. G. H. Sandars and S. J. Wright, Phys. Rev. Lett. **22** (1969), 1263.

395. M. C. Weisskopf *et al.*, Phys. Rev. Lett. **21** (1968), 1645.

396. R. W. Brown, V. K. Cung, K. O. Mikaelian and E. A. Paschos, Phys. Lett. **43B** (1973), 403;
K. O. Mikaelian, Phys. Lett. **55B** (1975), 219.

397. A. A. Sokolov and I. M. Ternov, Sov. Phys. Dokl. **8** (1964), 1203;
A. A. Sokolov and I. M. Ternov, *Synchrotron Radiation*, Pergamon Press (1968).

398. A. W. Chao, *Proceedings of the Conference on High Energy Particle Accelerators*, Fermilab Summer School, Batavia, Illinois, eds. R. A. Carrigan and F. R. Huson (1981), p. 395.

399. *HERA, a Proposal for a Large Electron-Proton Colliding Beam Facility at DESY*;
DESY HERA 81/10 (1981).

400. M. Davier, *Proceedings of Cargèse Summer Institute on Fundamental Interactions*, eds. M. Lévy et al. (1981), p. 283, Plenum Press, New York and London.

401. Sau Lan Wu, Phys. Rep. **107** (1984), 59.

402. M. J. Puhala, Z. J. Rek, Bing-Lin Young and Xue-Tian Zhu, Phys. Rev. **D25** (1982), 95;
M. J. Puhala, Z. J. Rek and Bing-Lin Young, Phys. Rev. **D23** (1981), 89.

403. J. Ellis and M. K. Gaillard, *Physics With Very High Energy e^+e^- Colliding Beams*, CERN76-18 (1976), 21.

404. K. G. Chetyrkin *et al.*, Phys. Lett. **85B** (1979), 277;
W. Celmaster and R. Gousalves, Phys. Rev. Lett. **44** (1980), 560.

405. D. P. Barber *et al.*, Phys. Rev. Lett. **43** (1979), 830; Phys. Lett. **89B** (1979), 139;
W. Bartel *et al.*, Phys. Lett. **91B** (1980), 142;
Ch. Berger *et al.*, Phys. Lett. **86B** (1979), 418;
R. Brandelik *et al.*, Phys. Lett. **86B** (1979), 243; DESY-Report 80/40 (1980);
H. B. Newman, *Proceedings of the XXth International Conference on High Energy Physics*, Madison, eds. L. Durand and L. G. Pondrom (1980), p. 627.

406. G. 't Hooft, Nucl. Phys. **B61** (1973), 455.

407. W. A. Bardeen *et al.*, Phys. Rev. **D18** (1978), 3998.

408. W. Celmaster and J. R. Gonsalves, Phys. Rev. **D20** (1979), 1420.

409. W. Bartel *et al.*, Phys. Lett. **101B** (1981), 361.

410. C. Møller, Ann. Phys. **14** (1932), 531.

411. C. H. Llewellyn Smith and D. V. Nanopoulos, Nucl. Phys. **B78** (1974), 205.

412. R. Gastmans and Y. Van Ham, Phys. Rev. **D10** (1974), 3629.

413. L. L. de Raad, Phys. Rev. **D11** (1975), 3228.

414. M. J. Puhala, T. G. Rizzo and B.-L. Young, Phys. Lett. **109B** (1982), 411.

415. T. Tsao, Preprint, Ph. D. Thesis SLAC-233 UC-34D (T/E) (1980).

416. W. Bernreuther and O. Nachtmann, Z. Phys. **C11** (1981), 235.

417. A. Rich, Rev. Mod. Phys. **53** (1981), 127.

418. B. Naroska, *Proceedings of the International Symposium on Lepton and Photon Interactions at High Energies*, Cornell, Ithaca. eds. D. G. Cassel and D. L. Kreinick (1983), p. 96;
A. Böhm, *Proceedings of the International Europhysics Conference on High Energy Physics*, Brighton (UK), eds. J. Guy and C. Costain (1983), p. 686, Rutherford Appleton Laboratory, Chilton, Didcot;
A. Böhm, Preprint, Aachen PITHA 84/11 (1984); PITHA 84/13 (1984);
R. Prepost, *Proceedings of the XXII International Conference on High Energy Physics*, Leipzig, eds. A. Meyer and E. Wieczorek, **Vol. I** (1984), p. 227;
C. K. Bowdery. *Proceedings of the XXII International Conference on High Energy Physics*, Leipzig, eds. A. Meyer and E. Wieczorek. **Vol. I** (1984), p. 229;
E. Wicklund, *Proceedings of the XXII International Conference on High Energy Physics*, Leipzig, eds. A. Meyer and E. Wieczorek, **Vol. I** (1984), p. 230.

419. H. J. Behrend *et al.*, Phys. Scripta **23** (1981), 610.

420. W. Bartel *et al.*, Phys. Lett. **88B** (1979), 171.

421. D. P. Barber *et al.*, Phys. Rep. **63** (1980), 339.

422. Ch. Berger *et al.*, Phys. Lett. **81B** (1979), 410.

423. R. Brandelik *et al.*, Phys. Lett. **83B** (1978), 261.

424. D. Rubin *et al.*, Nucl. Instr. Meth. **203** (1983), 119;
J. Chapman *et al.*, Nucl. Instr. Meth. **158** (1979), 387;
N. Harnew and D. Meyer, Nucl. Instr. Meth. **186** (1981), 513.

425. J. G. Smith, *Proceedings of the XVIIth Rencontre de Moriond*, Les Arcs-Savoie-France, ed. J. Tran Thanh Van, **Vol. 1** (1982), p. 131.

426. J. Dorfan, *Proceedings of Summer Institute on Particle Physics, the Strong Interactions*, Stanford University, SLAC Report No. 245, ed. A.Mosher (1981), p. 569.

427. H. Aihara *et al.*, Nucl. Instr. Meth. **217** (1983), 259;
H. Aihara *et al.*, Preprint LBL-17545, UT HE-84/03 (1984).

428. G. Wolf, Desy-Report 81-086 (1981).

429. F. A. Berends, K. J. F. Gaemers and R. Gastmans, Nucl. Phys. **B63** (1973), 381;
Nucl. Phys. **B68** (1974), 541;
F. A. Berends and R. Kleiss, DESY-Report 80-66 (1980);
F. A. Berends and G. J. Komen, Phys. Lett. **63B** (1980), 432.

430. F. A. Berends, S. Jadach and R. Kleiss, Acta Phys. Pol. **B14** (1983), 413.

431. D. A. Saxon, Hadronic J. **6** (1983), 455.

432. G. B. Chadwick, Preprint SLAC-PUB-3118 (1983).

433. JADE: W. Bartel *et al.*, Phys. Lett. **129B** (1983), 145;
MARK J: B. Adeva *et al.*, Phys. Rep. **109** (1984), 131;
TASSO: M. Althoff *et al.*, Phys. Lett. **138B** (1984), 441.

434. J. G. Branson, *Proceedings of the 10th International Symposium on Lepton and Photon Interactions at High Energies*, Bonn, ed. W. Pfeil (1981), p. 279.

435. JADE: W. Bartel *et al.*, Phys. Lett. **146B** (1984), 121; Phys. Lett. **146B** (1984), 437;
MARK J: B. Adeva *et al.*, Phys. Rep. **109** (1984), 131;
TASSO: M. Althoff *et al.*, Z. Phys. **C22** (1984), 219; Phys. Lett. **146B** (1984), 443; Phys. Lett. **126B** (1983), 493; Phys. Lett. **130B** (1983), 463 (Erratum);
MAC and TPC: J. M. Izen, Preprint DESY 84-104; *Proceedings of the XV. International Symposium on Multiparticle Dynamics*, Lund, Sweden (1984), p. 727;
HRS: M. Derrick *et al.*, Phys. Rev. Lett. **51** (1983), 1147; Phys. Rev. Lett. **53** (1984), 1971; Phys. Lett. **146B** (1984), 261.

436. J. Blietschau *et al.*, Phys. Lett. **71B** (1977), 231.

437. M. Holder *et al.*, Phys. Lett. **74B** (1978), 277.

438. V. Efremenko *et al.*, Phys. Lett. **88B** (1979), 181.

439. C. Baltay *et al.*, Phys. Rev.Lett. **39** (1977), 62;
C. Baltay, *Proceedings of the 19th International Conference on High Energy Physics*, Tokyo, eds. S. Homma, M. Kawaguchi and H. Miyazawa (1978), p. 882.

440. F. Buccella and L. Oliver, Nucl. Phys. **B162** (1980), 237.

441. G. J. Feldman *et al.*, Phys. Rev.Lett. **38** (1977), 1313.

442. G. Goldhaber *et al.*, Phys. Lett. **69B** (1977), 503.

443. K. H. Mess and B. H. Wiik, DESY-Report 82-011 (1982).

444. J. J. Sakurai, Preprint, Munich MPI-PAE/PTh 24/82 (1982).

445. F. Niebergall, *Proceedings of the XXII International Conference on High Energy Physics*, Leipzig, eds. A. Meyer and E. Wieczorek, **Vol. I** (1984), p. 240.

446. C. H. Llewellyn Smith, *Workshop on SPS Fixed Target Physics in the Years 1984-1989*, CERN 83-02 Vol. II, ed. I. Mannelli, p. 180.

447. J. F. Wheater and C. H. Llewellyn Smith, Nucl. Phys. **B208** (1982), 27; Phys. Lett. **105B** (1981), 486;
W. J. Marciano and A. Sirlin, Nucl. Phys. **B189** (1981), 442; Phys. Rev. **D29** (1984), 945;
W. J. Marciano, *Proceedings of the International Symposium on Lepton and Photon Interactions at High Energies*, Cornell, Ithaca, eds. D. G. Cassel and D. L. Kreinick (1983), p. 81.

448. E. Ma, *Proceedings of the International Europhysics Conference on High Energy Physics*, Brighton (UK), eds. J. Guy and C. Costain (1983), p. 259, Rutherford Appleton Laboratory, Chilton, Didcot.

449. J. Panman, *Workshop on SPS Fixed Target Physics in the Years 1984-1989*, CERN 83-02 Vol. II, ed. I. Mannelli, p. 146.

450. C. Busi *et al.*, *Proposal to Study Neutrino-Electron Scattering at the SPS - CHARM II Collaboration*; CERN/SPSC/83-24, SPSC/P186 (1983).

451. B. Kayser and S. P. Rosen, *AIP Conference Proceedings of Theoretical Symposium on Intense Medium Energy Sources of Strangeness*, Santa Cruz, eds. T. Goldman, H. E. Haber and H. F.-W. Sadrozinski (1983), p. 165.